PERFORMANCE EVALUATION AND FINITE ELEMENT ANALYSIS OF FIBER REINFORCED PRECAST CONCRETE UNDERGROUND STRUCTURES

by

ASHLEY WILSON

Presented to the Faculty of the Graduate School of
The University of Texas at Arlington in Partial Fulfillment
of the Requirements
for the Degree of

MASTER OF SCIENCE IN CIVIL ENGINEERING

THE UNIVERSITY OF TEXAS AT ARLINGTON
December 2012

ACKNOWLEDGEMENTS

I would like to express my sincere gratitude to my research adviser Dr. Ali Abolmaali for supporting me both academically and throughout my research. I am very grateful and sincerely appreciate all the knowledge and advice he has shared. I would also like to thank the other members of my committee, Dr. Shih-Ho Chao and Joe Lundy for their reviews and advice with this research project.

I would like to thank Hanson Pipe and Precast and Northern Concrete Pipe for volunteering their time and provisions of materials to make this research possible.

Special thanks goes to Ruth Bribiesca for all the time spent helping testing in The University of Texas at Arlington Civil Engineering Laboratory

Last but not least, I give my sincere thanks to my family who has been so loving and supportive throughout my studies.

November 15, 2012

ABSTRACT

PERFORMANCE EVALUATION OF FIBER
REINFORCED PRECAST CONCRETE
UNDERGROUND STRUCTURES

Ashley Wilson, M.S.

The University of Texas at Arlington, 2012

Supervising Professor: Ali Abolmaali

This study aimed at evaluating the performance of BASF Synthetic and Steel fibers as alternative reinforcements in concrete pipes. A total of 93 synthetic fiber and 60 steel fiber reinforced pipes were produced and tested based on the ASTM C497 in order to have a benchmark for comparison with conventionally reinforced concrete pipes. Three production sites with different production equipment were used in different geographical locations in the United States. Standard ASTM C76 diameters of up to 36 in. with “Wall-B” and “Wall-C” were used in this study for both synthetic and steel fibers. Vertical and horizontal load-deformation plots for the majority of the pipes were obtained by instrumenting the test pipes with linear variable displacement transducer (LVDT). The load-deformation plots were recorded for up to 5% of the pipe diameter. The load-deformation plots for steel and synthetic fibers were compared with each other. During production, compressive cylinder and beam specimens from the same mix designs were produced and cured for ASTM C39 and ASTM C1609 tests, respectively. A total of 353 cylinders and 77 beams were produced and tested. The ASTM C1609 beam load deformation

plots were compared for different fiber dosages and the area under this curve was calculated for each test specimen and modulus of toughness was calculated and documented. The patterns for material law (constitutive relationship) for low and high fiber dosages of both synthetic and steel fibers were identified. From the ASTM C39 and ASTM 1609 tests, a relationship between the tensile strength and square root of compressive strength was established on all the tests conducted.

This study showed that the use of BASF synthetic and steel fibers in concrete pipes as alternative reinforcement is feasible. This study recommends the use of synthetic fibers with adequate dosage for up to 21 in. concrete pipes with “B-Walls,” and up to 36 in. concrete pipes with “C-Walls.” BASF (Maccafferri) steel fiber pipes are recommended as alternative reinforcement with adequate fiber dosage for up to 24 in. concrete pipes with “B-Wall” and up to 36 in. concrete pipes with “C-Walls.” It should be noted that proper fiber dosage is a trial and error process based on local aggregate and cementitious materials and the type of production equipment used, which is also the case for the production of the conventionally reinforced concrete pipe

.

TABLE OF CONTENTS

LIST OF ILLUSTRATIONS

Figure Page

LIST OF TABLES

CHAPTER 1

INTRODUCTION, LITERATURE REVIEW AND GOALS AND OBJECTIVES

1.1 Introduction

Traditionally, concrete pipe is designed based on either a direct or indirect design procedure. In general, both procedures have three major steps for design; determining the total load that will be supported by the pipe, determining the required strength the pipe needs to support and the design of the wall strength required to support the total load on the pipe. Loads seen on a pipe are a combination of earth load, fluid load, wheel load, surcharge load, and the self-weight of the pipe. Both direct and indirect design procedures use similar methods in order to determine the loads described above. The magnitude and distribution of the loads being applied to a pipe determine the required strength. Designing the wall strength has many variables including the concrete strength, reinforcement size, reinforcement arrangement and wall thickness.

Indirect design utilizes the Marston-Spangler procedure in order to develop a bedding factor. Bedding factors (B_f) describe a relationship between the total field load and the three-edge bearing load so that it is no longer necessary to calculate the moments, shears and thrusts acting in the pipe wall. Trench condition bedding factors are based on the assumption that no lateral pressures are acting on the sides of the pipe. Embankment conditions, on the other hand, assume an active lateral pressure is applied on the sides of the pipe up to the height of the natural ground. Standard installations have been developed for each of the trench and embankment conditions and from this the correct bedding factor can be determined. The standard D-Load ($D_{0.01}$) calculation is then determined by dividing the total load by the product of the bedding factor and the diameter of the pipe. The ultimate strength design limit (D_{ult}) is the multiplication of the $D_{0.01}$ by a factor of safety which is a function of the class of the pipe. Indirect

design procedures encompass three-edge bearing results from previous test and evaluations in order to design for the required strengths needed.

In the direct design procedure the distribution of loads is dependent on one of two methods, uniform method or the radial method. The uniform method takes the total load on the pipe and evenly distributes it across the pipe compared to the radial method, which assumes the load acts radially around the pipe varying as a cosine function. The next step is to determine the bending moments, thrusts, and shears that result in the wall from the loads described above. Coefficients, which are multiplied by the total load, have been developed that describe the moments and thrusts at the crown, invert and springline of the pipe at given bedding angles. Once the moments, thrusts and shears are known, the pipe wall can be designed by determining wall thickness, concrete strength and conventional reinforcement design.

1.1.1 Reinforcement Needs for Conventional Reinforced Concrete Pipes

Small diameter pipe typically has a circumferential steel cage that is used to resist the ultimate flexural load exerted on the pipe. Circumferential reinforcement is an efficient solution to resist flexural ultimate loads but becomes increasingly less efficient for other failure modes which can occur as pipe diameter increases or as required pipe strengths increase. Figure 1.1 depicts the relation of the typical failure modes of a pipe depending on the inside reinforcing area of the wall and the height of earth cover. At lower heights, flexural control is the controlling failure method, which can be seen as acting linearly in the bottom left of the graph. As the fill heights increase the failure mode shortly turns to crack controlled then shear controlled design. The increase in the slope of the straight line indicates the circumferential steel becoming less efficient as the failure modes change. As a pipe diameter increases the graph in Figure 1.1 would show more extreme results.

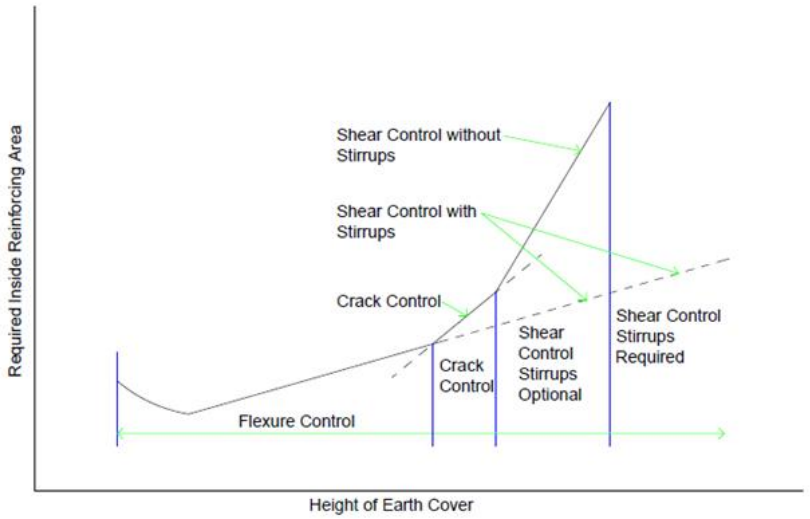

Figure 1.1 Plot of Required Inside Reinforcing Area vs. Design Height Earth Cover for Typical Design with Surface Wheel Loads (ASCE 15-98).

Circumferential steel is placed with within the wall at least one inch of concrete cover. It is with in this one-inch area that the initial tensile crack occurs and propagates through the section before the steel cage is engaged. The use of fibers is thought to resist cracking due to the dispersion of the fibers evenly throughout the entire wall thickness thereby more widely distributing the tensile stresses. Because each fiber is so small, in comparison with a traditional cage, the concrete surrounding each fiber is also small which results in less tensile force being released to each fiber. This process is thought to produce fine micro cracks but increases the overall tensile strain before a 0.01 in. crack is observed.

1.1.2 Intent and Justification of this Research

The above discussion (Figure 1.1) indicates that as the height of the fill increases the inside reinforcing area also increases. As pipe diameter increase the failure modes are met at lower fill heights. Thus, as the diameter of the pipe increases, the need for shear stirrups is imminent. Previous studies by Sustersic et al. showed that the addition of fibers into concrete, creating a matrix of fiber concrete, would increase the shear capacity of the concrete. In addition, it is documented in the study by Kwak et al. that fiber would enhance the crack resistance

capacity of concrete which acts as a crack control agent. Thus, considering the above benefits of the composite of fiber and concrete and the fact that steel fiber concrete pipes have been in service for many years in Europe, this study was undertaken. Even though the scope of this study did not include the large diameter pipes to demonstrate the full advantage of enhanced shear capacity by the introduction of fibers, it has set the ground work for future research for large diameter pipes.

It should be noted that even though the test results are compared with $D_{0.01}$ and D_{ult}, the concept of $D_{0.01}$ is irrelevant in fiber concrete pipe. Figure 1.2 shows the schematic of typical fiber concrete load deformation test results for low and high fiber dosages in which the D_{ult} is identified beyond which the load cannot be increased. However, due to fiber pull out resistance characteristics, significant deformation capacity without collapse beyond the D_{ult} is observed.

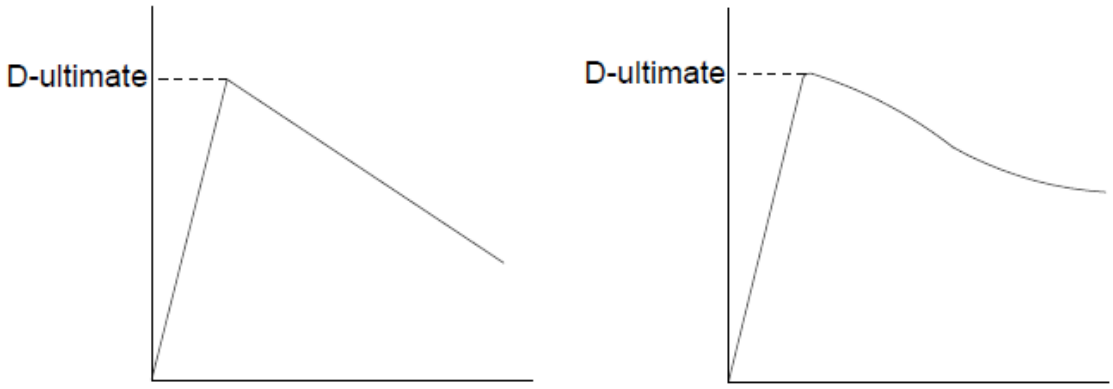

(a) (b)

Figure 1.2 Typical Behavior of Fiber Concrete for (a) Low Dosage of Fiber and (b) High Dosage of Fiber.

Currently, there is an ASTM standard specification which is being balloted that describes the behavior of steel fiber reinforced concrete pipe described in Figure 1.3. This figure shows the specification's proof of design concept in which the pipe is loaded until D_{ult} is reached. As a verification of bond, ductility, and toughness, the pipe is then unloaded and re-loaded until it reaches the specified service load, $D_{service}$. The load is held at $D_{service}$ level for one minute. The

value of $D_{service}$ is calculated based on taking a factor of safety of 1.5 with respect to D_{test} (i.e., $D_{service}$ = 2/3 D_{test}). As shown in Figure 1.3, the value of D_{test} is slightly lower than the value of D_{ult} and will be given as a pre-specified load in the upcoming ASTM Specification.

The dashed line presented in Figure 1.3 is to emphasize that additional displacement capacity (energy) exists in fiber concrete pipes beyond ultimate load. Therefore, the solid lines presented in Figure 1.3 does not represent the behavior of the pipe subject to loading, but instead merely shows the testing procedure for ensuring the bond and fiber quality.

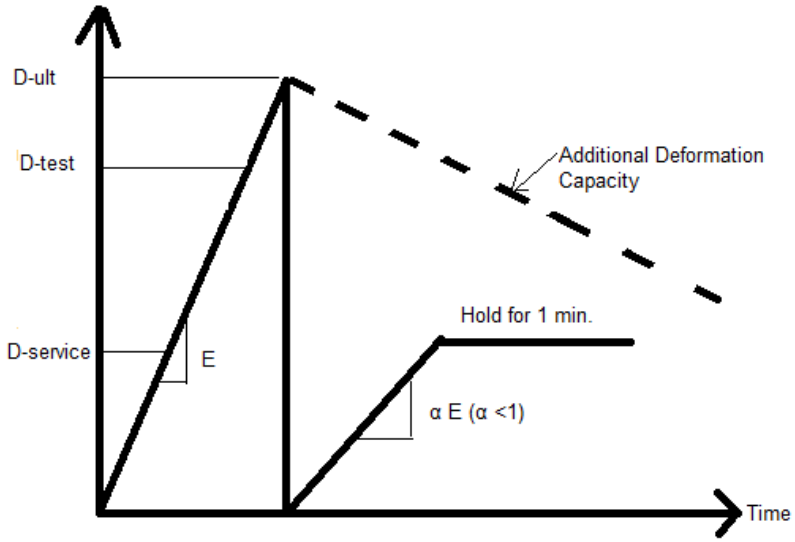

Figure 1.3 Behavior of Fiber Reinforced Pipe Design Concept

This study is the investigation of synthetic and steel fibers individually introduced into precast concrete pipes as a substitution for the conventional steel cage reinforcement. Concrete pipes were produced using two different fibers; BASF's Macrosynthetic fiber MasterFiber MAC Matrix, and BASF/Maccaferri fiber MasterFiber FS7. Multiple pipe sizes were investigated ranging between 15 in. to 36 in. (375 mm to 900 mm) diameters with varying dosages of each fiber. During this investigation, load-deformation plots for each pipe, as well as material proprieties including cylinder and beam testing were completed. As a result of the tests performed it was then possible to compare the fibers by deformation behavior, crack delay, crack control, Modulus of Elasticity, compressive strength and Modulus of Rupture.

1.1.3 Fibers

MasterFiber MAC Matrix is BASF's synthetic fiber that is manufactured from a blend of polypropylene resins that conforms to ASTM C1116 "Standard Specification for Fiber-Reinforced Concrete." Material properties for the MAC Matrix fiber can be found in Table 1.1. MAC Matrix fiber has previously been used in applications such as slab-on-grade and shotcrete as a replacement for welded wire reinforcement and other secondary reinforcement. Throughout testing performed by BASF, the MAC Matrix fibers have provided increased flexural toughness, increased impact resistance, improved residual strength and durability. Figure 1.4 (a) shows an image of the synthetic fibers.

MasterFiber FS7 is a steel fiber produced by Maccaferri that is manufactured using a low carbon drawn wire. This fiber conforms to ASTM A820 "Standard Specification for Steel Fibers for Fiber-Reinforced Concrete," as well as, international standards UNI-EN 10016, UNI-11037, and EN 14889-1. Material properties for FS7 are found in Table 1.1. BASF describes the benefits of MasterFiber FS7 as providing improved toughness, reduced cracking due to shrinkage, improved impact resistance, faster installation and improved durability of concrete mixes. Figure 1.4 (b) shows an image of the steel fibers used for this research.

Table 1.1 Fiber Properties

Fiber Type	Length	Diameter	Tensile Strength
MasterFiber MAC Matrix	1.9 in (48 mm)	n/a	85 ksi (585 MPa)
MasterFiber FS7	1.1 in (33 mm)	0.002 in (0.50 mm)	174 ksi (1200 MPa)

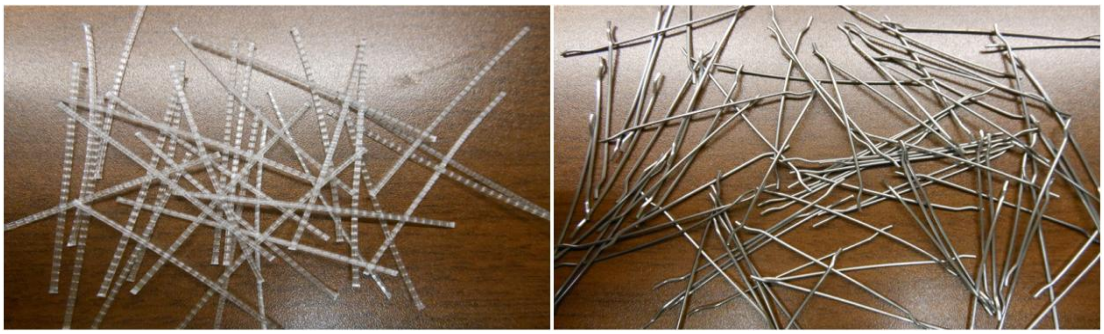

(a) (b)

Figure 1.4 Fibers (a) MasterFiber MAC Matrix Synthetic Fiber and (b) MasterFiber FS7 Steel Fiber.

1.1.4 Production Locations, Methods and Equipment

Three production sites were used during this study; Hanson Pipe and Precast in Grand Prairie, Texas, Hanson Pipe and Precast in Longview, Texas and Northern Concrete Pipe in Charlotte, Michigan. Two different production methods were used; Packerhead and Hawkeye, which will be described in detail in the following paragraphs. At each plant, the fiber was added directly into the mixer before the water was added. This approach helped to ensure that all fibers were distributed as evenly as possible throughout the concrete mix. Figure 1.5 (a) and (b) show the steel fibers being added into the concrete mixer and a typical conveyor system, respectively. After casting the pipes, each was removed from the outer form and then cured using a low-pressure steam system in which the steam is introduced into a controlled, closed environment (kiln) providing 100% humidity at temperatures between 80-100°F (26-37°C). It is essential to have high humidity, as close to saturation as is possible so that drying of the concrete doesn't occur during the curing process. Curtains are draped over a group of pipes to provide a barrier in order to retard the condensation of the steam. A typical curing curtain can be seen in Figure 1.5 (c). Curing time, temperature and moisture are the important factors needed to properly cure concrete. Not all concrete mixtures need the same relationship of these factors and must be determined by experience for each type of product. Due to the experience of the pipe producers, all pipes are left under the steam curing curtain overnight in order to accelerate the rate of

hydration in the concrete. This process allows the pipes to reach higher strengths in a shorter time frame.

Packerhead equipment was used at the Hanson Grand Prairie plant. This system involves placing a three-piece jacket onto a rotating table, creating the outside diameter of the pipe. Roller heads that rotate at high speeds are then placed inside the jacket. These roller heads spin while the concrete is introduced into the pipe form from above. The inside diameter of the pipe is created by the spinning of the rollers which force the concrete to the outer edges against the jacket by radial compaction. Packerhead equipment, seen in Figure 1.6, was the most challenging equipment used in this investigation due to the large amounts of dynamic movement during the jacket stripping process, which would cause pipes with higher water-to-cement ratios to collapse. To prevent pipes from falling, the water/cement ratio was reduced compared to typical production and pipes were retained in the jackets for 30 seconds to one minute before being stripped.

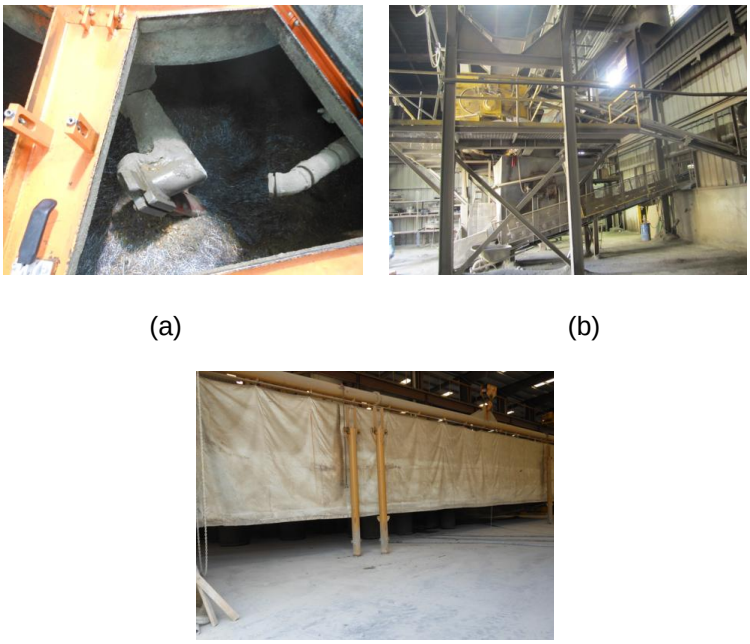

(a) (b)

(c)

Figure 1.5 Production Methods (a) Steel Fibers in Mixer, (b) Concrete Mix Conveyor System, (c) Steam Curing Curtains.

Figure 1.6 Packerhead Equipment.

Hawkeye equipment used was located at the Hanson Longview plant and the Northern Concrete Pipe plant. All production was completed using a dry cast process in which low frequency-high amplitude vibration is used to compact the concrete into the pipe molds. This system involves placing both outer and inner forms onto a vibrating table. As the concrete batch is added, the entire table vibrates and the concrete densely compacts. Once the pipe is fully compacted the machine then rotates the table so that the bell of the pipe can be formed. After that process the pipe can be lifted from the table and placed on the floor of the plant to be de-jacketed. The de-jacketing system is different with Hawkeye because the jacket is lifted from above slowly releasing the pipe. This process causes less dynamic stess on the pipe. All Hawkeye equipment is 100% automated resulting in a process that is much smoother helping to ensure the pipes are in good condition when placed into the curing location. This process also allowed for higher water contents to be achieved within the mixture. The Hawkeye equipment process is shown in Figure 1.7.

Figure 1.7 Hawkeye Equipment.

1.2 Literature Review

1.2.1 Steel Fibers

Previous research utilizing steel fibers has found a decrease in crack width for a given stress, and an increase in structural strength, ductility, impact resistance and freeze-thaw resistance. Research has recently begun in the United States using steel fibers in concrete pipes. Over the past two decades, Europe has produced performance-based guidelines which allow the use of steel fibers in concrete gravity pipelines. The current European Standards are predominately based from EN 1916 (2002) and include French NF P16-345-2 (2003), Belgium NBN-B21-106 (2004), Italian UNI EN 1916 (2004), Netherlands NEN 7126 (2004) and Spain UNE 127916 (2004).

A study by Swamy and Kent (1974) evaluated the use of steel fibers in two applications, deck slabs and concrete pipes. In the deck application, square slabs of two thicknesses with varying fiber dosages were subjected to a point load test in which they were loaded to twice the required design load. It was found that none of the specimens showed any sign of cracking while under working load stresses and that they also passed the load recovery tests. The concrete pipe testing covered a range of pipe diameters. It was found that all tests satisfy the proof load and ultimate load as required by British Standard BSS 556.

MacDonald and Trangsrud (2004) investigated the addition of steel fibers into wet and dry cast concrete pipes. The fiber dosages used were 0.25, 0.50, and 0.75 percent per volume (20, 39, and 59 kg/m3). Through compressive strength, average residual strength, and three-edge bearing tests, it was determined that fiber type and dosage amount greatly influenced the overall strength of the pipes. In addition to the above tests, pipes were tested for the first hairline crack, the first 0.25mm crack and ultimate load. Ultimate load was compared between fabric reinforcement, steel fiber reinforcement and a combination of both fabric and steel fiber reinforcement. It was determined from this study that steel fiber reinforcing adds strength to pipes but dosages should be optimized depending on the application and desired strength.

A study completed by Robert Henry (1974) investigated the concept of replacing traditional cage reinforcement with steel fibers in large diameter concrete pipes. For 60 in. pipes, the higher percent by volume ratios (between 0.8 and 1.08 percent) passed the ASTM C76 $D_{0.01}$ and $D_{ultimate}$ load requirements. The lower dosages did not pass the $D_{0.01}$ requirement but did however pass $D_{ultimate}$. All fiber percentages for the 54 in pipe did not pass the ASTM $D_{0.01}$ or $D_{ultimate}$ load requirements. Henry concludes that to use steel fiber instead of conventional reinforcement was not effective unless high dosages and thicker wall types were going to be used.

Thomas and Ramaswamy (2007) studied the material properties (compressive strength, tensile strength, modulus of rupture, post-cracking response, poisson's ratio, modulus of elasticity and strain) of steel fiber reinforced concrete with varying concrete strengths. The steel fibers had strengths of 35, 65, and 85MPa and were produced with a 1.5% volume fraction. Compression strength increased 8.33, 6.10, and 4.60% for normal, moderately high, and high-strength concrete respectively. Much higher increases were seen for split tensile tests; being 38.2% for normal concrete, 41.2% for moderately high-strength concrete and 38.5% for high-strength concrete. Modulus of rupture increased by 46.2, 38.8, and 40.0% for normal, moderately high-strength and high-strength concrete, respectively. Strain increased by 29.5% for normal concrete, 29.4% in moderately high-strength concrete and 27.0% for high-strength concrete. Modulus of elasticity

increased only slightly for normal, moderately high-strength, and high-strength concrete by8.3, 9.2, and 8.2%, respectively. It was found that Poisson's ratio had no significant change and was between 0.18 and 0.22 for all grades of the concrete mixes. Finally, as steel dosages increased the post cracking response was intensified.

Shende and Pande (2011) investigated the effects of steel reinforced concrete beams for flexural and deflection comparisons. Three steel fibers used had aspect ratios of 50, 60 and 67. The concrete mixture was constant except for the change in fiber dosages of 0%, 1%, 2%, and 3% by volume. It was determined that the addition of steel fibers increased the flexural strength compared to the plain concrete by 8.80-10.40 MPa, 8.40-10.00 MPa, and 8.27-9.73 MPa for 1%, 2%, and 3% by volume of steel fibers, respectively. The variations in the flexural strength are due to the change in aspect ratio and increase as the ratio increases. Deflection curves followed similar patterns for all fiber types and fiber dosages with a noticeable reduction for 3% of steel by volume.

Pullout behavior of steel fibers research was completed by Cunha, Barros and Sena-Cruz (2010). One hooked end type and one straight type of steel fiber were introduced into a self-compacting concrete application to determine the failure modes, load-slip curve and the relationships between embedded length and inclination angle. The most common type of failure for both fiber types when aligned was complete pullout. This resulted in the bent fibers hook to straighten out after debonding with the concrete. For inclined fibers the most common failure was rupture. The load-slip curves showed that the load significantly dropped once peak load was reached for aligned straight fibers. Following this, the load would continue to decrease as the slip increased. Hooked fibers had less of an abrupt decrease and would slip for length of the hook before acting as a straight fiber. It was found that embedded length had a significant impact on the pullout of the aligned fibers and very little to no impact with the inclined fibers. The peak load was observed to increase up to an angle of 30 degrees then decrease from 30 to 60 degrees.

Gencel et al. (2011) investigated the workability of steel fibers when used in a self-compacting concrete application. This research was completed to develop materials that would

help increase the workability of fiber reinforced concrete that currently caused difficulties on job sites. The same mix was used throughout the study except that the fiber dosages changed. It was found through slump flow and V-funnel tests that all fiber dosages were within the range necessary to deform as needed, as well as, avoid segregation. Fiber with hooked ends did cause some blockage of the aggregates and material during flow. Compressive strength was seen to initially increase, then decrease as high fiber dosage began to enable the concrete to behave in a homogeneous state that is highly important for strength. Flexural and toughness strengths of the mixes significantly increased in comparison to the plain concrete mix and continued to increase as more fiber was added.

1.2.2 Synthetic Fibers

Synthetic fibers are a newer material, which are being used in concrete applications, including slab-on-grade construction. Through previous research, it has been found that synthetic fibers can increase the impact resistance and toughness, and reduce crack width and plastic shrinkage seen in concrete. Research has not been completed until now for the application of synthetic fibers in concrete pipes.

An investigation by Song, Hwang, and Sheu (2005) determine the compressive strength, splitting tensile strength, modulus of rupture and impact resistance for nylon and polypropylene fiber reinforced concrete compared to plain concrete. It was found that the compressive strength of the polypropylene-fiber-reinforced concrete had an increase of 5.8% and nylon-fiber-reinforced had an increase of 12.4% compared to plain concrete. Splitting tensile strength was increased by 9.7% and 17.1% for polypropylene- and nylon-fiber reinforced concrete, respectively. It was observed that the fibers bridged over the split and eventually supported the entire load after the splitting had occurred. The increase in the modulus of rupture was found to be 1.5% for polypropylene and 5.6% for nylon fiber due to the fibers intersecting the crack. Impact resistance increased for polypropylene by 11.9% for first crack and 17% for failure strength. The nylon fiber increased by 19% and 30.5% for first crack and failure strength, respectively. In conclusion, the

nylon fiber performed better than the polypropylene fiber but both showed an increase in material properties compared to the plain concrete sample.

Another study was completed by Alhozaimy, Soroushian, and Mirza (1996) which used polypropylene fiber reinforced concrete at low volume fractions of 3% or less and evaluated the effects in regards to compression strength, flexural strength and impact resistance. Compressive strength test showed an increase between 21 and 23% but the compressive toughness was not significantly affected due to the fiber percentage. During flexure testing it was found that the flexural strength was not affected at the 95% level of confidence but the flexural toughness was affected at the 99% level of confidence. Impact resistance testing showed a very large range of results. However, multiple tests showed that at 2% fiber volume fraction there was a notable difference from the plain concrete. Overall, this study concluded that polypropylene fibers had no effect on the compressive strength, toughness and flexural strength of the concrete with the fiber dosages used. Flexural toughness, first crack and failure impact resistance all increased with the addition of fiber.

Kurtz and Balaguru (2000) performed an investigation that compared polypropylene and nylon fibers with dosages of 1.5 lb/yd^3 (0.9 kg/m^3). The experimental program consisted of compressive strength, post crack load-deflection behavior and time-dependent post crack load-deflection behavior tests. At the completion of this testing it was determined that polypropylene and nylon fibers can resist small percentages of post crack load. Nylon was found to creep faster and for less time compared to the polypropylene fiber. Final net creep deformation was not significantly different between to two fiber types.

Wang (1998) investigated the toughness characteristics of aramid, high-strength, and undrawn synthetic fibers as reinforcement in concrete. Aramid fibers were found to be 40-90% higher in toughness than undrawn fibers, depending on the fiber length and volume fraction. Strength increase in the armaid fibers were partly due to the fibers bundling causing the crack to be deflected by the fibers. Once the crack occurred aramid fibers showed the crack opening, as well as, a quick decrease in stress. High-strength and undrawn fibers had overall lower

strengths, however, were opposite in that the crack openings increased while the stress increases less rapidly.

A study completed by Hsie, Chen, and Song (1997) investigated fiber reinforced concrete, comparing four types of steel and one polypropylene fiber for abrasion resistance. Three of the steel fibers were various sizes with hooked-ends and the remaining was crimped. During compression strength testing the polypropylene fiber increased the strength more than the remaining steel fibers. The steel fiber that performed the best was the middle size (40 mm) hooked-end. Modulous of rupture (MOR) tests produced results showing higher MOR for fibers with large aspect ratios. This was due to the increase in stress resistance after the failure of flexural loading and an increased embedment depth in the failed surface. It was finally concluded that because of the low specific weight, the polypropylene fibers contributed the most to abrasion control.

An investigation by Atis et al. (2009) researched the compressive, flexural and abrasion resistance of varying steel and synthetic and fly ash quantities in reinforced fiber concrete. The volume ratios used for the synthetic and steel fibers were 0.05, 0.1, and 0.2% and 0.25, 0.5, 1, and 1.5% respectively. It was determined that adding and increasing the percentage of steel fibers produced higher abrasion resistance and increased flexural strength, but did not affect the compressive strength. Polypropylene fiber showed no increase in abrasion resistance when used in either plain concrete or fly ash concrete. The addition of fly ash only reduced the abrasion resistance compared to plain concrete and continues to decrease resistance as more fly ash was added.

Roesler et al. (2004) completed testing fiber reinforced slabs under monotonic loading and compared the results of plain concrete, two dosages of synthetic fiber and two steel fibers. Through flexural strength tests of the slabs it was determined that and volume fraction percentage less than 1% did not show a difference from plain concrete. Synthetic and hooked-end fibers showed an increase of 30% and the crimped steel fiber increased by 55% in flexural

strength compared to the plain concrete. Steel fibers had the most increase of ultimate load as compared to plain concrete. Failure behavior of all steel fibers was similar.

1.3 Goals and Objectives

The general goal of this study is to evaluate the performance of BASF MasterFiber (FS7) steel fiber and Macrosynthetic (Mac Matrix) synthetic fiber in the application of concrete pipes. This evaluation is then intended to identify possible improvements to pipe production and to facilitate further steps in the investigation of this advancing technology. The objectives of this study focus mainly on the production of concrete pipes of various sizes between 15 in. and 36 in. (375 mm-900 mm) with varying fiber amounts. The pipe sizes were determined due to previous research showing that the failure modes of small diameter pipes are typically hoop or flexural failure. While each pipe is being tested, a Load-Deformation plot is produced showing the fiber characteristics after initial crack. Another key objective is to determine the material properties of the fiber concrete and its relationships between their compressive cylinder and flexural beam tests.

CHAPTER 2

EXPERIMENTAL PROGRAM (MATERIAL PROPERTIES)

2.1 Introduction

This chapter presents the material behavior results of steel and synthetic fiber reinforced concrete when tested in flexural beam (ASTM C1609) and compressive cylinder (ASTM C39) applications. Each of the tests was completed using the same concrete mix for the corresponding concrete pipes which were produced simultaneously. All curing of the test specimens were completed at the respective production plant alongside the concrete pipes. In addition, the mix properties for each batch are also described in the following section, as well as in Appendix A.

Each pipe, beam and cylinder was designated by a unique name which displayed all important information. The following is the format which was used for all specimens from Hanson Grand Prairie.

"BASF-(Fiber Type)-Pipe Diameter-Wall Type-Test Type-Fiber Dosage (lbs/yd^3)-Test Number"

In the above designation, the test type is defined as DL for D-Load, BM for ASTM 1609 Beam and **CC** for Compressive Cylinders. Modification to the name designation format was made to accommodate beams and cylinders produced by the Hawkeye equipment at the Hanson Longview and Northern Concrete Pipe plants. This was necessary because one mix was used to produce up to three pipe diameters but only one set of beams and cylinders was needed for material properties testing. Therefore, the following format was used for Hanson Longview and Northern Concrete specimens.

"BASF-(Fiber Type)- Wall Type-Test Type-Fiber Dosage(lbs/yd^3)-Test Number-Production Plant"

In the above designation the production plant is defined as LV for Hanson Longview plant and NC for Northern Concrete plant.

All production was based off values in lbs/yd^3 and then was later converted into fiber volume fraction percentages for easier comparison purposes. All volume fraction calculations were based on the relative density of water (1.0). Steel fibers were determined to have a relative density of 7.85 and a mass per volume value of 13,226 (lbs/yd^3). Synthetic fibers were determined to have a relative density of 0.91 and a mass per volume value of 1,533 (lbs/yd^3). The following equation shows the calculation for fiber volume percentage.

$$Fiber\ Volume\ \% = \frac{Relative\ Density}{Mass\ per\ Volume}\ (100)$$

Table 2.1 is a summary of the fiber dosages for synthetic and steel fibers in terms of lbs/cy^3 and fiber volume fraction percentage.

Table 2.1 Fiber Volume Percentage Summary

Fiber Type	Synthetic							Steel				
Dosage (lbs/yd3)	4	6	8	10	12	16	18	22	33	44	66	88
Fiber Volume (%)	0.26	0.39	0.52	0.65	0.78	1.04	1.17	0.17	0.25	0.33	0.5	0.67

2.2 Dry Cast Mix Design

In pre-cast concrete production there are two different methods that can be used, dry cast and wet cast. Dry cast production uses low frequency-high amplitude forces which distribute and compact the concrete. This could be in the form of vibration, packing, spinning, or a combination which forces the concrete towards the form and creates the desired shape. Dry cast forms are usually removed right away and therefore create the ability to produce multiple pipes in a production day with one form. Due to the removal of the forms, the early curing time becomes essential to the pipes overall strength. The concrete mix is made to have a low water-to-cement ratio with zero slump resulting in the consistency of slightly wetted soil. This kind of concrete mix is less workable than other variations of concrete mixtures. Wet cast production has a slightly higher water-to-cement ratio with a slump of less than 4 inches. This creates a more workable concrete mix design. This procedure requires that each pipe has its own freestanding form in

which the concrete is poured and cured overnight. Typically, wet cast procedures are used in large diameter pipe production.

Within the pipe industry, it is up to each producer to prepare mix designs which enable their pipes to pass the D-Load testing requirement. As the class requirements of pipes move from Class I to V, the overall strength needs to increase in order to pass the required load. One common option is to increase the reinforcement area within the pipe wall in order to increase the strength. The second common option is to modify the cement and mix design while keeping the reinforcement the same in order to increase the overall strength of the pipe. Hanson in Grand Prairie mix designs increase the cement amount within the mix. These mix designs can be found in Appendix A. The Longview plant typically uses one mix design and then increases the steel area depending on the class of pipe, therefore in order to increase the cement amount the Grand Prairie mix designs were used in the Longview location as well. Hawkeye equipment is capable of making multiple sizes of pipe during one batch so the Class IV mix for 24 in. (600 mm) pipe was chosen to be used for all Hanson Longview pipe production. The Northern Concrete Pipe plant in Charlotte, Michigan produced the batches individually depending how large of a batch they were going to need for each fiber dosage. All the batches from this plant were overall very similar and only had slight variations in amounts.

Throughout this investigation, the mix designs were to be kept constant with each specific plant in order to keep a consistency for each production method. Consequently, the varying factor at each production location was the water content and fiber dosage. Due to initial difficulties with the Packerhead equipment at the Hanson Grand Prairie plant, the water was reduced by 10% in order to insure that the pipes stood up. Reducing the water, however, reduced the strengths. The mixes were then increased to a Class IV mix design which would be tested in accordance to Class III design strengths to account for the decrease in water. Pipes produced during colder months, as well as, produced on a bi-directional Packerhead machine at Grand Prairie produced smooth finished pipes and higher pipe strengths. At the Longview plant, the water-to-cement ratio was reduced from 4.0 to 3.2. This was the case for all mixes except when

high dosages og synthetic fiber were being used, then 10-20 lbs of additional water was added. Water was added to high synthetic dosages because the additional surface area increased water demand. Hanson Longview and Northern Concrete Pipe plants produced good finished surfaces on the pipe dut to higher water content and the one-piece jackets being stripped overhead.

2.3 Flexural Beam Test

Beams were produced throughout this study for each mix design. Each beam test was performed in accordance with ASTM C1609 “Standard Test Method for Flexural Performance of Fiber-Reinforced Concrete (Using Beam with Third-Point Loading).” Flexural beams produced were 6 by 6 by 20 in (150 by 150 by 500 mm) in size and tested after 7 days of curing. This test is conducted with a simply supported beam that has three-point load application set-up. From this test, it is then possible to determine first-peak loads, peak load, modulus of rupture, and load-deflection plot. This information then can be used to establish specimen toughness.

All beams were produced using steel forms of the appropriate size. Molds were placed onto a vibrating table located near the concrete mixer and layers of concrete were added and compacted until the entire beam mold was full. Each layer was dispersed in even thicknesses and distributed over the whole area of the beam. After curing, each beam was de-molded, labeled and marked in preparation for the flexural test.

Concrete is a brittle material by itself, but with the addition of fiber reinforcement concrete can transition into a ductile material. Failure modes, seen throughout the testing show the progression of cracking moving from brittle to ductile behavior as the fiber dosage was increased. With low dosages of fiber a typical failure crack would move vertically along the centerline of the beam specimen. High dosage showed a more ductile behavior as failure cracks would begin to travel vertically then move to a 45-degree angle with the crack heading in the direction of the top support. Typical crack failures can be seen in Figures 2.1 for synthetic fibers and Figure 2.2 for steel fibers.

(a)

(b)

(c)

Figure 2.1 Synthetic Fiber Crack Behaivors (a) 4 lbs/yd^3 (0.26% VF), (b) 10 lbs/yd^3 (0.65% VF), and (c) 16 lbs/yd^3 (1.04% VF)

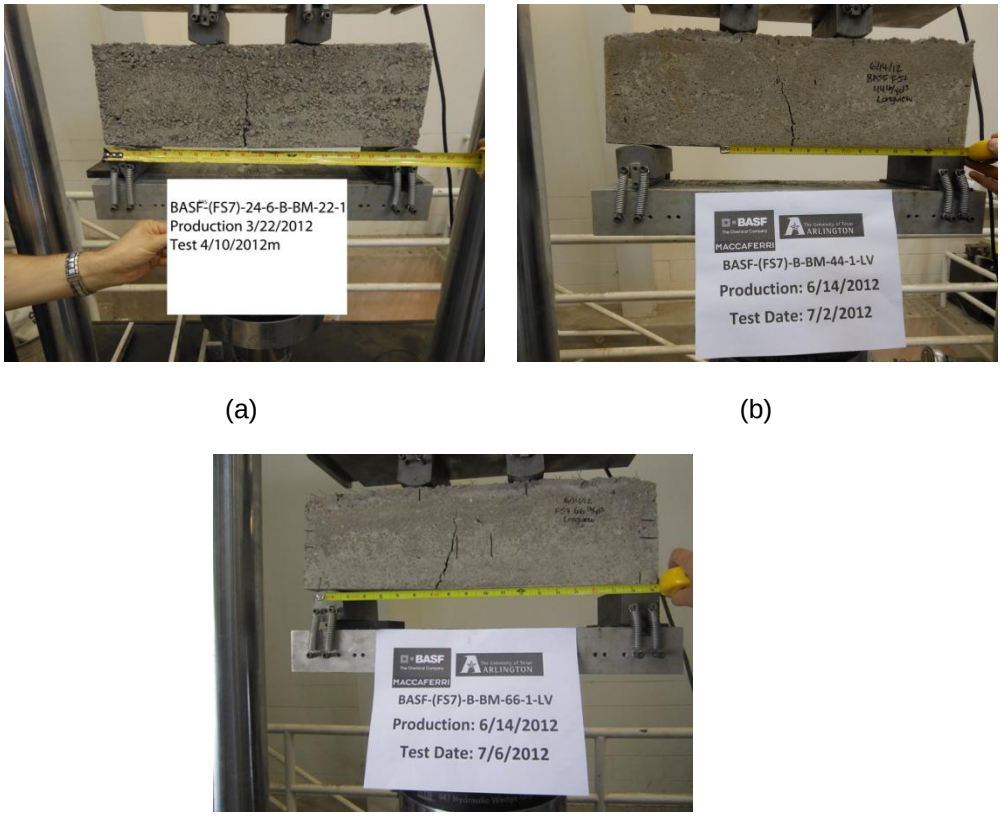

(a) (b)

(c)

Figure 2.2 Steel Fiber Crack Behaviors (a) 22 lbs/yd^3 (0.17% VF), (b) 44 lbs/yd^3 (0.33% VF), and (c) 66 lbs/yd^3 (0.50% VF).

2.3.1 Test Set Up

The MTS testing apparatus is hydraulic pump operated and is capable of applying constant displacement. The attachments used for flexural testing ensured that the beam was placed and centered inside the testing area in a three-point load, simply supported beam set up. The bottom supports for the beam were 18 in (457 mm) apart and the top supports were positioned 3 in (76 mm) on both sides of the centerline. A typical beam test set up can be seen in Figure 2.3.

The specimen was measured and marked to ensure the correct placement of a rectangular frame, which is attached to the specimen in order to hold the Linear Variable Displacement Transducers (LVDTs) in place. The frame was placed so that the LVDT's were

centered in the middle of the beam, both horizontally and vertically. The specimen was then placed into the MTS machine and positioned on the supports. A schematic showing the frame placement is in Figure 2.4.

Figure 2.3 Typical Beam Set Up.

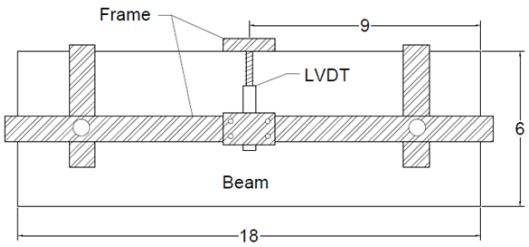

Figure 2.4 Schematic of Frame.

2.3.2 Instrumentation

StrainSmart Data Acquisition software, in addition to a Vishay scanner were the primary sources for collecting data. The high-voltage channels were connected to the MTS testing apparatuses in order to record the machines output for load and displacement. This information was critical in order to produce load-deformation plots.

LVDT's were used to collect displacement data independent from the MTS displacement in order to observe deflection of the beam specimen. As mentioned above, they are positioned along the mid-span of the beam and supported by the rectangular frame which is placed along the centerline of the beam. The LVDT's are also connected to the high-voltage inputs and recorded using the StrainSmart data recording system. Pictures showing the instrumentation configuration can be found in Figure 2.5.

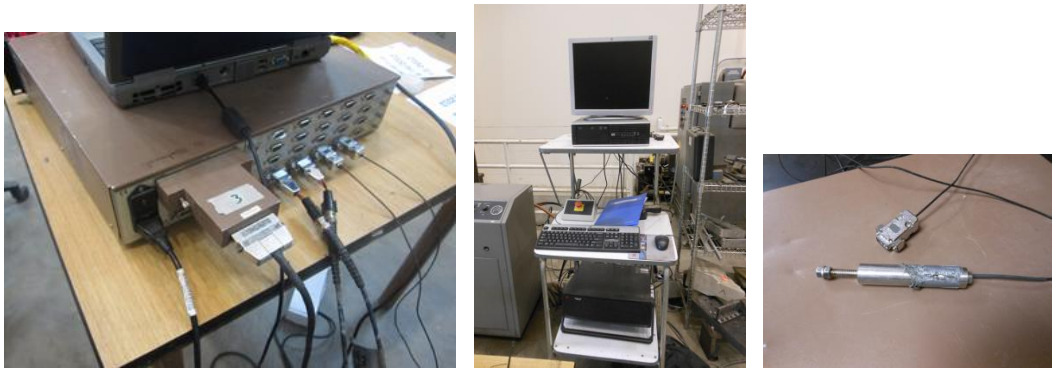

(a) (b) (c)

Figure 2.5 Beam Testing Equipment (a) Vishay Connections, (b) MTS computer and (c) LVDT.

2.3.3 Loading History

ASTM C1609 states that a loading rate of 0.002 to 0.012 in/min (0.05 to 0.30 mm/min) should be used for net deflections greater than L/900. Therefore, the MTS was programmed to apply a constant displacement of 0.002 in/min (0.05 mm/min) during testing. It is recommended that the test continue until the net deflection reached a value of at least L/150, which is 0.12 in. (3 mm) for the length of beam specimens used in this study.

2.3.4 Test Cases

Throughout this study a total of 77 beams were tested, 43 synthetic fiber reinforced and 34 steel fiber reinforced. Multiple cases for each fiber dosage from each production location were tested. The breakdown of this information can be seen below in Table 2.2 and Table 2.3.

Table 2.2 Total Amount of Synthetic Beams Based on Fiber Dosage and Production Plant

Synthetic	**Fiber Dosage (lbs/yd^3)**							
	4	**6**	**8**	**10**	**12**	**16**	**18**	**Total**
Hanson-Grand Prairie	2	3	5	6	6	5	4	31
Hanson-Longview	0	1	3	1	1	1	0	7
Northern Concrete	0	0	1	1	1	1	1	5
Total	2	4	9	8	8	7	5	**43**

Table 2.3 Total Amount of Steel Beams Based on Fiber Dosage and Production Plant

Steel	Fiber Dosage (lbs/yd^3)					
	22	**33**	**44**	**66**	**88**	**Total**
Hanson-Grand Prairie	6	5	10	3	0	24
Hanson-Longview	0	3	1	1	1	6
Northern Concrete	0	1	1	1	1	4
Total	6	9	12	5	2	**34**

2.3.5 Test Results

Flexural beams tests produced load-deflection plots for each specimen, which relates the average deflection seen by the LVDT's to the corresponding load being applied to the beam. Load-deflection plots display first-peak, peak load, and material property behaviors. The definition of first-peak and peak loads are defined based on ASTM C1609, which states that first-peak is the first point on the load-deflection curve where the slope is zero. ASTM C1609 defines the peak load is defined as the maximum load shown on the load-deformation plot. In some cases in this report peak load may also be referred to as ultimate load. In most cases the first-peak load was the same as the overall peak load. In general, at the initial crack the load significantly decreases and then depending on the fiber type and amount determined how much, if any, of the load is regained throughout the remaining of the test. Figure 2.6 shows a typical plot of the first-peak load being the same as the peak load. Figure 2.7 shows a representation of a typical plot where peak load is greater than first-peak.

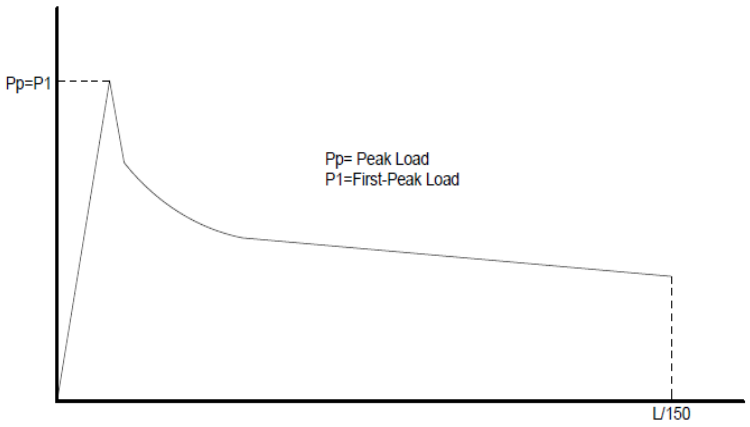

Figure 2.6 Typical Schematic Showing First-Peak Equal to Peak Load

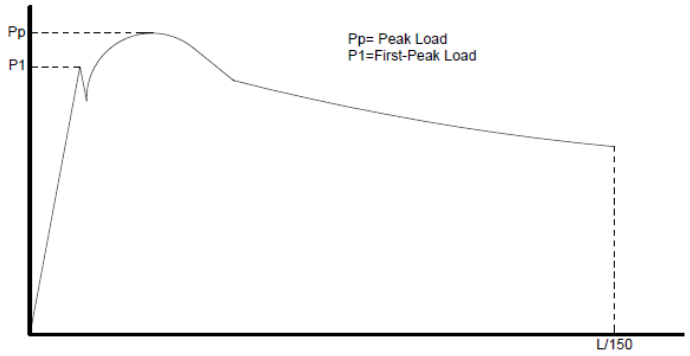

Figure 2.7 Typical Schematic Showing Peak Load Greater than First-Peak Load

Low dosages of synthetic fibers typically dropped in load significantly at failure, then would remain constant showing the ability to allow deflection and displacement to occur without decreasing the load. This behavior is also described as a hardening phenomenon which occurs as the fibers are engaged after the failure of the beam. As fiber dosages increased the initial drop in load was reduced and the fiber began to not only allow for deflection, but the hardening behaviors become more pronounced. As hardening increased the load capacity began to increase as well. From the fiber dosages tested, synthetic fiber were not observed passing the

first-peak load, however, 18lbs/yd^3 (1.17% VF) testing did come close to regaining first-peak load value. Sample graphs for low-, medium-, and high-dosage of synthetic fiber can be found in Figure 2.8 and all steel beam graphs and synthetic beam graphs are located in Appendix B and Appendix C, respectively.

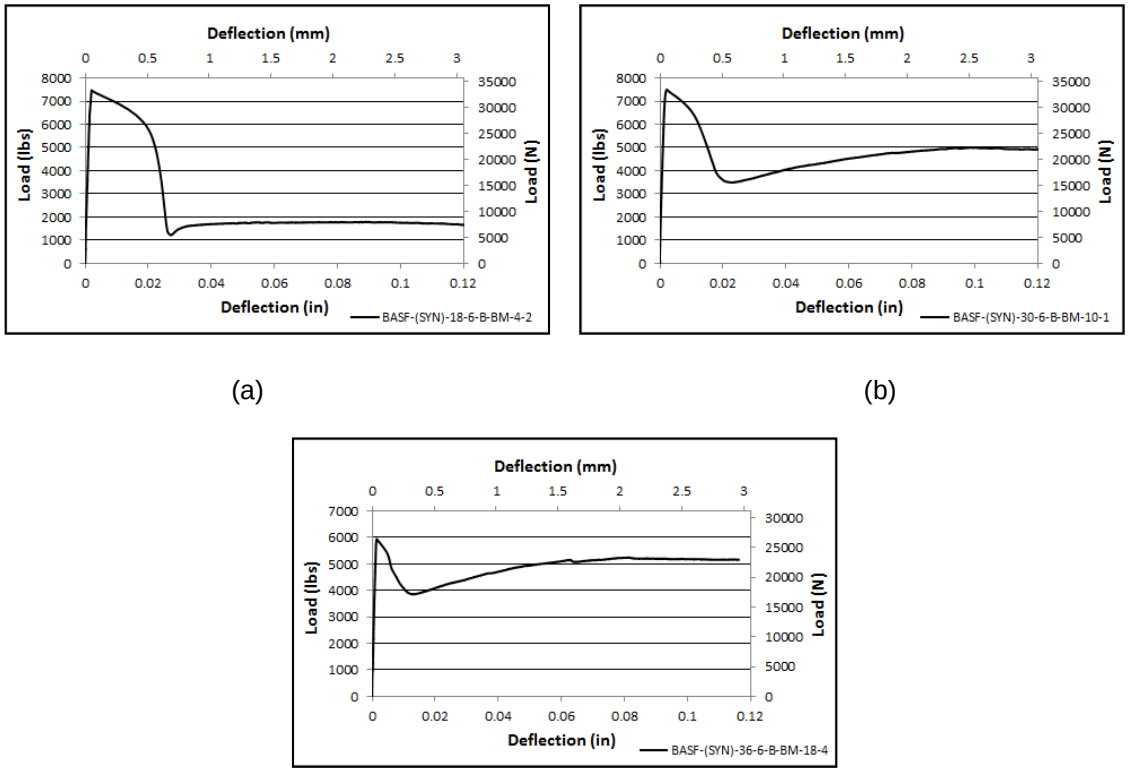

Figure 2.8 Load-Deformation Plots for Various Synthetic Fiber Dosages (a) 4 lbs/yd^3 (0.26% VF), (b) 10 lbs/yd^3 (0.65% VF), and (c) 18 lbs/yd^3 (1.17% VF).

Steel fibers also showed similar load-deflection plots for low-dosages of fiber with the exception of the hardening behavior. The initial drops in load at failure were not as significant as synthetic, but as more deflection in the specimen occurred low-dosage fibers continued to decrease in load capacity. As fiber dosages increased, the graphs showed smaller drops in load and began to regain some of the first-peak load. Medium fiber dosages, typically 44 lbs/yd^3 (0.33% VF), were observed to begin increasing in load then after about 0.03 to 0.05 in. (0.76 to 1.27 mm) deflection, load would begin to decrease again. As seen in Figure 2.9 (c) 66 lbs/yd^3

(0.5% VF) had a high enough fiber dosage that there is a difference in first-peak and peak load. In this case, the initial crack occurred and briefly affected the beam and then the fibers engaged and resumed increasing load capacity for roughly 0.04 in. (1.02 mm) of deflection before decreasing load (negative slope) occurs.

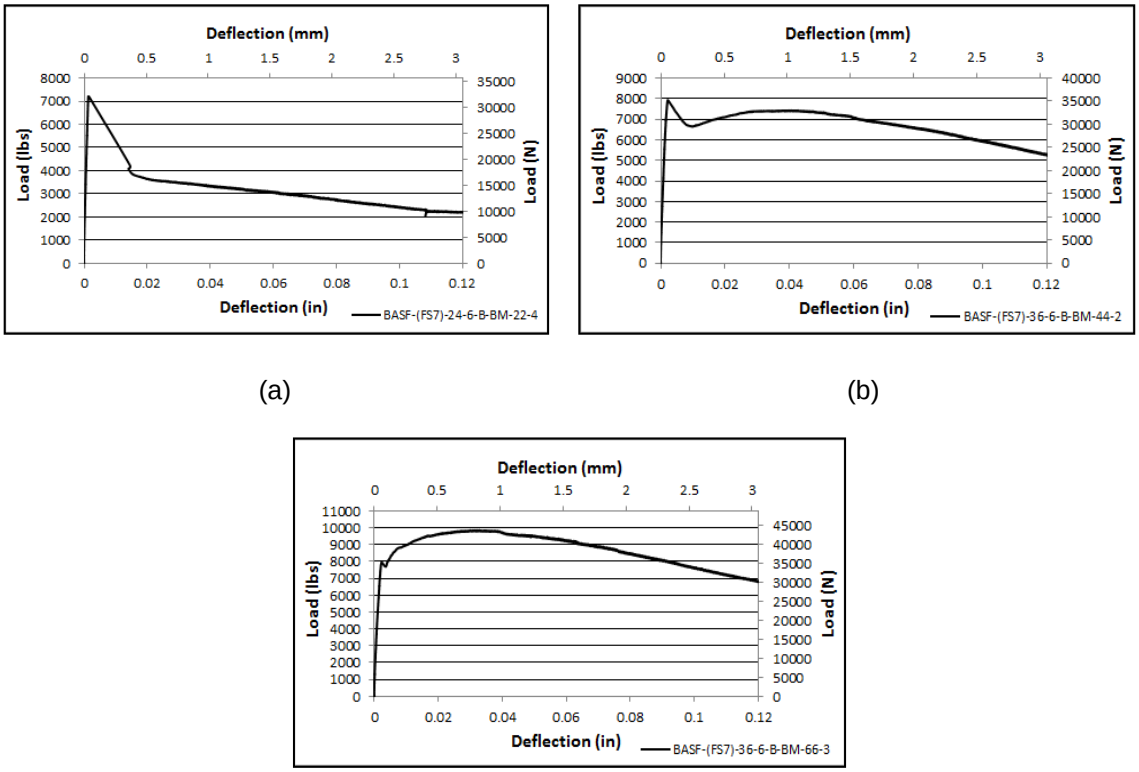

(a) (b)

(c)

Figure 2.9 Load-Deformation Plots for Various Steel Fiber Dosages (a) 22 lbs/yd^3 (0.17% VF), (b) 44 lbs/yd^3 (0.33% VF), and (c) 66 lbs/yd^3 (0.50% VF).

Modulus of rupture is the force needed to break a flexural beam per square inch of cross-sectional area. This factor can be determined from the following equation:

$$f_t = \frac{PL}{bd^2}$$

Where, P is the first-peak load, 'L' is the length, 'b' is the width, and 'd' is the depth of the specimen. The modulus of rupture in comparison with fiber dosage is shown in Figure 2.10 for both steel and synthetic fibers. On average the modulus of rupture for steel fibers was f_t = 999 psi (7 MPa) for the Northern Concrete Pipe plant, f_t = 650 psi (4 MPa) for the Hanson Longview plant

and f_t = 610 psi (4 MPa) for the Hanson Grand Prairie plant. Synthetic fiber modulus of rupture was on average f_t = 887 psi (6 MPa), f_t = 550 psi (4 MPa) and f_t = 559 psi (4 MPa) for the Northern Concrete, Hanson Longview and Hanson Grand Prairie plants, respectively. In all cases, the addition of fibers had very little effect on the rupture factor and values from each production plant were within a close range. These values also indicate that the strength required at failure was overall higher for beam specimens which used steel fibers as reinforcement.

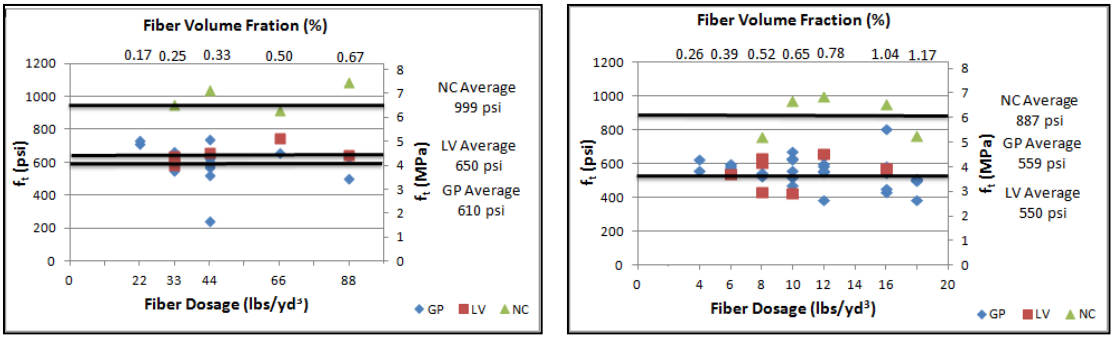

(a) (b)

Figure 2.10 Fiber Dosage vs. Modulus of Rupture (a) Steel Fibers and (b) Synthetic Fibers.

Material toughness is a description of the energy absorbed by the fibers. Toughness is calculated by finding the area under the load-deflection curve up to a deflection of L/150 (0.12 in. or 3 mm), according to ASTM C1609. Plots found in Figure 2.11 show the fiber dosage compared to material toughness for steel and synthetic fiber, respectively. From both plots it can be observed that the increase in fiber dosage, in general, increases the overall toughness of the specimen. The average toughness for steel fibers from Hanson Grand Prairie is 52 ft-lb (70 J), 56 ft-lb (76 J) from the Hanson Longview plant, and 80 ft-lb (108 J) from Northern Michigan. The average toughness for the synthetic fibers is 39 ft-lb (53 J) from Hanson Grand Prairie, 38 ft-lb (52 J) from Hanson Longview, and 75 ft-lb (102 J) from Northern Michigan.

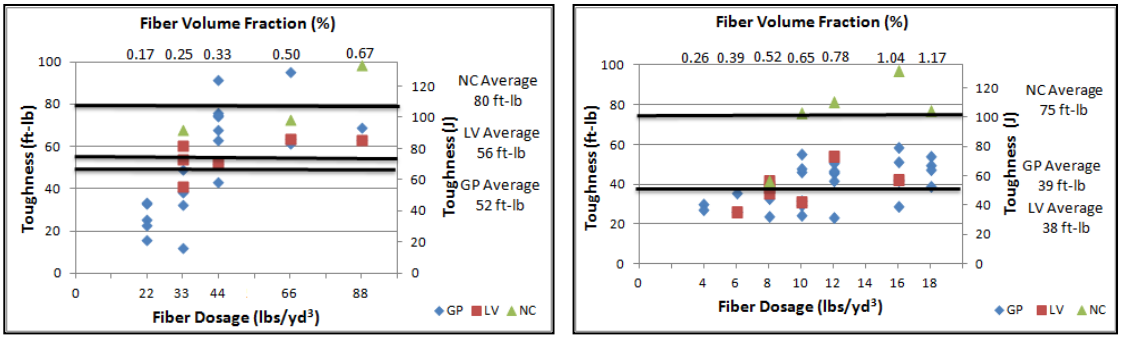

(a) (b)

Figure 2.11 Fiber Dosage vs. Toughness (a) Steel Fiber and (b) Synthetic Fiber.

Another common caparison of material properties is the strength ratio (η) for the matrix of fiber and concrete. This factor describes the relationship between the modulus of rupture (f_t) and average compressive strength (f_c) found in compressive cylinder testing. The equation is as follows:

$$\eta = \frac{f_t}{\sqrt{f_c}}$$

Figure 2.12 displays the comparison of f_t and η for both steel and synthetic fibers. From these graphs it can be observed that as the modulus of rupture increase so does the strength ratio. This comparison shows that even though the rupture strength is increasing the compressive strength of the concrete is decreasing. The average strength ratios for steel fibers were found to be η = 8.42 from Hanson Grand Prairie, η = 10.02 from Hanson Longview, and η = 12.01 from Northern Michigan. The strength ratio averages for synthetic fibers were η = 8.29 from Hanson Grand Prairie, η = 8.11 from Hanson Longview and η =12.61 from Northern Michigan. Compressive strength is discussed more in detail in the following section.

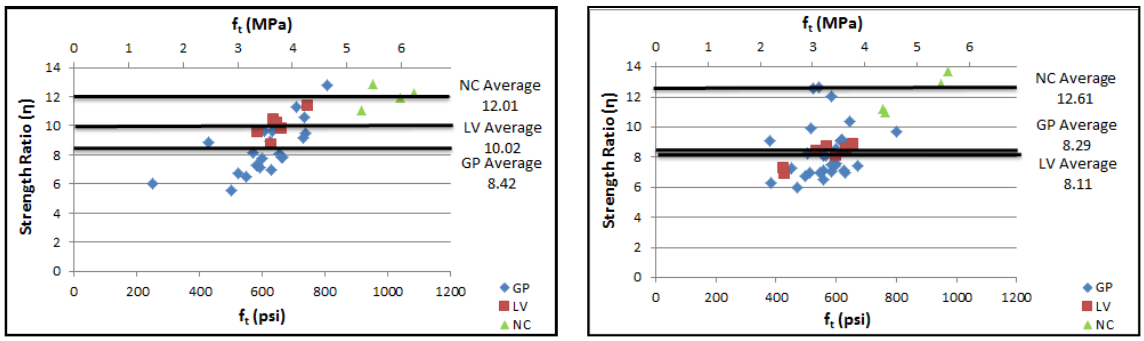

(a) (b)

Figure 2.12 Modulus of Rupture vs. Strength Ratio (a) Steel Fibers and (b) Synthetic Fibers.

2.4 Compressive Cylinder Tests

Cylinders were produced for each different batch and tested according to the ASTM C39 "Standard Test Method for Compressive Strength of Cylindrical Concrete Specimens." This method is the process of applying a compressive force onto the cylinder, through its axis in order to find the maximum load per square inch of surface concrete at failure. Cylinders were produced having a 4 in. (100 mm) diameters at Hanson Grand Prairie and Longview plants and 6 in. (150 mm) diameter specimens at the Northern Concrete Pipe plant. Cylinders were tested at 1, 3, 7, and in some cases, 28 days after production. From this test, the compressive strength and the failure methods can be determined. Values acquired from this test procedure are influenced by the batching procedures, moisture content of mixture, curing temperatures and methods, and age at testing.

All cylinder specimens were produced using plastic molds which ensure the correct size and diameter. Molds were placed and secured onto a vibrating table near the batching location. Concrete mixture was placed in multiple lifts, compacted and tamped while under vibration. After curing, the cylinders were stripped from their molds and capping was applied at each end. This procedure is accomplished by heating silica until it is in liquid form. The liquid silica is then poured into a mold and the cylinder is placed into the liquid while it begins to cool and harden forming the "cap". Capping was used to ensure that neither end displaced more than 0.5 degrees (0.009 rad.) from the perpendicular of the axis and to creating a smooth and level testing surface.

The most frequent failure type for cylinders in low dosages was a series or vertical cracks, which traveled directly up or down the length of the cylinder from the initial failed location. As fiber dosages begin to increase the failure modes have a tendency to crack in a 45-degree (0.78 rad.) angle spanning throughout the entire length of the cylinder acting as a ductile material. Intermediate stages can be observed in the middle fiber dosage range where the 45-degree (0.78 rad.) crack occur but do not extend the entire length of the cylinder forming a dome like crack at typically two-thirds the height of the cylinder. Figures 2.13 and 2.14 show the stages most frequently observed in the synthetic and steel fiber compression tests, respectively.

(a) (b) (c)

Figure 2.13 Synthetic Fiber Cylinder Failure Stages (a) 4 lb/yd^3 (0.26% VF), (b) 8 lbs/yd^3 (0.52% VF), and (c) 12 lbs/yd^3 (0.78% VF).

(a) (b) (c)

Figure 2.14 Steel Fiber Cylinder Failure Stages (a) 22 lb/yd^3 (0.17% VF), (b) 44 lbs/yd^3 (0.33 %VF), and (c) 88 lbs/yd^3 (0.67% VF).

Additional failure modes observed including crushing of the concrete cylinder where no single distinct failure cracks could be followed. Crushing resembled many small hairline cracks dispersed throughout the entire surface area of the specimen. Another failure mode which occurred included internal failures where the cylinder would no longer resist additional load but showed no visible cracking on the outside surface.

2.4.1 Test Set Up

The testing apparatus used had compressive capabilities up to 500 kips. The machine was power operated and had the ability to apply load continuously at the prescribed loading rate as described in the section below. Within the machine testing area there were two stationary steel bearing blocks which bear on the upper and lower surfaces of the cylinder while testing. Each of the bearing blocks were at least 3% greater in diameter than the testing specimen. Cylinders were placed in the machine and centered relative to the upper bearing block. Before the start of the test the machine was manually moved up until the cylinder and the upper block made contact. A typical test set up can be seen in Figure 2.15.

Figure 2.15 Compressive Cylinder Testing Machine.

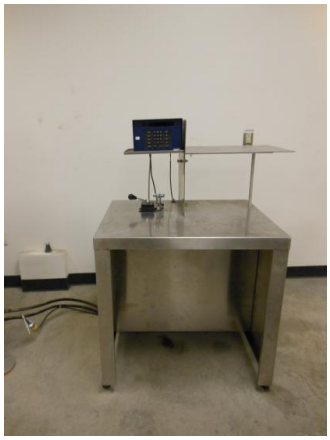

Figure 2.16 Loading Apparatus.

2.4.2 Loading History

The rate at which each cylinder was tested was 35 ± 7 psi/s (0.25 ± 0.05 MPa/s) and applied continuously, without shock, throughout the test. ASTM C39 states that this loading rate can be increased during the first half of the test but must be controlled so that the specimen is not shock loaded which can cause a premature failure. As the ultimate load is being reached no adjustments to the rate should be made for the remainder of the test. The completion of the test is when the cylinder has reached the maximum load, failed showing a defined fracture pattern, and the load has reduced to at least 95% of the peak load. Loading rate was applied manually and displayed visually by use of a digital reader. Figure 2.16 shows the part of the testing apparatus which controls the rate.

2.4.3 Test Cases

Throughout this study a total of 353 cylinders were tested, 191 synthetic fiber reinforced and 162 steel fiber reinforced. Multiple cases for each fiber dosage at each location were tested. The breakdown of this information can be seen below in Tables 2.4 and 2.5.

Table 2.4 Total Amount of Synthetic Cylinders Based on Fiber Dosage and Production Plant

Synthetic MAC Matrix	Fiber Dosage (lbs/yd^3)							
	4	**6**	**8**	**10**	**12**	**16**	**18**	**Total**
Hanson-Grand Prairie	6	10	18	25	36	18	12	125
Hanson-Longview	0	6	12	6	6	6	0	36
Northern Concrete	0	0	6	6	6	6	6	30
Total	6	16	36	37	48	30	18	**191**

Table 2.5 Total Amount of Steel Cylinders Based on Fiber Dosage and Production Plant

Steel FS7	Fiber Dosage (lbs/yd^3)					
	22	**33**	**44**	**66**	**88**	**Total**
Hanson-Grand Prairie	24	42	18	18	6	108
Hanson-Longview	0	12	6	6	6	30
Northern Concrete	0	6	6	6	6	24
Total	24	60	30	30	18	**162**

2.4.4 Test Results

After completion of all cylinder tests, data was accumulated and compared in order to determine the effect of both synthetic and steel fiber reinforced concrete. The water content in the original mix design can significantly influence the final compressive results and therefore must also be evaluated when analyzing this data. The average compressive strength for steel fibers is 5,411 psi (37 MPa) at the Hanson Grand Prairie plant, 4,671 psi (32 MPa) for the Hanson Longview plant and 6,923 psi (48 MPa) for the Northern Concrete Pipe plant. In both locations the results for steel fibers provided higher strengths on average. Figure 2.17 shows all the compressive cylinders separated by production plant for steel fibers.

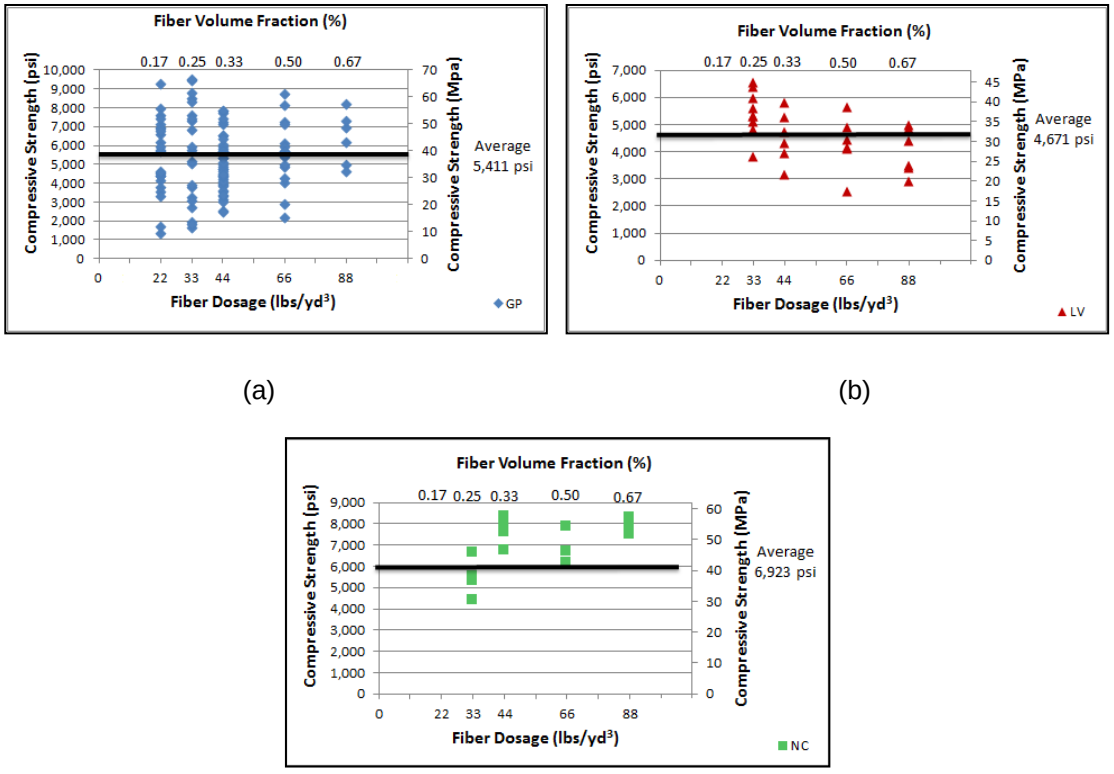

Figure 2.17 Steel Compression Cylinder Strength Test Results for (a) Hanson Grand Prairie Plant, (b) Hanson Longview Plant, and (c) Northern Concrete Plant.

Figure 2.18 compares the overall compressive average strengths based on production plant and steel fiber dosage. Based on observation of the average values, in general compressive strengths increased as the amount of steel fibers were increased in the mix.

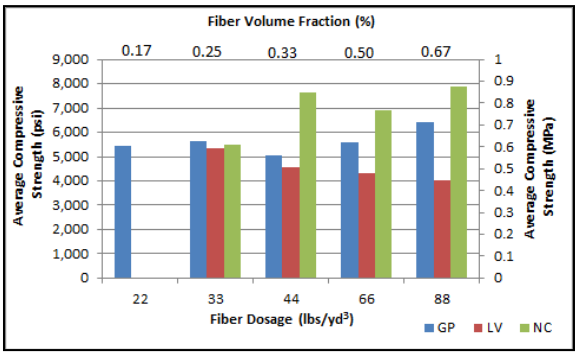

Figure 2.18 Steel Fiber Compressive Cylinder Average Strengths

The average 7-day compressive strengths for steel fiber in Hanson Grand Prairie and Hanson Longview were 5,876 psi (41 MPa) and 4,828 psi (33 MPa), respectively. Seven-day compressive strength data was plotted based on the fiber dosage, and compared between the two plants. This plot can be found in Figures 2.19 representing the steel fibers. As can be observed from Figure 2.19 below the Hanson Longview data has less of variation as compared to Hanson Grand Prairie plant. Although, Hanson Longview has significantly less test specimens, this could be a more accurate display of results because all the cylinders were produced during the same day, with the same concrete mixture, water content and curing environment. The only variable that changed was the fiber dosage.

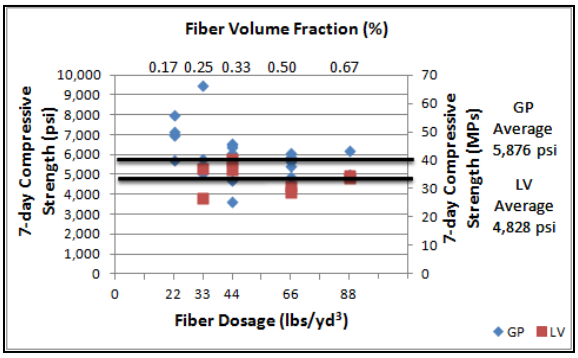

Figure 2.19 Steel Fiber 7-day Compressive Strengths vs. Fiber Dosage Comparison.

The average compressive strength for synthetic fibers is 4,958 psi (34 MPa) for the Hanson Grand Prairie plant and 4,433 psi (31 MPa) for the Longview plant, and 4,394 psi (30 MPa) for the Northern Concrete Pipe plant. All cylinder tests can be seen in Figure 2.20 for each of the production plants. As described above the Longview and Northern Concrete have less variation in the compressive strengths tested.

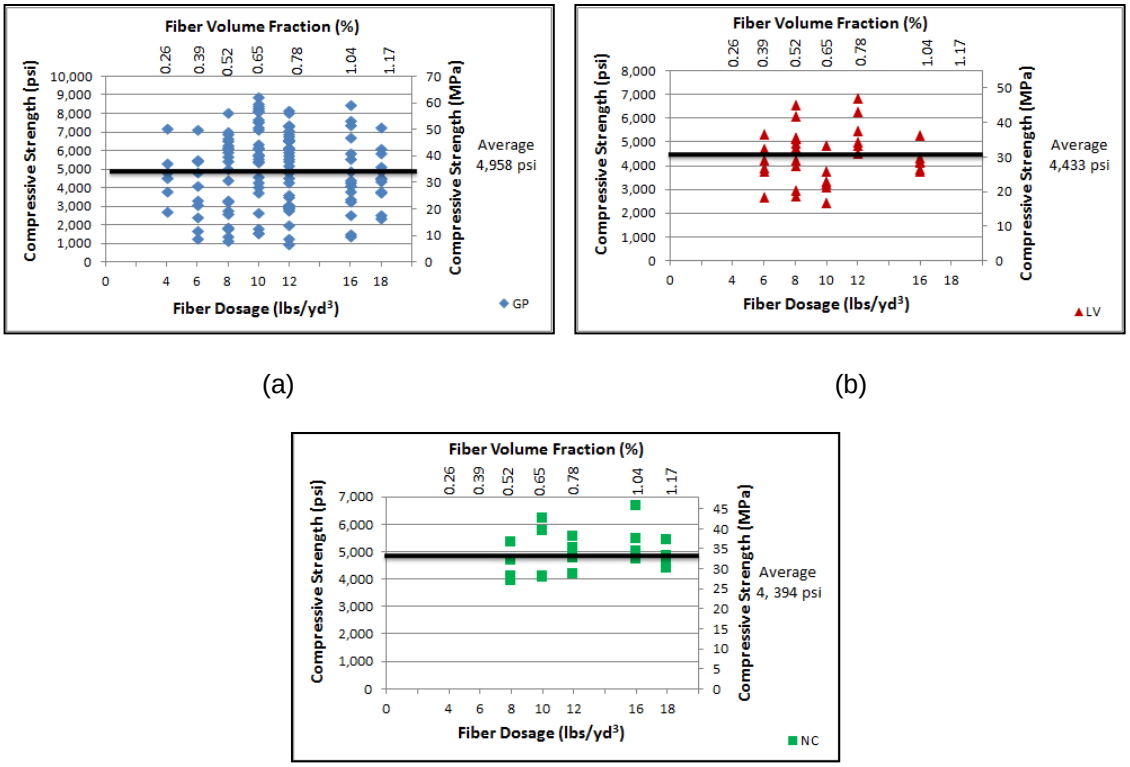

Figure 2.20 Synthetic Compression Cylinder Strength Test Results for (a) Hanson Grand Prairie Plant, (b) Hanson Longview Plant, and (c) Northern Concrete Plant.

Figure 2.21 compares the overall compressive average strengths based on production plant and steel fiber dosage. Based on the observation of the averages displayed in the figure below; the compressive strengths increase with the addition of synthetic fibers up to 10 lbs/yd^3 (0.65% VF), then the trend is that the strength is decreasing as more synthetic fiber is added.

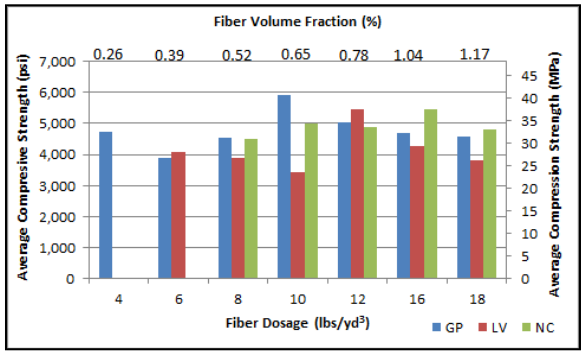

Figure 2.21 Synthetic Fiber Compressive Cylinder Average Strengths

Synthetic fiber 7-day strength is 5,325 psi (37 MPa) for the Grand Prairie plant and 3,811 psi (26 MPa) for the Longview plant. As can be observed from the Figure 2.22 below the addition of synthetic fiber has which vary and is believed to be primarily due to water hydration variations. During production it was observed that higher dosages of synthetic fibers required more water to be added into the concrete mixture in order to have sufficient finishes and concrete quality that was expected. Due to the Packerhead equipment it was difficult to obtain the required water for these fiber dosages and still produce a pipe that would stand up. Whereas, the Hawkeye equipment was able to add additional water to the mix and still produce a standing pipe. Additional research needs to be completed with a variety of equipment in order to confirm Longview's increase results.

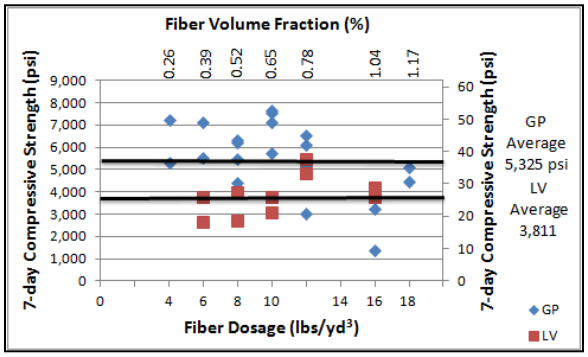

Figure 2.22 Synthetic Fiber 7-day Compressive Strengths vs. Fiber Dosage Comparison.

CHAPTER 3

EXPERIMENTAL PROGRAM (STRUCTURAL PIPE)

3.1 Introduction

This chapter presents the results of steel and synthetic fiber reinforced concrete pipes tested in accordance to ASTM C76 “Standard Specification for Reinforced Concrete Culvert, Storm Drain, and Sewer Pipe”. The metric version of the ASTM specification (ASTM C76M) is referenced for the metric conversions regarding this chapter. Fiber pipe D-Load characteristics were determined in accordance with ASTM C76 so that they could be compared to conventional reinforced concrete pipes. All concrete pipe manufacturers identify their pipes by one of five classes; Class 1, Class II, Class III, Class IV and Class V. All of which have corresponding prescribed strength requirements.

Typical acceptance of concrete pipe is based on a sample of pipes passing the D-Load 0.01 in. crack and D-ultimate strength load tests which is determined by a three-edge bearing test associated with each class of pipe. Acceptance can also be obtained by material tests or drilled core samples of the pipes. D-Load tests are described more in detail in the following section. Material tests include compressive strength testing cylinders prepared on the day of pipe production or by using drilled cores taken from the pipe wall. The average cylinder compressive strength must meet strength requirements with only 10% of the specimens tested being less than the required strength but greater than 80% of the required strength. Drilled core samples can be used as acceptance if the cores tested reach strengths equal to or greater than prescribed in ASTM C76.

All concrete pipes must be produced within a given range of the required physical characteristics. Internal diameter must remain within 2% and 1.5% of design diameter for pipe diameter of 12 in. and 24 in. (300 mm and 600 mm), respectively. Interpolation can be competed for pipe diameters in between those sizes. For diameters greater than 27 in. (675 mm) the

internal diameter must not vary more than the greater of 1% or $^3/_8$ in. (10 mm). Wall thickness must not vary more than the greatest of 5% or $^3/_{16}$ in. (5 mm). All circumferential reinforcement must have 1 in. (19 mm) of cover to either edge of pipe.

During this investigation the goal was to achieve an optimized design for synthetic fiber and steel fiber reinforcement that reached or exceeded Class 3 ultimate loading for each of the pipe diameters being tested. Ultimate load was focused on due to fiber characteristics. Through previous research, it was observed that when fiber reinforced pipe reach 0.01 in. crack no additional load was seen. Therefore, D-load and D-ultimate load essentially become the same and the higher required value is used as a reference. Fiber reinforced concrete pipes also do not have the 1 in. (25 mm) of concrete cover described above because there is no way to enforce this when fiber are added directly into the concrete mixture. Where there is optimized water-to-cement ratio and smooth finishing surfaces the fibers rarely show excessively on the outer edge of the pipe.

3.2 D-Load Test

The D-Load test can be described by the three-edge bearing method in ASTM C497 “Standard Test Methods for Concrete Pipe, Manhole Sections, or Tile”. The procedure describes a test which requires a machine capable of applying a force along the length of the specimen in order to establish either a 0.01 in. crack or an ultimate load. The machine must be rigid, able to distribute the load evenly, and not deform or yield to any part while testing. The D-Load test can be used for either quality control or proof of design purposes.

The test specimen must be supported by two parallel lower bearing strips and one upper bearing strip. The upper bearing strip is to be made of a single wood beam attached to a rigid steel beam that will not deflect under pressure. The upper bearing strip can be used with or without a hard rubber strip attached to the face which comes in contact with the concrete pipe. The lower bearing strips are to be made of wood beams or rubber strips which have a cross-section of 2 in. (50 mm) in width and 1 to 1 ½ in. (25 to 38 mm) in height. The lower bearing strips

must then be fastened to a rigid beam of either wood or steel which is then connected directly to a concrete base. A testing schematic can be seen in Figure 3.1.

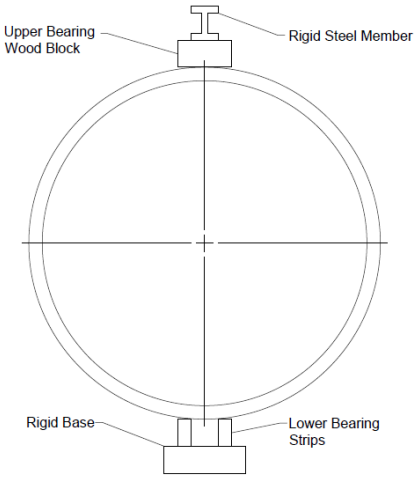

Figure 3.1 Schematic of Three-Edge Bearing Test

The D-Load is defined as the load per foot of pipe length and per foot of pipe diameter. This loading can be determined based on a three edge bearing test which loads the pipe along its length until a crack width of 0.01 in. is observed. A crack width of 0.01 in. is determined when a 0.01 in. gage can fit between the crack to a depth of at least $^{1}/_{16}$ in. (1.6 mm) without being forced and the crack is a minimum of 1 ft. (3005 mm) of continuous length. The ultimate load is also tested by the same apparatus and is the load at which the pipe can no longer resist additional load. Ultimate load should be calculated by taking the max load divided by the pipe diameter in feet multiplied by the length of the pipe in feet as shown in the Equation below.

$$D_{ULT} = \frac{Maximum\ Load}{Diameter\ X\ Length}$$

3.2.1 *Test Set Up*

The D-Load testing rack is capable of applying a constant loading rate desired for each pipe diameter and class. The two supports at the bottom of the machine are adjusted for the specific pipe diameter being tested. The pipe is then aligned to the machine and rolled into place, resting level on the two bottom supports. Each pipe is marked in preparation of placing the equipment by measurement and leveling devices. Measurements were taken from 6 in. (150

mm) from the edge of pipe both vertically and horizontally. The marked locations were then drilled so the instrumentation could be securely attached.

A typical test set up can be seen in Figure 3.2, showing how the pipe is placed into the testing rack, the pipe in final position, and leveled for instrumentation.

(a)

(b)

(c)

Figure 3.2 Typical Test Set Up (a) Placing Pipe, (b) Final Position of Pipe, (c) Leveling for Instrumentation.

3.2.2 *Instrumentation*

Each pipe had two Linear Variable Displacement Transducers (LVDT's) secured within the interior of the pipe in order to read the displacement in both the vertical and horizontal directions. Deflection of each pipe was recorded up to 5% of the pipe diameter in both horizontal and vertical directions. This information was again recorded using a StrainSmart software and

Vishay scanner, which could then be plotted into load-deformation plots. This set up can be seen in Figure 3.3 (a). Typical computer outputs during testing can be seen in Figure 3.3 (c).

Load-deflection equipment is not typically used in traditional concrete pipe testing, therefore modifications to the Hanson Grand Prairie test equipment had to be made in order to retrieve the necessary data. In order to accomplish this, the machines load reading connection was unplugged and replaced with a connection capable from the testing computer. This connection was calibrated to the Hanson Grand Prairie machine to ensure accurate readings while testing and can be seen in Figure 3.3 (d). All pipes from the Hanson Longview and Northern Concrete Pipe plants were shipped to Grand Prairie in order to be tested using consistent test methods.

3.2.3 *Loading History*

As specified in ASTM C497 the loading rate for reinforced concrete pipes is to be any rate up to 7500 lbf/foot (10.2 kNm/m) of length of pipe. This rate should be applied up to 75% of the design strength followed by a continuous, uniform loading of $^1/_3$ of the design strength per min. After reaching the design strength, no loading rate must be continued.

3.2.4 *Test Cases*

Throughout this study a total of 153 fiber reinforced concrete pipes were tested, 93 synthetic fiber and 60 steel fiber pipes. Multiple cases for each fiber dosage at each location were tested. The breakdown of this information can be seen below in Tables 3.1 and 3.2.

(a)

(b)

(c)

(d)

(e)

Figure 3.3 Pipe Testing Instrumentation: (a) LVDT Placement, (b) Vishay Connections, (c) Typical Display while Testing, (d) Load Connection Cord, (d) Main Power Supply for Applying Load.

Table 3.1 Total Amount of Synthetic Pipes Based on Fiber Dosage and Production Plant

Synthetic Plant	Pipe Diameter	Fiber Dosage (lbs/yd^3)							Total
		4	6	8	10	12	16	18	
Hanson Grand Prairie	18	3	3	3	2	-	-	-	11
	21	-	2	3	3	2	-	-	10
	24	-	-	4	2	8	-	-	14
	30	-	-	2	4	2	2	-	10
	36	-	-	-	-	2	4	4	10
Hanson Longview	15	-	4	2	-	-	-	-	6
	24	-	-	5	2	2	-	-	9
	36	-	-	1	-	2	2	-	5
Northern Concrete	24	-	-	2	2	2	-	-	6
	30	-	-	-	2	2	2	-	6
	36	-	-	-	-	2	2	2	6
Total									93

Table 3.2 Total Amount of Steel Pipes Based on Fiber Dosage and Production Plant

Steel Plant	Pipe Diameter	Fiber Dosage (lbs/yd^3)					Total
		22	33	44	66	88	
Hanson Grand Prairie	18	2	2	2	-	-	6
	21	2	2	1	-	-	5
	24	5	2	5	-	-	12
	30	-	2	2	2	-	6
	36	-	-	4	4	2	10
Hanson Longview	15	-	3	-	-	-	3
	24	-	4	2	-	-	6
	36	-	-	-	1	1	2
Northern Concrete	24	-	2	2	-	-	4
	36	-	-	2	2	2	6
Total							60

3.2.5 *Test Results*

D-Load pipe tests produced load-deformation plots for each specimen tested with instrumentation. The load-deformation plots describe the deflection in the horizontal and vertical directions of the pipe due to the load being applied along its length. The plots also show the maximum load obtained per foot of diameter per foot of length of the pipe as described above. In addition to the data received from instrumentation, crack propagation along the length of pipe and crack width was able to be observed.

During the initial stages of this investigation a sample of pipes were tested to a deflection much greater than 10%. This was done to observe if the fiber pipes would collapse under extreme deflection. For both steel and synthetic fiber test pipes it was determined that the fiber allowed for excessive deflection and none of the pipes collapsed while on the testing apparatus. The synthetic pipe test had to be stopped due to the testing machine maximum deflection allowance. Figure 3.4 shows an end view of the deflected pipe and a close up of the crack opening showing the fibers holding the pipe together. Figure 3.5 shows the steel fiber reinforced pipe that was taken to extreme deflection and also a close up of the crack opening with fibers holding the pipe together.

(a) (b)

Figure 3.4 Synthetic Pipe at Extreme Deflection (a) Cross-Section View and (b) Crack Opening

(a) (b)

Figure 3.5 Steel Pipe at Extreme Deflection (a) Length of Pipe View and (b) Crack Opening

From the load-deformation plots it can be observed that at the time of failure (initial crack) all pipes have a decrease (negative slope) in load at the time of initial crack. For steel fiber pipes this load, generally, stayed constant or slightly had an increase in slope until a 5% deflection was reached in both directions and the test was stopped. Examples of load-deformation plots for steel fiber reinforced pipes with varying dosage amounts can be found in Figure 3.6. From these figures it should be noted that for low dosages the load significantly decreases, compared to higher dosages, due to failure and also has the most visible change of slope once the fibers become engaged within the pipe.

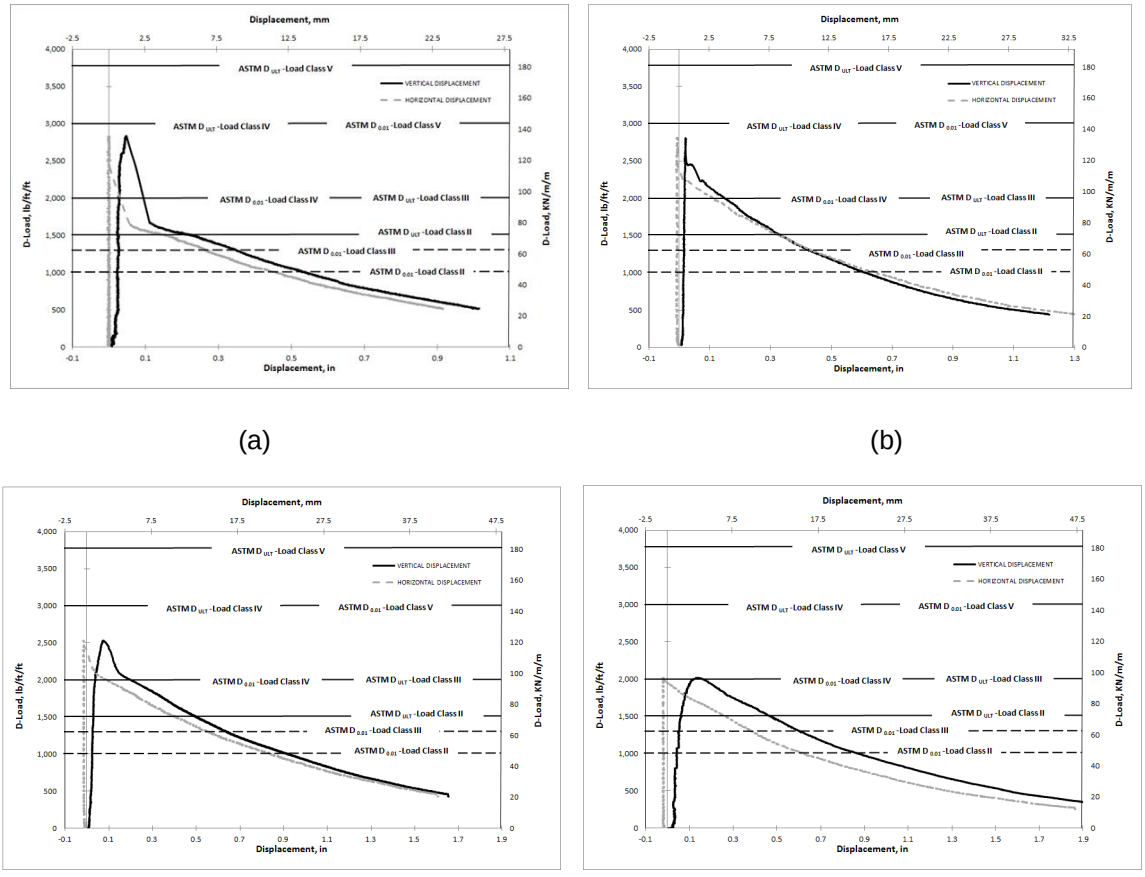

(a) (b)

(c) (d)

Figure 3.6 Steel Fiber Reinforced Concrete Pipes Load-Deformation Plots for Dosages of (a) 33 lbs/yd^3 (0.25% VF), (b) 44 lbs/yd^3 (0.33% VF), (c) 66 lbs/yd^3 (0.50% VF), and (d) 88 lbs/yd^3 (0.67% VF).

As mentioned above, all pipes tested had a decrease in load at the time of failure. However, with synthetic fiber reinforcement the load did not behave in the same fashion as steel

fiber. As can be seen from Figure 3.7, synthetic fibers began to increase load (positive slope). The smaller the initial drop and higher the increase in load was typically associated with increasing the fiber dosage. In no instance, did a pipe gain an ultimate load in which was greater than the initial crack (failure) load.

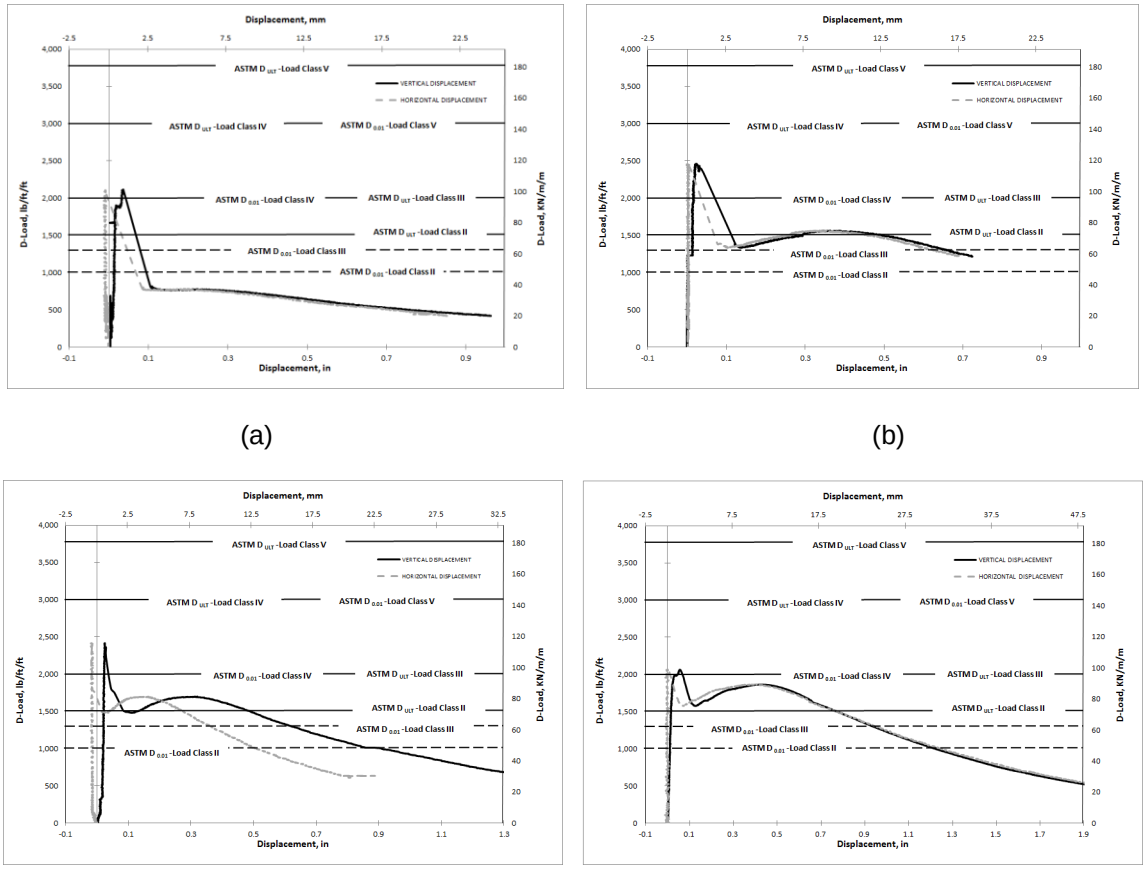

Figure 3.7 Synthetic Fiber Reinforced Concrete Pipes Load-Deformation Plots for Dosages of (a) 4 lbs/yd^3 (0.26% VF), (b) 8 lbs/yd^3 (0.52%VF), (c) 10 lbs/yd^3 (0.65% VF), and (d) 16 lbs/yd^3 (1.04% VF).

The maximum load was plotted based on fiber type and diameter size for each of the tested pipes. These comparisons can be seen in Figure 3.8 showing D_{ult} comparisons. From these graphs it can be observed that when steel fibers are used the increase of fiber dosage will generally increase the pipe strength within the same diameter of pipes. This can be seen for Hanson Grand Prairie, Hanson Longview, and Northern Concrete plants.

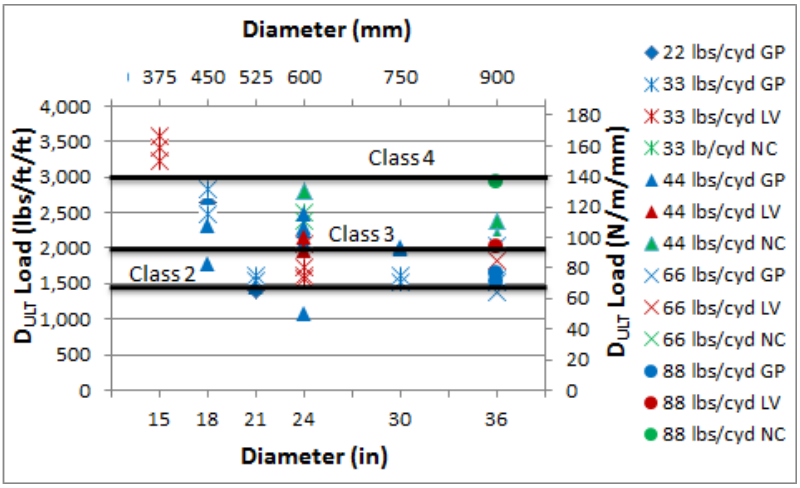

Figure 3.8 D_{ult} Load vs. Diameter and Steel Fiber Dosage for all Production Plants.

When ultimate load requirements were compared, the steel fibers were about 50% above the Class 3 ultimate strength requirements. This passing rate is higher for pipe diameter sizes of 24 in. (600 mm) and smaller. The use of Hawkeye equipment and larger wall sizes increased the ability for large diameter pipes pass. In general, pipe sizes of 24 in. (600 mm) and smaller have the capability of meeting the requirement of Class 3 ultimate design when fiber dosages were above 44 lbs/yd^3 for 24 in. (600 mm) diameter and above 22 lbs/yd^3 for 15 and 18 in. (375 mm and 450 mm) diameter pipes. Figure 3.9 displays test results for steel fibers based on each productions site.

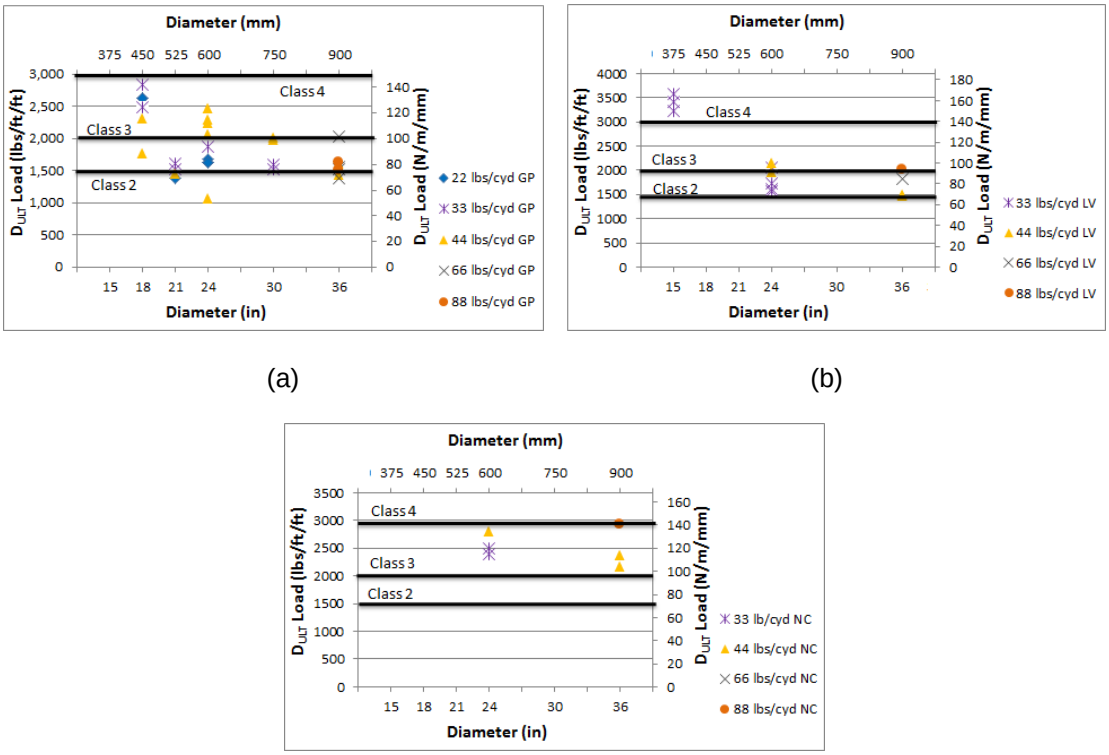

Figure 3.9 D_{ult} Load vs. Fiber Dosage for each Pipe Diameter for (a) Hanson Grand Prairie Plant, (b) Hanson Longview Plant, and (c) Northern Michigan Plant.

It was also observed that the water content of the mix is sensitive to weather conditions and must be adjusted due to extreme heat. The higher dosages of synthetic fiber required more water to be added to the mix in order to have sufficient finish and strength. Also, due to the Packerhead equipment restrictions, there were difficulties in moving the high dosages of synthetic fibers through the machine without stopping production. Figure 3.10 shows D_{ult} comparisons for synthetic fibers compared to each plant

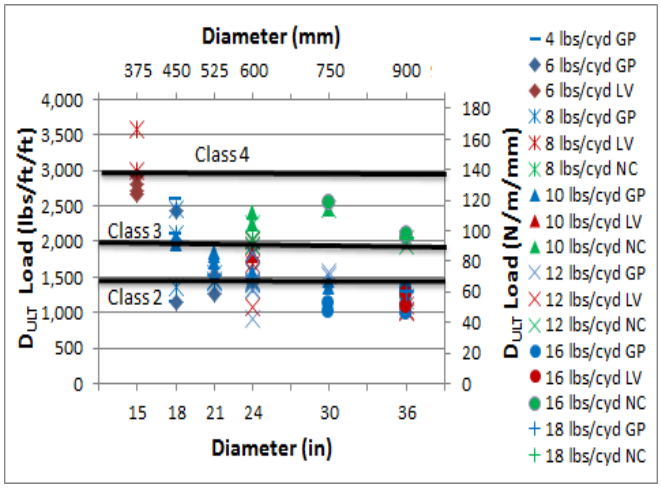

Figure 3.10 Dult Load vs. Diameter and Synthetic Fiber Dosage for all Production Plants.

Synthetic fibers, overall, had a much less percentage for passing Class 3 ultimate. Although, pipe sizes of 15, 18, and 21 in. (375, 450, and 525 mm) diameter passed the majority of the time. Synthetic fibers in 24 in. (600 mm) pipes were very close to Class 3 ultimate, typically closer when produced at the Hanson Longview plant and passing when produced at the Northern Concrete plant. Figure 3.11 displays test results for steel fibers based on each productions site.

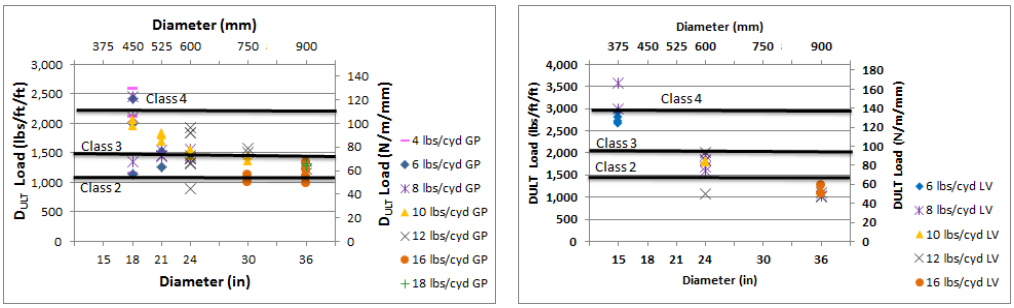

(a) (b)

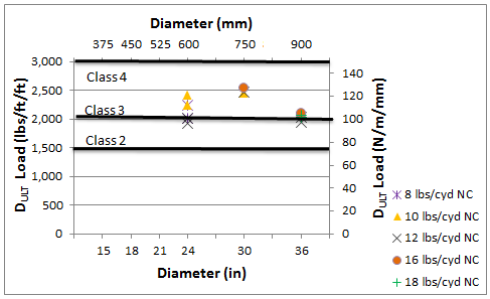

(c)

Figure 3.11 D_{ult} Load vs. Fiber Dosage for each Pipe Diameter for (a) Hanson Grand Prairie Plant, (b) Hanson Longview Plant, and (c) Northern Michigan Plant.

CHAPTER 4

THREE DIMENSIONAL FINITE ELEMENT ANALYSIS

4.1 Finite Element Model

A three dimensional linear-elastic finite element model (FEM) was developed to investigate the effect of tooling and production equipment on the material properties of fiber concrete that pipes actually experience. Throughout this research it was noticed that production of ASTM material test specimens such as beams and compressive cylinders experience different compaction processes that the pipe experiences. Since the load deformation plots for pipe test specimens were obtained during structural pipe testing, the FEM analysis was calibrated to obtain the same load deformation up to ultimate load which is approximately the load of first crack as shown in Figure 4.1. Thus, only the linear elastic region of the load-deformation plot is required to be calibrated for this purpose. Upon calibrating material properties to mimic experimental load-deformation plots, the normal stresses at the crown and springlines can easily be obtained from FEM analyses results. These correspond to cracking stresses or modulus of rupture that pipes actually experience, which are compared with the modulus of rupture observed from ASTM beam tests. In addition, pipes modulus of elasticity can similarly be compared to the beam test. These are important information that has challenged researchers while modeling fiber reinforced concrete pipes with different material properties that structure experiences compared with those obtained from ASTM material tests.

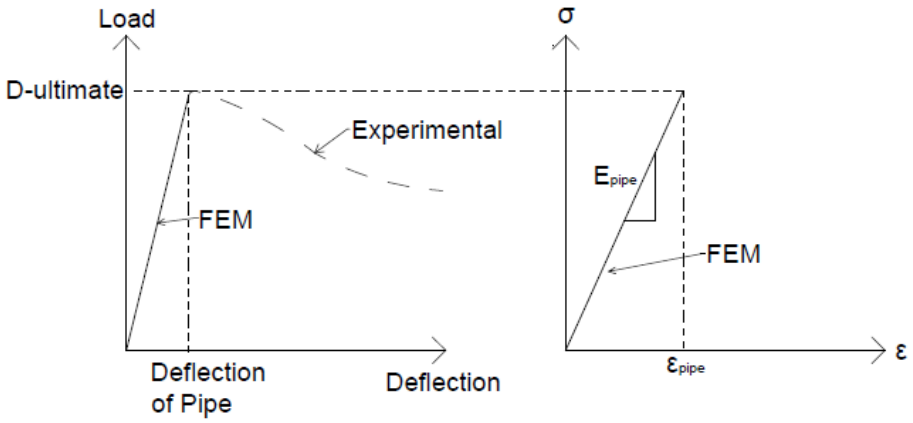

Figure 4.1 Determination of FEM Based Material Properties that Pipe Experience (a) Load Deformation from Pipe Test, and (b) Material Properties that Pipe Experience.

The FEM for this project was developed to simulate the three edge bearing test set up and loading. The model consisted of the three dimensional models of the pipe and load strip with supports being modeled identical to those provided during testing (Figure 4.2). Due to linear elastic nature of the model, the computational time was insignificant, and thus the entire pipe and test set up were modeled without taking advantage of the plane of symmetry. This is due to the fact that material, geometric, and contact nonlinearities were not incorporated into the analysis algorithm. In almost all finite element analyses the geometric nonlinearity formulation, the large displacement using Almansi (Eulerian) strain complemented by Cauchy stress tensor during the total Lagrangian analysis consumes significant amount of computation time which was not the case in here. Thus, modeling the entire structure was justifiable.

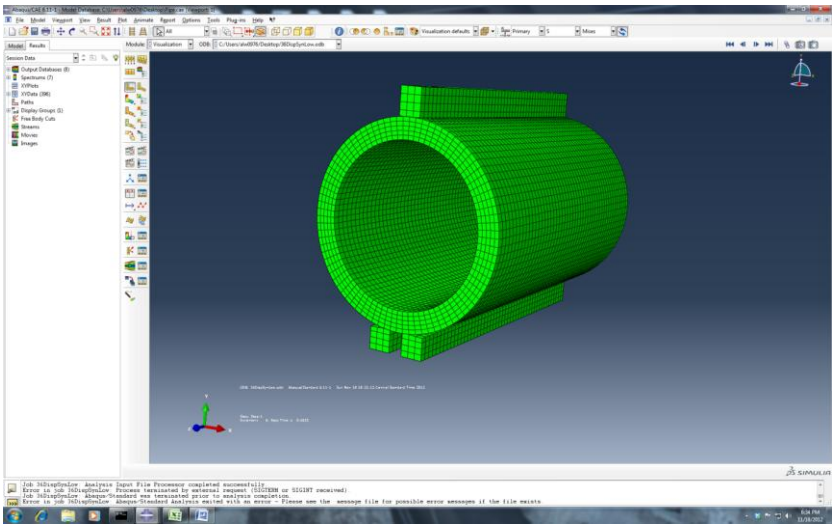

Figure 4.2 Finite Element Model of Three Edge Bearing Test for Fiber Concrete Pipe

Both three-dimensional shell and solid elements was used to optimize the mesh. All the classical convergence criteria were employed to check for the converged solution, which includes P-, H-, P-H, and the energy based convergences. The H-convergence is tested by increasing the number of degrees-of-freedom (DOF) of the model as a result of decreasing the element sizes. In the P-convergence, higher order polynomials are used in defining the assumed displacement function, which is equivalent to use higher order elements. The P-H convergence employed both P- and H- methods. Since convergence of the linear elastic problems is monotonic given proper displacement-based finite element is employed, the energy-based convergence was not adopted. Also, the H-convergence for each model was tested by using Hilbert L-2 norm, coupled with equating the external and the virtual work done to the internal strain energy at each load increment. Different element types were examined for optimized and efficient solution of the fiber concrete pipe test set up.

The model used three dimensional isoparametric continuum elements. These elements are capable of predicting the complete three dimensional stresses and deformations throughout model. Both linear and quadratic thick shell and brick elements were used in order to obtain the optimized 3-D mesh model. This FEM analysis particularly focused on not using thin shell element theory due to their potential well-known shortcomings with regard to membrane and

shear locking behavior. Also, in using linear or quadratic brick or shell continuum elements, both the Kirchhoff theory, in which the shear deformation is neglected and plane sections remain plane, and the Reissner/Mindlin theory, in which shear deformations are included, was considered. The typical isoparametric continuum elements proposed as alternative to thick shell elements for the modeling of the entire pole, mast arm, and end plate system is shown in Figure 4.3.

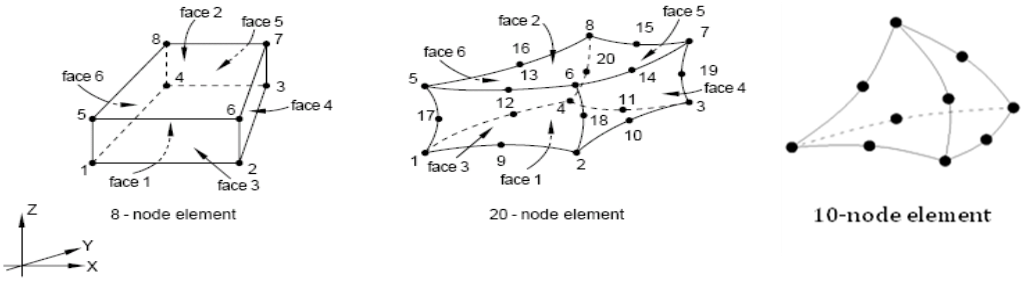

Figure 4.3 Linear and Quadratic Brick and Tetrahedral Elements

4.2 Finite Element Results

Figure 4.4 shows typical normal stress contour lines obtained from FEM at crown and springlines. The color red indicates the tensile stresses while compressive stresses are shown in blue color.

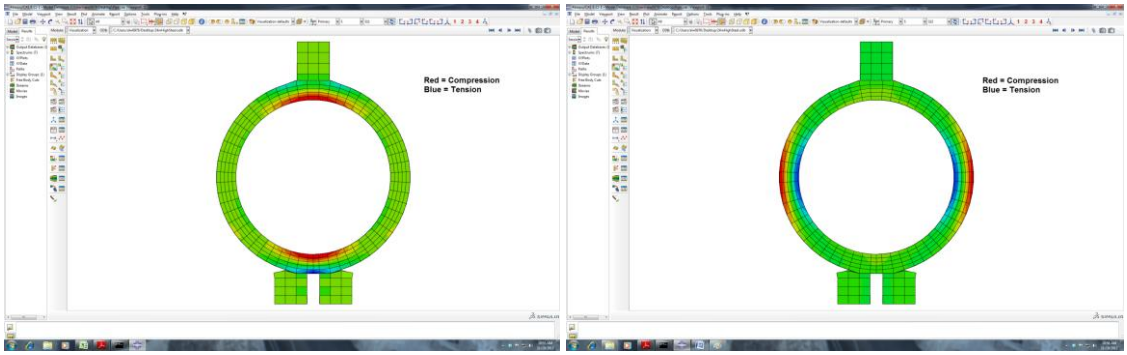

(a) (b)

Figure 4.4 Normal Stress Contour at (a) Crown and (b) Springlines

This figure shows that the FEM concisely predicts anticipated stresses at both locations which are tensile stresses at inside face at the crown and outside face at the springlines. Figure

4.5 compares the FEM load deformation results compared with the experimental tests for low and high dosage steel and synthetic fiber concrete pipes, which shows FEM is predicting the test tests accurately.

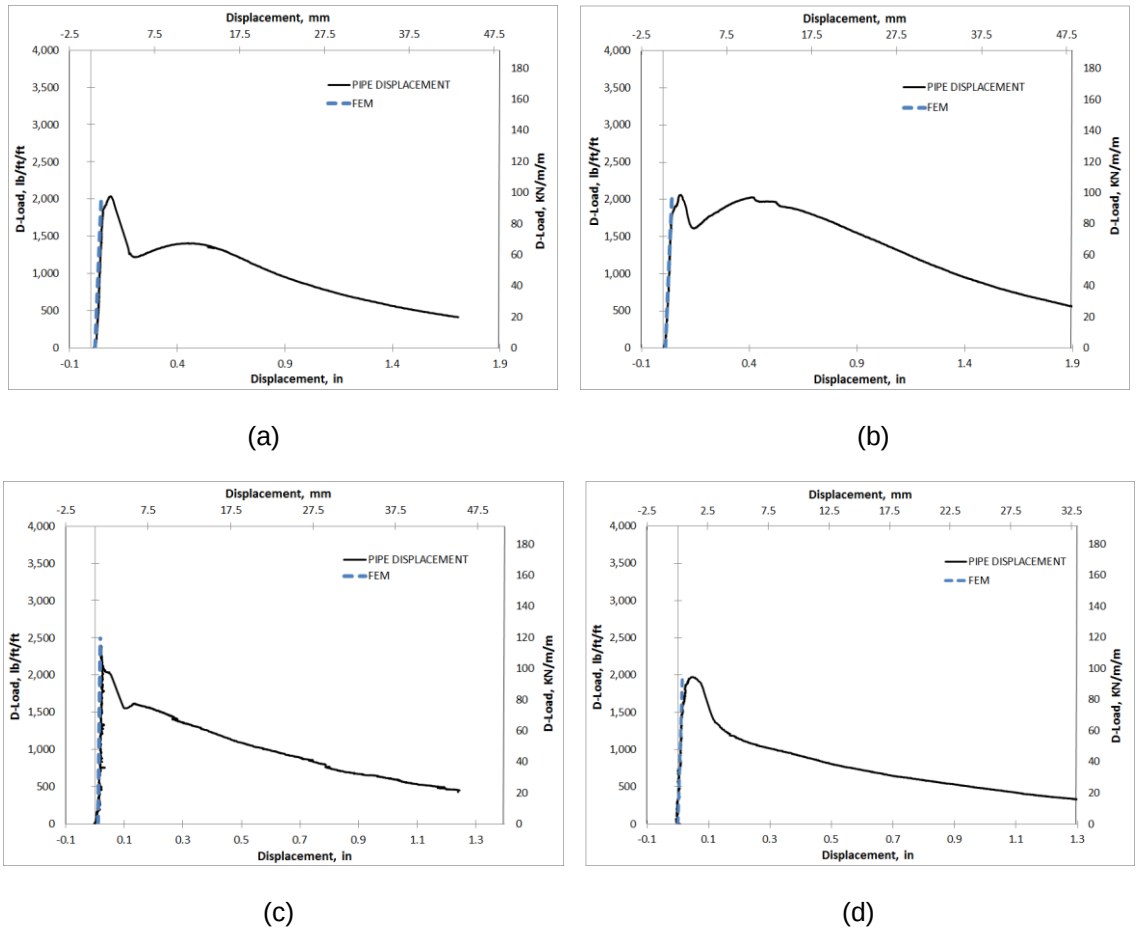

Figure 4.5: Experimental Pipe vs. FEM results for (a) 36in. Synthetic Low Dosage, (b) 36in. Synthetic High Dosage, (c) 24in. Steel Low Dosage, (d) 24in. Steel High Dosage.

The FEM was used to identify the actual material properties that the manufactured pipes would experience compared with the ASTM material testing. Figure 4.6 (a) shows the comparison between pipe material modulus of elasticity and those obtained from the ASTM beam tests. A line with the slope of 1:1 is also drawn for qualitative comparison purposes. As shown in this figure, better correlations are observed between the moduli of elasticity of the pipe and ASTM beams for the 24 in. pipe diameter as compared to the 36 in. diameter pipe. Same comparisons are also presented in Figure 4.6 (b) for the modulus of rupture of the pipe versus the ASTM beam. It is

evident that in most cases a 1:1 relationship between the material properties of the pipe and ASTM is not observed. Even though in some cases close relationships exist, in most cases significant differences are depicted.

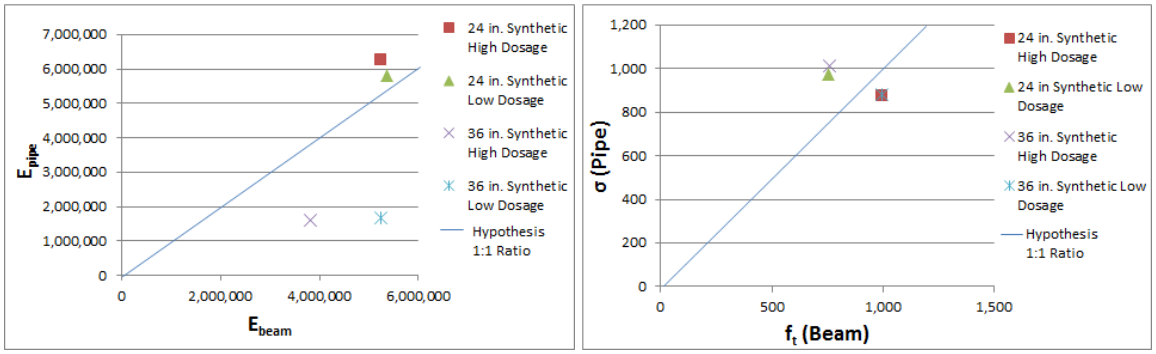

(a) (b)

Figure 4.6 Comparison of Elastic Modulus Experienced by Pipe vs. ASTM Beam Test for Synthetic Fiber Concrete (a) Comparison of Modulus of Elasticity, (b) Comparison of Normal. Stresses.

Similarly, Figures 4.7 (a) and (b) show the comparison of moduli of elasticity and rupture of the pipe material versus the ASTM beam materials for steel fiber concrete, respectively. Once again the majority of the data indicates differences in material properties of pipe after manufacturing process versus ASTM beams. The discussion presented here is based on limited data, therefore, to reach to a more informative conclusion, a more comprehensive study in future is recommended.

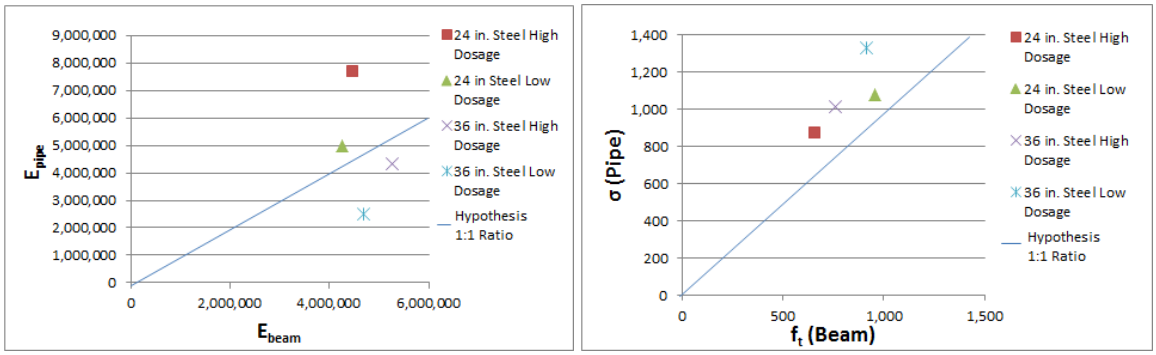

(a) (b)

Figure 4.7 Comparison of Elastic Modulus Experienced by Pipe vs. ASTM Beam Test for Steel Fiber Concrete (a) Comparison of Modulus of Elasticity, (b) Comparison of Normal Stresses.

CHAPTER 5

SUMMARY, CONCLUSIONS, AND RECOMMENDATIONS

5.1 Summary

This study is aimed at investigating the performance of BASF synthetic and steel fibers in concrete pipes without the conventional steel cage in three different manufacturing plants. A total of 93 Synthetic and 60 steel pipes were tested based on ASTM C497 in order to have a benchmark for comparison with conventional reinforced concrete pipes. The majority of the pipes were tested with linear variable displacement transducer (LVDT) equipment in order to obtain the load-deflection plots in both the horizontal and vertical directions of the pipe. The load-deflection plots were recorded for up to 5% deflection of the pipe diameter. During production, compressive cylinder and beam specimens from the same mix designs were produced and cured for ASTM C39 and ASTM C1609 tests, respectively. A total of 353 cylinders and 77 beams were produced and tested.

5.2 Conclusions

Throughout this investigation, a total of 43 synthetic fiber reinforced ASTM 1609 beams were tested with fiber dosages ranging from 4 lbs/yd^3 to 18 lbs/yd^3 (0.26% VF to 1.17% VF) and 34 steel fiber reinforced beams ranging from 22 lbs/yd^3 to 88 lbs/yd^3 (0.17% VF to 0.67% VF). The load deformation plots for the beams were obtained for all the test specimens and their behavior for low and high fiber dosages were documented. For low fiber dosage beams, the peak (ultimate) load was observed before or at the same time as the first-peak load. Please note that the first-peak load and ultimate load definitions are adopted from the ASTM 1609 designations which were introduced in Chapter 2. For convenience, the figures corresponding to the above definitions are repeated and presented in this chapter as Figures 5.1 and 5.2.

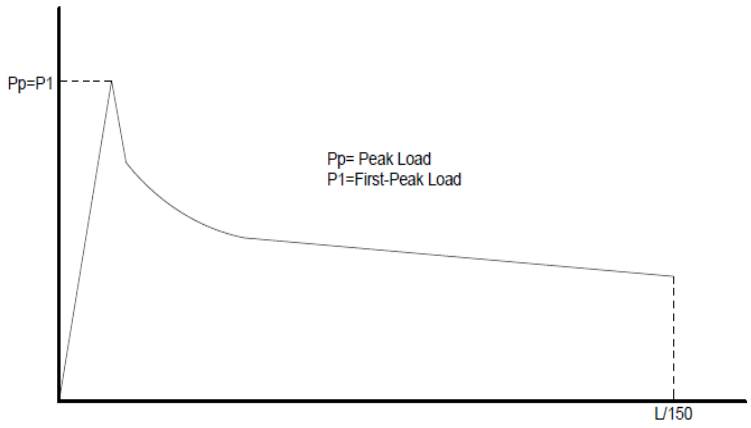

Figure 5.1 Typical Schematic Showing First-Peak Equal to Peak Load.

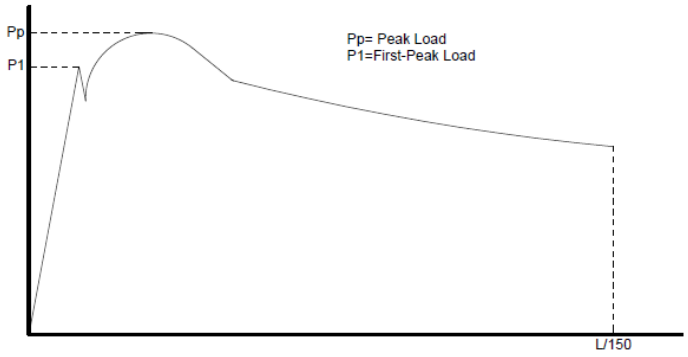

Figure 5.2 Typical Schematic Showing Peak Load Greater than First-Peak Load.

For the low dosage steel fiber beams, after the ultimate load is reached the load drops with a steep negative slope, and as the deflection continues beyond the first crack, the unengaged fibers would begin to be engage causing the rate of negative slope to decrease (refer to Figure 5.3). A similar phenomenon was observed in low dosage synthetic beam test specimens with the exception that after first crack hardening phenomenon was detected, which was more pronounced for higher fiber dosages.

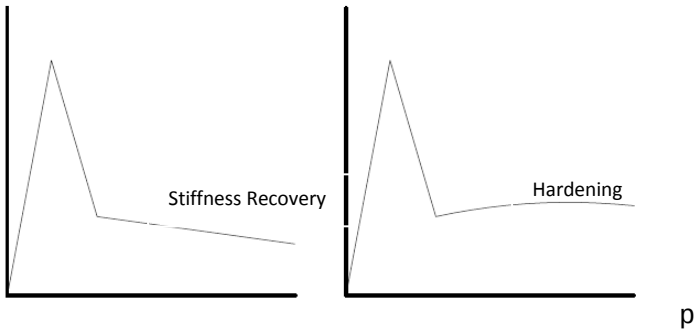

(a) (b)

Figure 5.3 Typical Load-Deflection Plot for ASTM C1609 Beams with Low Dosages of (a) Steel Fiber and (b) Synthetic Fiber.

The behaviors of the beams for high dosage steel and synthetic fibers are shown in Figure 5.4. High dosages of steel fiber reinforcement showing a slight decrease in load at failure but when the fibers began to be engaged, they demonstrated a hardening affect. In some cases, the first-peak load was passed and ultimate load was reached before the beams began to decrease (negative slope) in load capacity. Synthetic fibers showed very similar behaviors as steel fibers for high dosages, with the exception that hardening was never greater than the first-peak load.

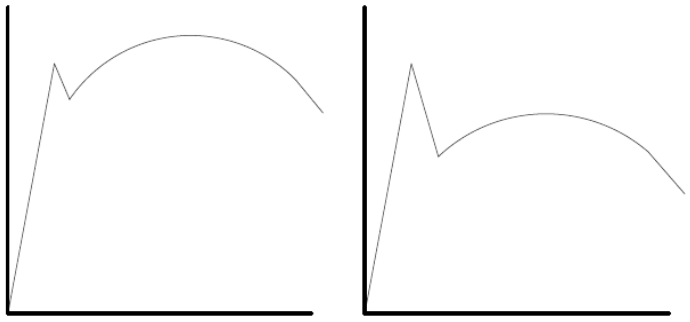

(a) (b)

Figure 5.4 Typical Load-Deflection Plot for ASTM C1609 Beams with High Dosages of (a) Steel Fiber and (b) Synthetic Fiber.

The average of modulus of rupture for steel fibers was 610 psi (4 MPa), 650 psi (4 MPa), and 999 psi (7 MPa) for Hanson Grand Prairie, Hanson Longview, and Northern Concrete plants,

respectively. The synthetic fibers had an average of 559 psi (4 MPa), 550 psi (4 MPa), and 887 psi (6 MPa) for Hanson Grand Prairie, Hanson Longview and Northern Concrete Pipe plants, respectively. The above values show that the averages of modulus of rupture values, in general, are enhanced by introducing synthetic or steel fibers when compared with plane concrete with a compressive strength of 5,000 psi based on 7.5 √f'c.

Material toughness was also determined from beam tests resulting in averages of 52 ft-lb (70 J) at Hanson Grand Prairie, 56 ft-lb (76 J) at Hanson Longview, and 80 ft-lb (108 J) at Northern Concrete for steel fibers. Material toughness averages of synthetic fibers were 39 ft-lb (53 J) at Hanson Grand Prairie, 38 ft-lb (52 J) at Hanson Longview, and 75 ft-lb (102 J) at Northern Concrete.

The strength ratio identified by value of eta, (η) was determined from a function of modulus of rupture and average compressive strength; $\eta = \frac{f_t}{\sqrt{f_c}}$. Overall, the strength value increased as the modulus of rupture increased. The strength ratios from Hanson Grand Prairie were η=8.42 for steel fiber and η=8.29 for synthetic fiber. For Hanson Longview the averages were η=10.02 for steel fiber and η=8.11 for synthetic fiber. The Northern Concrete plant had an average of η=12.01 for steel fiber and η=12.61 for synthetic fibers. In general, the synthetic and steel fibers enhanced the strength ratio for the matrix of fiber and concrete when compared with ACI value of η = 7.5.

During compressive cylinder testing it was observed that as fiber dosages increase the failure crack tendency moves toward a 45 degree (0.78 rad.) angle. This crack pattern describes ductile material properties, which is due to the introduction of fibers into the concrete matrix. As fiber dosages were reduced, the 45 degree (0.78 rad.) angle would decrease in length and begin to straighten. Another failure mode frequently observed was crushing. The average 7-day compressive strengths for steel fibers at the Hanson Grand Prairie and Longview plants were 5,878 psi (41 MPa) and 4,828 psi (33 MPa), respectively. Average 7-day strengths for synthetic fibers at Hanson Grand Prairie and Longview plants were 5,325 psi (37 MPa) and 3,811 psi (26 MPa), respectively. Overall average compressive strengths for steel fibers were 5,411 psi (37

MPa), 4,671 psi (32 MPa), and 6,923 psi (48 MPa) for the Hanson Grand Prairie, Hanson Longview, and Northern Concrete plants, respectively. Synthetic fiber average compressive strengths were 4,958 psi (34 MPa) at Hanson Grand Prairie, 4,433 psi (31 MPa) at Hanson Longview and 4394 psi (30 MPa) at Northern Concrete.

The pipe test results for both synthetic and steel fibers showed that both fibers were able to resist crack widths up to 1.0 in. when the pipe was at extreme deflection (i.e., over 10% of pipe diameter). Examination of the open cracks at final deflection during the testing showed that steel and synthetic fibers were mostly intact on each side of the crack and exhibited high pull out capacity. In certain steel test specimens, a few steel fibers were separated from the middle which indicated failure by yielding rather than pull-out. In the case of synthetic fibers neither pull out nor yielding were observed (refer to Figure 3.4).

Typically, pipes which were reinforced with steel fibers showed characteristics of increasing pipe strength as the fiber dosages increased. However, it should be noted that as fiber dosage increases, the addition of water in the mix becomes necessary. Thus, producing a mix that is dry enough to permit the pipe to withstand vertical casting but wet enough to assist the hydration process for strength becomes an art in casting, which producers can easily achieve based on their experience and the nature of the local aggregates and other materials in the mix. Also, this study showed the amount of water needed in a mix with fibers is highly sensitive to weather conditions. For example, during extreme summer months (95°F), the combination of dried aggregates and addition of fiber will cause a higher water demand than normal weather conditions. Therefore, it is not practical to predetermine the amount of water that will be required in fiber concrete. Thus, the experience of the plant manager is instrumental in producing successful steel or synthetic fiber concrete.

In general, the results of this study showed that the use of both BASF MasterFiber MAC Matrix synthetic fiber and BASF MasterFiber FS7 steel fiber in concrete pipes is a viable alternative to conventional reinforcing. This study recommends the use of synthetic fibers (BASF MasterFiber MAC Matrix) with adequate dosage for up to 21 in. diameter concrete pipes with “B-

Walls," and up to 36 in. diameter concrete pipes with "C-Walls." Steel fiber (BASF MasterFiber FS7) pipes are recommended as alternative reinforcement with adequate fiber dosage for up to 24 in. diameter concrete pipes with "B-Wall" and up to 36 in. diameter concrete pipes with "C-Walls." It should be noted that proper fiber dosage is a trial and error process based on local aggregate and cementitious materials and the type of production equipment used, which is also the case for the production of the conventional reinforced concrete pipes.

5.3 Recommendations

The recommendations for future research studies are at the following forefronts:

1. To test additional pipe sizes with "C-Wall" and different production machinery such as Packerhead.
2. Additional mix design optimization studies to include different local aggregates and manufacturing processes. This study focused on employing the current mix design used in regular RCP production with optimization of the amount of water due to the introduction of fiber. Further studies on mix designs are recommended.
3. Conduct a long term (up to one year) fiber pipe performance evaluation on installed pipes with simulated design backfill heights. The primary objective is to compare long-term load responses between fiber reinforced concrete pipes and RCP as measure by deflections.
4. It is recommended that the long term structural performance of concrete pipes with galvanized and un-galvanized steel fibers be evaluated under installed conditions.

APPENDIX A

MIX DESIGNS

Table A1 Hanson Grand Prairie Mix Designs

Mix #	Size of pipe	Class	Total Cement (lbs)	Fly Ash (%)	3/8" Stone (lbs)	5/8" Stone (lbs)	Concrete Sand (lbs)	MFG Sand (lbs)	Cement I/II (lbs)	Fly Ash (lbs)	Admix Sika PI100 (oz)	Admix Sika Rapid (as needed) (oz)	W/C (%)	Water (gal.)
GP1	12", 15",18"	3	505	25	1315	0	2051	0	380	125	2.5	2.5	0.387	26
GP2	12", 15",18"	4	564	25	1315	0	1958	0	424	140	2.5	2.5	0.369	28
GP3	12", 15",18"	5	611	25	1315	0	1887	0	461	150	2.5	2.5	0.36	29
GP4	21", 24", 27"	3	505	25	1450	0	960	957	380	125	2.5	2.5	0.387	26
GP5	21", 24", 27"	4	564	25	1450	0	912	912	424	140	2.5	2.5	0.369	28
GP6	21", 24", 27"	5	611	25	1450	0	876	876	461	150	2.5	2.5	0.36	29
GP7	30", 33", 36"	3	505	25	1300	370	850	848	380	125	2.5	2.5	0.387	26
GP8	30", 33", 36"	4	564	25	1300	370	805	800	424	140	2.5	2.5	0.369	28
GP9	30", 33", 36"	5	611	25	1300	370	767	767	461	150	2.5	2.5	0.36	29

Table A2 Hanson Longview Mix Designs

Mix #	Size of pipe	Class	Total Cement (lbs)	Fly Ash (%)	3/8" Stone (lbs)	5/8" Stone (lbs)	Concrete Sand (lbs)	MFG Sand (lbs)	Cement I/II (lbs)	Fly Ash (lbs)	Admix Sika PI100 (oz)	Admix Sika Rapid (as needed) (oz)	W/C (%)	Water (gal.)
LV1	15", 24", 36"	4	564	25	1450	0	912	912	424	140	2.5	2.5	0.32	28

Table A3 Northern Concrete Pipe Mix Designs

Mix #	Size of Pipe	Class	Total Cement (lbs)	Fly Ash (%)	3/8" Stone (lbs)	5/8" Stone (lbs)	Sand (lbs)	Cement I/II (lbs)	Fly Ash (lbs)	Admix #1 (1000 NP)	Admix #2 (1000 R)	W/C (lbs/lbs)	Water (lbs)
NC1	24"	3	718	22	1990	0	1503	561	157	21	27	27.6	26
NC2	24", 30"	3	718	20	2105	0	1370	572	146	21	27	28.7	25
NC3	24", 30", 36"	3	709	21	1952	0	1533	561	148	21	27	22.2	27
NC4	30", 36"	3	718	21	2000	0	1565	569	149	21	27	23.2	31
NC5	36"	3	713	20	1980	0	1637	569	144	21	27	22.3	32
NC6	24"	3	708	20	1957	0	1520	569	139	21	27	26.2	27
NC7	24", 36"	3	708	20	1917	0	1536	569	139	21	27	26.2	27
NC8	36"	3	718	21	1917	0	1767	567	151	21	27	26.6	27
NC9	36"	3	708	20	1982	0	1615	564	144	21	27	27.2	26

APPENDIX B

STEEL BEAM GRAPHS

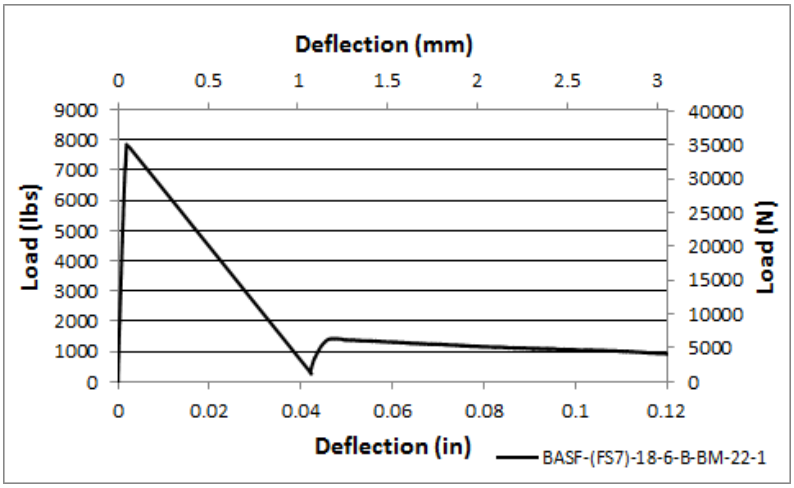

(a)

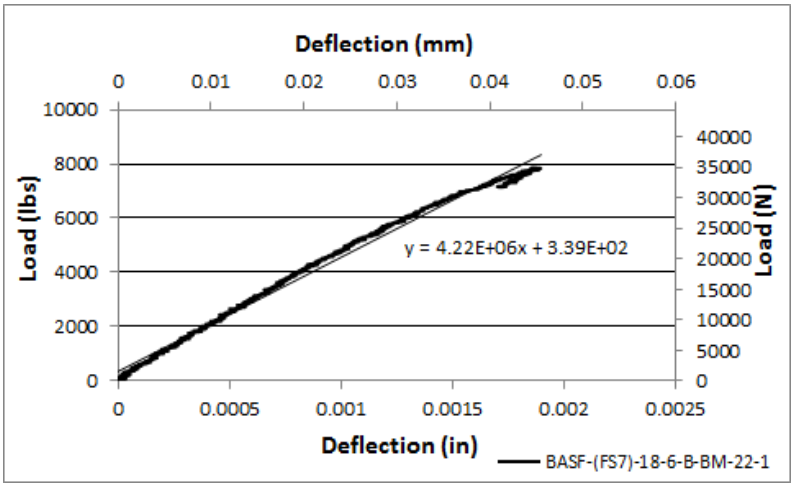

(b)

(c)

Figure B1 BASF-(FS7)-18-6-B-BM-22-1 (a) Load-Deflection Plot, (b) Modulus of Elasticity Plot, and (c) Crack Picture.

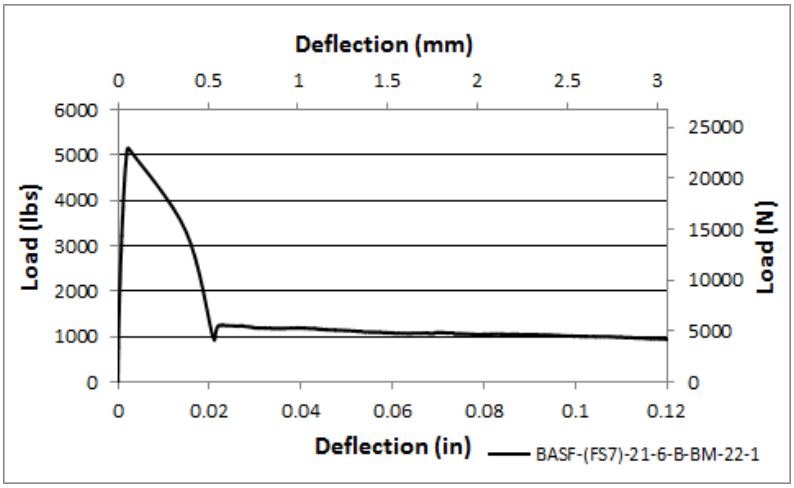

(a)

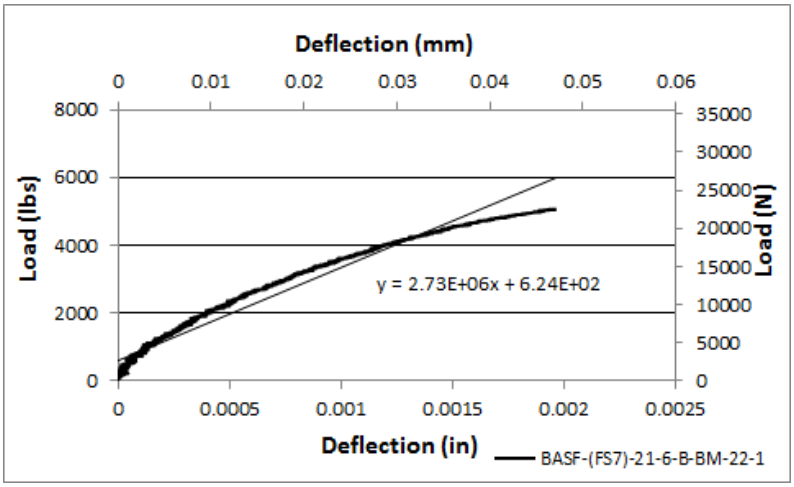

(b)

(c)

Figure B2 BASF-(FS7)-21-6-B-BM-22-1 (a) Load-Deflection Plot, (b) Modulus of Elasticity Plot, and (c) Crack Picture.

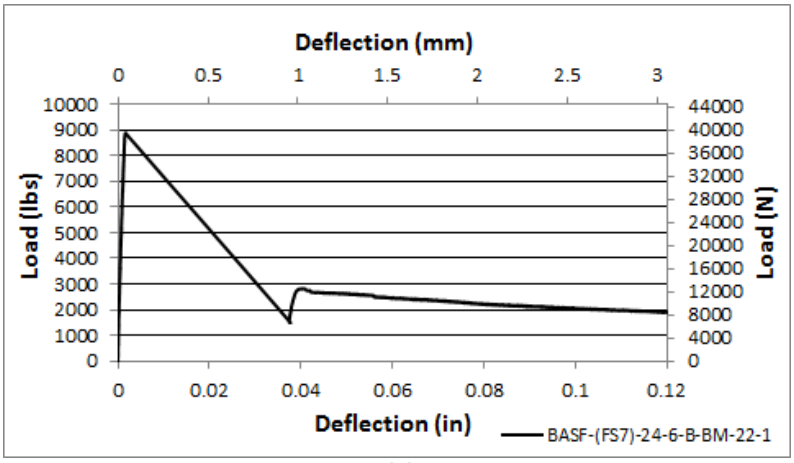

(a)

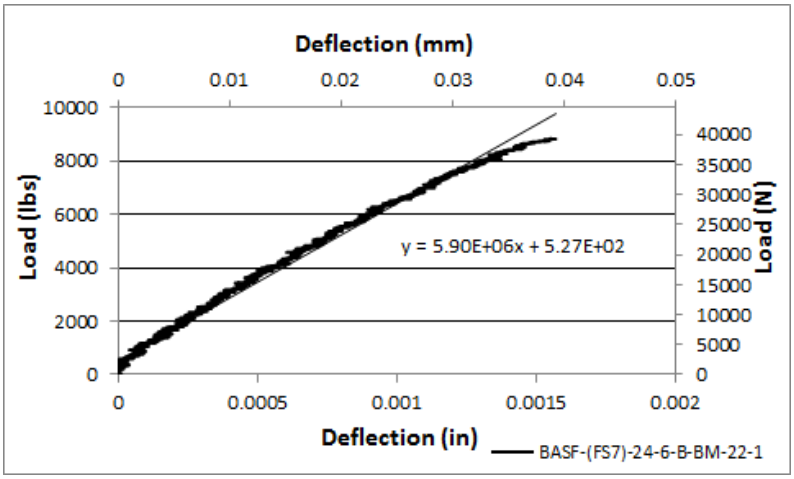

(b)

(c)

Figure B3 BASF-(FS7)-24-6-B-BM-22-1 (a) Load-Deflection Plot, (b) Modulus of Elasticity Plot, and (c) Crack Picture.

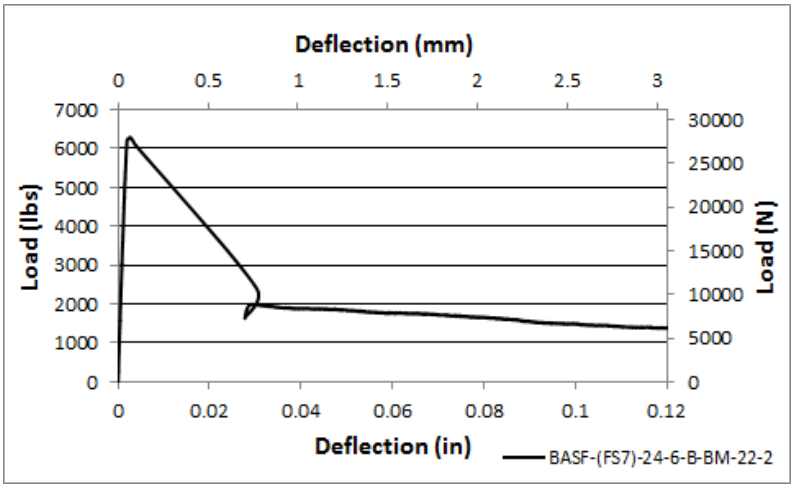

(a)

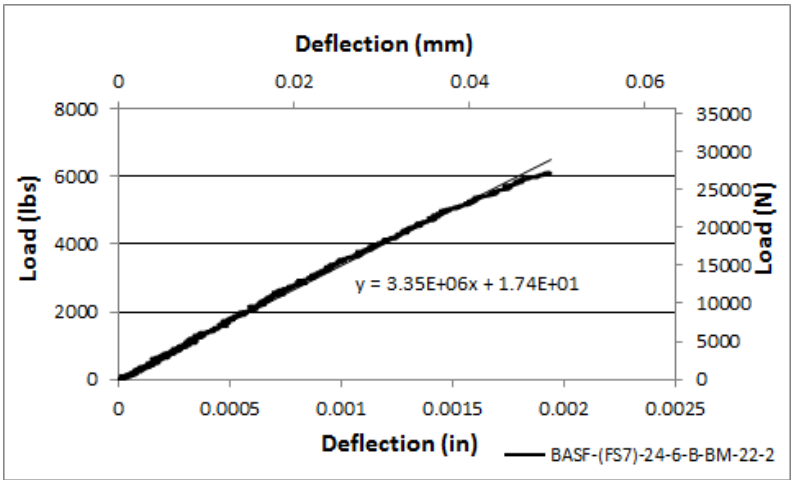

(b)

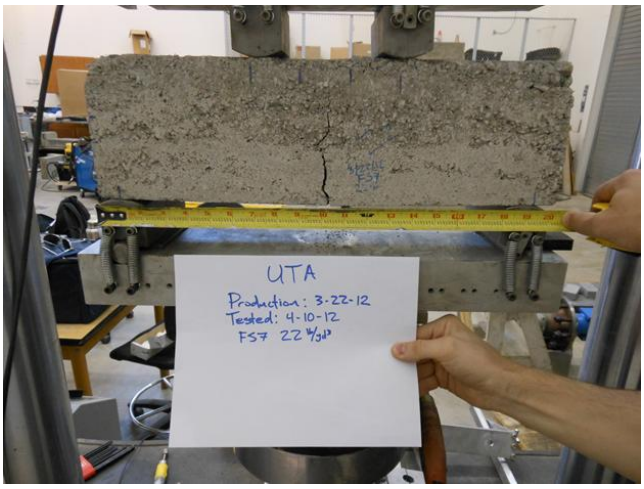

(c)

Figure B4 BASF-(FS7)-24-6-B-BM-22-2 (a) Load-Deflection Plot, (b) Modulus of Elasticity Plot, and (c) Crack Picture.

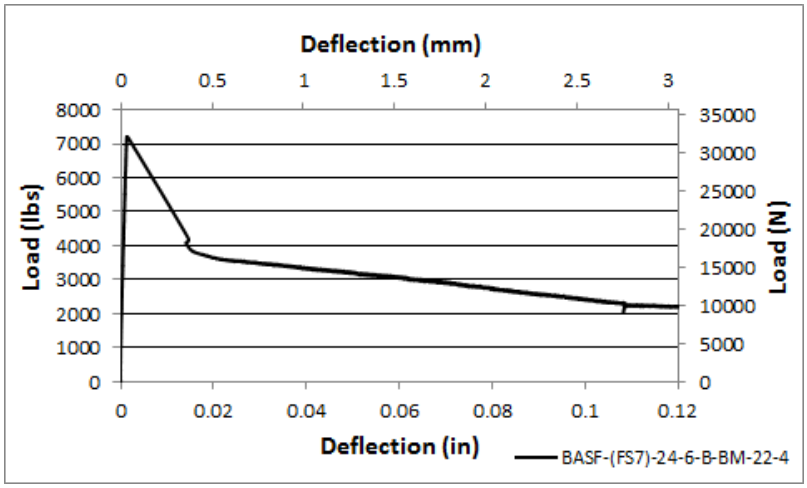

(a)

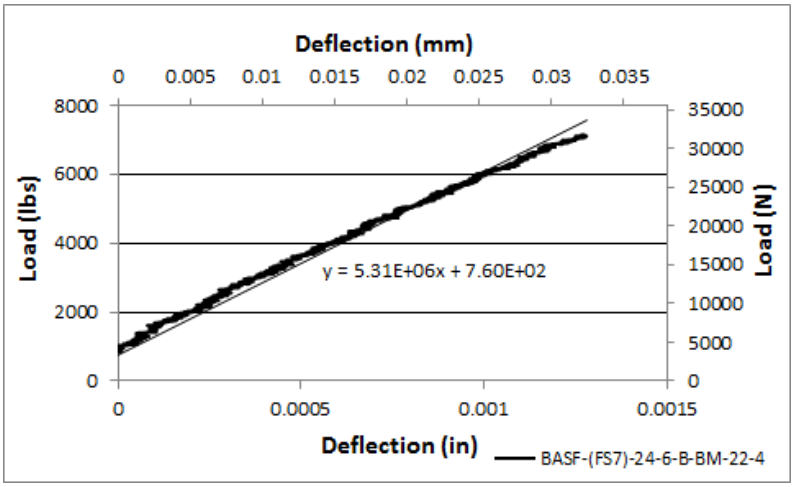

(b)

(c)

Figure B5 BASF-(FS7)-24-6-B-BM-22-4 (a) Load-Deflection Plot, (b) Modulus of Elasticity Plot, and (c) Crack Picture.

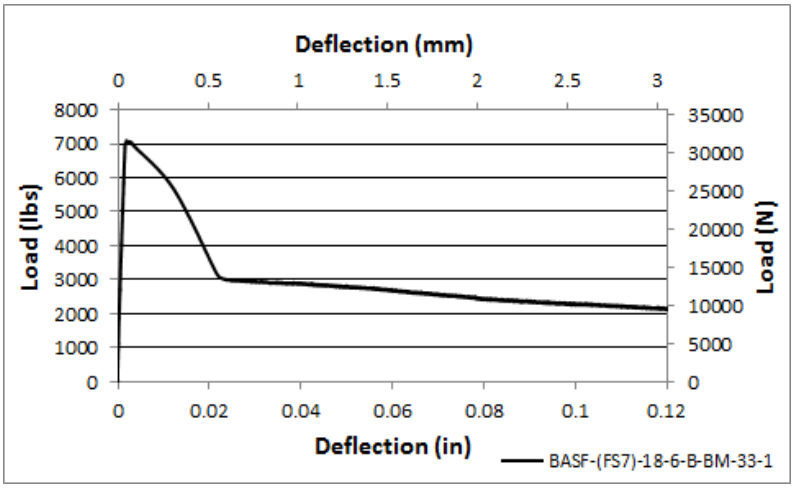

(a)

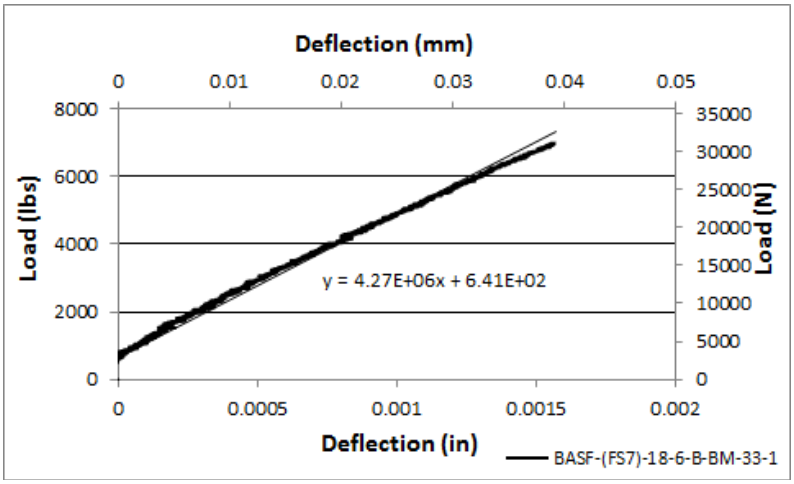

(b)

(c)

Figure B6 BASF-(FS7)-18-6-B-BM-33-1 (a) Load-Deflection Plot, (b) Modulus of Elasticity Plot, and (c) Crack Picture.

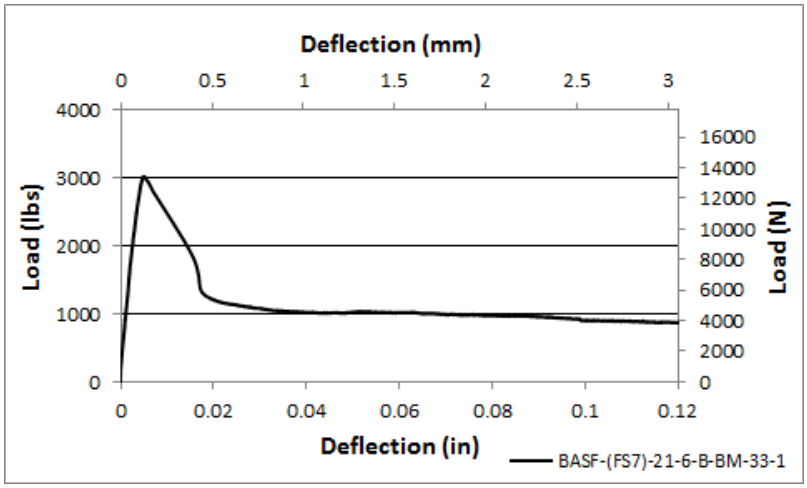

(a)

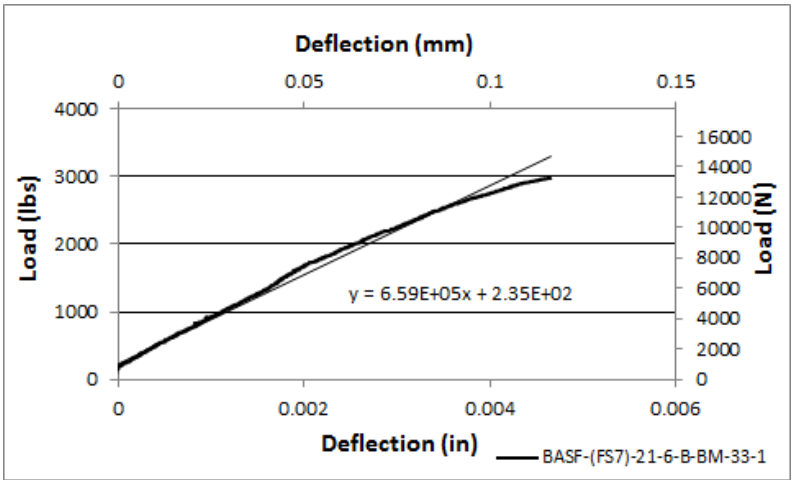

(b)

(c)

Figure B7 BASF-(FS7)-21-6-B-BM-33-1 (a) Load-Deflection Plot, (b) Modulus of Elasticity Plot, and (c) Crack Picture.

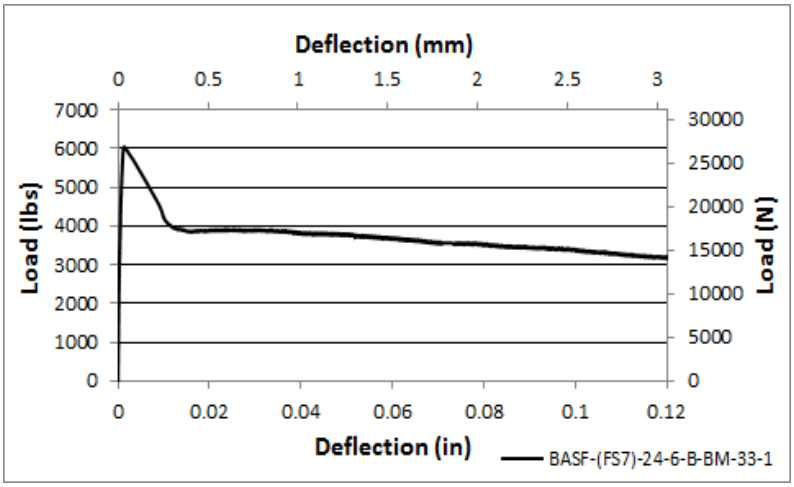

(a)

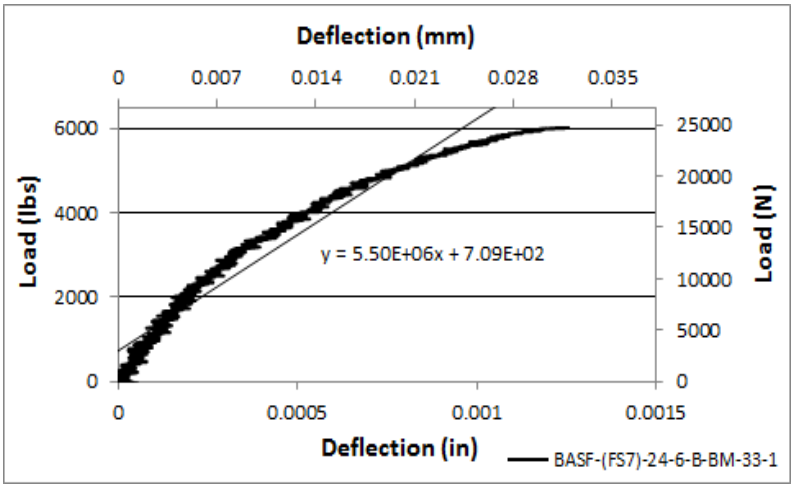

(b)

(c)

Figure B8 BASF-(FS7)-24-6-B-BM-33-1 (a) Load-Deflection Plot, (b) Modulus of Elasticity Plot, and (c) Crack Picture.

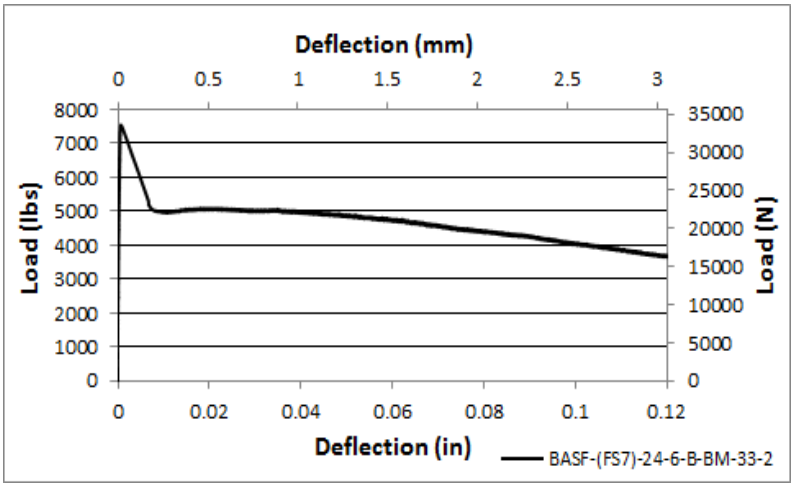

(a)

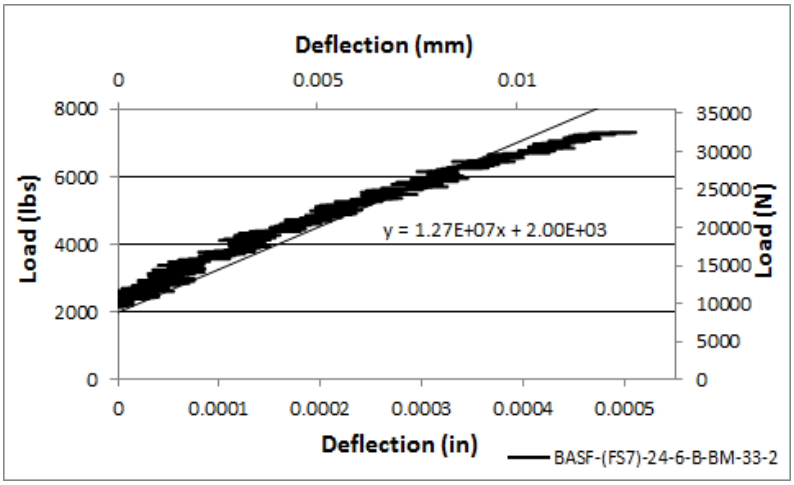

(b)

(c)

Figure B9 BASF-(FS7)-24-6-B-BM-33-2 (a) Load-Deflection Plot, (b) Modulus of Elasticity Plot, and (c) Crack Picture.

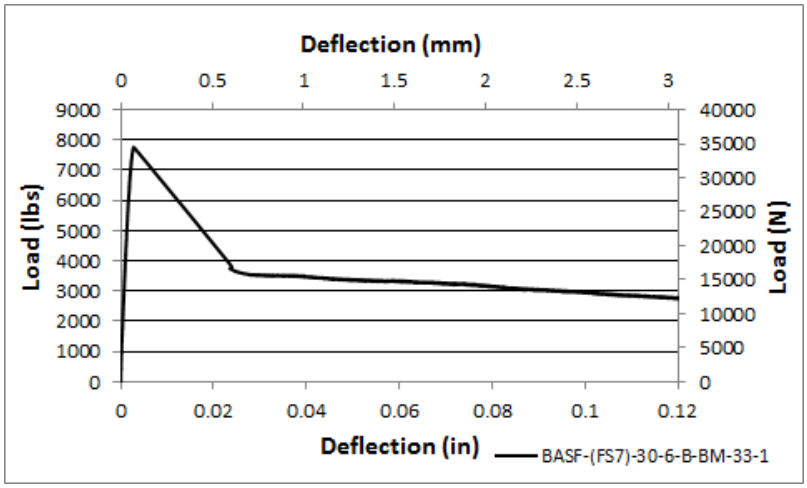

(a)

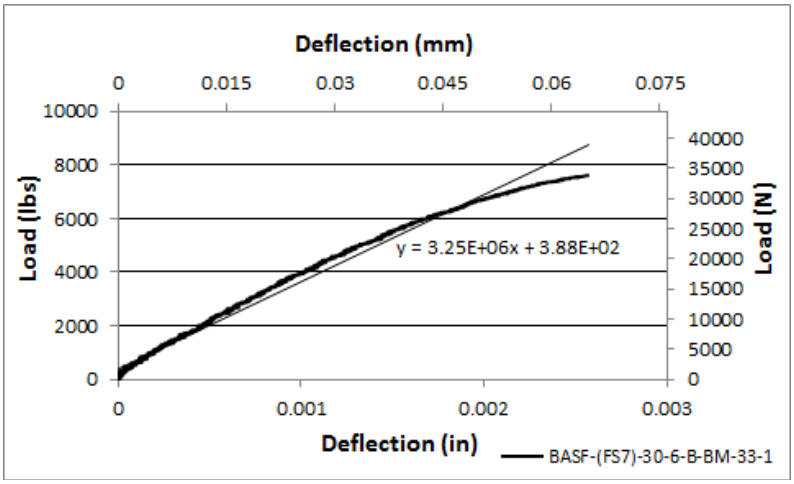

(b)

(c)

Figure B10 BASF-(FS7)-30-6-B-BM-33-1 (a) Load-Deflection Plot, (b) Modulus of Elasticity Plot, and (c) Crack Picture.

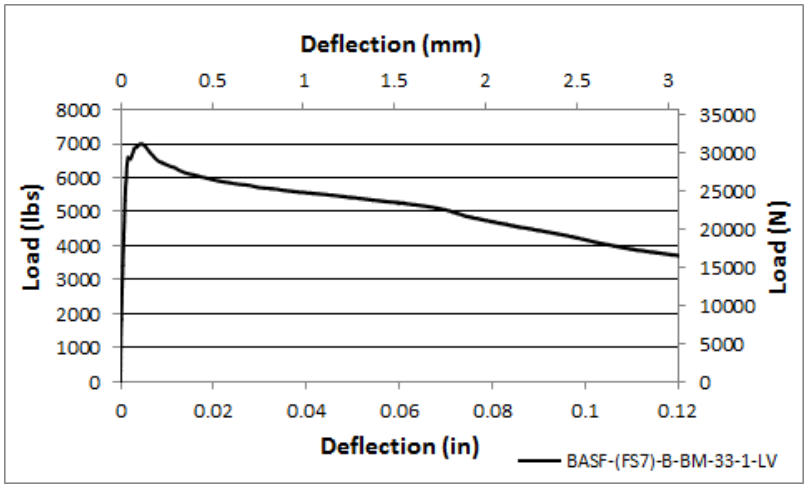

(a)

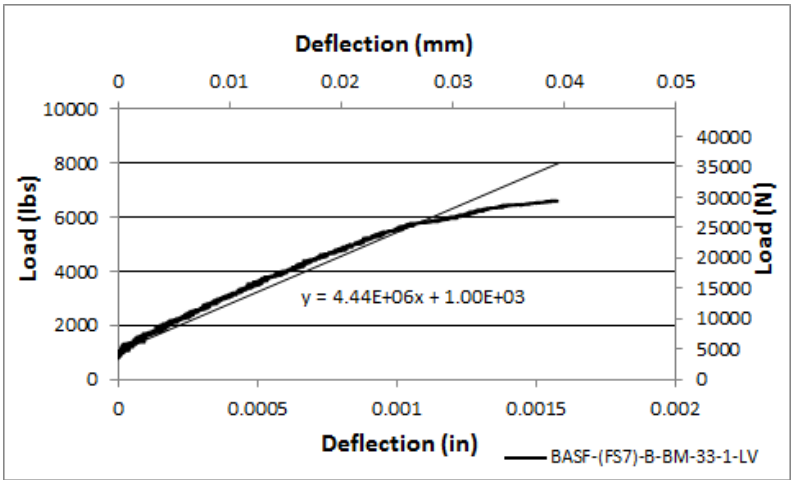

(b)

(c)

Figure B11 BASF-(FS7)-B-BM-33-1-LV (a) Load-Deflection Plot, (b) Modulus of Elasticity Plot, and (c) Crack Picture.

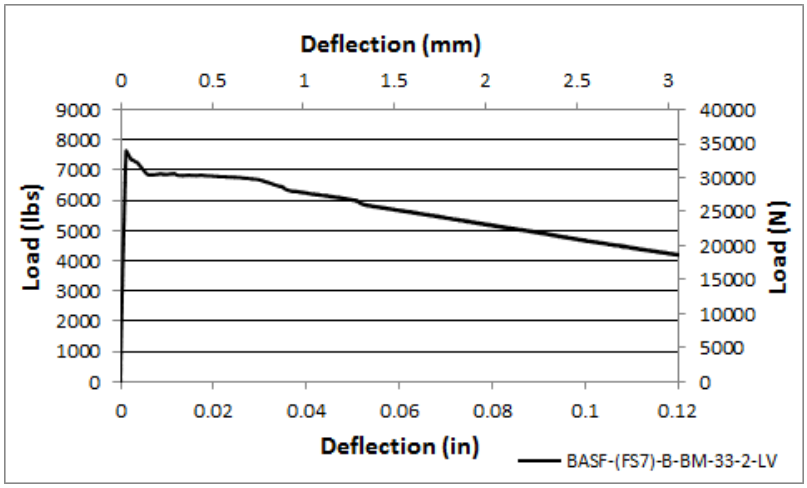

(a)

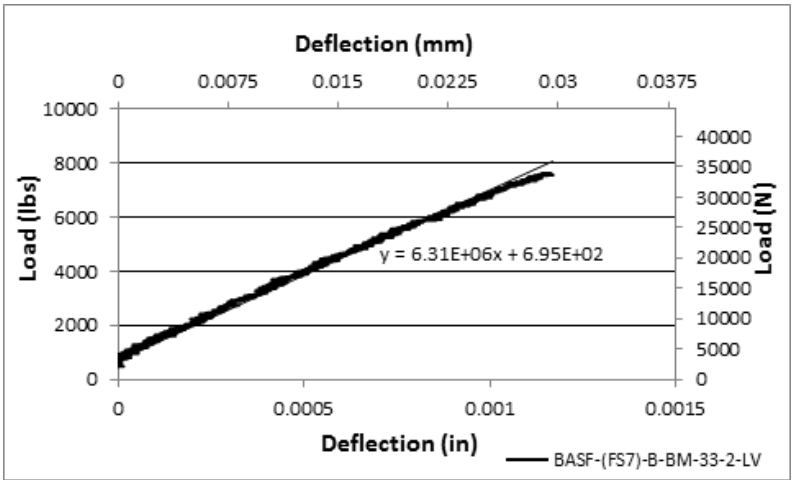

(b)

(c)

Figure B12 BASF-(FS7)-B-BM-33-2-LV (a) Load-Deflection Plot, (b) Modulus of Elasticity Plot, and (c) Crack Picture.

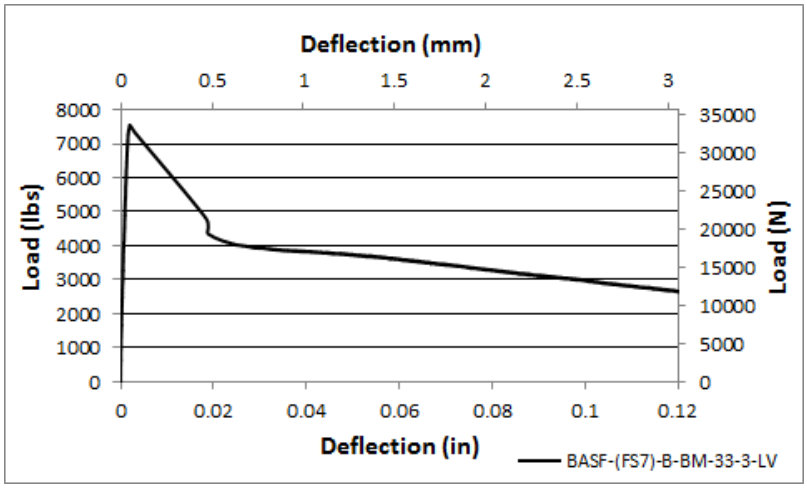

(a)

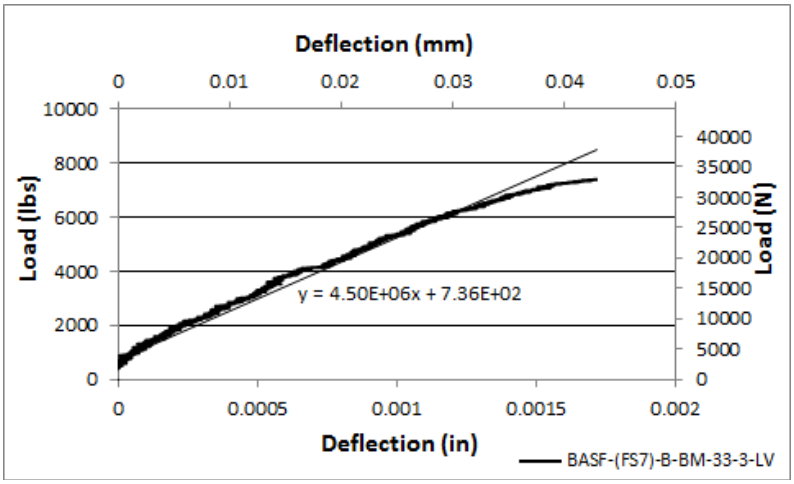

(b)

(c)

Figure B13 BASF-(FS7)-B-BM-33-3-LV (a) Load-Deflection Plot, (b) Modulus of Elasticity Plot, and (c) Crack Picture.

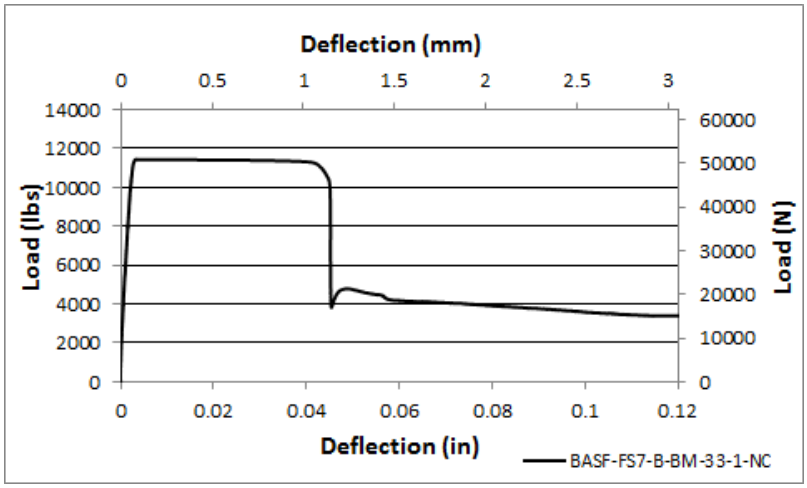

(a)

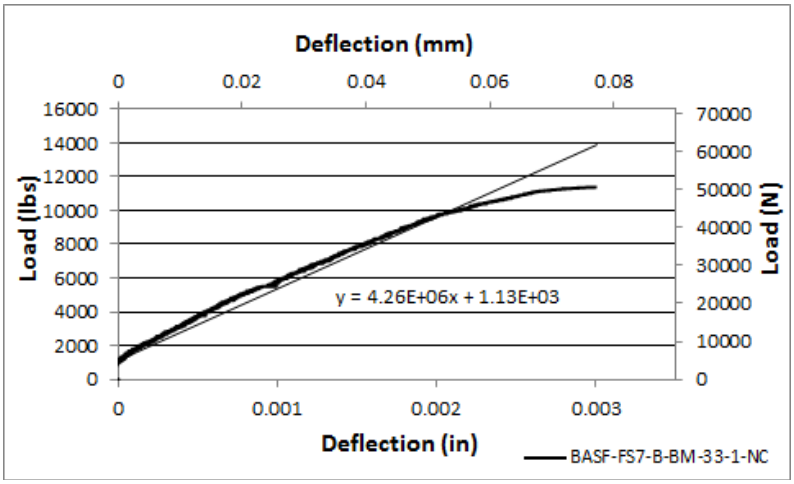

(b)

(c)

Figure B14 BASF-(FS7)-B-BM-33-1-NC (a) Load-Deflection Plot, (b) Modulus of Elasticity Plot, and (c) Crack Picture.

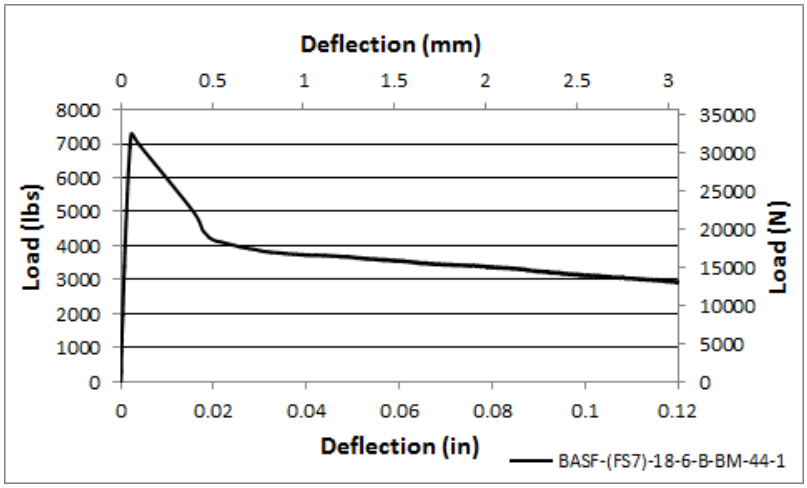

(a)

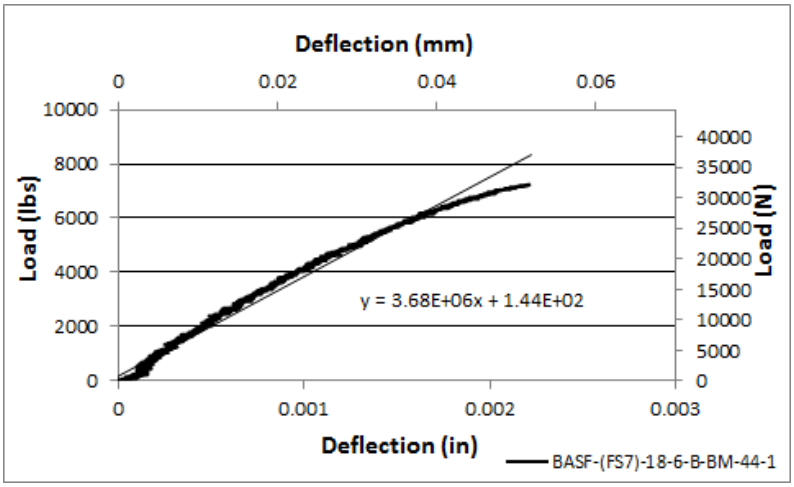

(b)

(c)

Figure B15 BASF-(FS7)-18-6-B-BM-44-1 (a) Load-Deflection Plot, (b) Modulus of Elasticity Plot, and (c) Crack Picture.

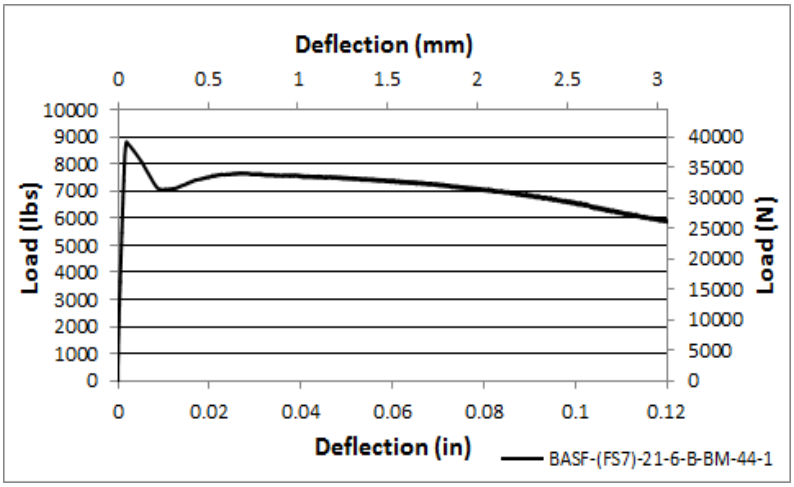

(a)

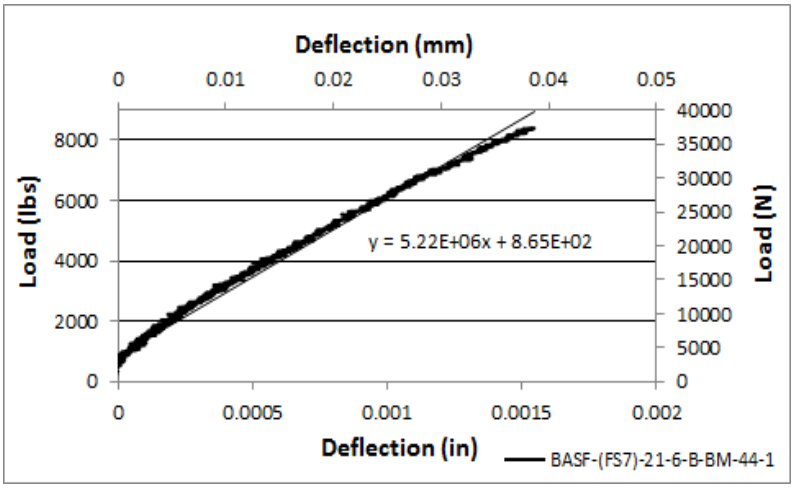

(b)

(c)

Figure B16 BASF-(FS7)-21-6-B-BM-44-1 (a) Load-Deflection Plot, (b) Modulus of Elasticity Plot, and (c) Crack Picture.

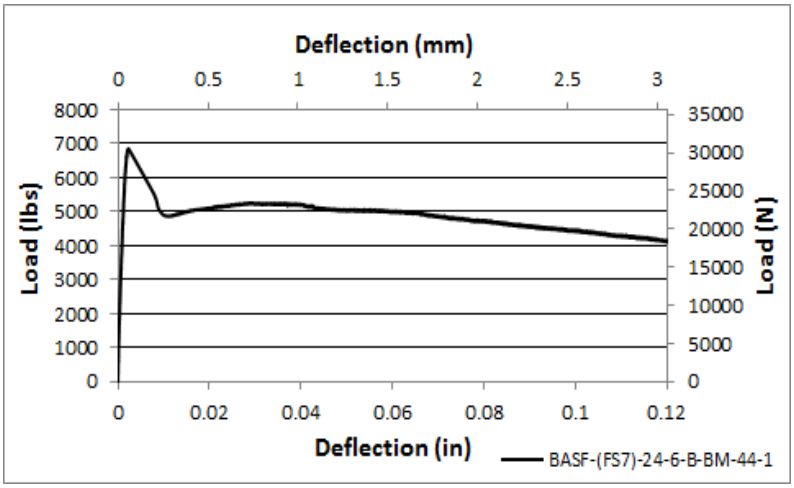

(a)

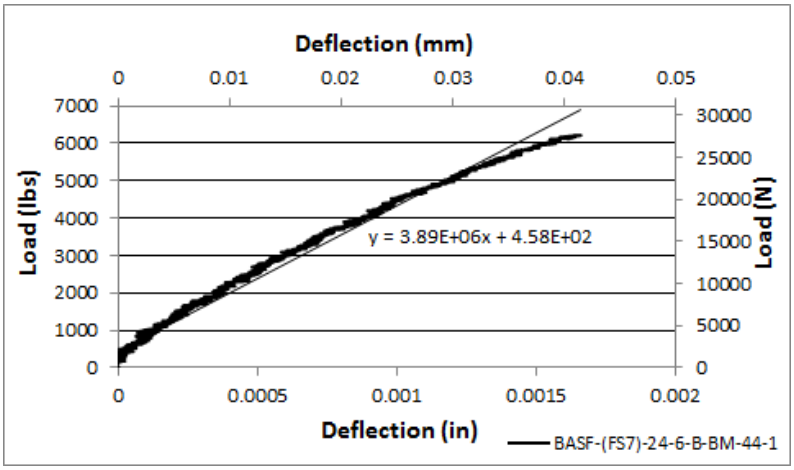

(b)

Figure B17 BASF-(FS7)-24-6-B-BM-44-1 (a) Load-Deflection Plot and (b) Modulus of Elasticity Plot.

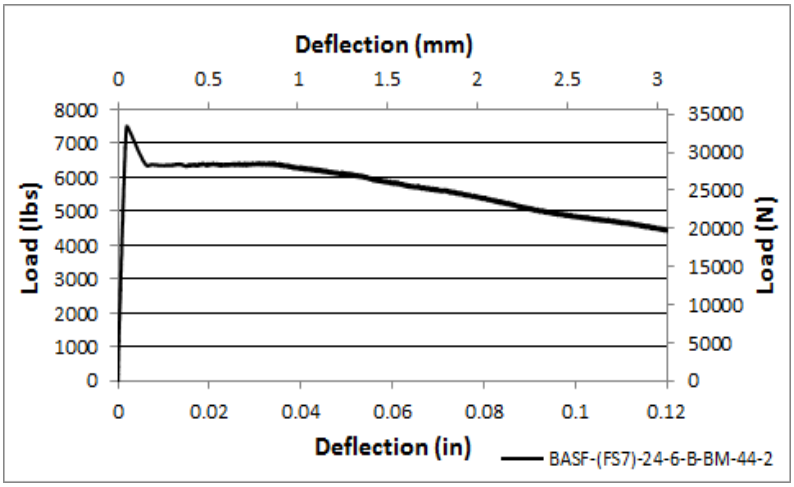

(a)

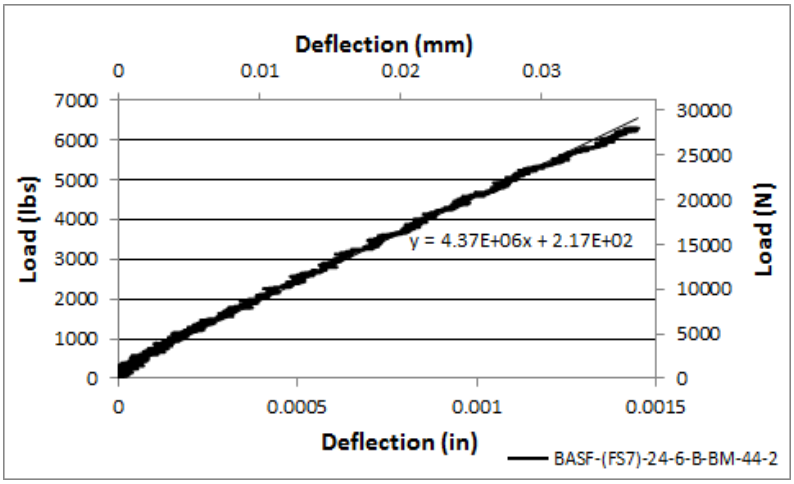

(b)

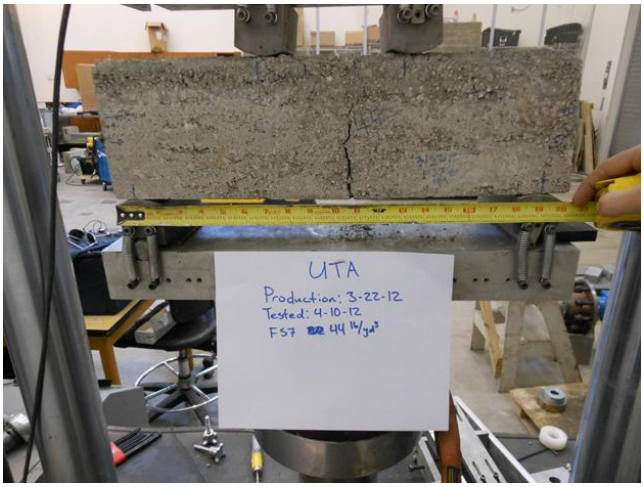

(c)

Figure B18 BASF-(FS7)-24-6-B-BM-44-2 (a) Load-Deflection Plot, (b) Modulus of Elasticity Plot, and (c) Crack Picture.

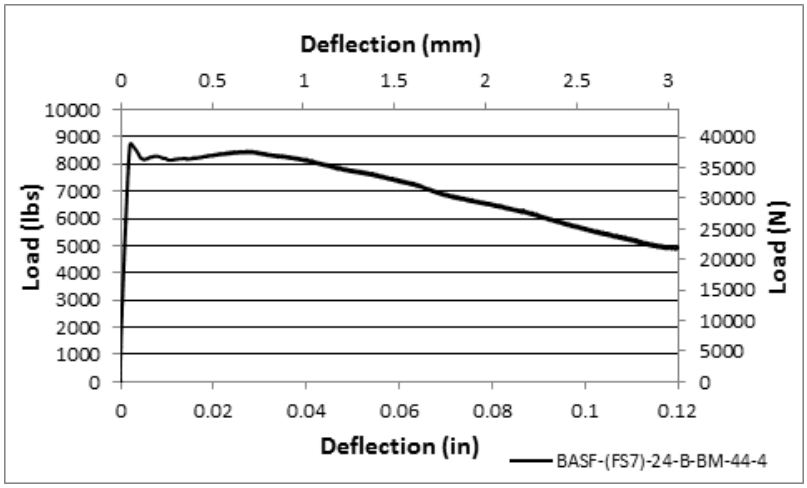

(a)

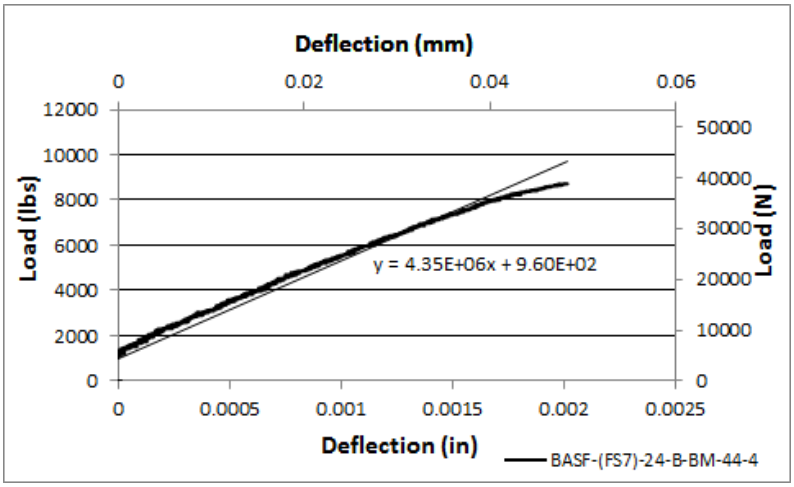

(b)

(c)

Figure B19 BASF-(FS7)-24-6-B-BM-44-4 (a) Load-Deflection Plot, (b) Modulus of Elasticity Plot, and (c) Crack Picture.

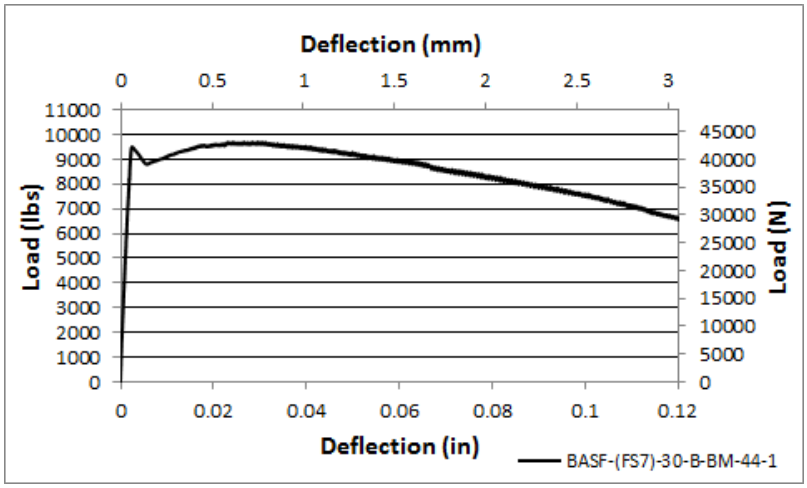

(a)

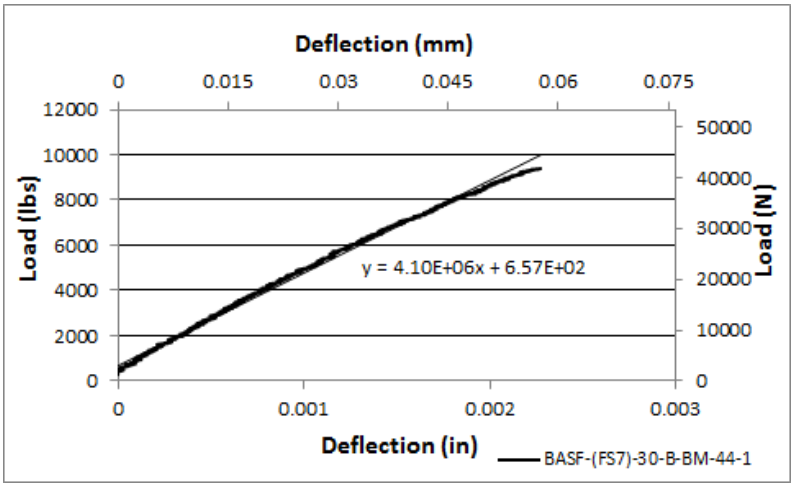

(b)

(c)

Figure B20 BASF-(FS7)-30-6-B-BM-44-1 (a) Load-Deflection Plot, (b) Modulus of Elasticity Plot, and (c) Crack Picture.

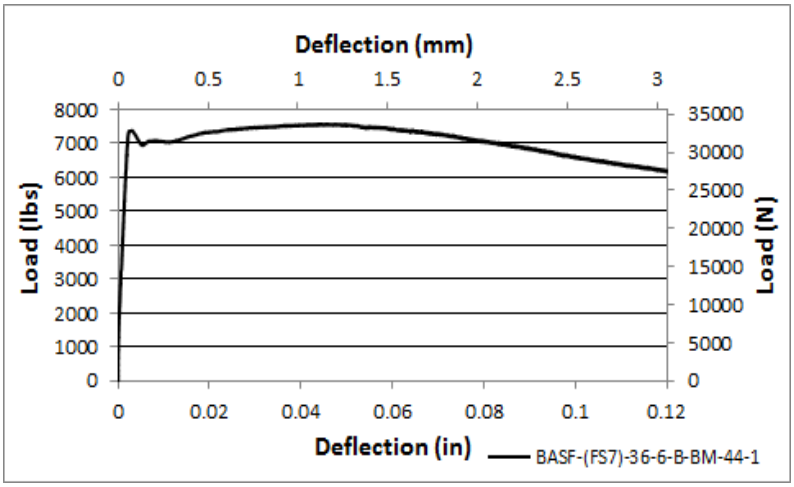

(a)

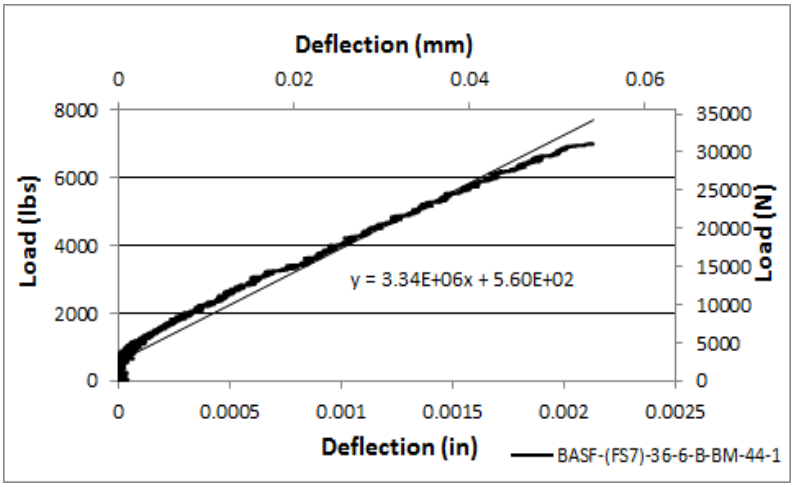

(b)

Figure B21 BASF-(FS7)-36-6-B-BM-44-1 (a) Load-Deflection Plot and (b) Modulus of Elasticity Plot.

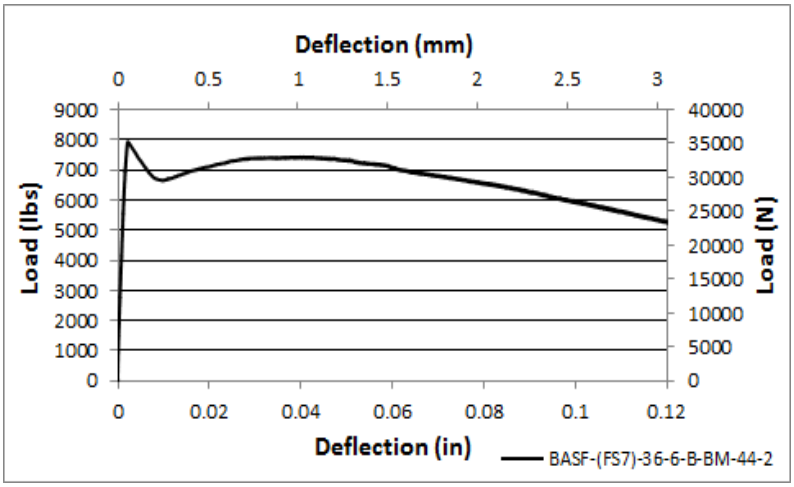

(a)

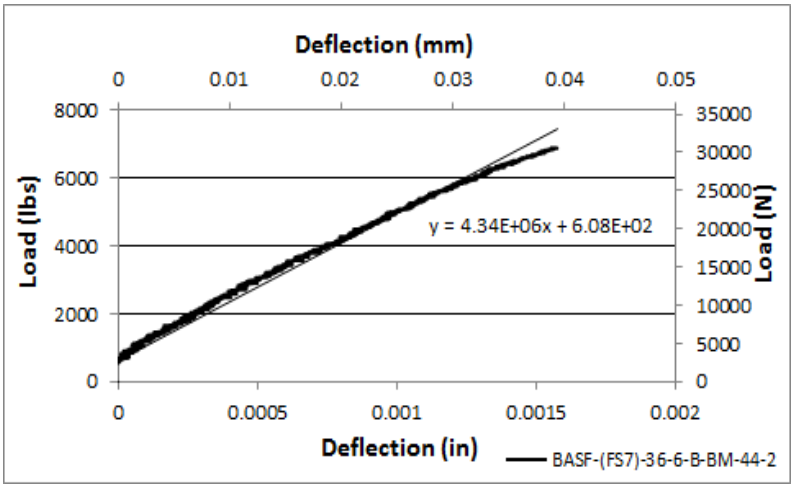

(b)

(c)

Figure B22 BASF-(FS7)-36-6-B-BM-44-2 (a) Load-Deflection Plot, (b) Modulus of Elasticity Plot, and (c) Crack Picture.

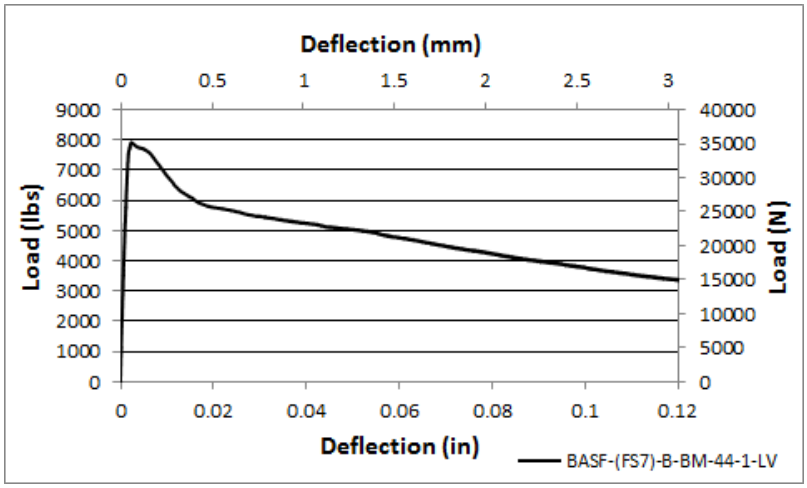

(a)

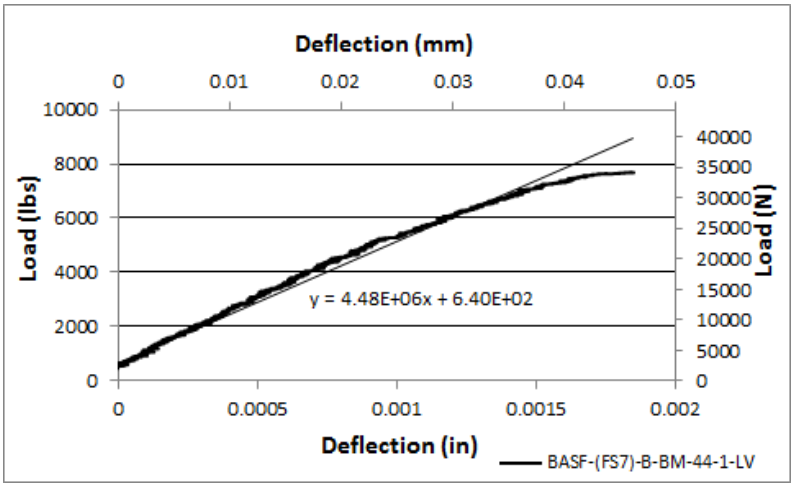

(b)

(c)

Figure B23 BASF-(FS7)-B-BM-44-1-LV (a) Load-Deflection Plot, (b) Modulus of Elasticity Plot, and (c) Crack Picture.

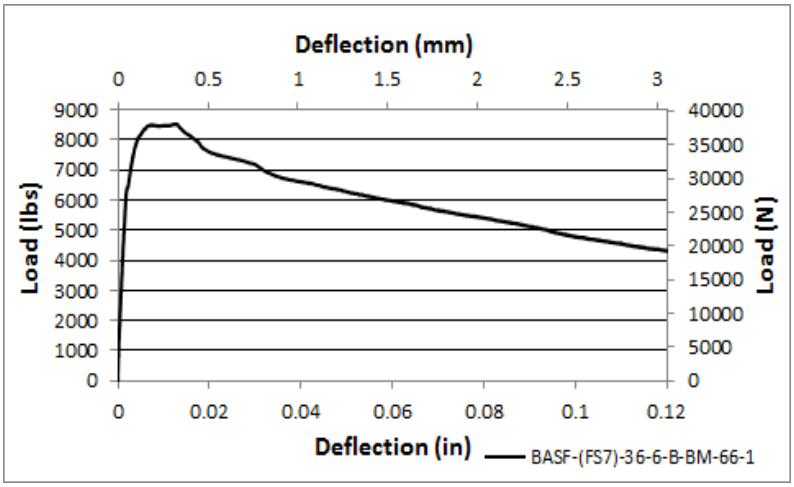

(a)

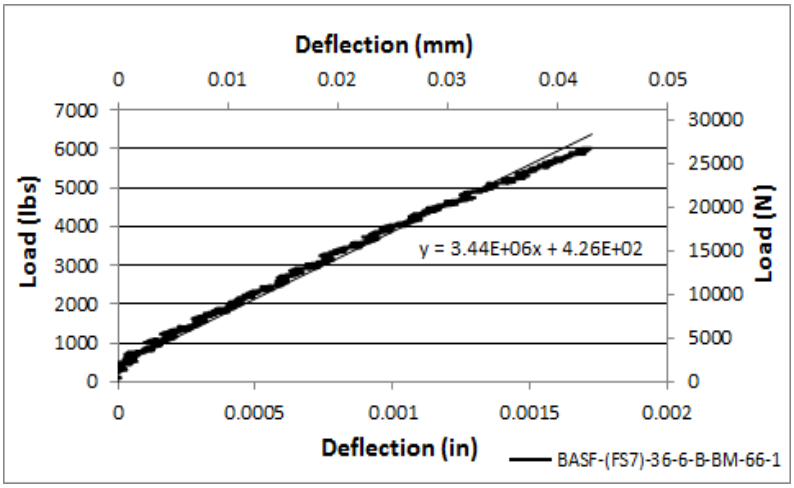

(b)

(c)

Figure B24 BASF-(FS7)-36-6-B-BM-66-1 (a) Load-Deflection Plot, (b) Modulus of Elasticity Plot, and (c) Crack Picture.

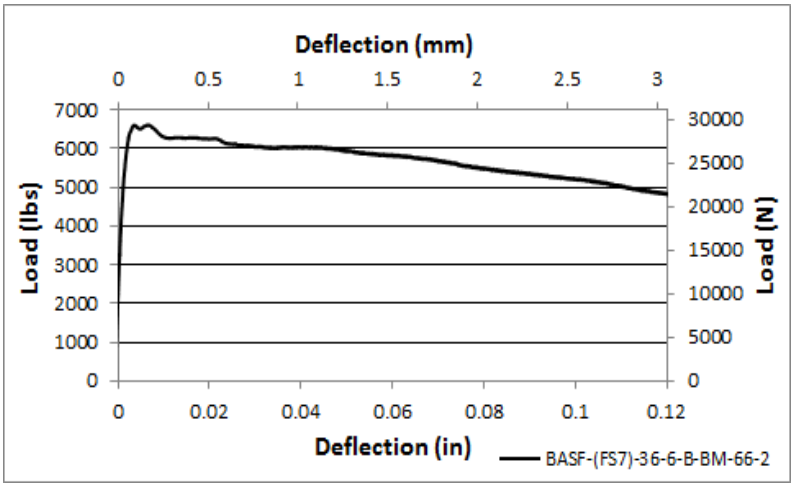

(a)

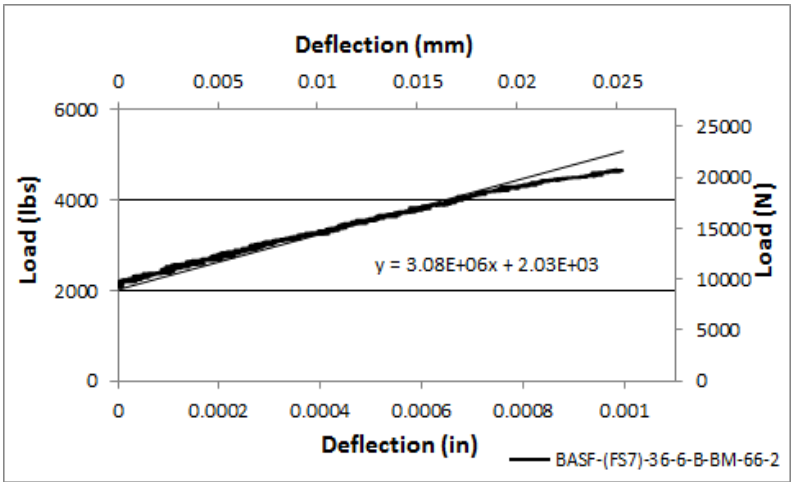

(b)

(c)

Figure B25 BASF-(FS7)-36-6-B-BM-66-2 (a) Load-Deflection Plot, (b) Modulus of Elasticity Plot, and (c) Crack Picture.

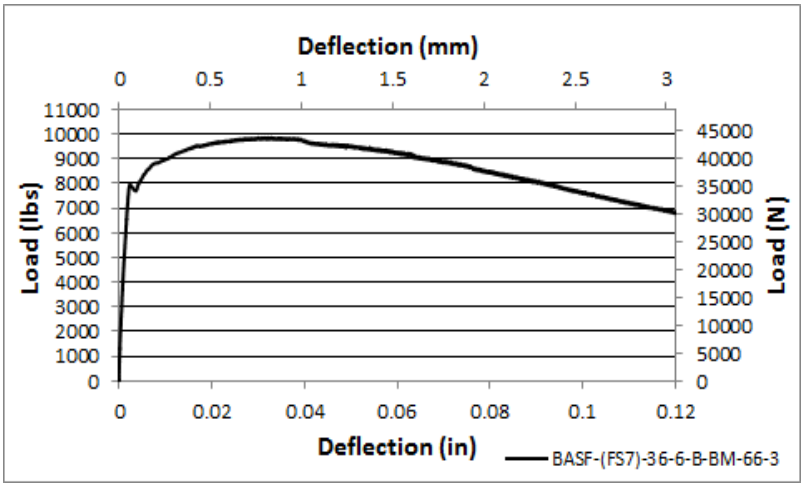

(a)

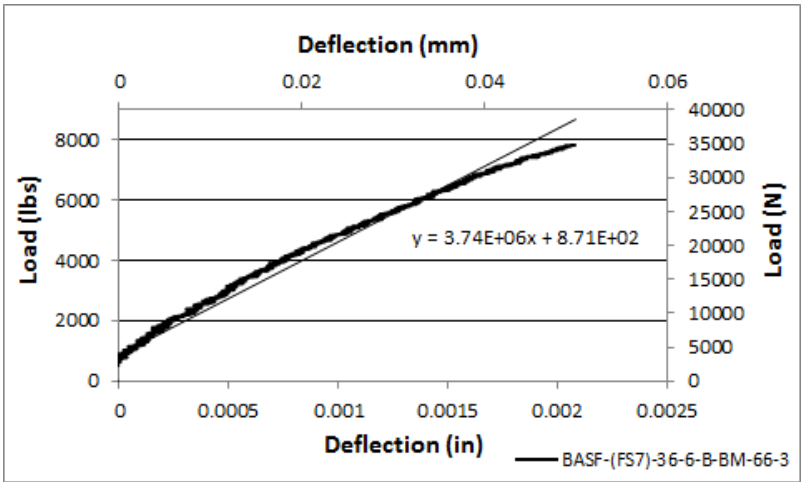

(b)

(c)

Figure B26 BASF-(FS7)-36-6-B-BM-66-3 (a) Load-Deflection Plot, (b) Modulus of Elasticity Plot, and (c) Crack Picture.

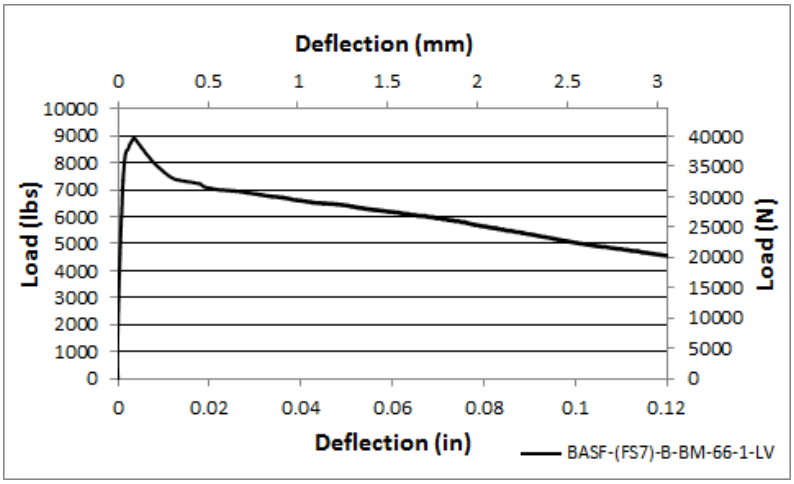

(a)

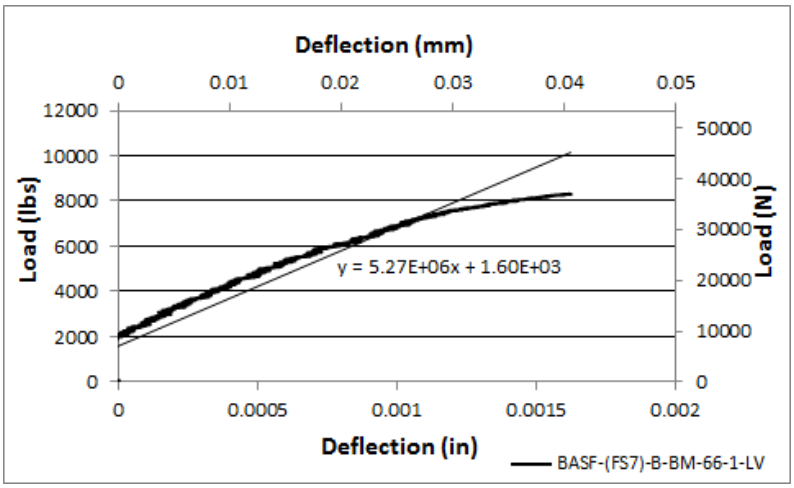

(b)

(c)

Figure B27 BASF-(FS7)-B-BM-66-1-LV (a) Load-Deflection Plot, (b) Modulus of Elasticity Plot, and (c) Crack Picture.

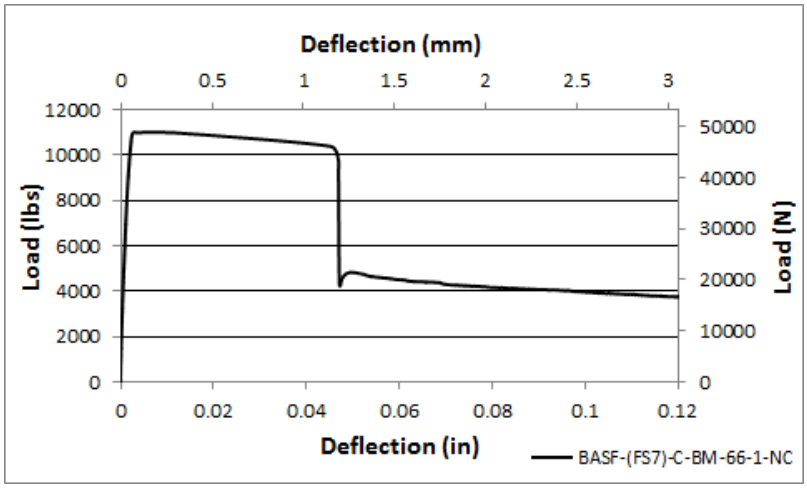

(a)

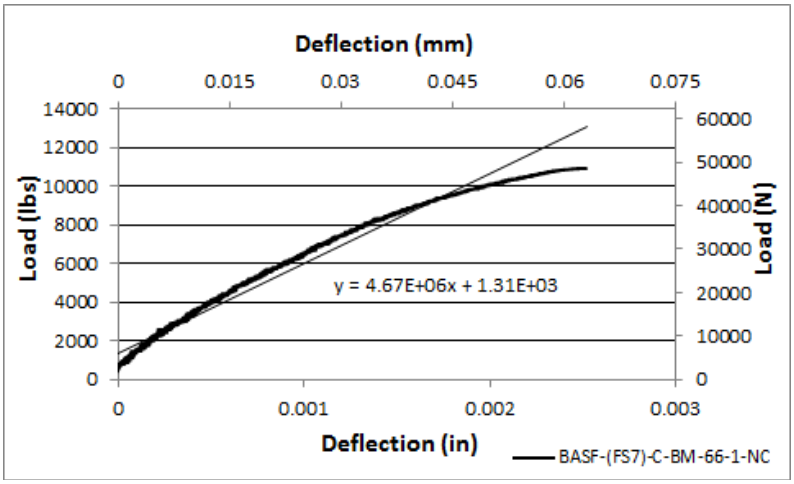

(b)

(c)

Figure B28 BASF-(FS7)-C-BM-66-1-NC (a) Load-Deflection Plot, (b) Modulus of Elasticity Plot, and (c) Crack Picture.

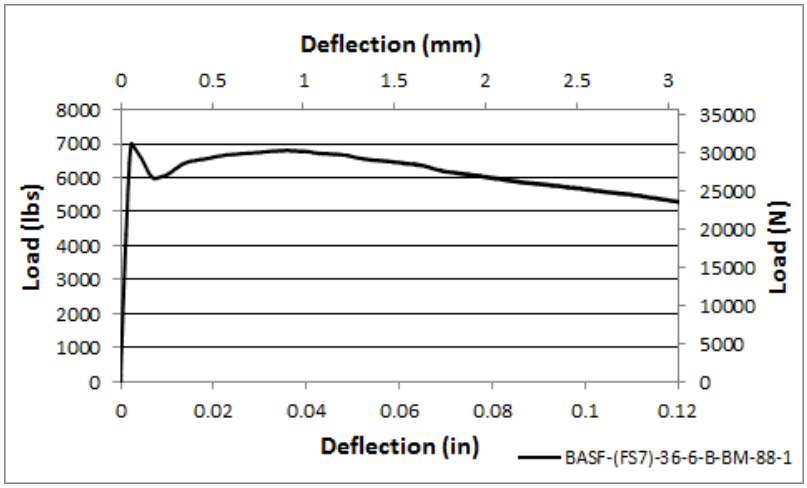

(a)

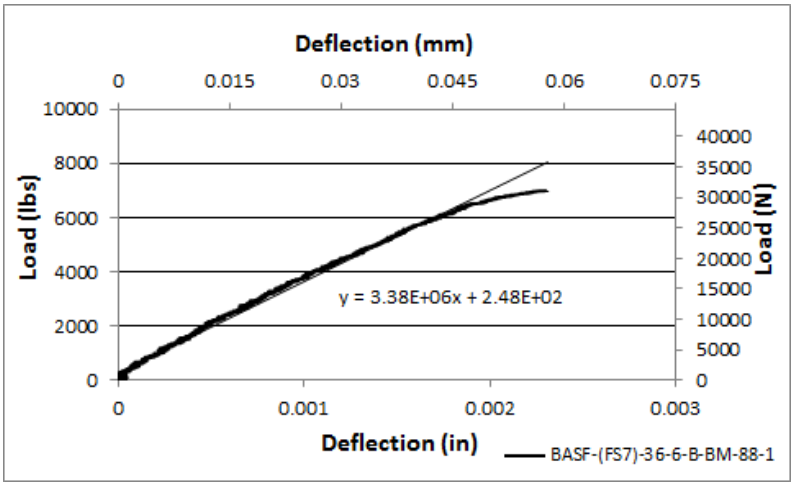

(b)

Figure B29 BASF-(FS7)-36-6-B-BM-88-2 (a) Load-Deflection Plot and (b) Modulus of Elasticity Plot.

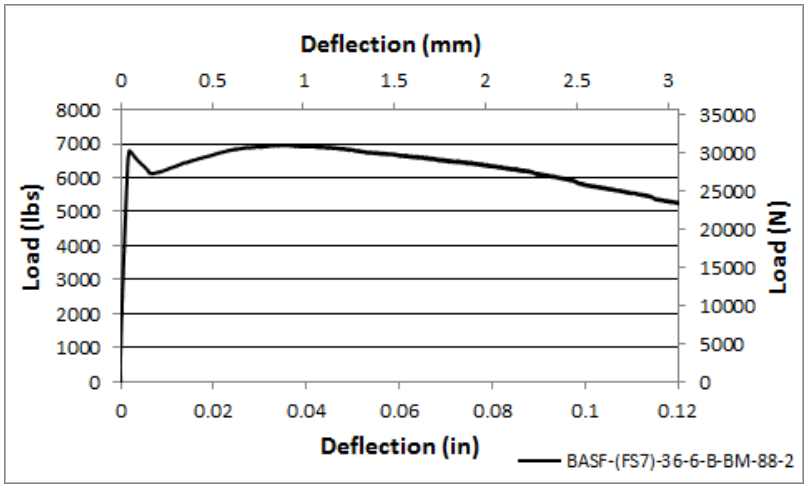

(a)

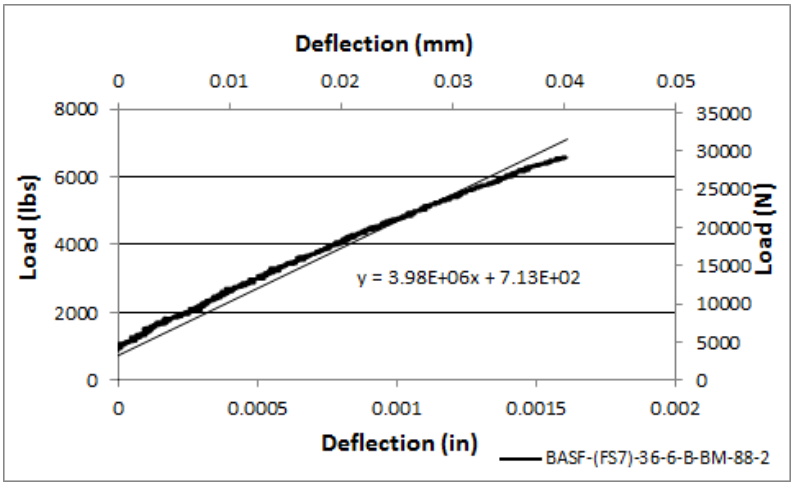

(b)

Figure B30 BASF-(FS7)-36-6-B-BM-88-2 (a) Load-Deflection Plot and (b) Modulus of Elasticity Plot.

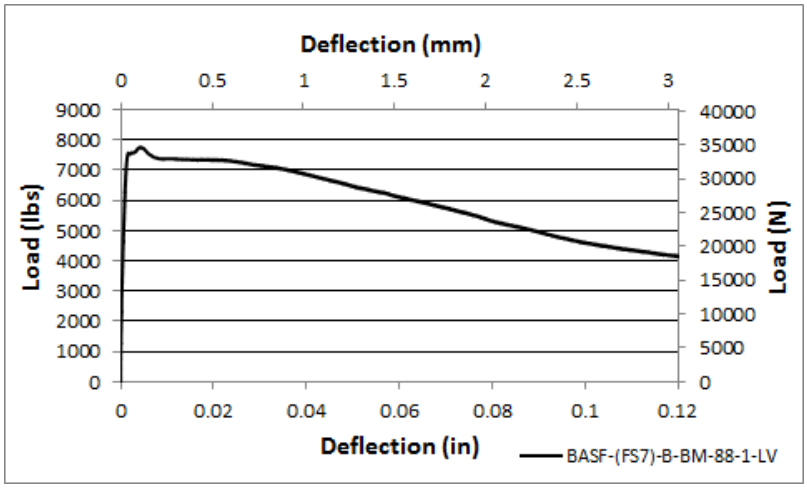

(a)

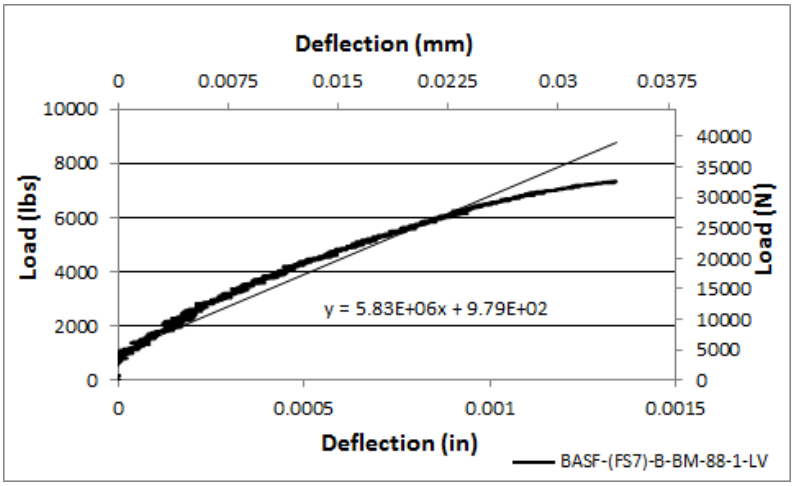

(b)

(c)

Figure B31 BASF-(FS7)-B-BM-88-1-LV (a) Load-Deflection Plot, (b) Modulus of Elasticity Plot, and (c) Crack Picture.

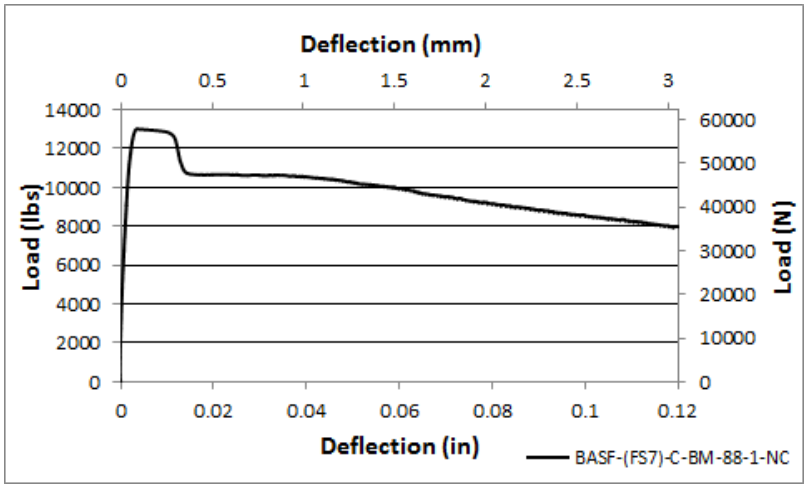

(a)

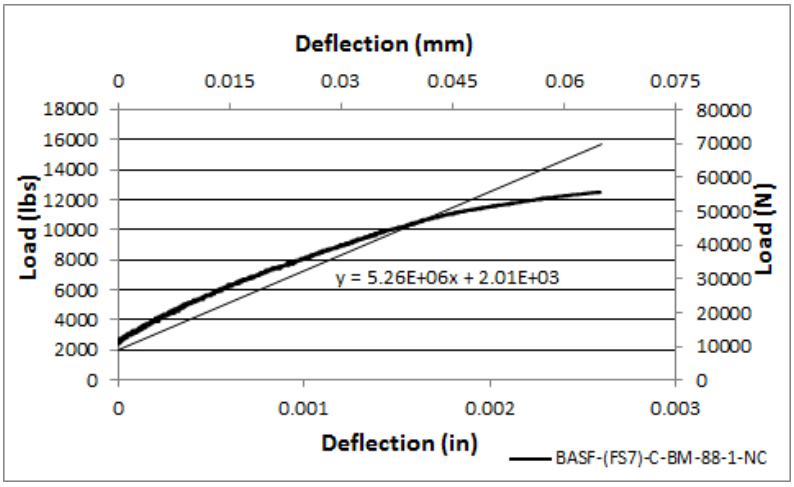

(b)

(c)

Figure B1 BASF-(FS7)-C-BM-88-1-NC (a) Load-Deflection Plot, (b) Modulus of Elasticity Plot, and (c) Crack Picture.

APPENDIX C

SYNTHETIC BEAM GRAPHS

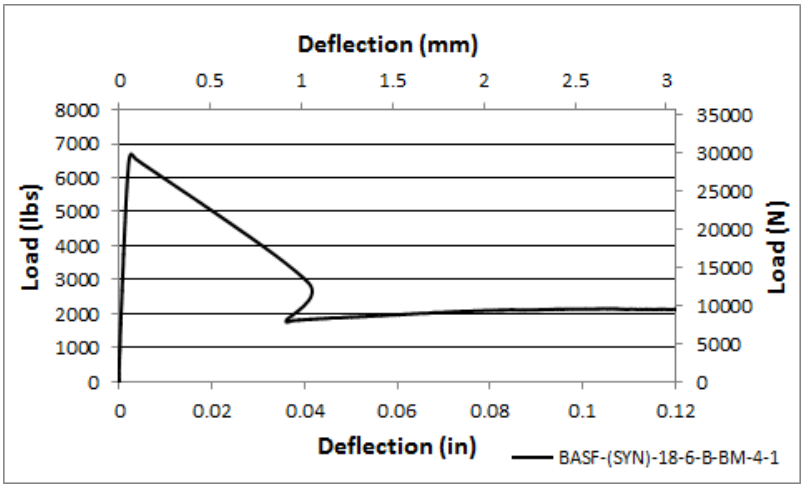

(a)

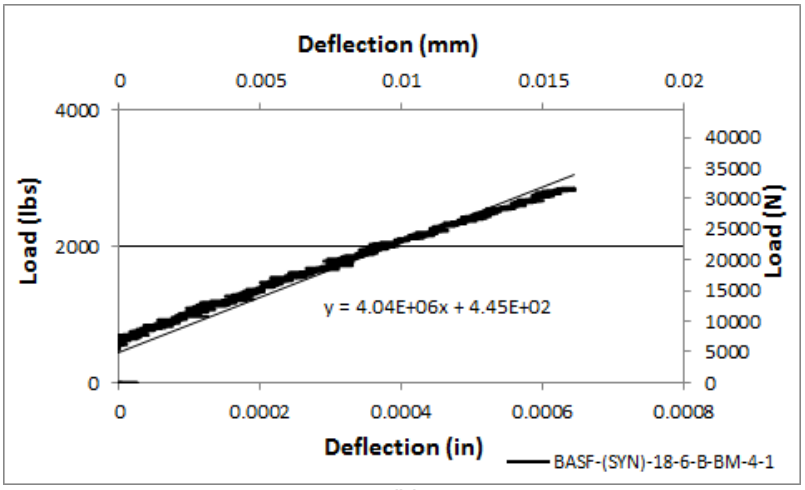

(b)

(c)

Figure C1 BASF-(SYN)-18-6-B-BM-4-1(a) Load-Deflection Plot, (b) Modulus of Elasticity Plot, and (c) Crack Picture.

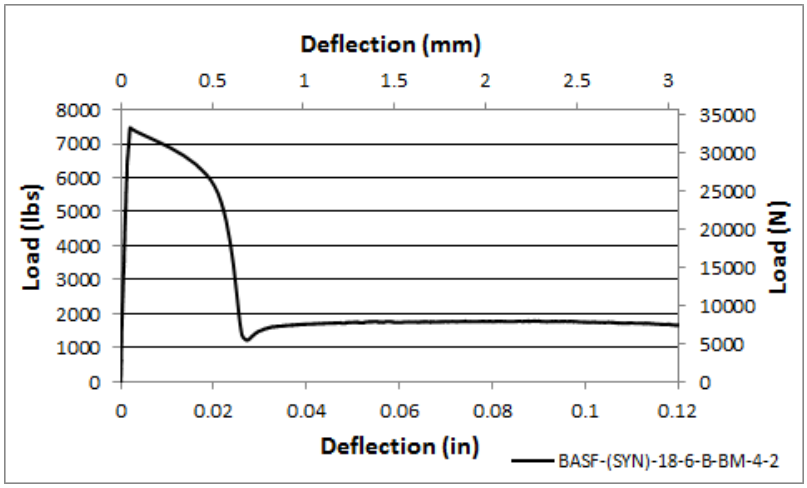

(a)

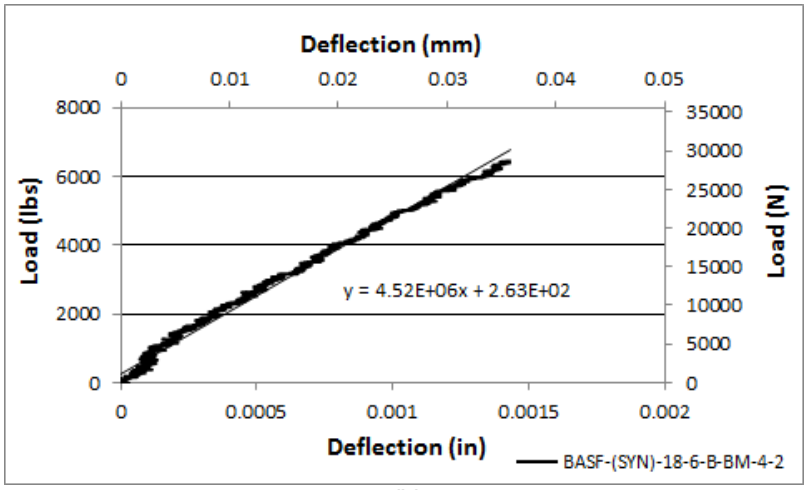

(b)

(c)

Figure C2 BASF-(SYN)-18-6-B-BM-4-2 (a) Load-Deflection Plot, (b) Modulus of Elasticity Plot, and (c) Crack Picture.

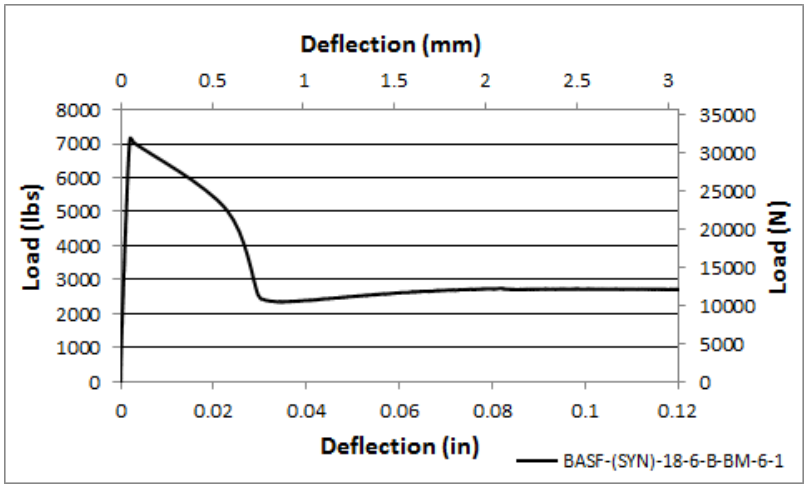

(a)

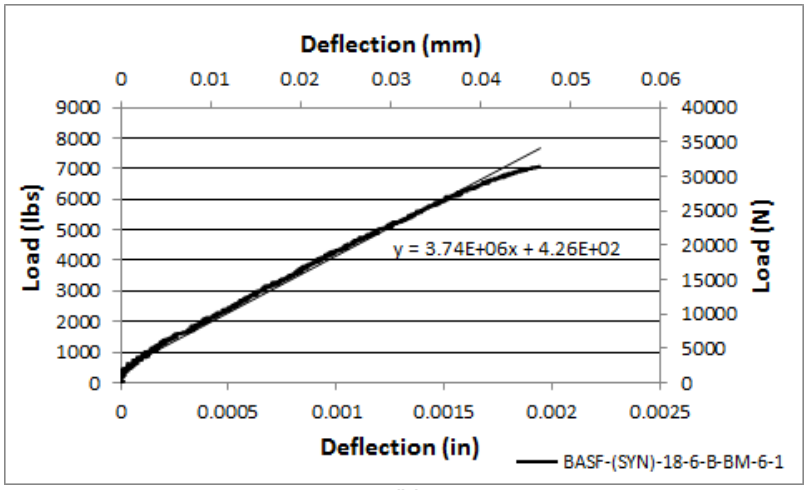

(b)

(c)

Figure C3 BASF-(SYN)-18-6-B-BM-6-1(a) Load-Deflection Plot, (b) Modulus of Elasticity Plot, and (c) Crack Picture.

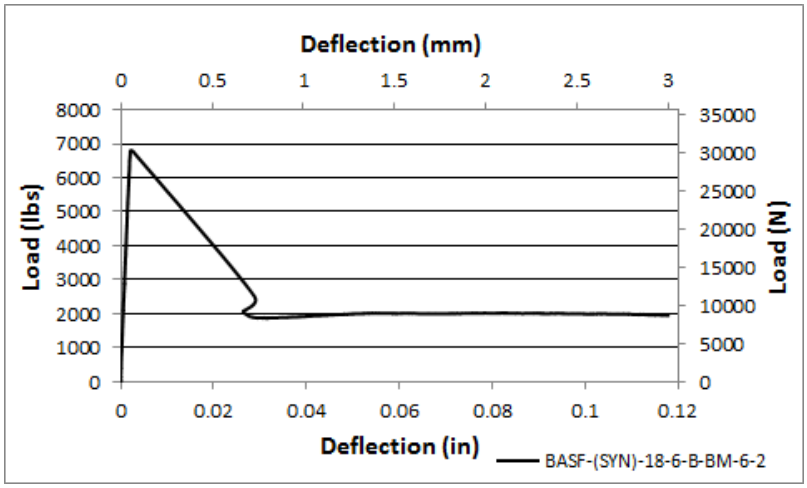

(a)

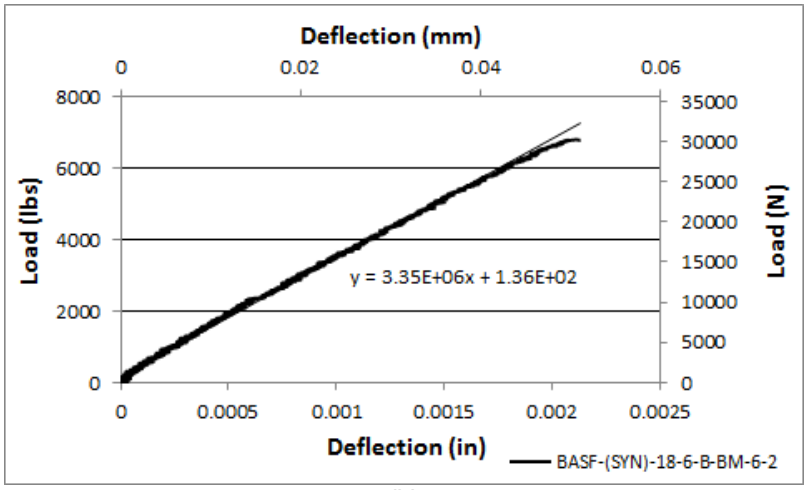

(b)

(c)

Figure C4 BASF-(SYN)-18-6-B-BM-6-2 (a) Load-Deflection Plot, (b) Modulus of Elasticity Plot, and (c) Crack Picture.

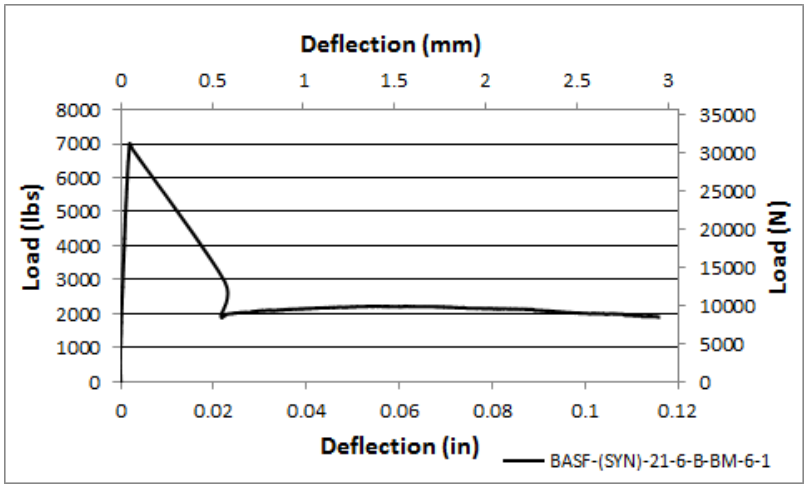

(a)

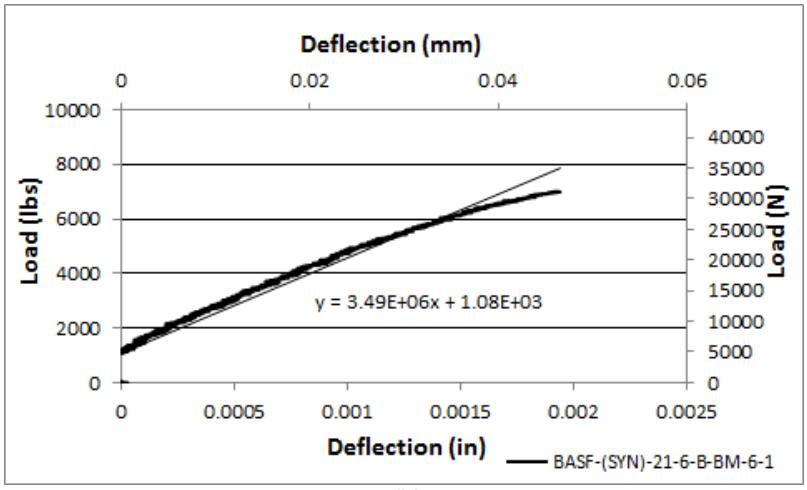

(b)

(c)

Figure C5 BASF-(SYN)-21-6-B-BM-6-1(a) Load-Deflection Plot, (b) Modulus of Elasticity Plot, and (c) Crack Picture.

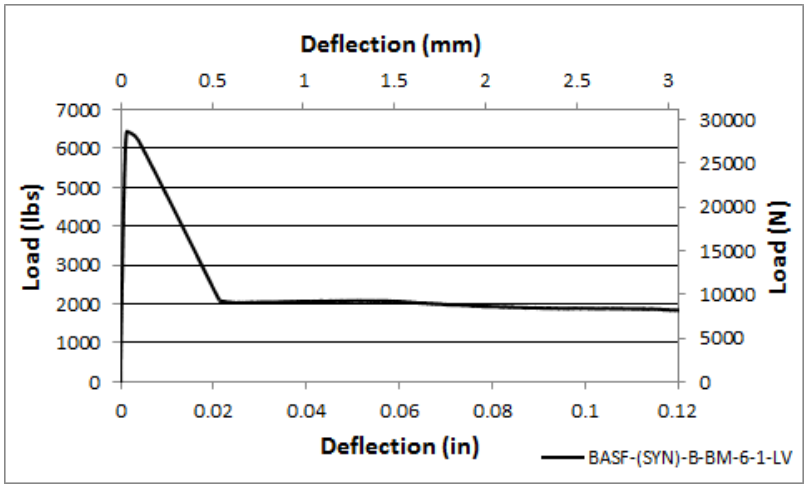

(a)

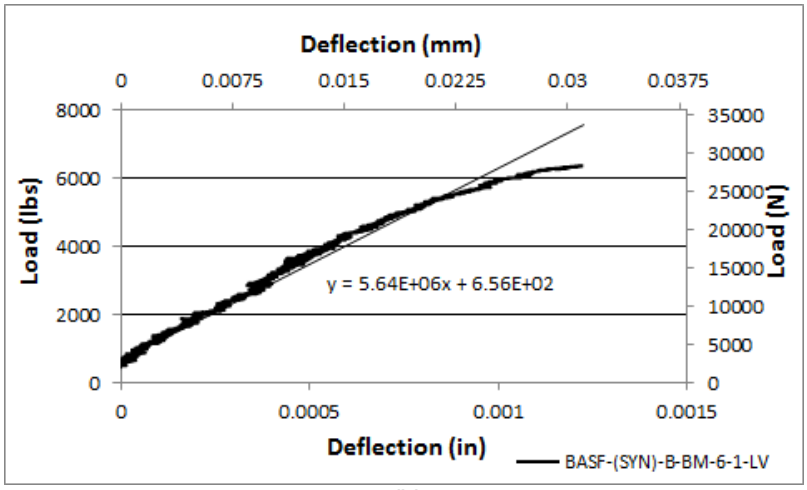

(b)

(c)

Figure C6 BASF-(SYN)-B-BM-6-1-LV (a) Load-Deflection Plot, (b) Modulus of Elasticity Plot, and (c) Crack Picture.

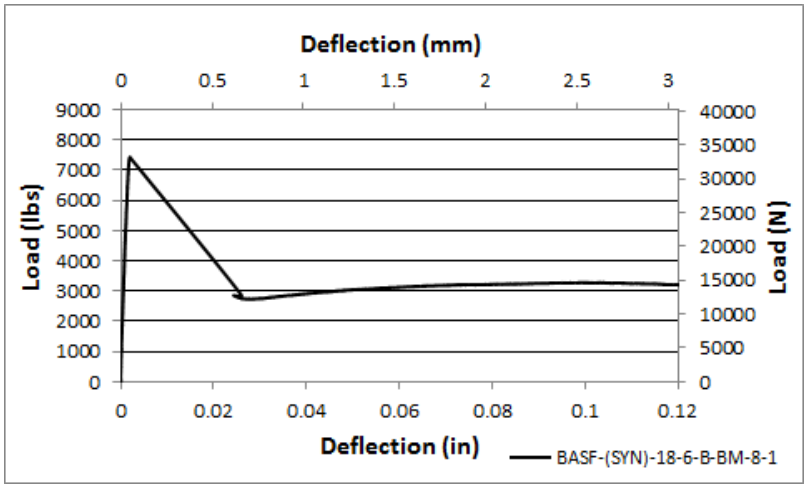

(a)

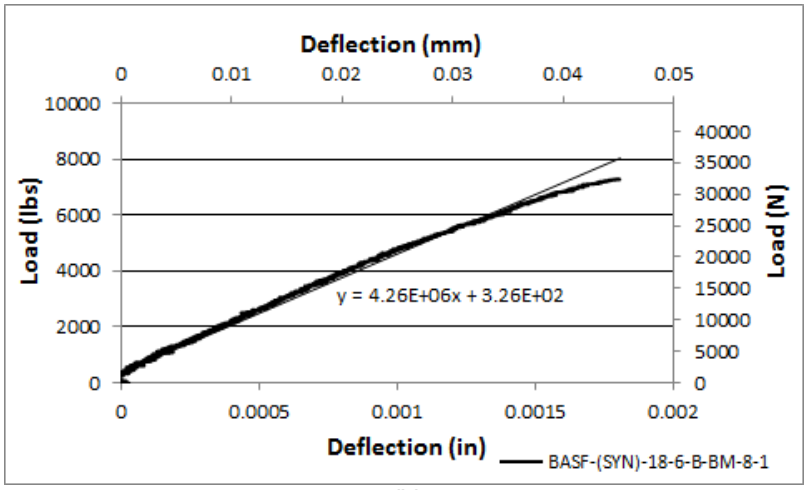

(b)

(c)

Figure C7 BASF-(SYN)-18-6-B-BM-8-1(a) Load-Deflection Plot, (b) Modulus of Elasticity Plot, and (c) Crack Picture.

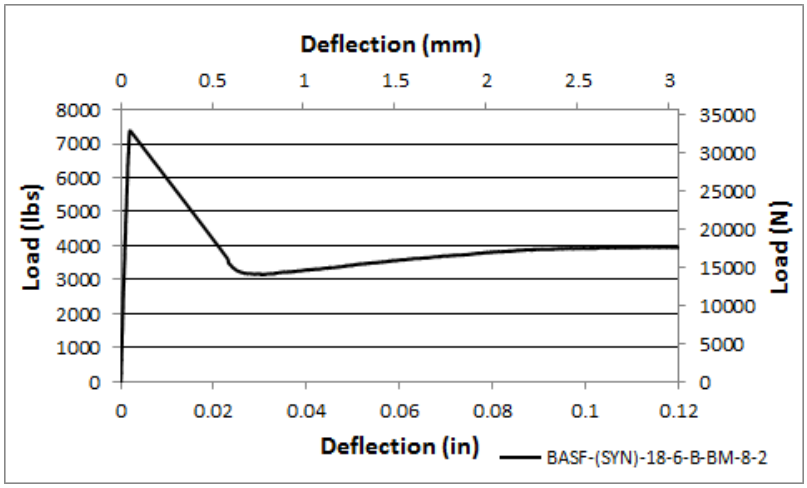

(a)

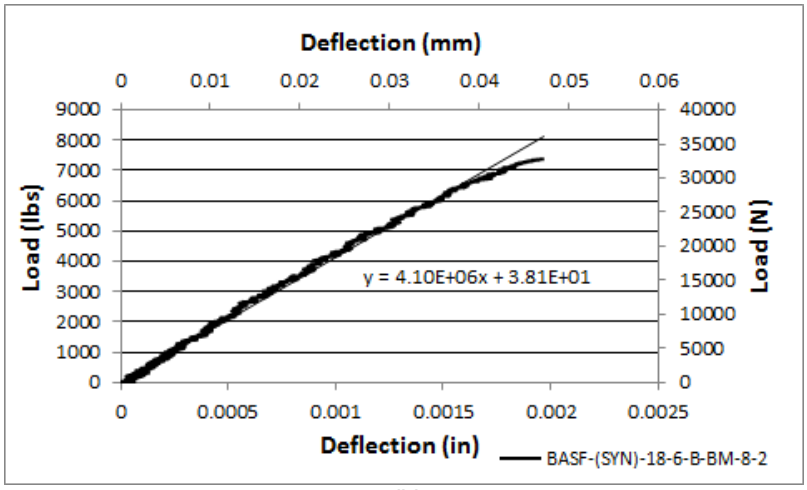

(b)

Figure C8 BASF-(SYN)-18-6-B-BM-8-2(a) Load-Deflection Plot and (b) Modulus of Elasticity Plot.

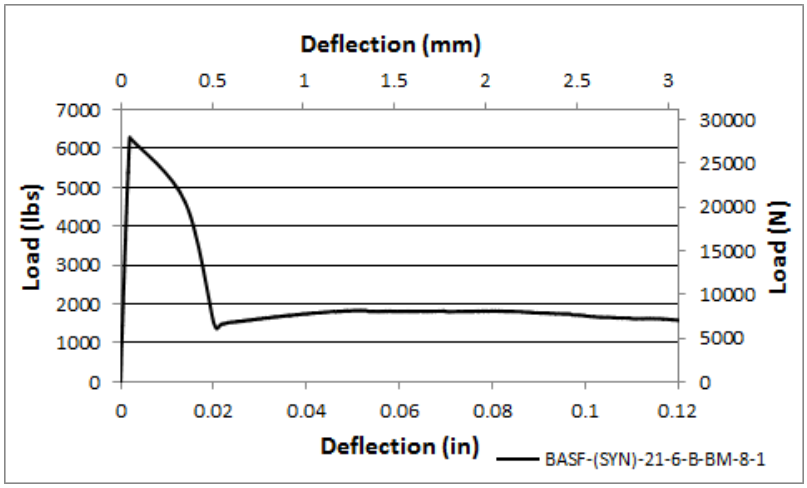

(a)

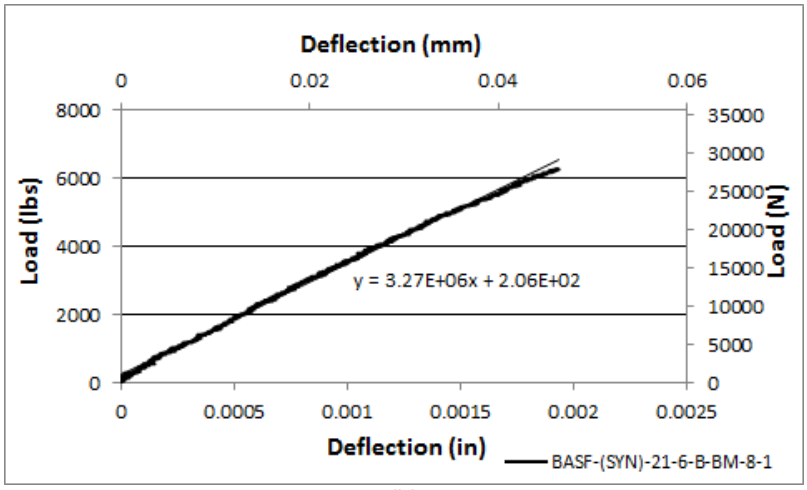

(b)

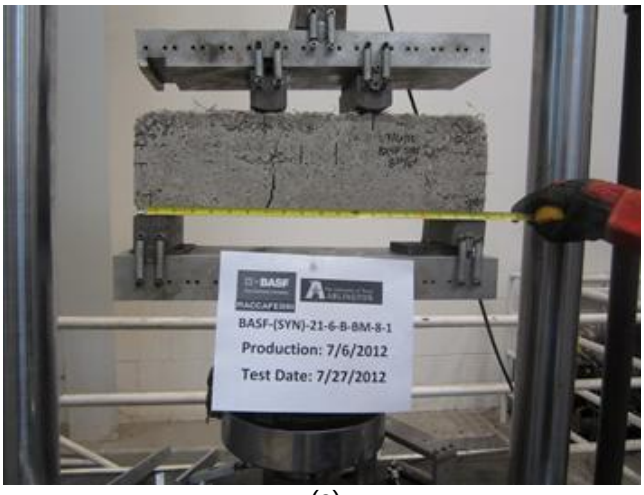

(c)

Figure C9 BASF-(SYN)-21-6-B-BM-8-1NC (a) Load-Deflection Plot, (b) Modulus of Elasticity Plot, and (c) Crack Picture.

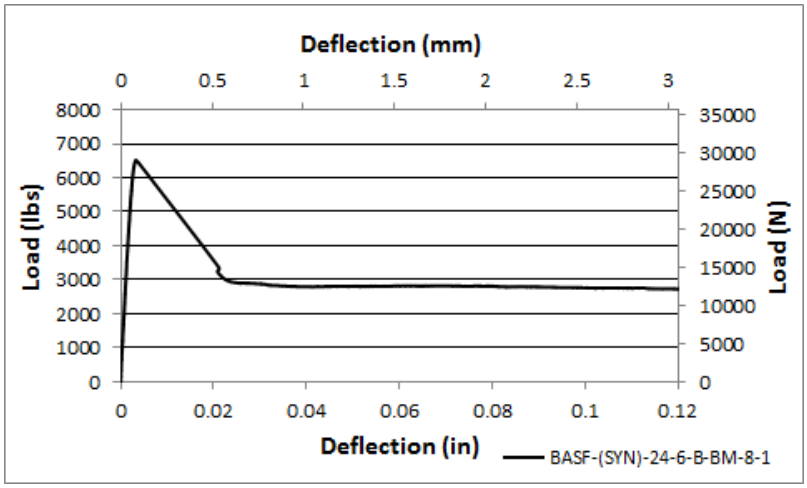

(a)

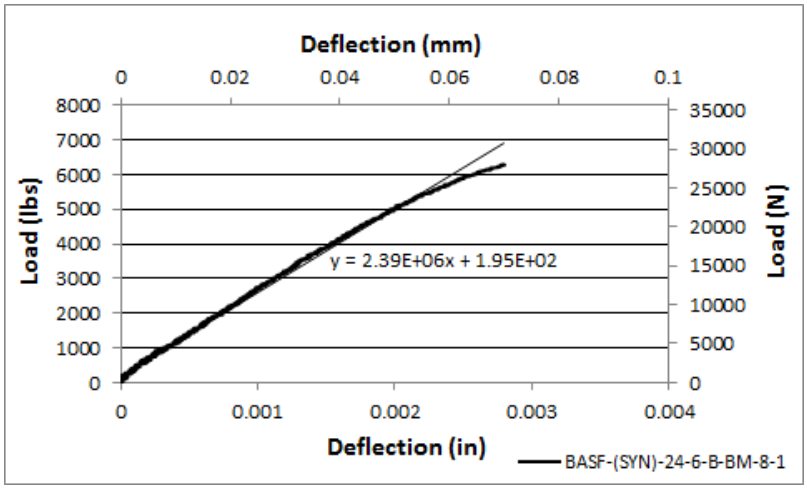

(b)

(c)

Figure C10 BASF-(SYN)-24-6-B-BM-8-1(a) Load-Deflection Plot, (b) Modulus of Elasticity Plot, and (c) Crack Picture.

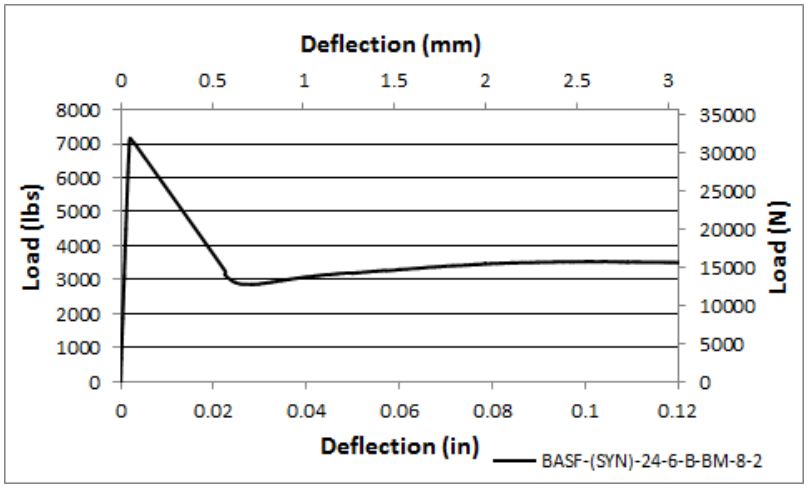

(a)

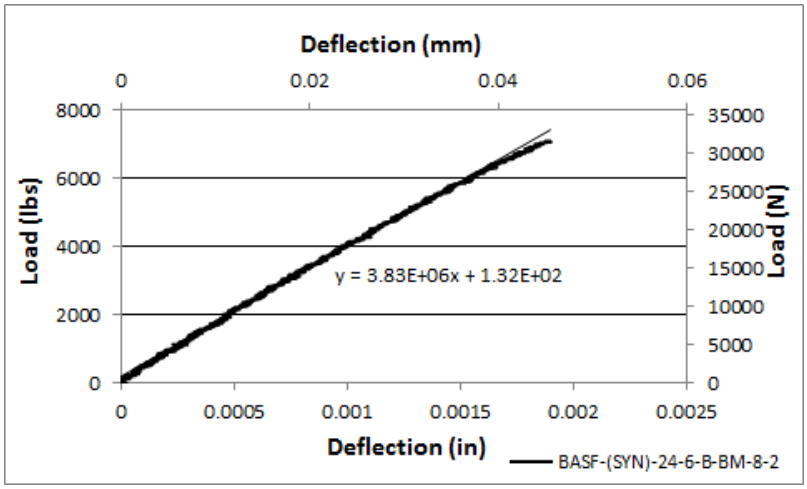

(b)

(c)

Figure C11 BASF-(SYN)-24-6-B-BM-8-2 (a) Load-Deflection Plot, (b) Modulus of Elasticity Plot, and (c) Crack Picture.

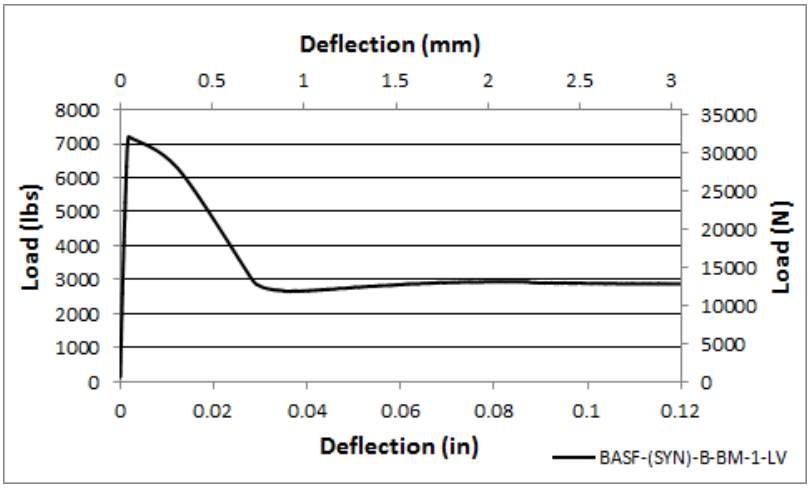

(a)

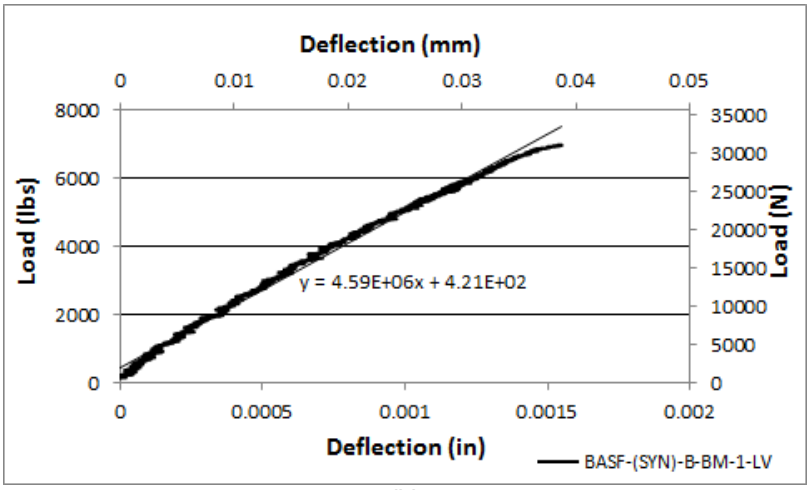

(b)

(c)

Figure C12 BASF-(SYN)-B-BM-8-1-LV (a) Load-Deflection Plot, (b) Modulus of Elasticity Plot, and (c) Crack Picture.

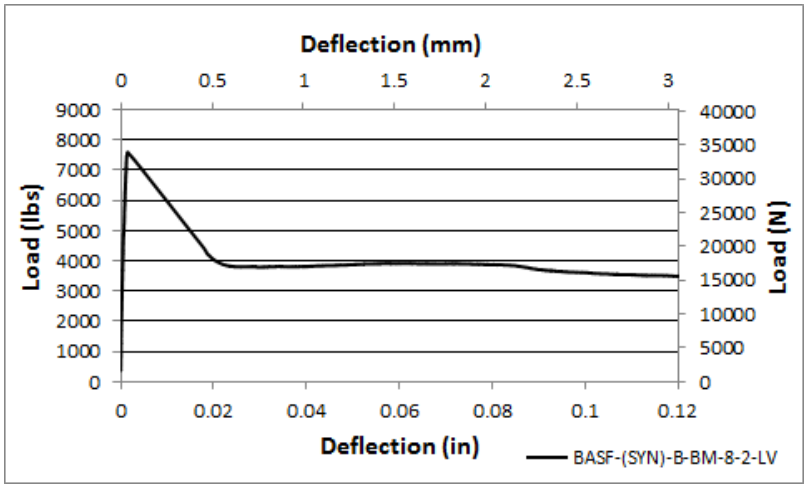

(a)

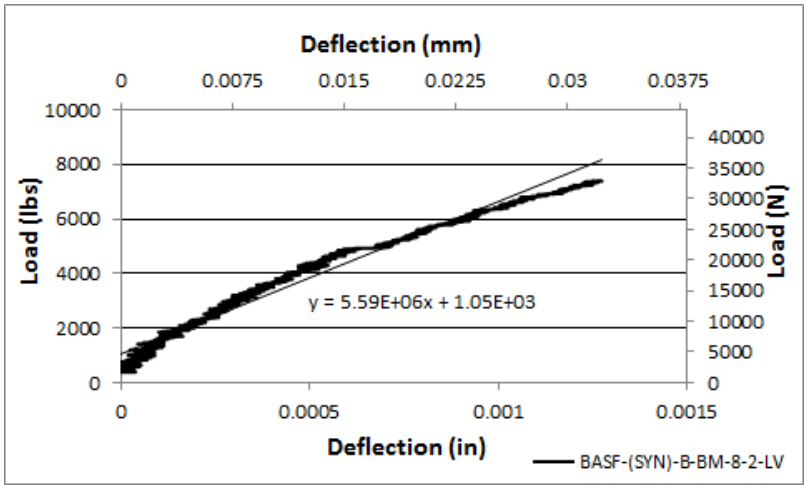

(b)

(c)

Figure C13 BASF-(SYN)-B-BM-8-2-LV (a) Load-Deflection Plot, (b) Modulus of Elasticity Plot, and (c) Crack Picture.

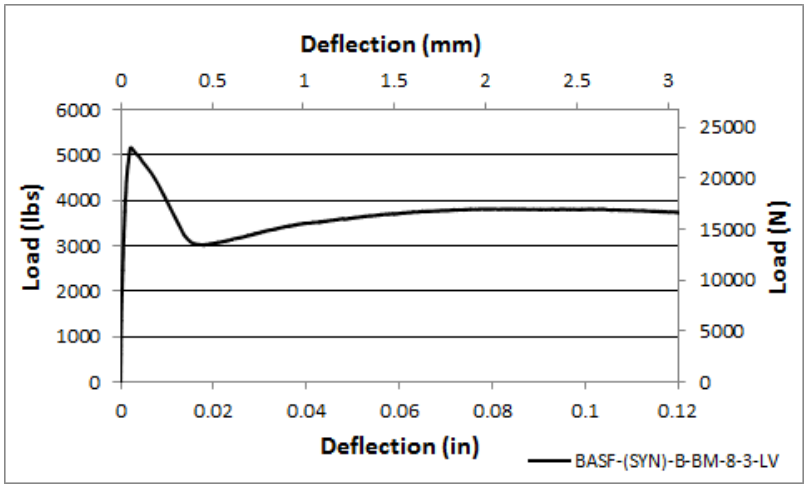

(a)

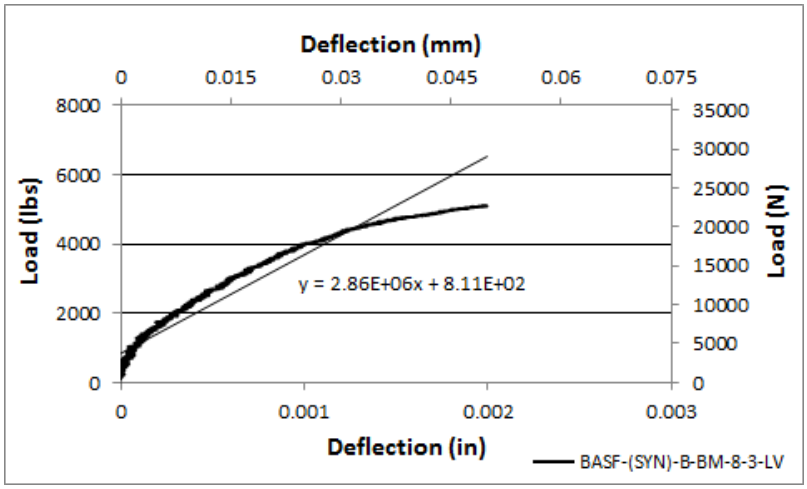

(b)

(c)

Figure C14 BASF-(SYN)-B-BM-8-3-LV (a) Load-Deflection Plot, (b) Modulus of Elasticity Plot, and (c) Crack Picture.

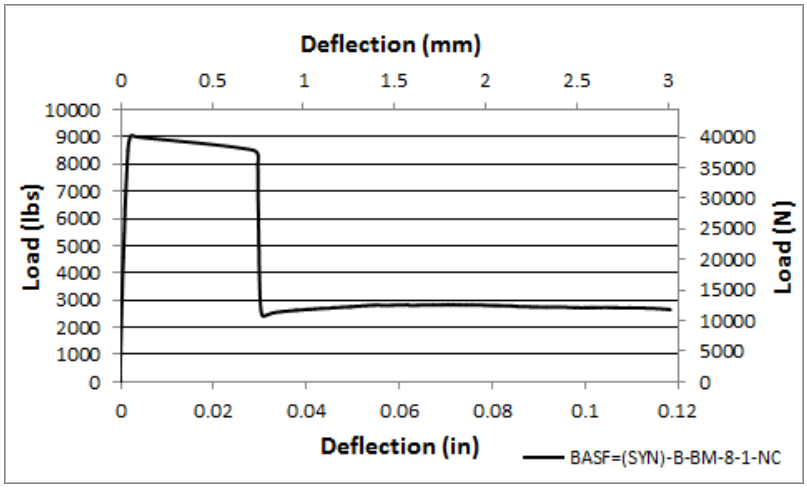

(a)

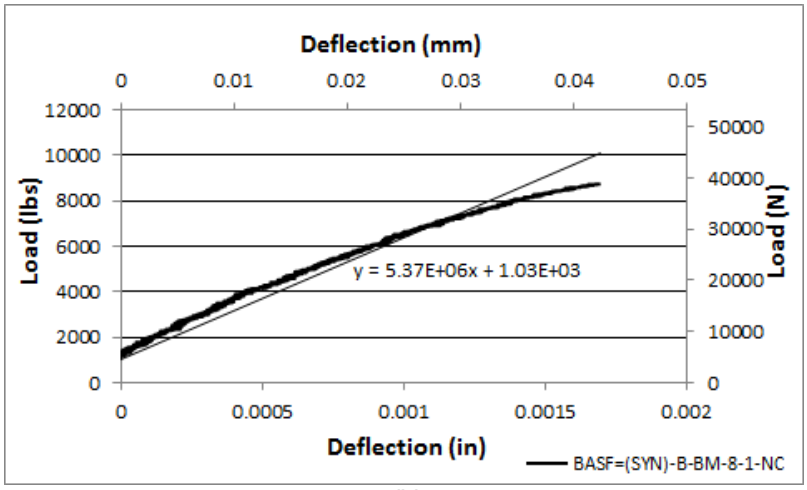

(b)

(c)

Figure C15 BASF-(SYN)-B-BM-8-1-NC (a) Load-Deflection Plot, (b) Modulus of Elasticity Plot, and (c) Crack Picture.

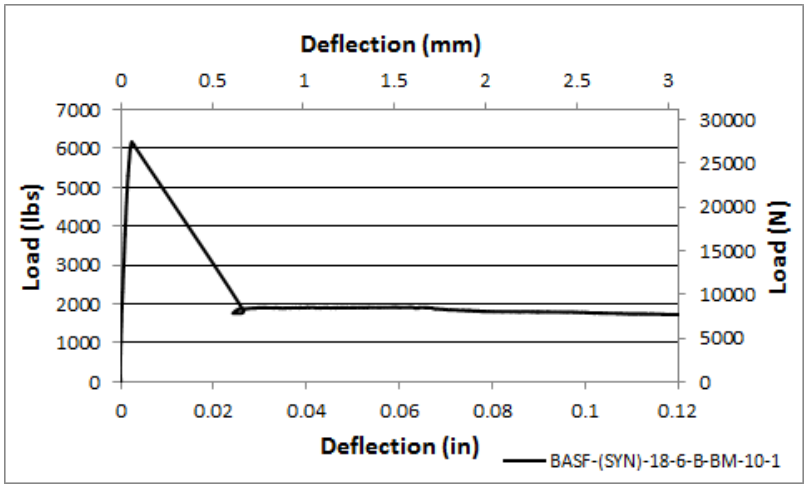

(a)

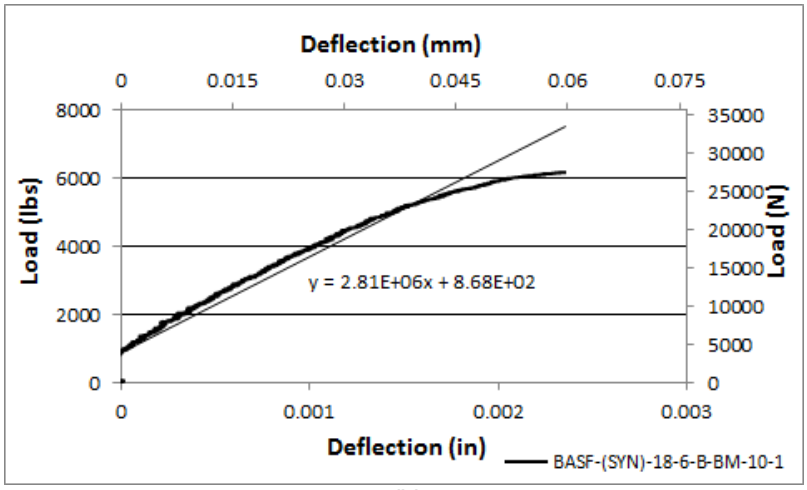

(b)

(c)

Figure C16 BASF-(SYN)-18-6-B-BM-10-1(a) Load-Deflection Plot, (b) Modulus of Elasticity Plot, and (c) Crack Picture.

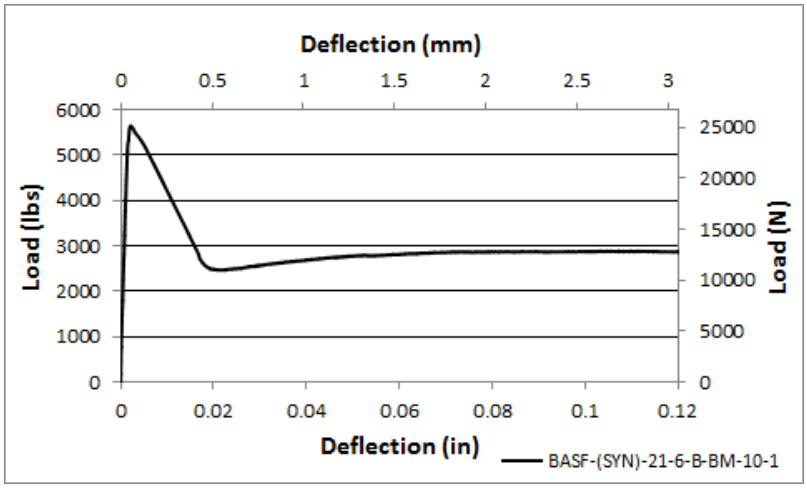

(a)

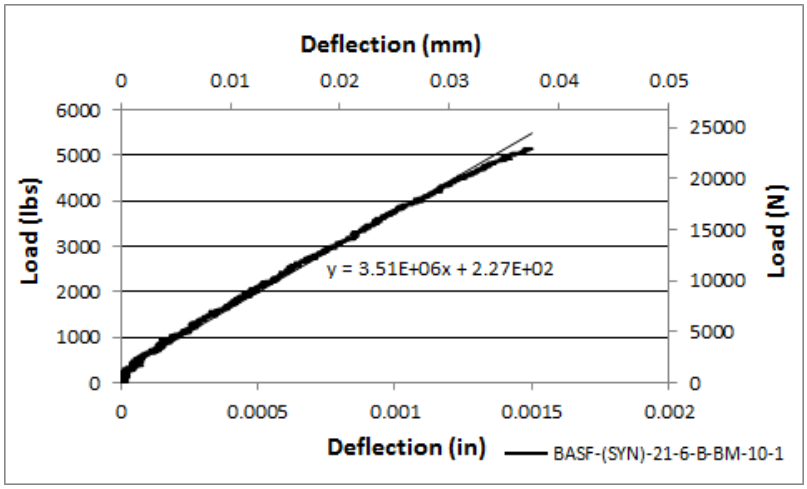

(b)

(c)

Figure C17 BASF-(SYN)-21-6-B-BM-10- (a) Load-Deflection Plot, (b) Modulus of Elasticity Plot, and (c) Crack Picture.

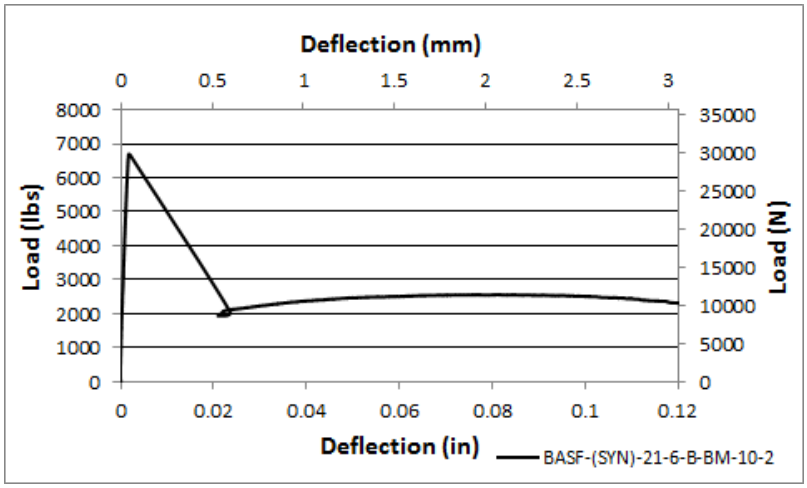

(a)

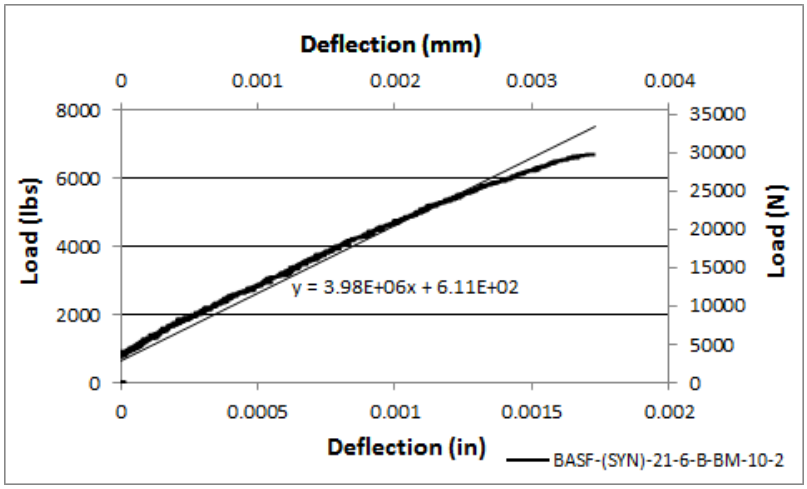

(b)

(c)

Figure C18 BASF-(SYN)-21-6-B-BM-10-2 (a) Load-Deflection Plot, (b) Modulus of Elasticity Plot, and (c) Crack Picture.

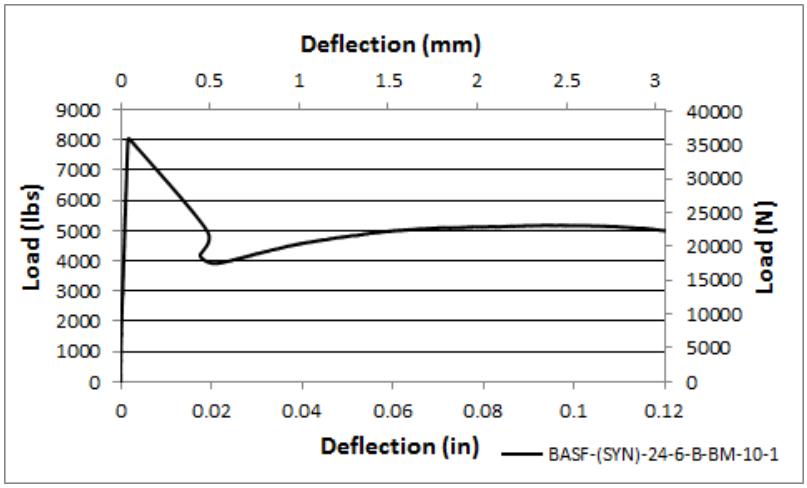

(a)

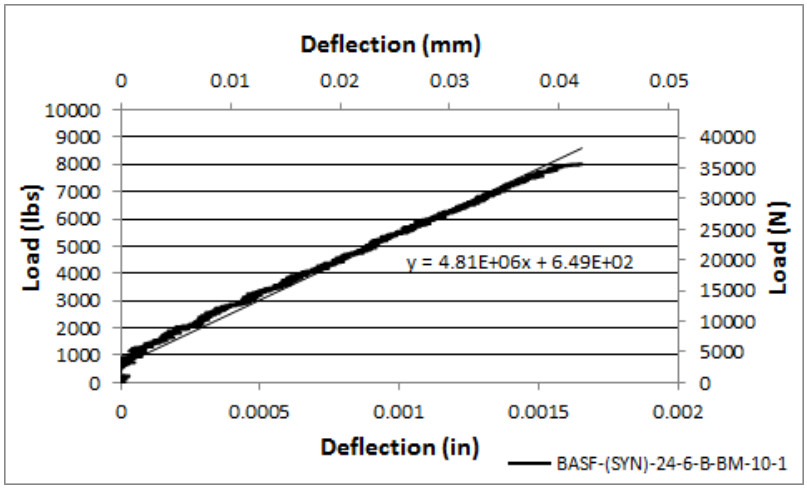

(b)

(c)

Figure C19 BASF-(SYN)-24-6-B-BM-10-1(a) Load-Deflection Plot, (b) Modulus of Elasticity Plot, and (c) Crack Picture.

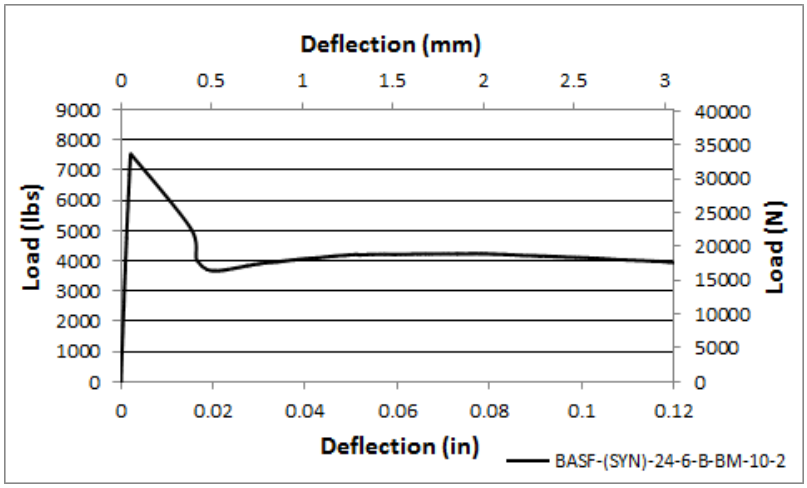

(a)

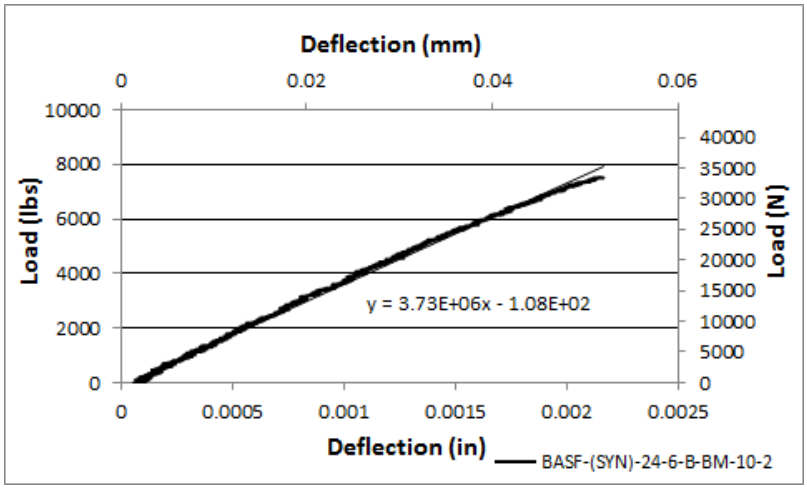

(b)

(c)

Figure C20 BASF-(SYN)-24-6-B-BM-10-2 (a) Load-Deflection Plot, (b) Modulus of Elasticity Plot, and (c) Crack Picture.

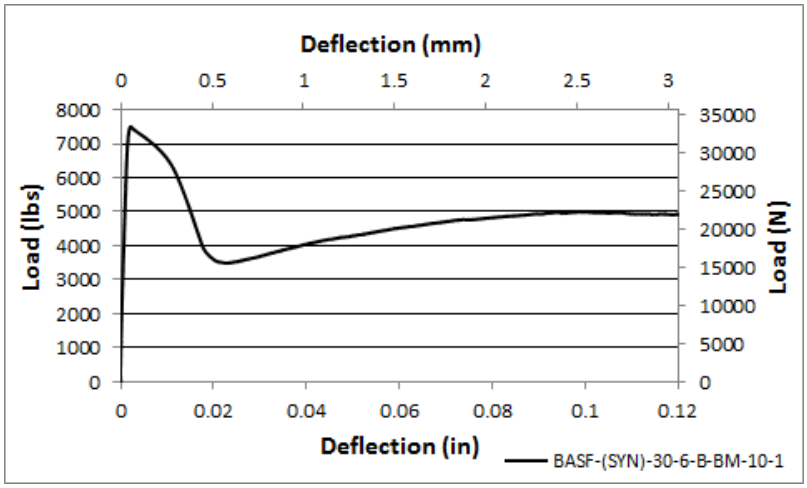

(a)

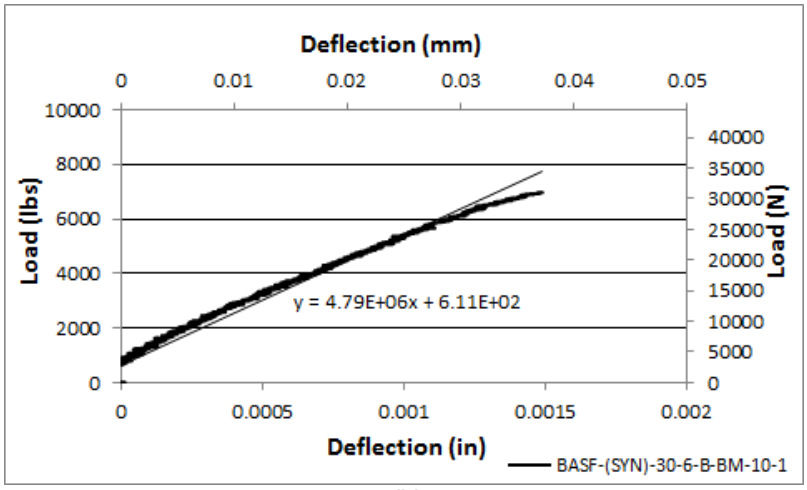

(b)

(c)

Figure C21 BASF-(SYN)-30-6-B-BM-10-1(a) Load-Deflection Plot, (b) Modulus of Elasticity Plot, and (c) Crack Picture.

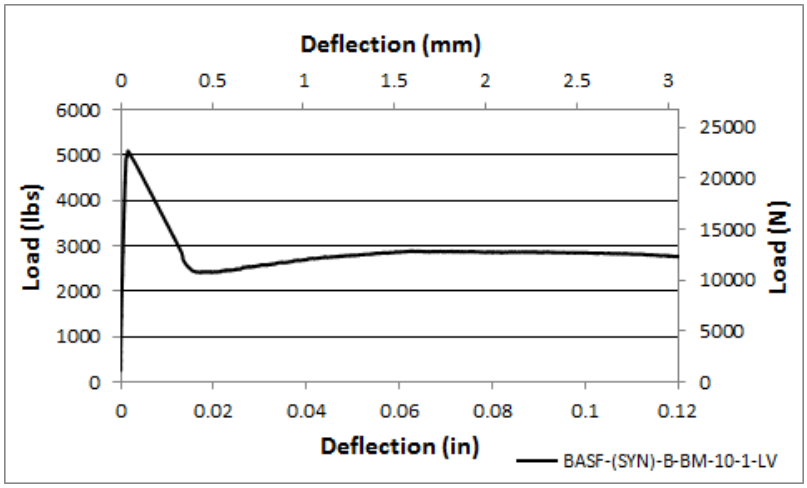

(a)

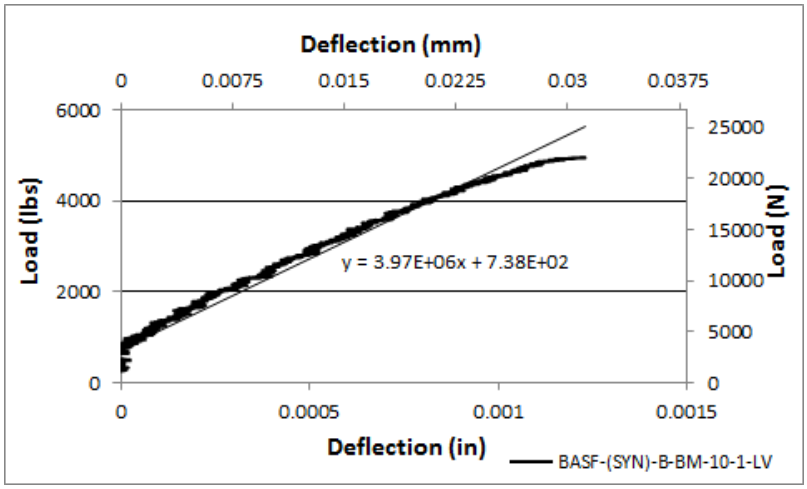

(b)

(c)

Figure C22 BASF-(SYN)-B-BM-10-1-LV (a) Load-Deflection Plot, (b) Modulus of Elasticity Plot, and (c) Crack Picture.

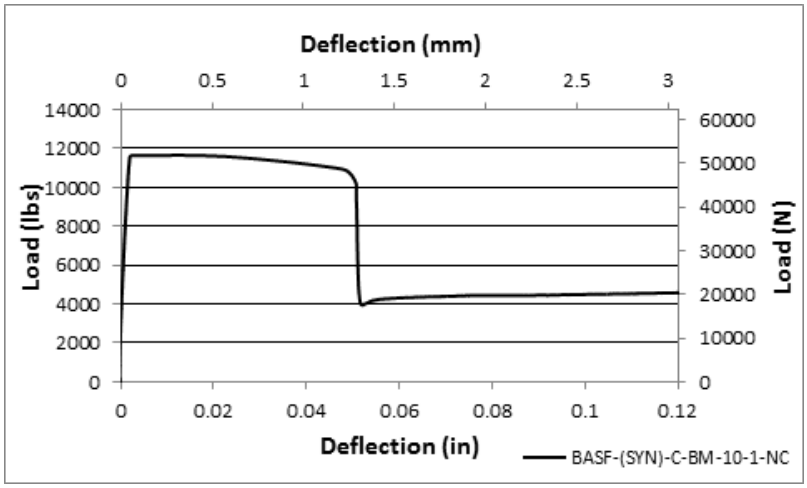

(a)

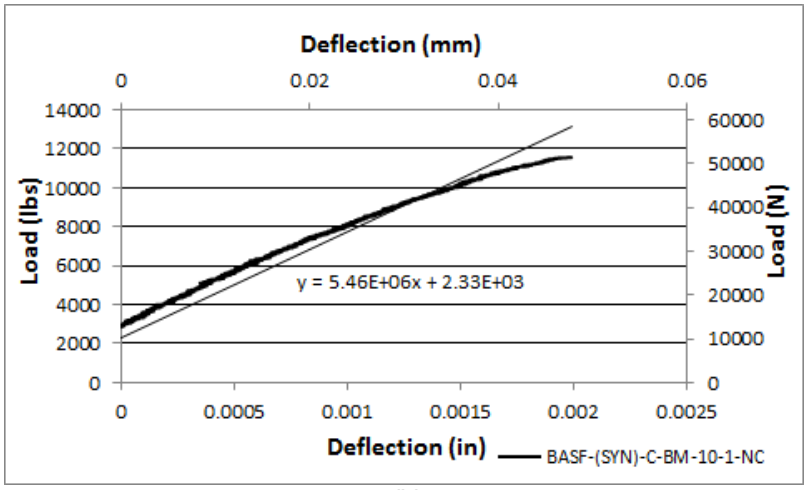

(b)

(c)

Figure C23 BASF-(SYN)-C-BM-10-1-NC (a) Load-Deflection Plot, (b) Modulus of Elasticity Plot, and (c) Crack Picture.

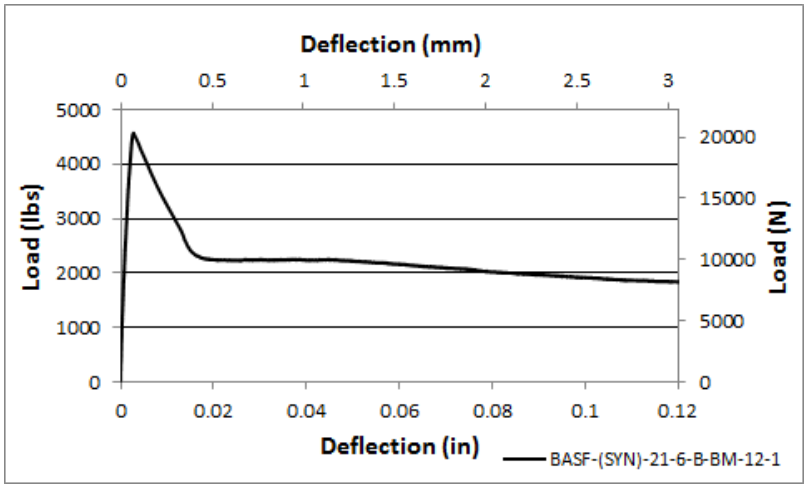

(a)

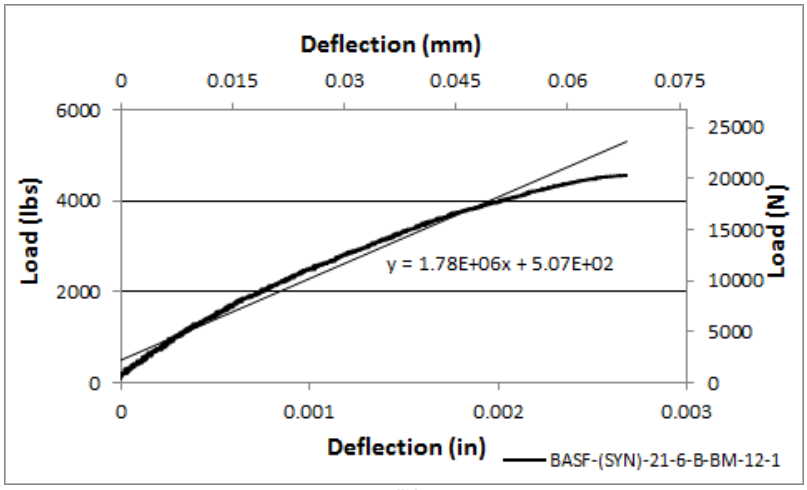

(b)

(c)

Figure C24 BASF-(SYN)-21-6-B-BM-12-1(a) Load-Deflection Plot, (b) Modulus of Elasticity Plot, and (c) Crack Picture.

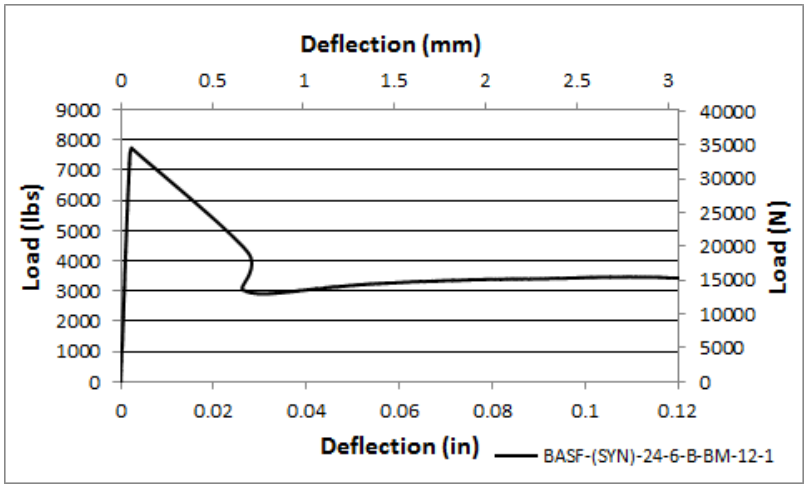

(a)

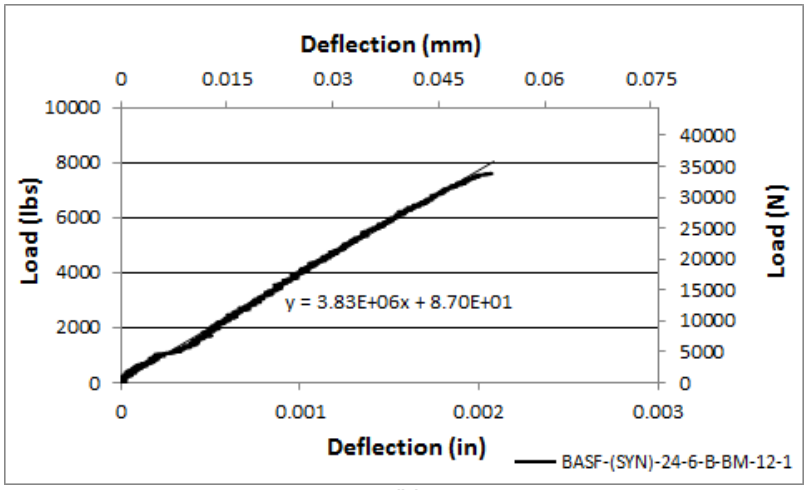

(b)

(c)

Figure C25 BASF-(SYN)-24-6-B-BM-12-1(a) Load-Deflection Plot, (b) Modulus of Elasticity Plot, and (c) Crack Picture.

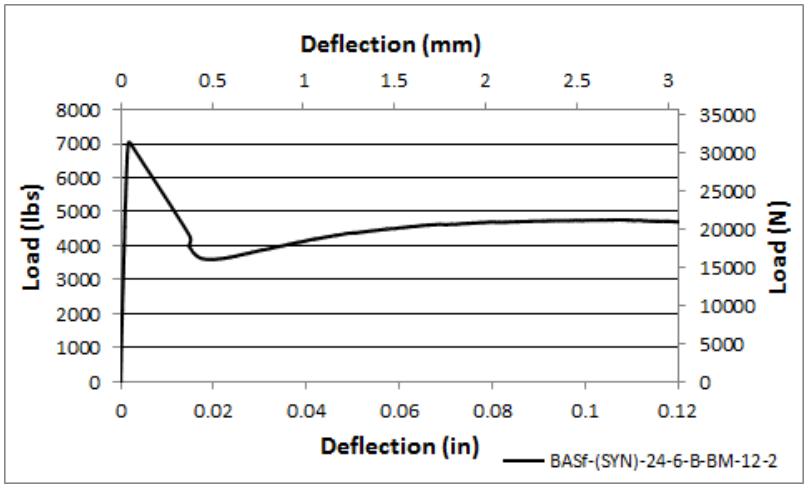

(a)

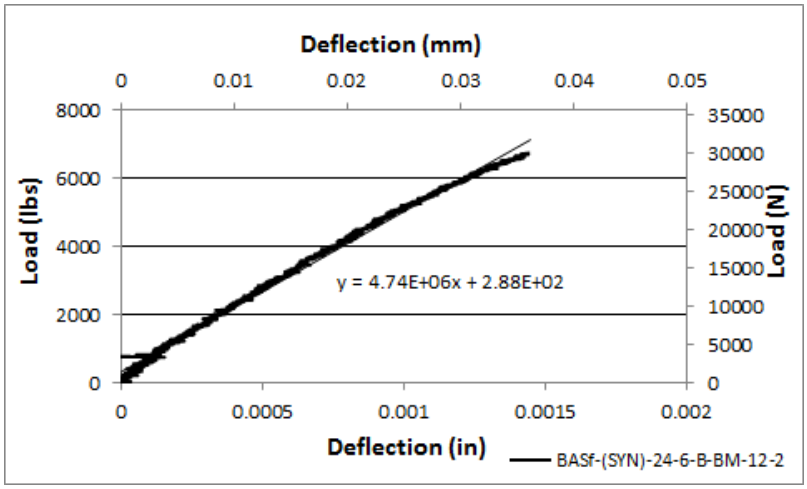

(b)

Figure C26 BASF-(SYN)-24-6-B-BM-12-2(a) Load-Deflection Plot and (b) Modulus of Elasticity Plot.

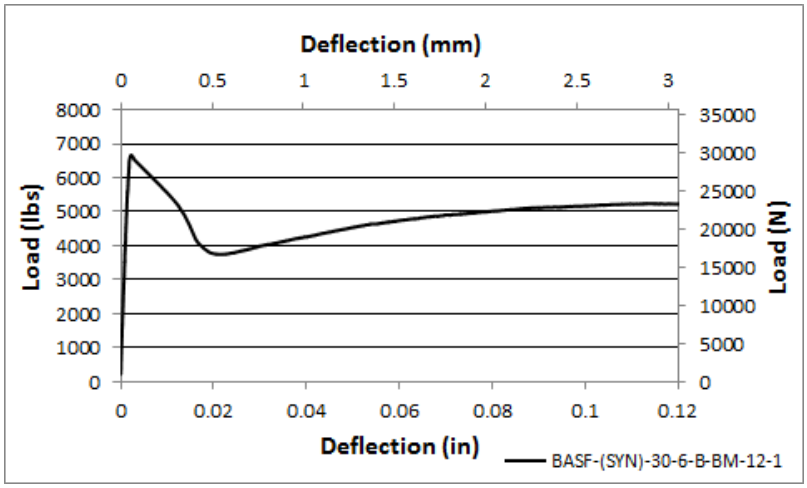

(a)

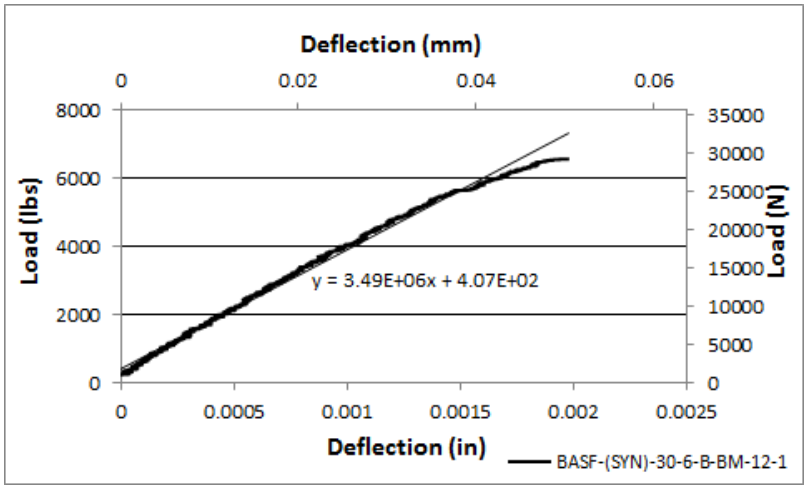

(b)

(c)

Figure C27 BASF-(SYN)-30-6-B-BM-12-1(a) Load-Deflection Plot, (b) Modulus of Elasticity Plot, and (c) Crack Picture.

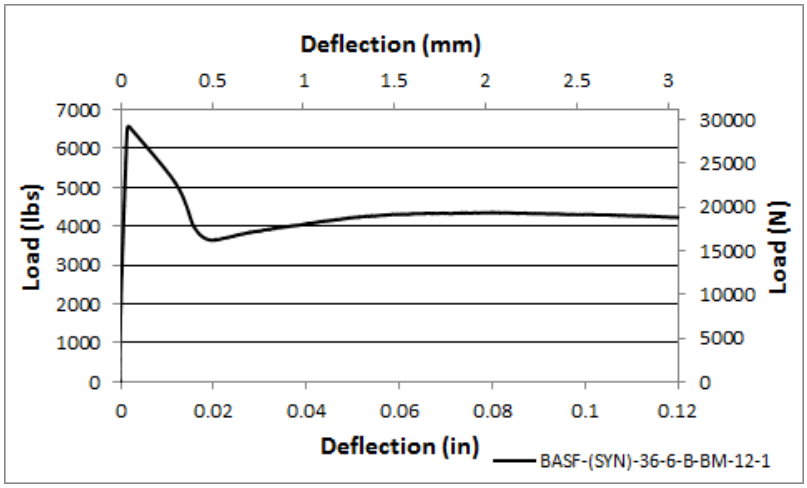

(a)

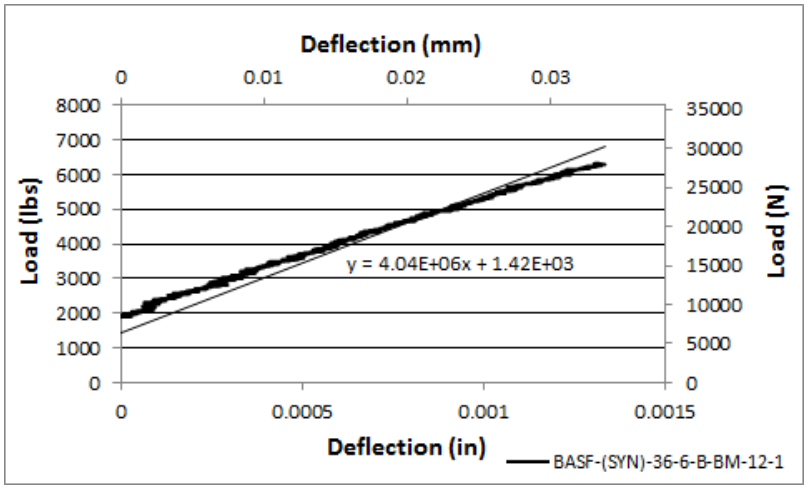

(a)

(c)

Figure C28 BASF-(SYN)-36-6-B-BM-12-1(a) Load-Deflection Plot, (b) Modulus of Elasticity Plot, and (c) Crack Picture.

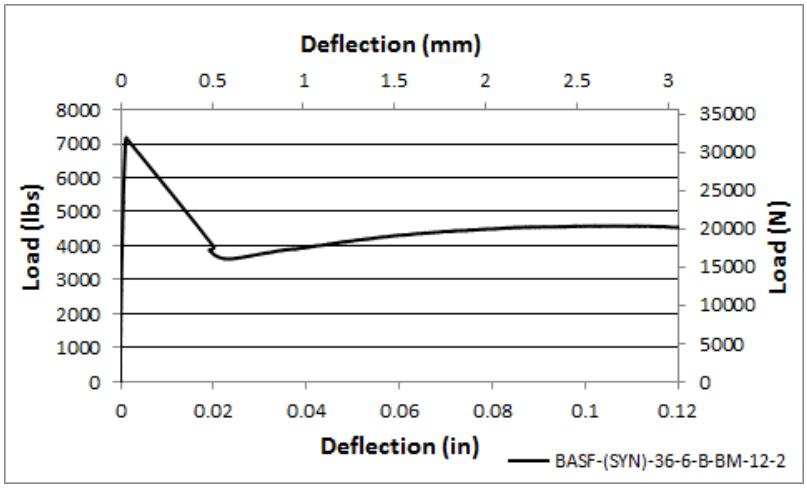

(a)

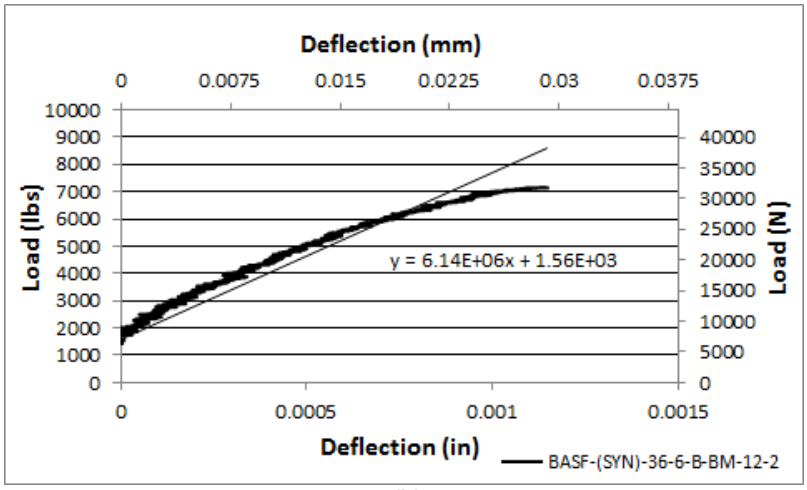

(b)

(c)

Figure C29 BASF-(SYN)-36-6-B-BM-12-2 (a) Load-Deflection Plot, (b) Modulus of Elasticity Plot, and (c) Crack Picture.

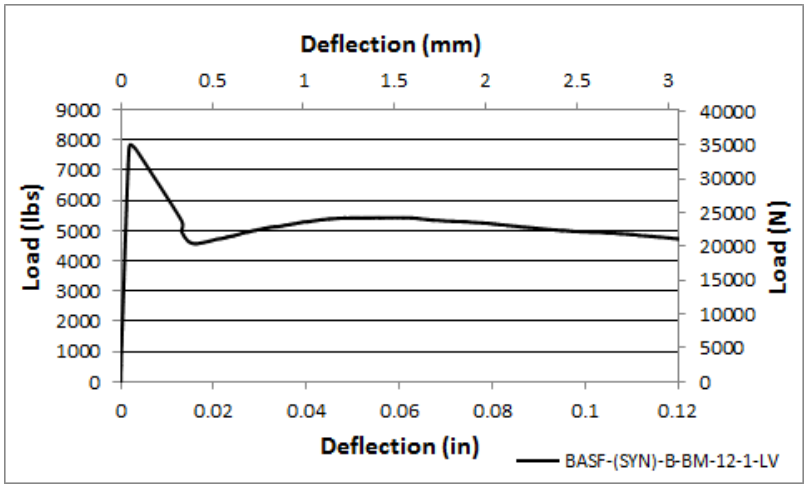

(a)

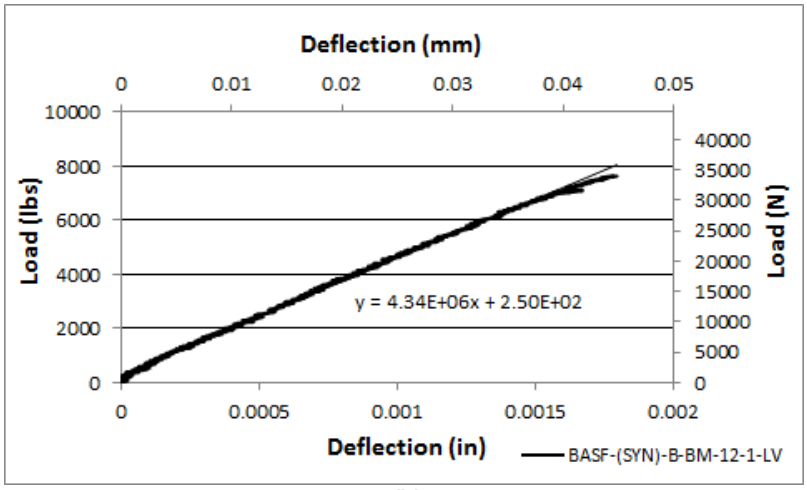

(b)

(c)

Figure C30 BASF-(SYN)-B-BM-12-1-LV (a) Load-Deflection Plot, (b) Modulus of Elasticity Plot, and (c) Crack Picture.

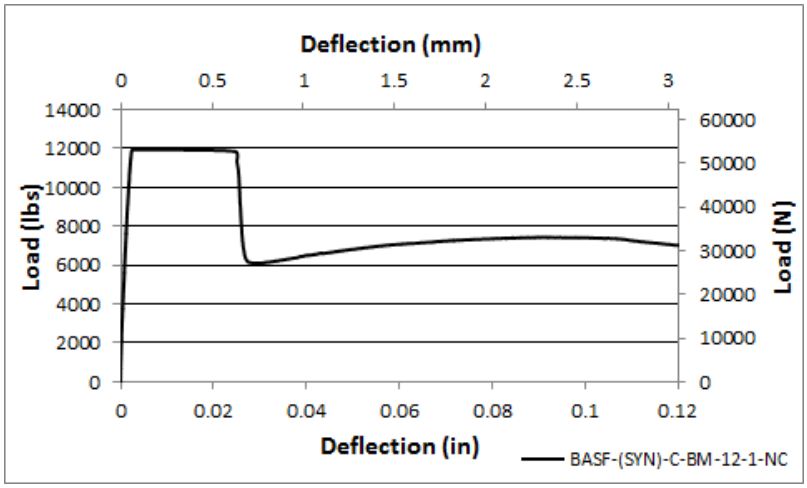

(a)

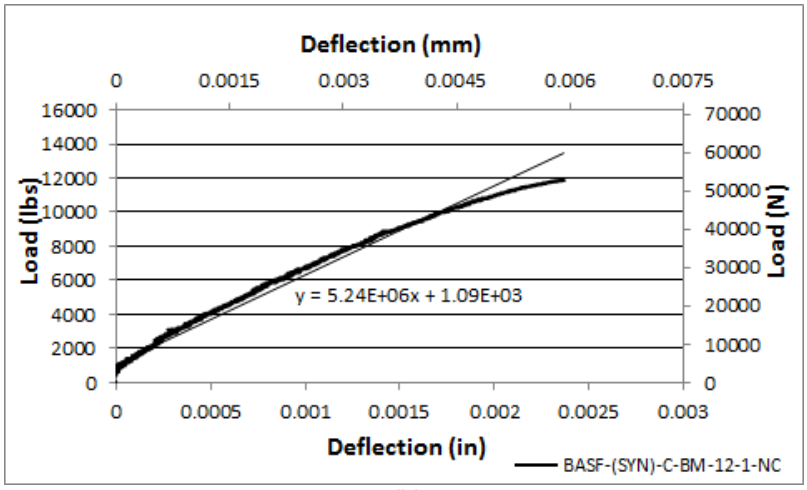

(b)

(c)

Figure C31 BASF-(SYN)-C-BM-12-1-NC (a) Load-Deflection Plot, (b) Modulus of Elasticity Plot, and (c) Crack Picture.

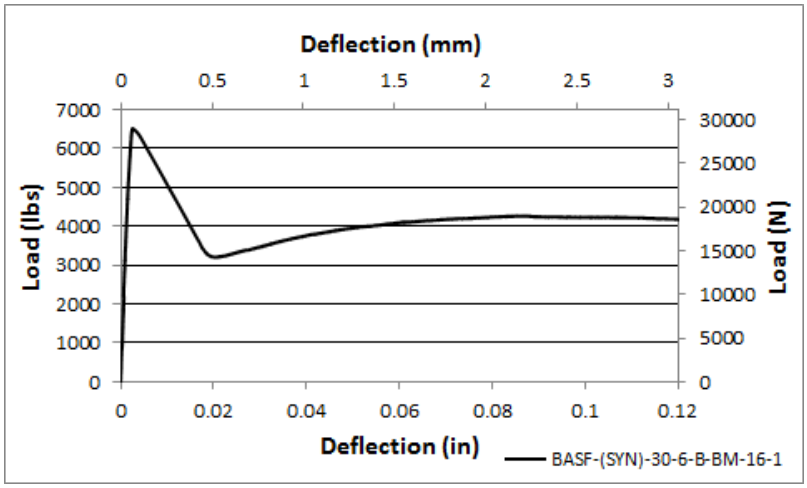

(a)

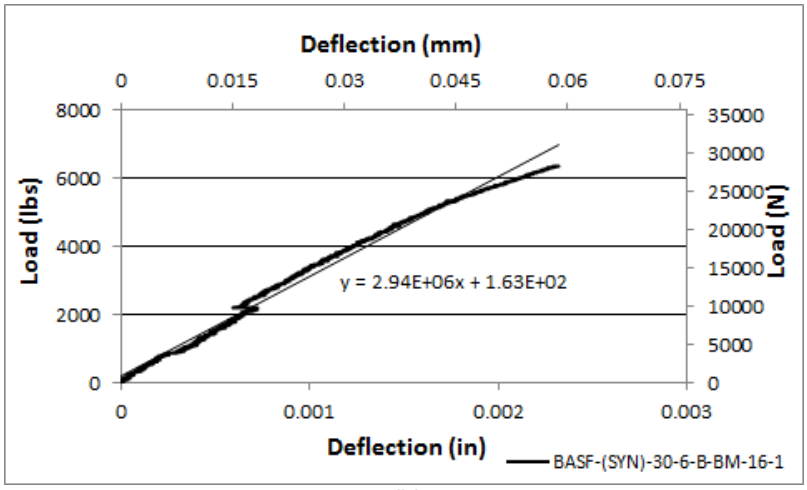

(b)

(c)

Figure C32 BASF-(SYN)-30-6-B-BM-16- (a) Load-Deflection Plot, (b) Modulus of Elasticity Plot, and (c) Crack Picture.

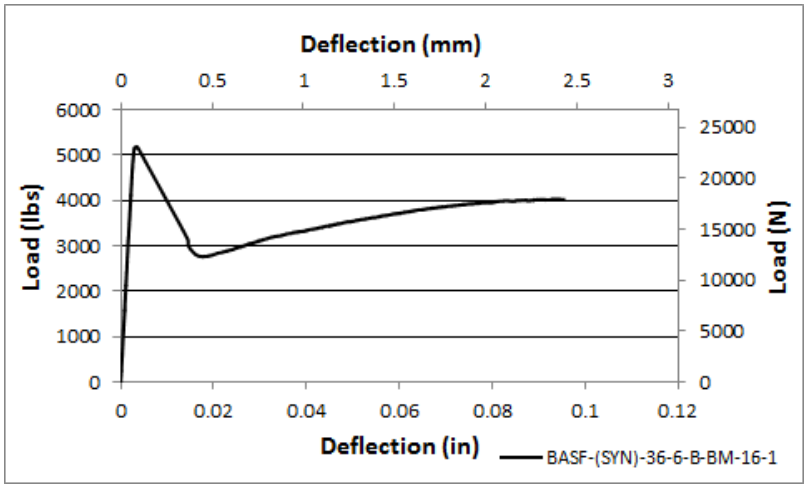

(a)

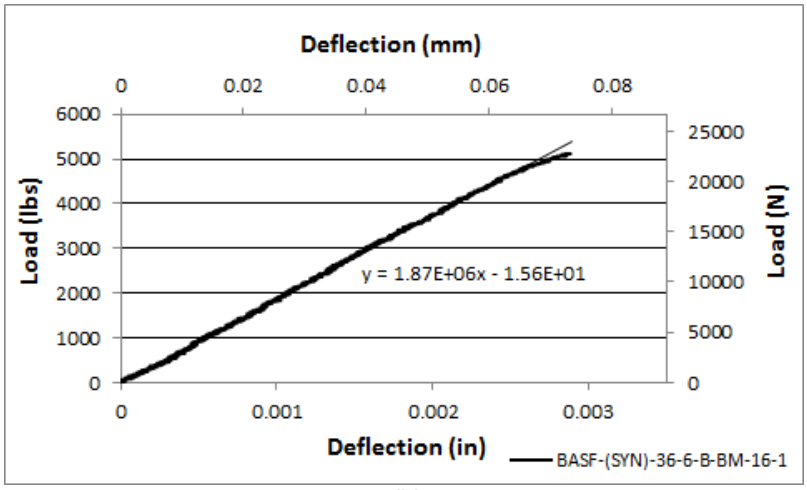

(b)

(c)

Figure C33 BASF-(SYN)-36-6-B-BM-16-1(a) Load-Deflection Plot, (b) Modulus of Elasticity Plot, and (c) Crack Picture.

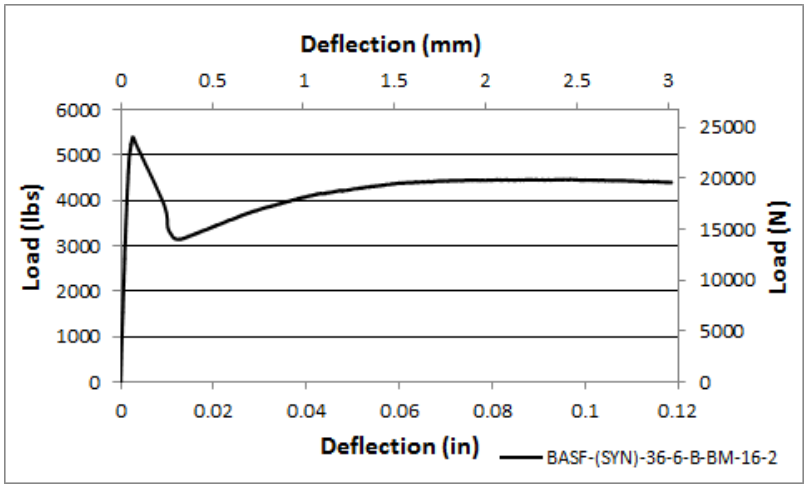

(a)

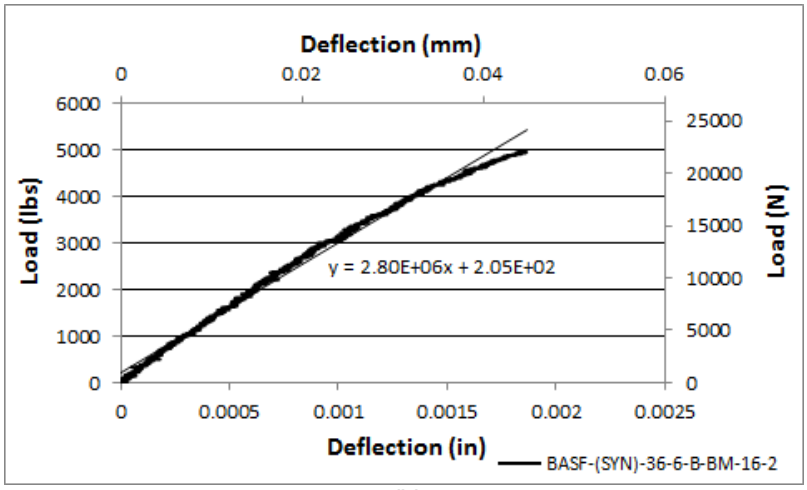

(b)

(c)

Figure C34 BASF-(SYN)-36-6-B-BM-16-2 (a) Load-Deflection Plot, (b) Modulus of Elasticity Plot, and (c) Crack Picture.

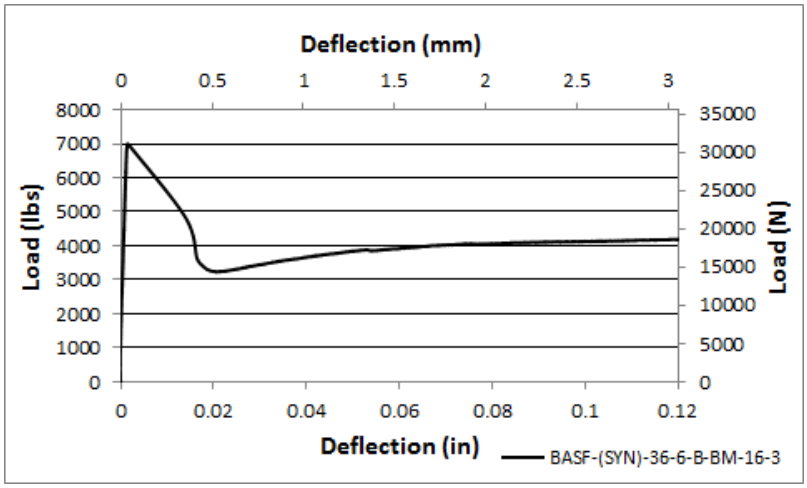

(a)

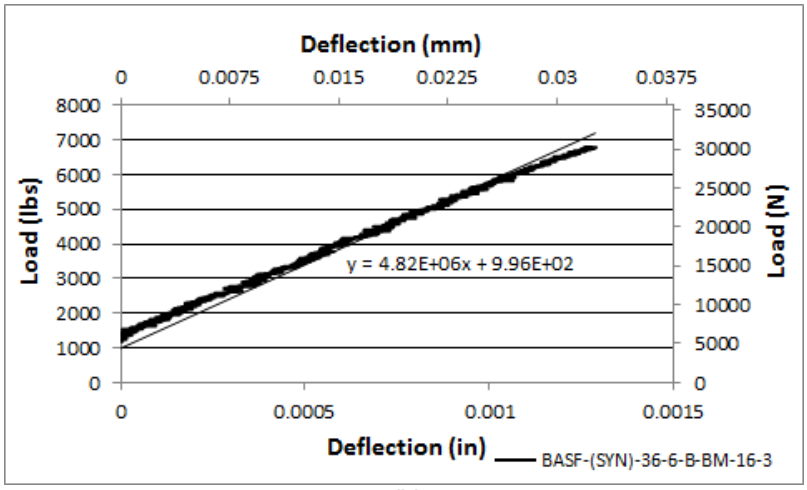

(b)

(c)

Figure C35 BASF-(SYN)-36-6-B-BM-16-3 (a) Load-Deflection Plot, (b) Modulus of Elasticity Plot, and (c) Crack Picture.

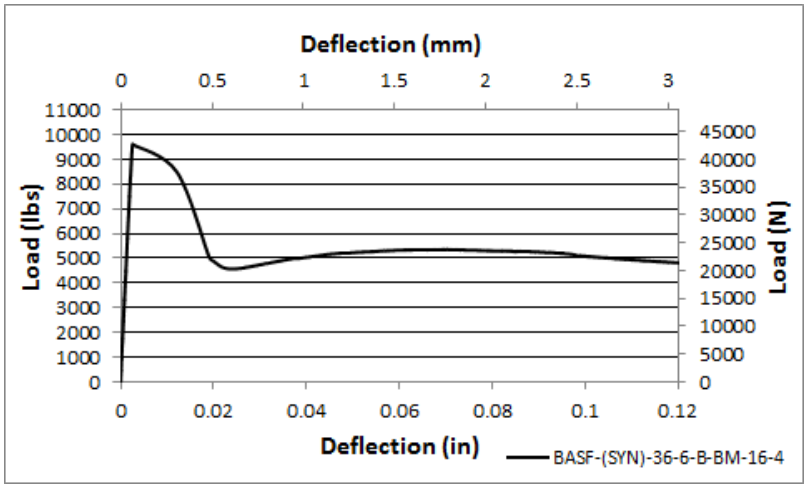

(a)

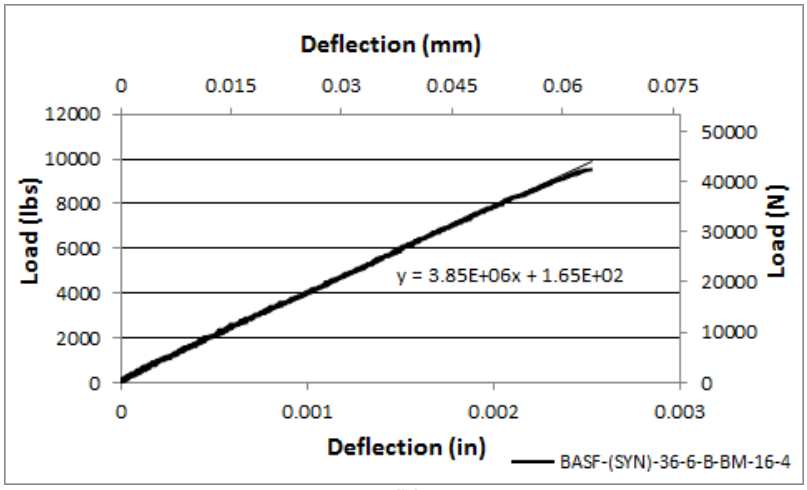

(b)

(c)

Figure C36 BASF-(SYN)-36-6-B-BM-16-4 (a) Load-Deflection Plot, (b) Modulus of Elasticity Plot, and (c) Crack Picture.

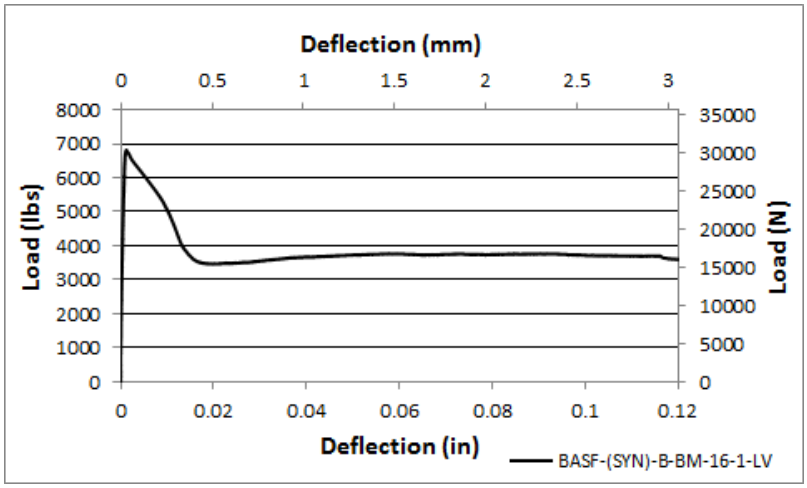

(a)

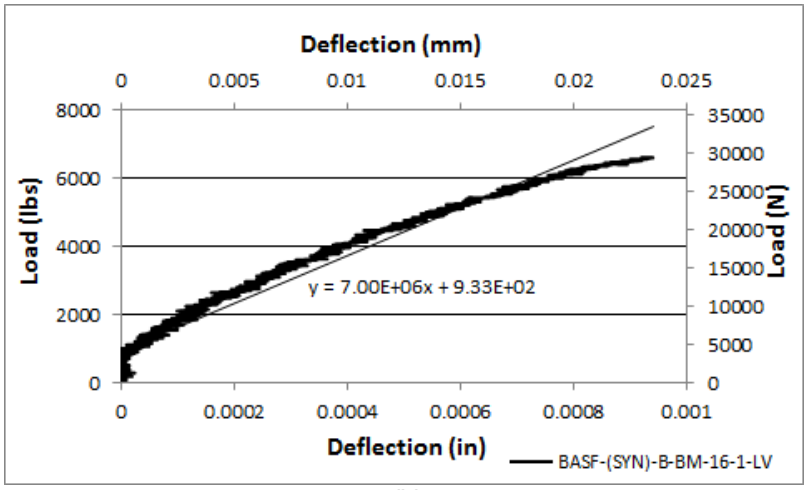

(b)

(c)

Figure C37 BASF-(SYN)-B-BM-16-1-LV (a) Load-Deflection Plot, (b) Modulus of Elasticity Plot, and (c) Crack Picture.

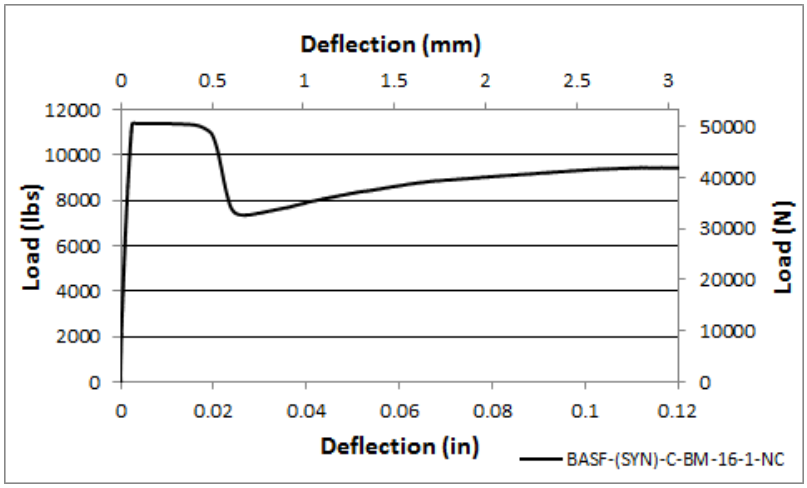

(a)

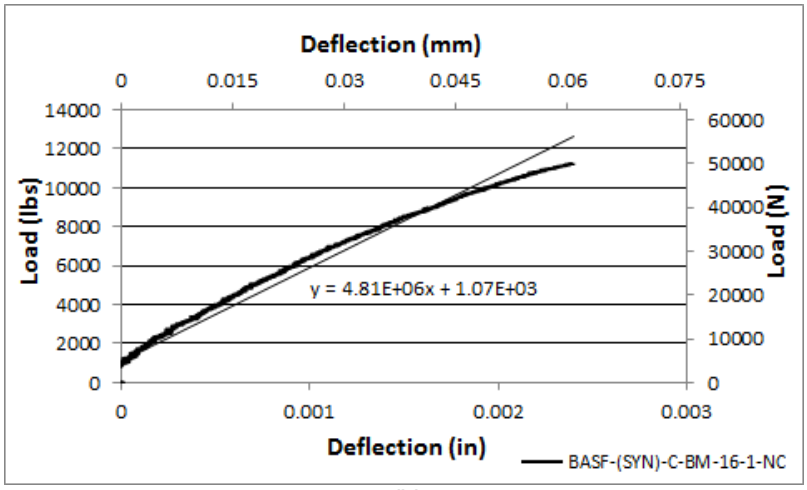

(b)

(c)

Figure C38 BASF-(SYN)-C-BM-16-1-NC (a) Load-Deflection Plot, (b) Modulus of Elasticity Plot, and (c) Crack Picture.

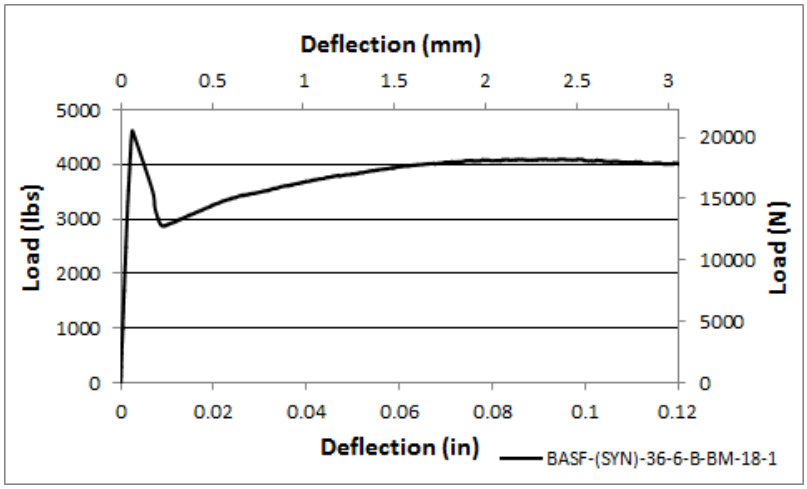

(a)

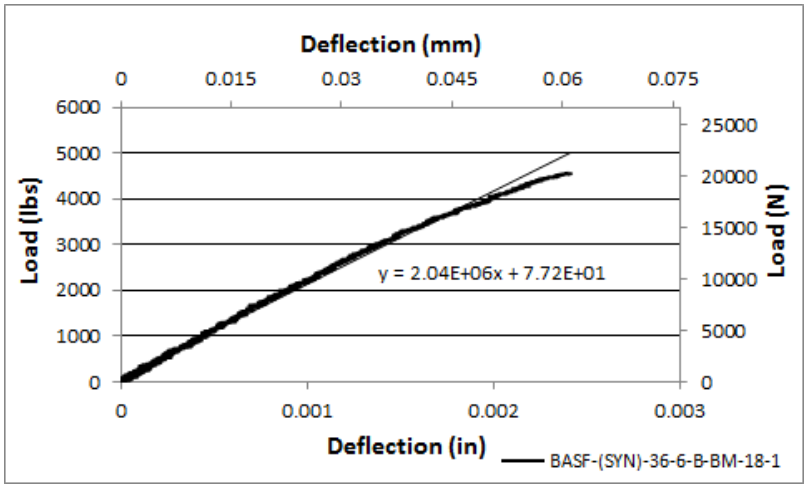

(b)

Figure C39 BASF-(SYN)-36-6-B-BM-18-1 (a) Load-Deflection Plot and (b) Modulus of Elasticity Plot.

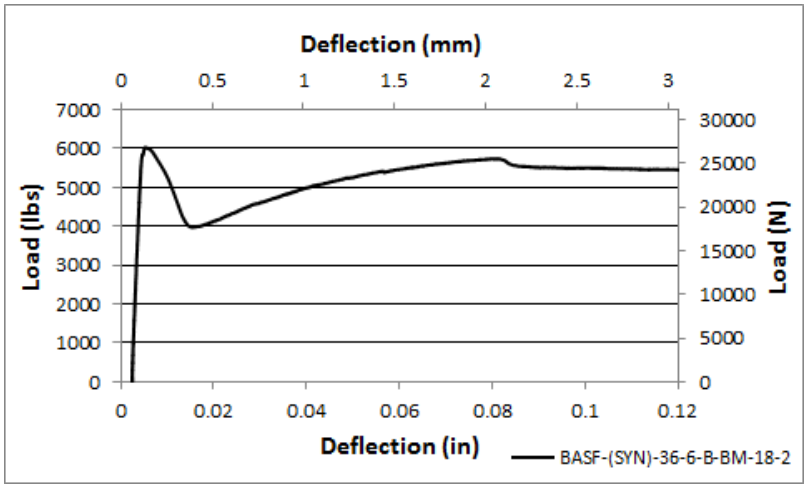

(a)

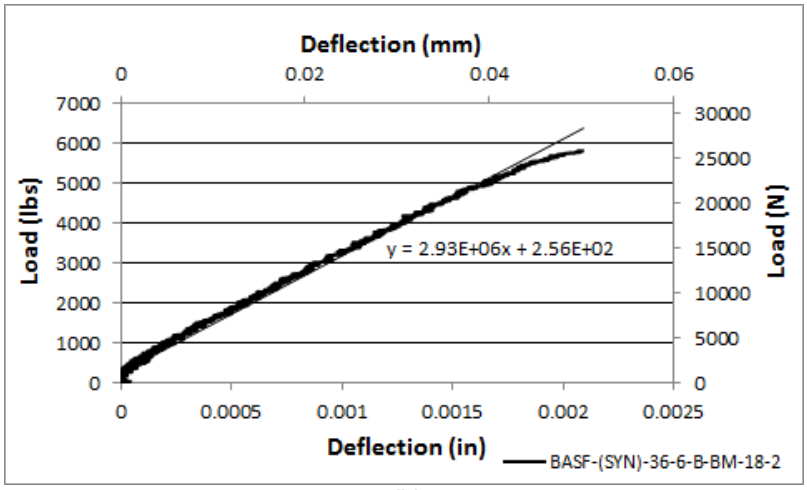

(b)

Figure C40 BASF-(SYN)-36-6-B-BM-18-2(a) Load-Deflection Plot and (b) Modulus of Elasticity Plot.

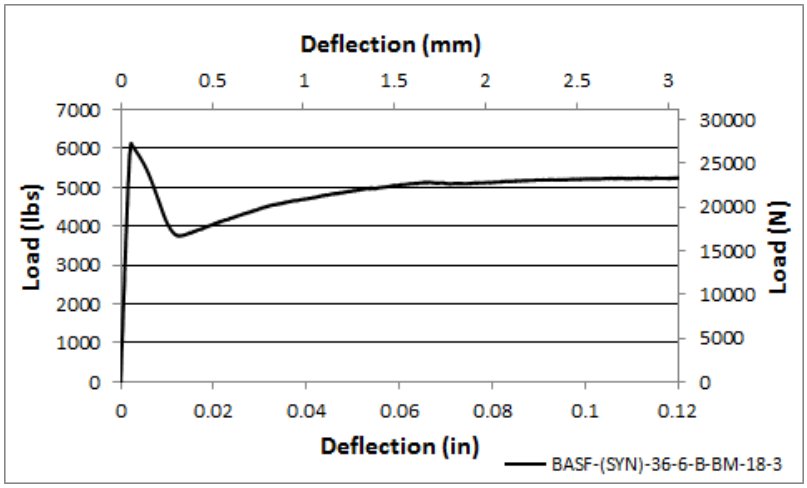

(a)

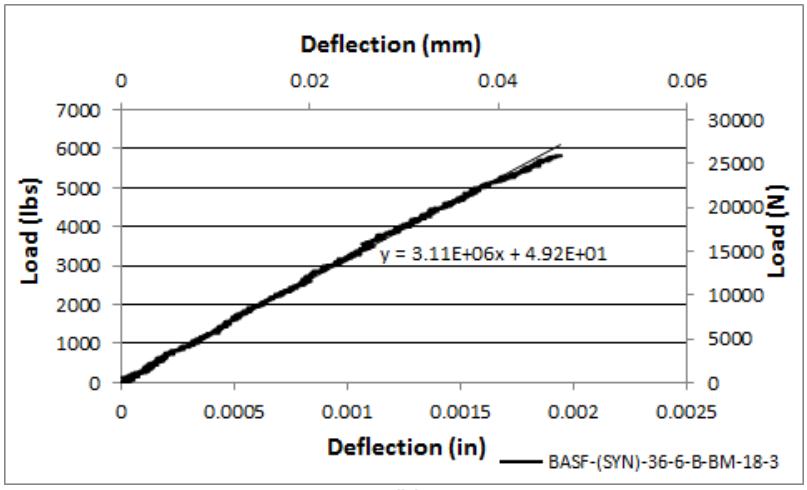

(b)

(c)

Figure C41 BASF-(SYN)-36-6-B-BM-18-3 (a) Load-Deflection Plot, (b) Modulus of Elasticity Plot, and (c) Crack Picture.

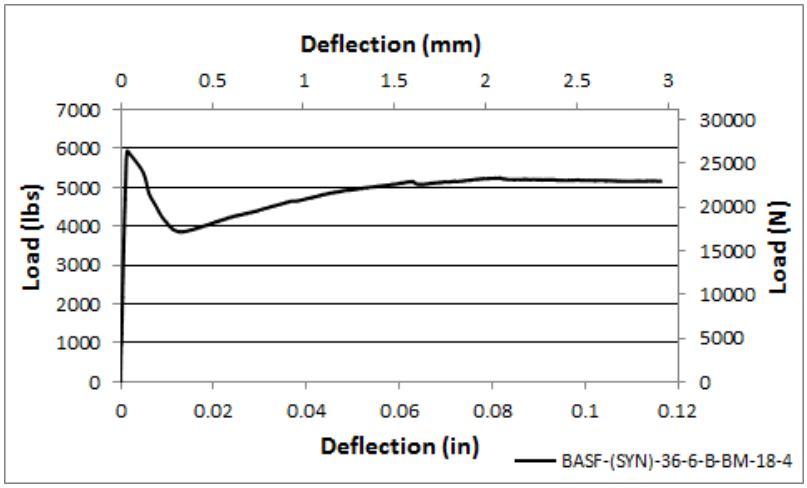

(a)

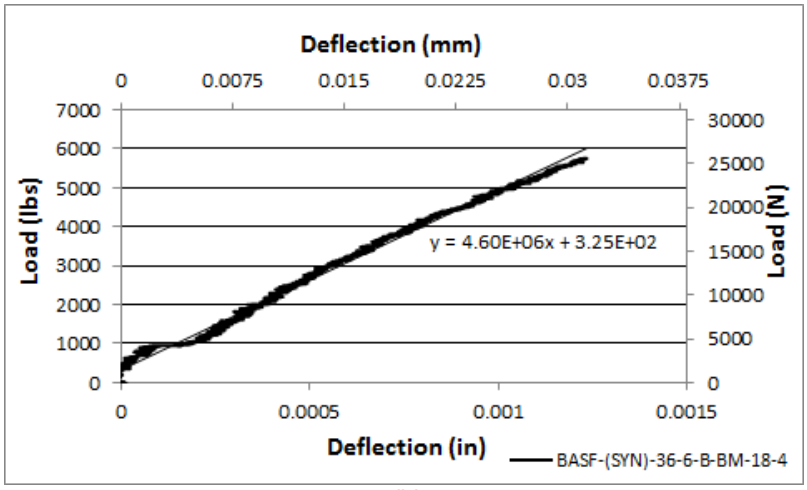

(b)

(c)

Figure C42 BASF-(SYN)-36-6-B-BM-18-4 (a) Load-Deflection Plot, (b) Modulus of Elasticity Plot, and (c) Crack Picture.

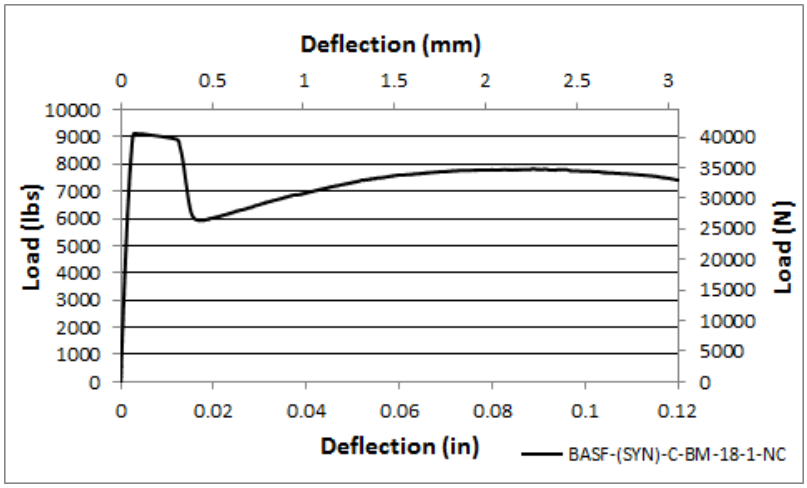

(a)

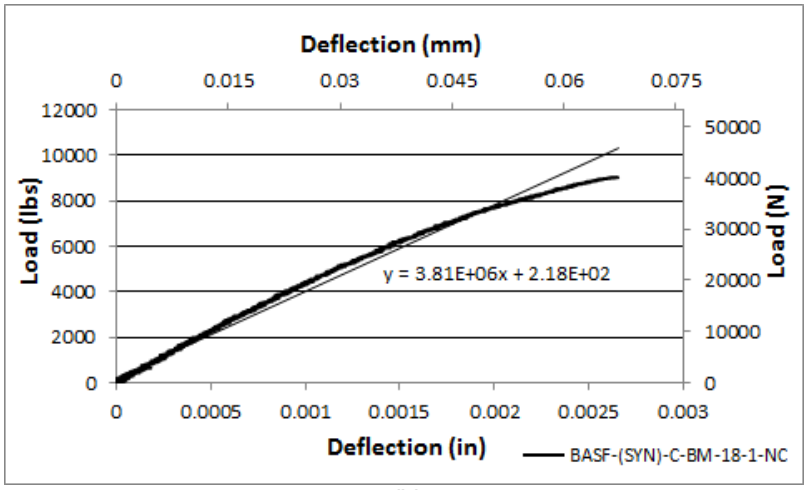

(b)

(c)

Figure C43 BASF-(SYN)-C-BM-18-1-NC (a) Load-Deflection Plot, (b) Modulus of Elasticity Plot, and (c) Crack Picture.

APPENDIX D

STEEL PIPE GRAPHS

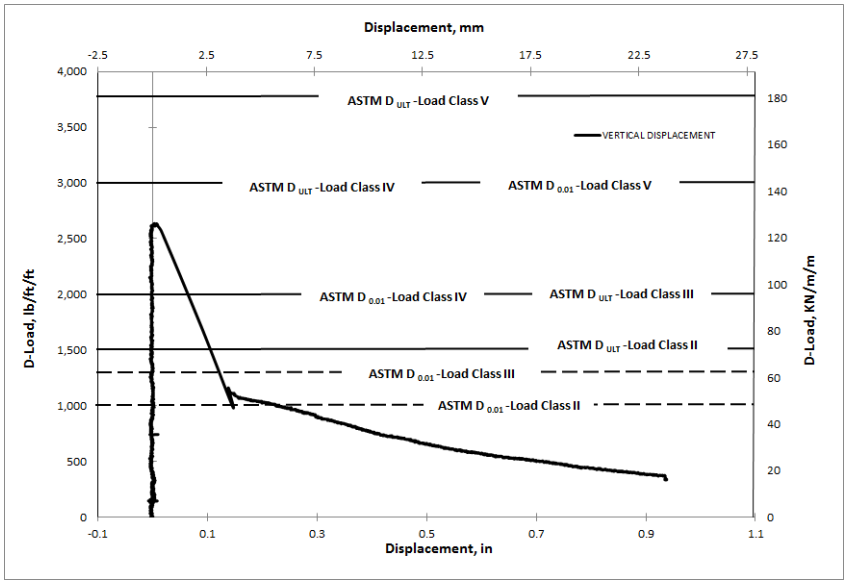

(a)

(b)

(c)

(d)

Figure D1 BASF-(FS7)-18-6-B-DL-22-1(a) Load-Deformation Plot, (b) Crack Propagation, (c) Cross-section Deformation, (d) Crack Width.

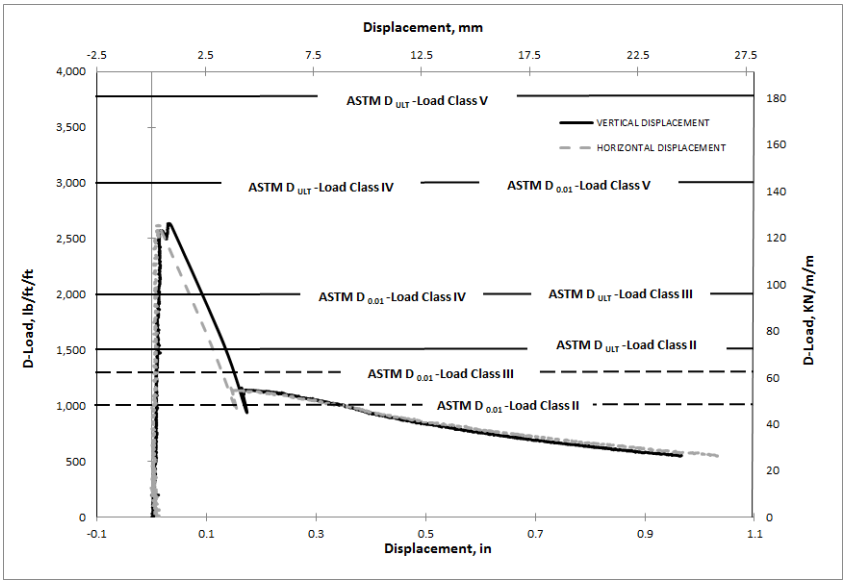

(a)

(b)

(c)

(d)

Figure D2 BASF-(FS7)-18-6-B-DL-22-2 (a) Load-Deformation Plot, (b) Crack Propagation, (c) Cross-section Deformation, (d) Crack Width.

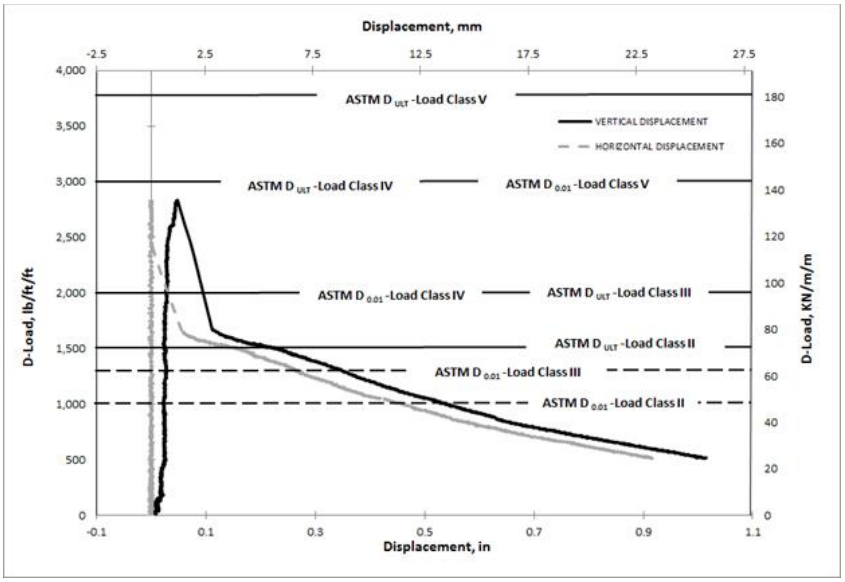

(a)

(b)

(c)

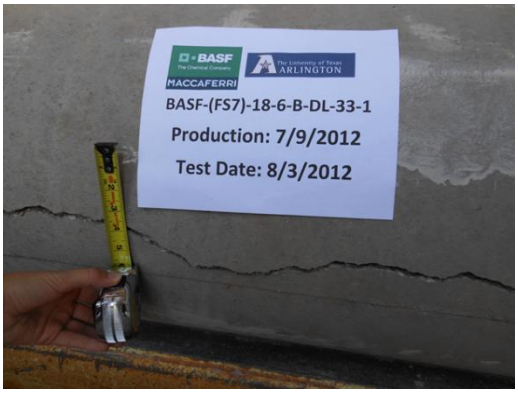

(d)

Figure D3 BASF-(FS7)-18-6-B-DL-33-1(a) Load-Deformation Plot, (b) Crack Propagation, (c) Cross-section Deformation, (d) Crack Width.

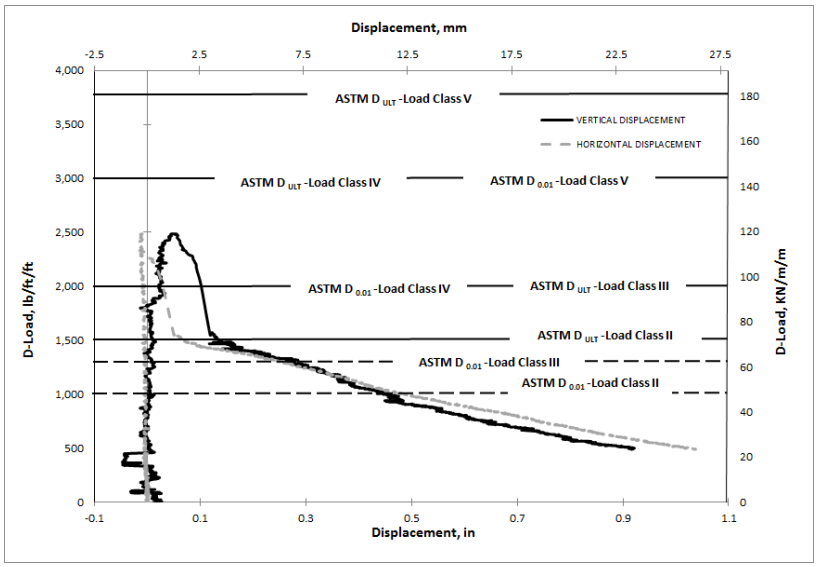

(a)

(b)

(c)

(d)

Figure D4 BASF-(FS7)-18-6-B-DL-33-2 (a) Load-Deformation Plot, (b) Crack Propagation, (c) Cross-section Deformation, (d) Crack Width.

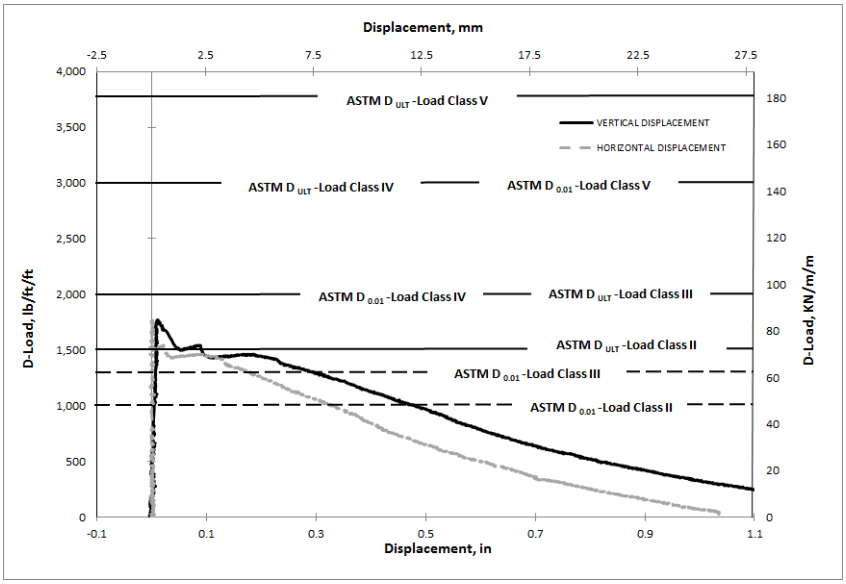

(a)

(b)

(c)

(d)

Figure D5 BASF-(FS7)-18-6-B-DL-44-1(a) Load-Deformation Plot, (b) Crack Propagation, (c) Cross-section Deformation, (d) Crack Width.

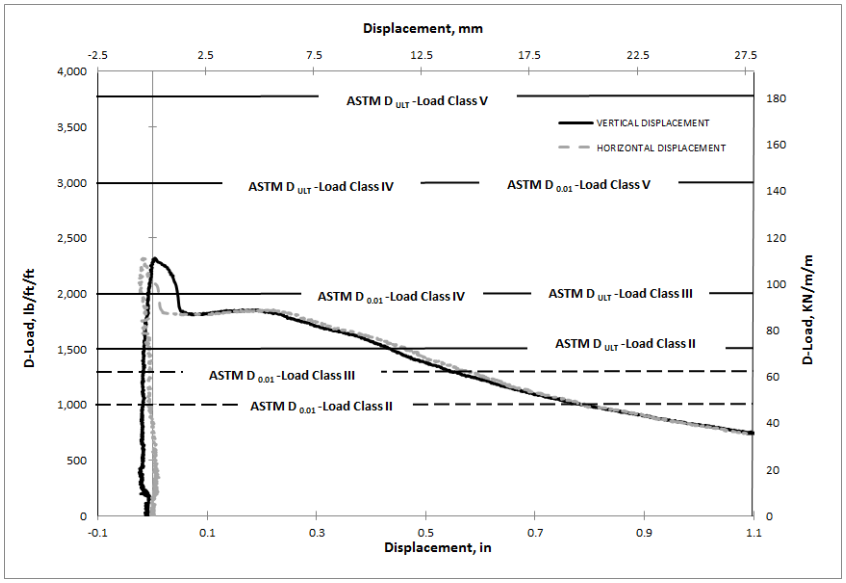

(a)

(b)

(c)

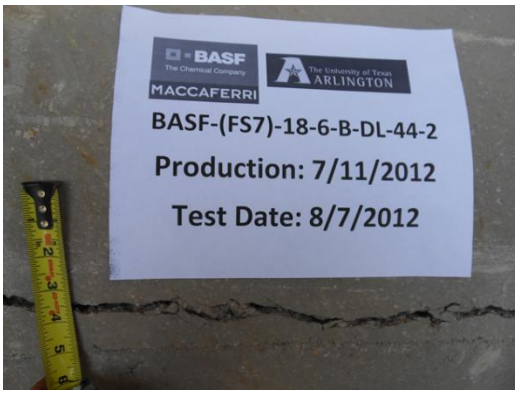

(d)

Figure D6 BASF-(FS7)-18-6-B-DL-44-2 (a) Load-Deformation Plot, (b) Crack Propagation, (c) Cross-section Deformation, (d) Crack Width

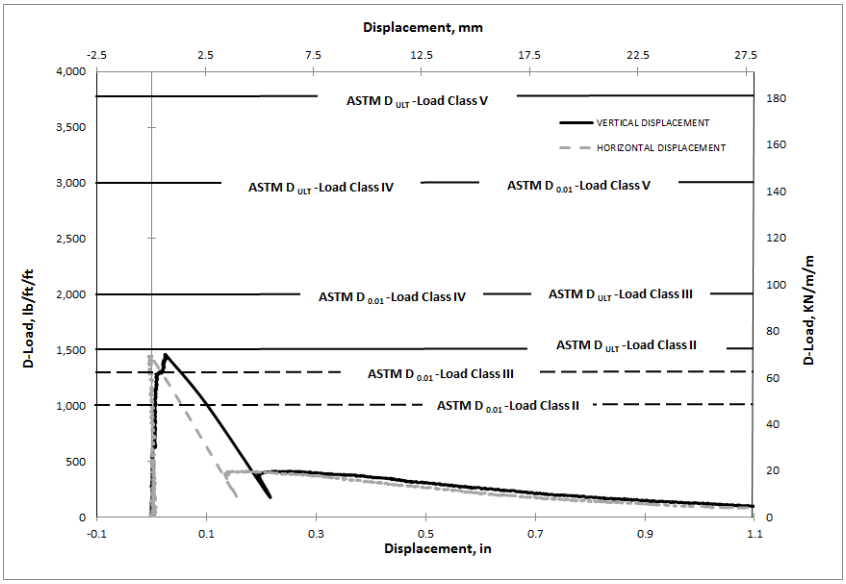

(a)

(b)

(c)

(d)

Figure D7 BASF-(FS7)-21-6-B-DL-22-1(a) Load-Deformation Plot, (b) Crack Propagation, (c) Cross-section Deformation, (d) Crack Width.

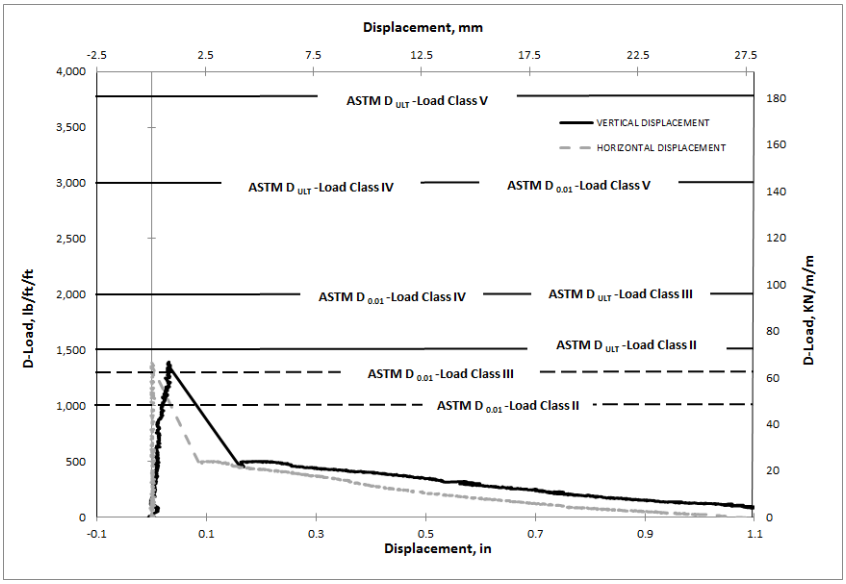

(a)

(b)

(c)

(d)

Figure D8 BASF-(FS7)-21-6-B-DL-22-2 (a) Load-Deformation Plot, (b) Crack Propagation, (c) Cross-section Deformation, (d) Crack Width.

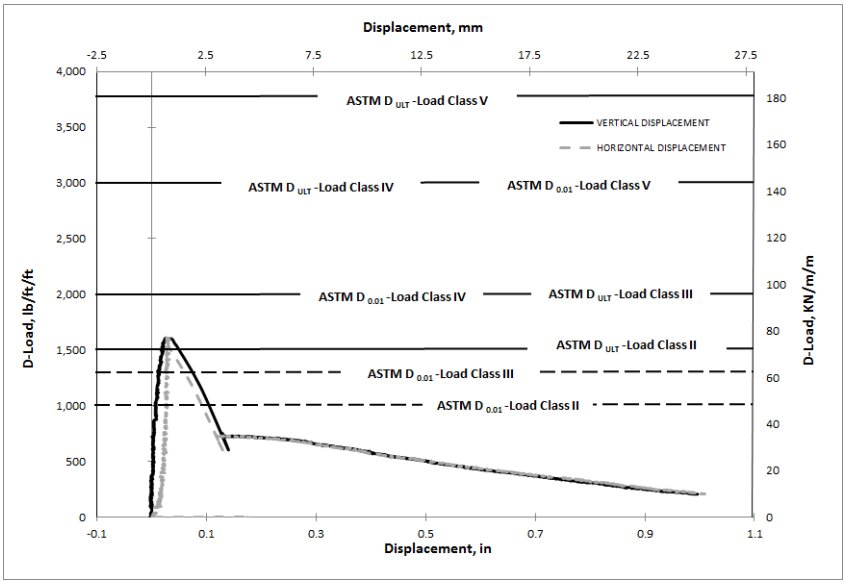

(a)

(b)

(c)

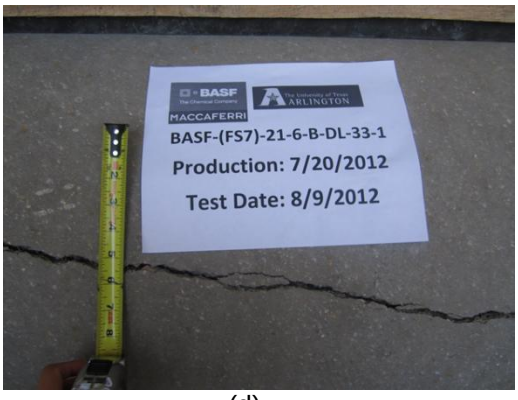

(d)

Figure D9 BASF-(FS7)-21-6-B-DL-33-1(a) Load-Deformation Plot, (b) Crack Propagation, (c) Cross-section Deformation, (d) Crack Width.

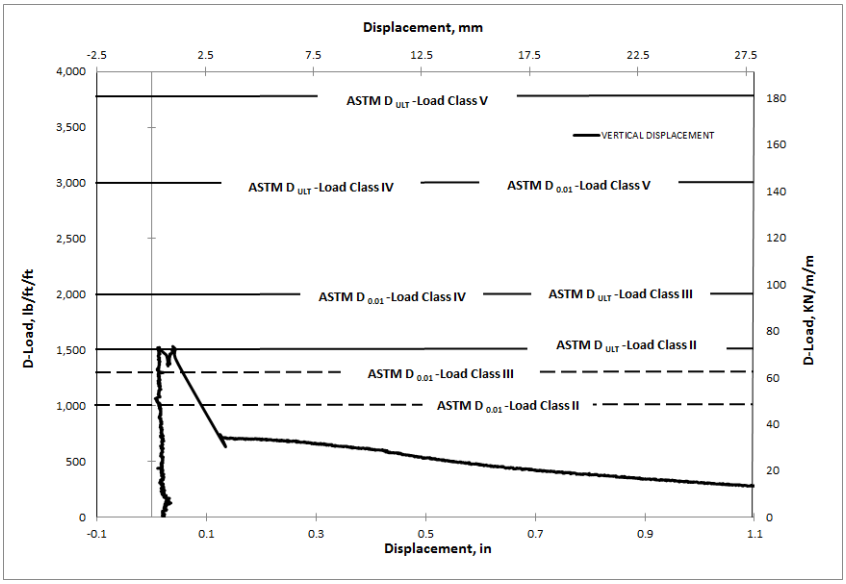

(a)

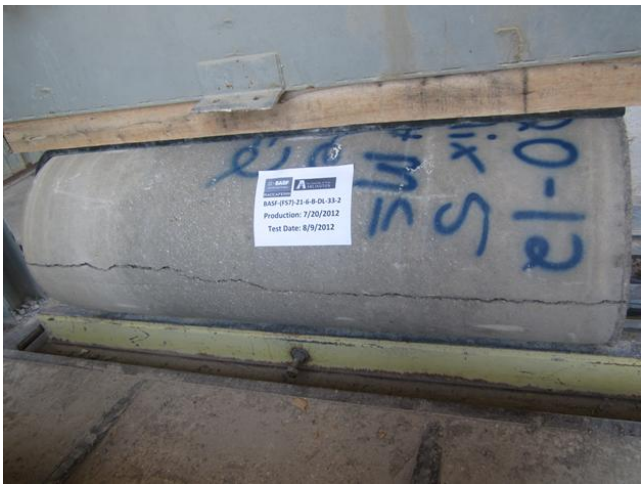

(b)

(c)

(d)

Figure D11 BASF-(FS7)-21-6-B-DL-33-2 (a) Load-Deformation Plot, (b) Crack Propagation, (c) Cross-section Deformation, (d) Crack Width.

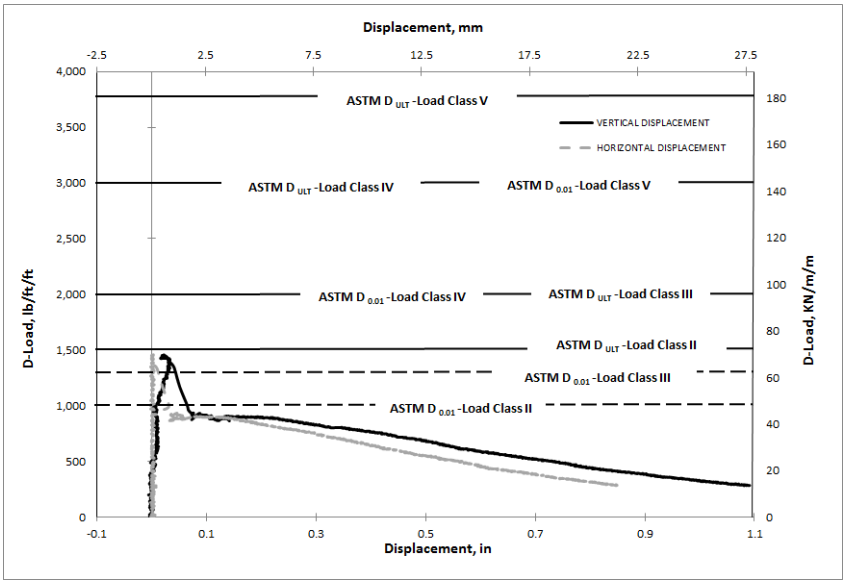

(a)

(b)

(c)

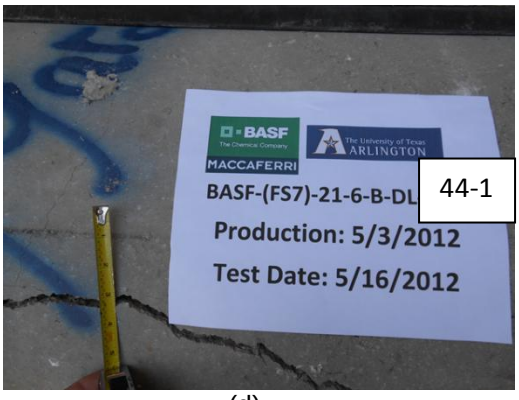

(d)

Figure D11 BASF-(FS7)-21-6-B-DL-44-1(a) Load-Deformation Plot, (b) Crack Propagation, (c) Cross-section Deformation, (d) Crack Width.

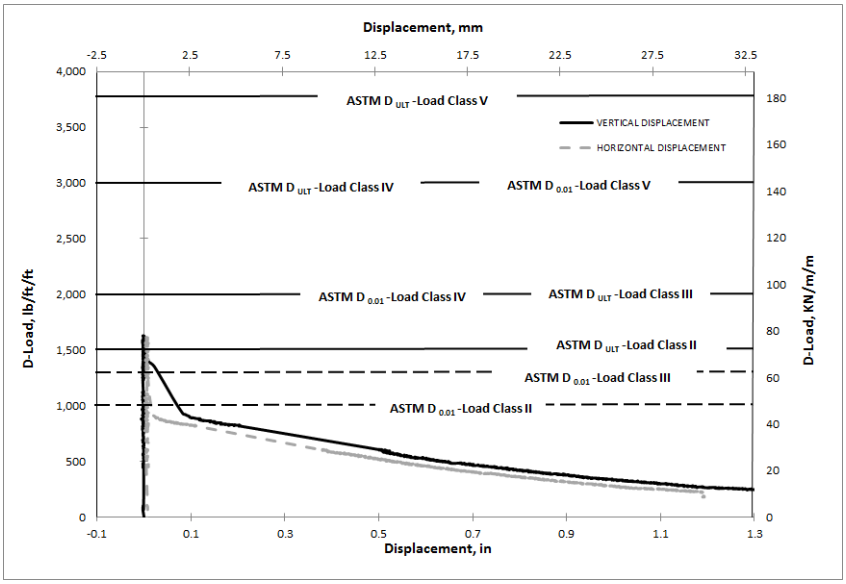

(a)

(b)

(c)

(d)

Figure D12 BASF-(FS7)-24-6-B-DL-22-1(a) Load-Deformation Plot, (b) Crack Propagation, (c) Cross-section Deformation, (d) Crack Width.

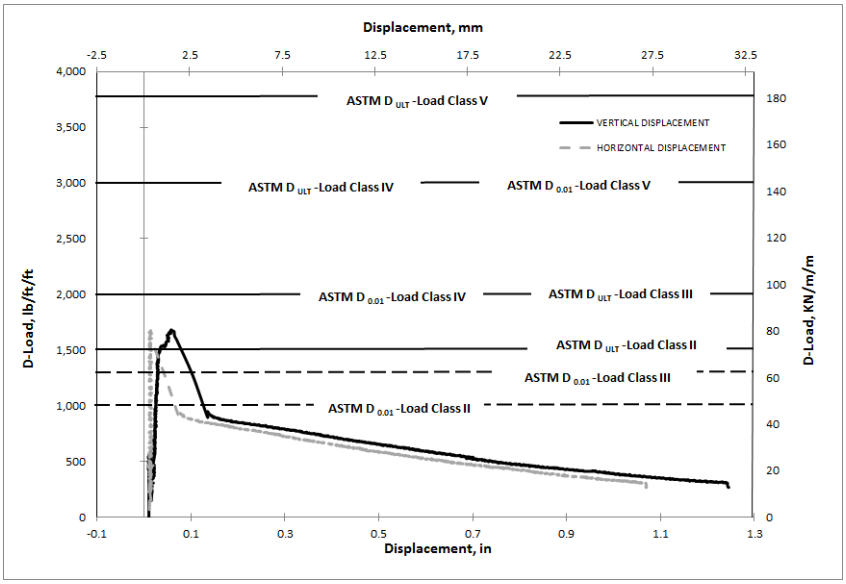

(a)

(b)

(c)

Figure D13 BASF-(FS7)-24-6-B-DL-22-2 (a) Load-Deformation Plot, (b) Crack Propagation and (c) Crack Width.

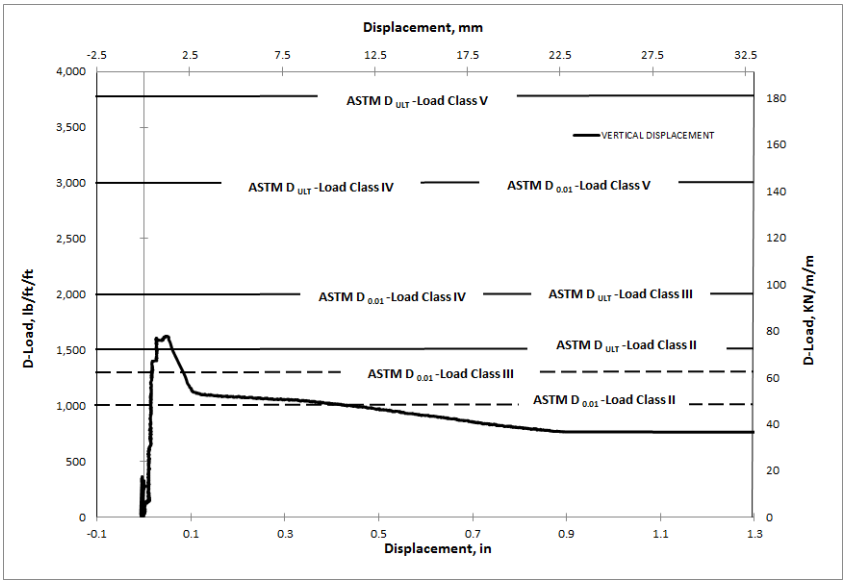

(a)

(b)

(c)

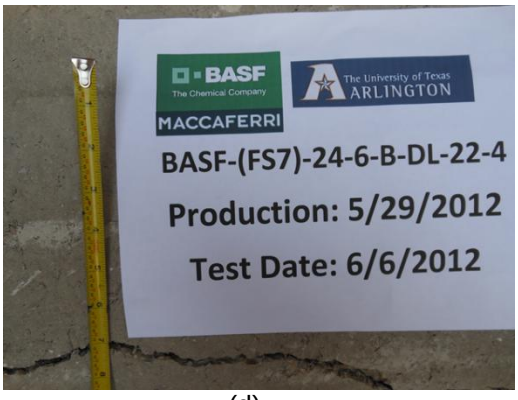

(d)

Figure D14 BASF-(FS7)-24-6-B-DL-22-4 (a) Load-Deformation Plot, (b) Crack Propagation, (c) Cross-section Deformation, (d) Crack Width.

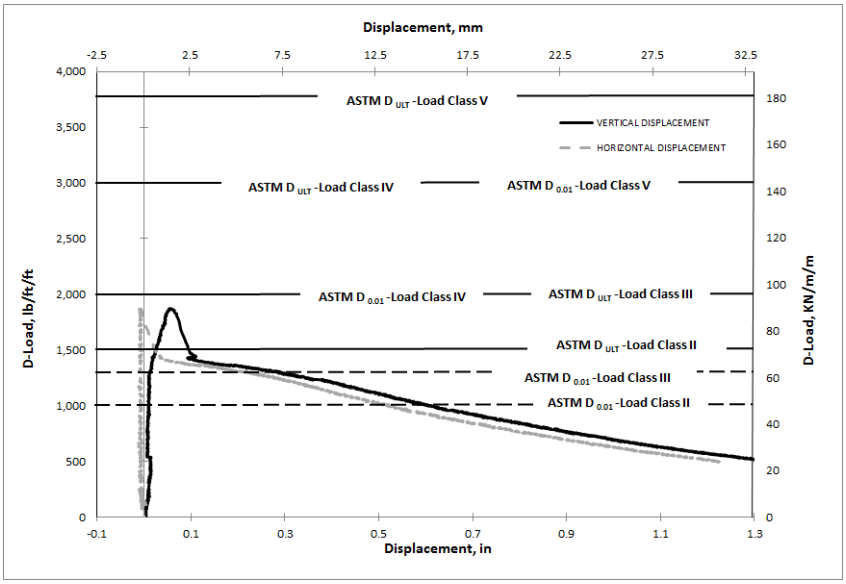

(a)

(b)

(c)

(d)

Figure D15 BASF-(FS7)-24-6-B-DL-33-2(a) Load-Deformation Plot, (b) Crack Propagation, (c) Cross-section Deformation, (d) Crack Width.

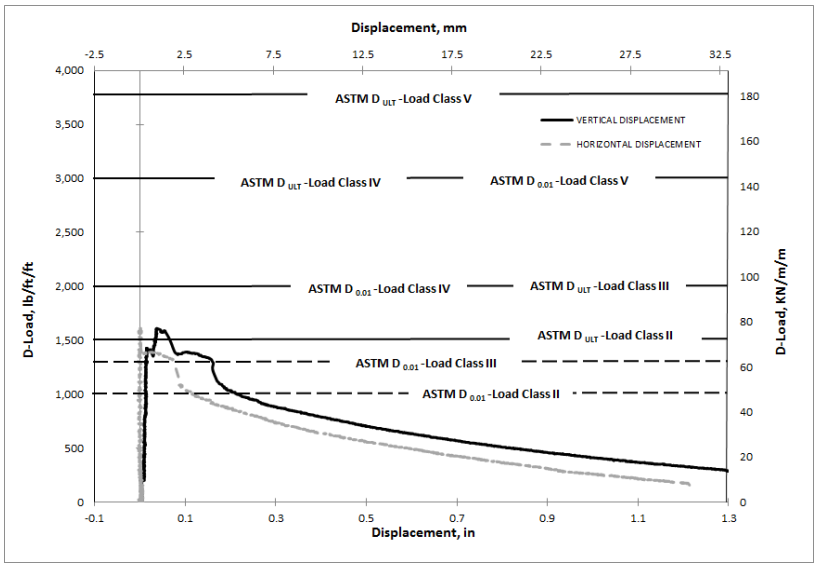

(a)

(b)

(c)

(d)

Figure D16 BASF-(FS7)-24-8-B-DL-33-3-LV (a) Load-Deformation Plot, (b) Crack Propagation, (c) Cross-section Deformation, (d) Crack Width.

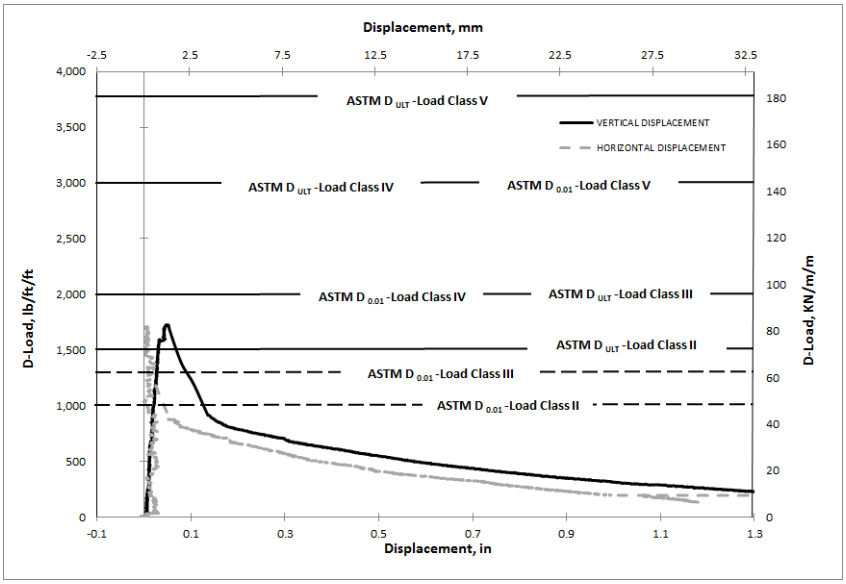

(a)

(b)

(c)

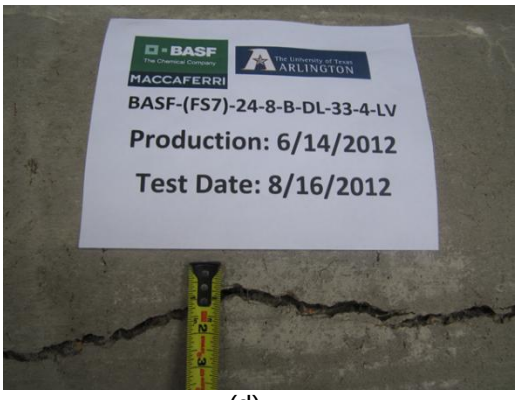

(d)

Figure D17 BASF-(FS7)-24-8-B-DL-33-4-LV(a) Load-Deformation Plot, (b) Crack Propagation, (c) Cross-section Deformation, (d) Crack Width.

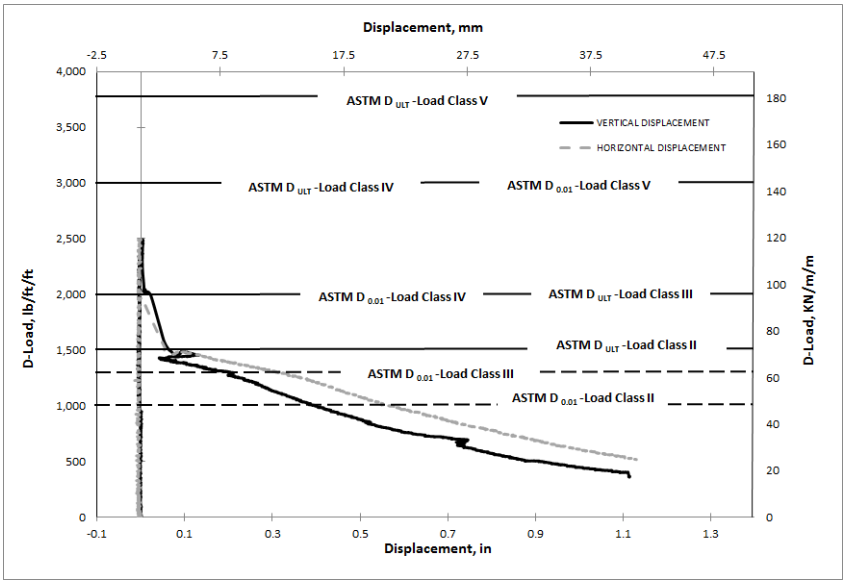

(a)

(b)

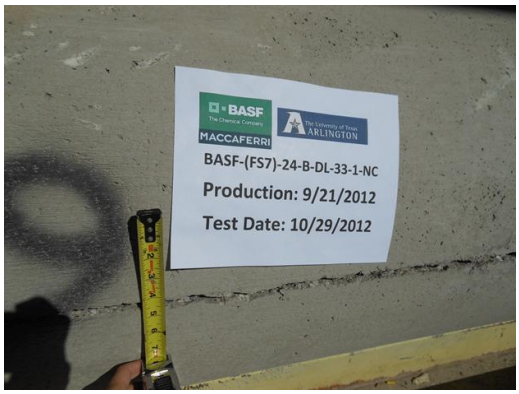

(c)

Figure D18 BASF-(FS7)-24-8-B-DL-33-1-NC(a) Load-Deformation Plot, (b) Crack Propagation and (c) Crack Width.

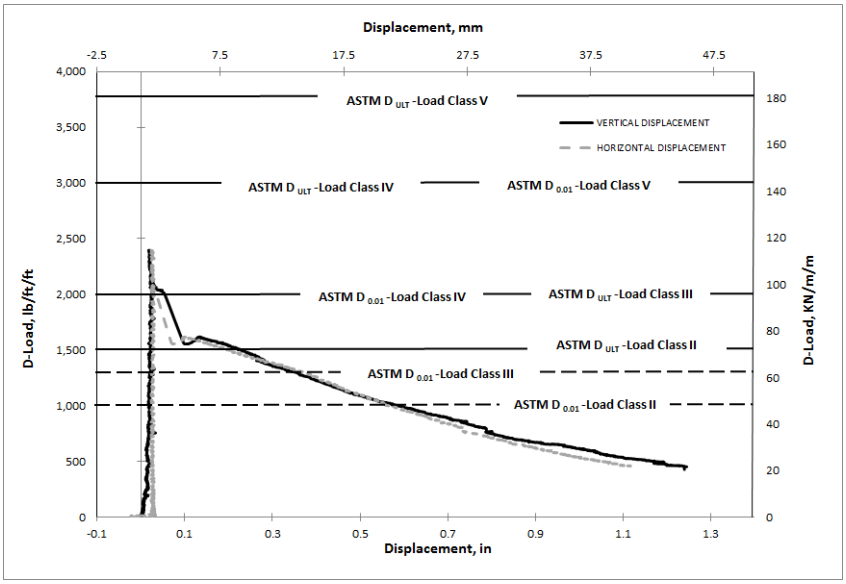

(a)

(b)

(c)

Figure D19 BASF-(FS7)-24-8-B-DL-33-1-NC(a) Load-Deformation Plot, (b) Crack Propagation and (c) Crack Width.

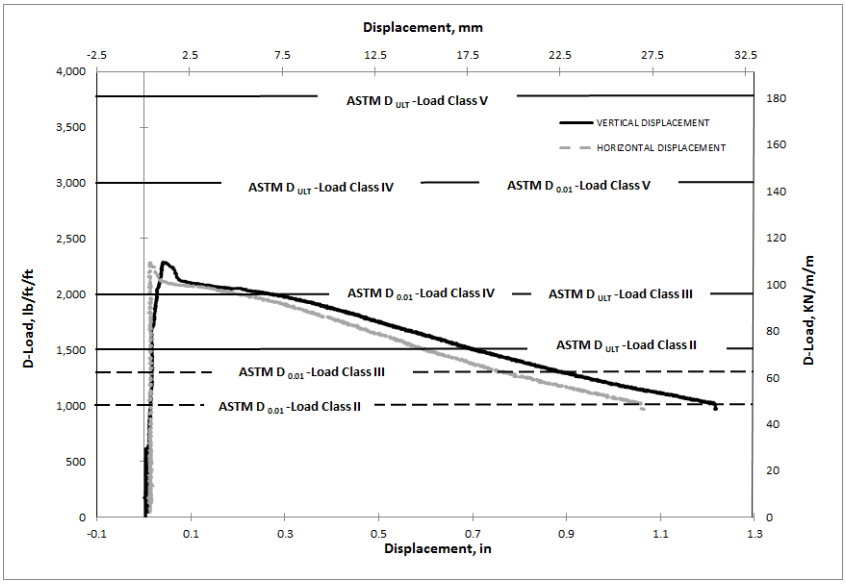

(a)

(b)

(c)

(d)

Figure D20 BASF-(FS7)-24-6-B-DL-44-1(a) Load-Deformation Plot, (b) Crack Propagation, (c) Cross-section Deformation, (d) Crack Width.

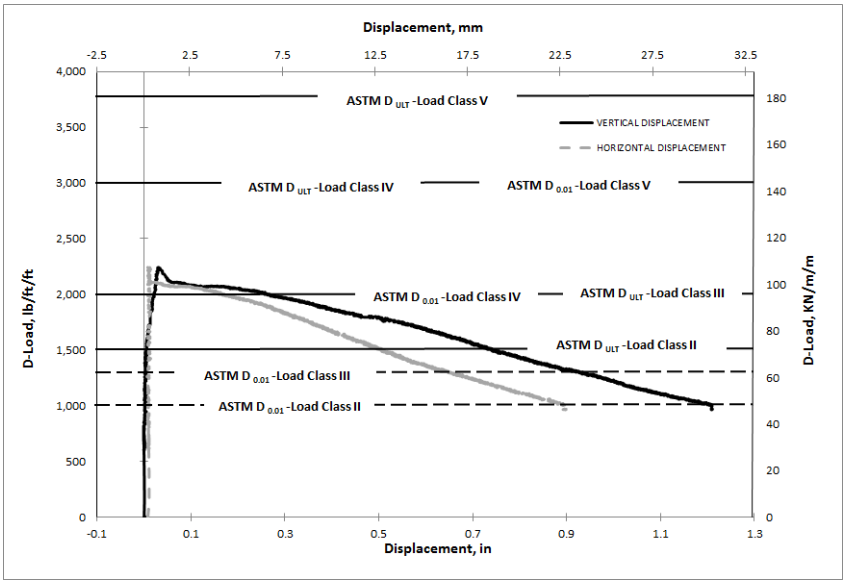

(a)

(b)

(c)

Figure D21 BASF-(FS7)-24-6-B-DL-44-2 (a) Load-Deformation Plot, (b) Crack Propagation and (c) Crack Width.

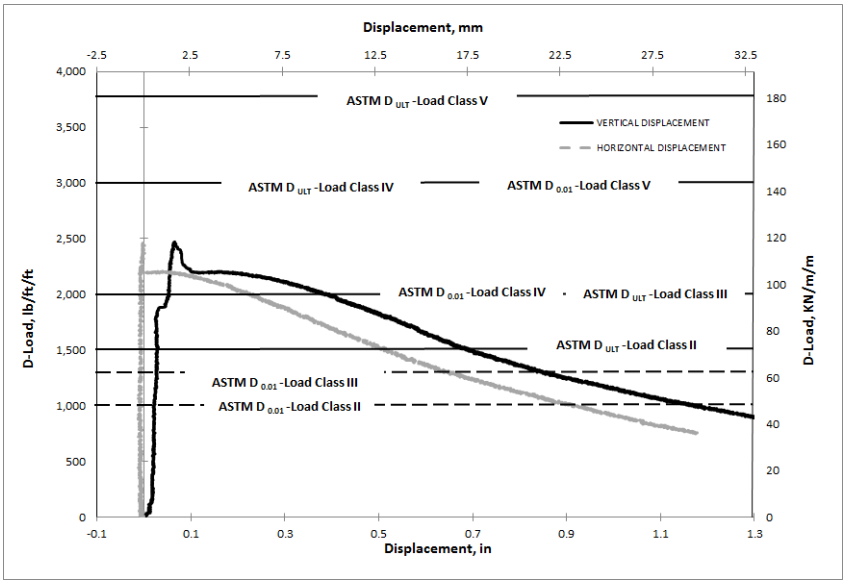

(a)

(b)

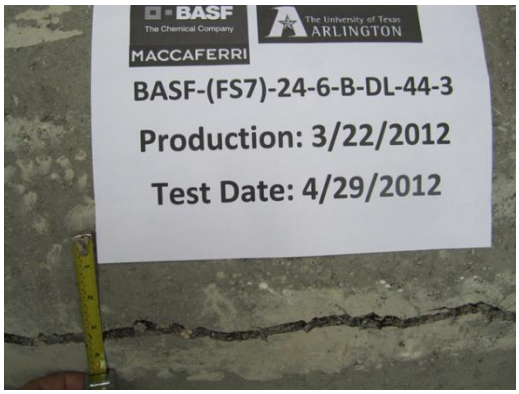

(c)

Figure D22 BASF-(FS7)-24-6-B-DL-44-3 (a) Load-Deformation Plot, (b) Crack Propagation and (c) Crack Width.

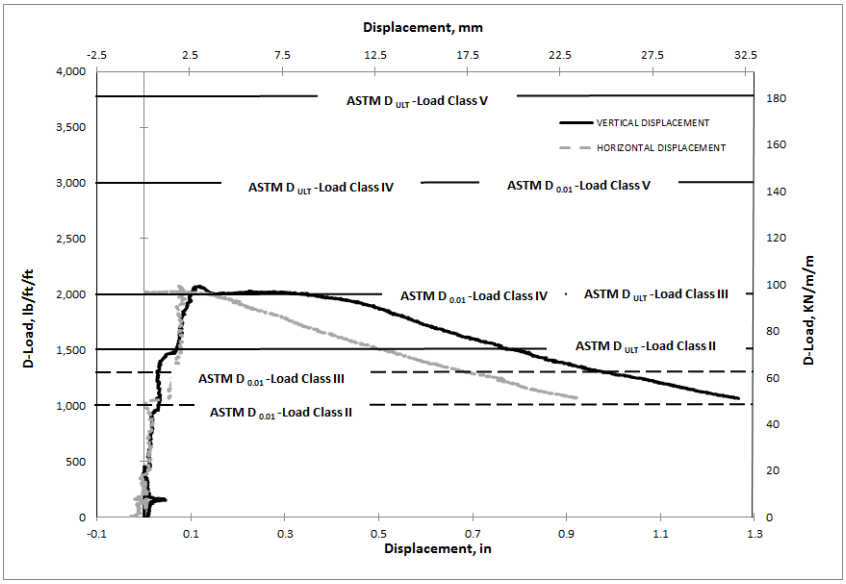

(a)

(b)

(c)

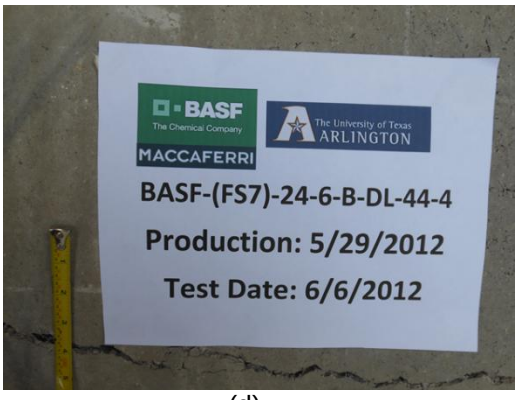

(d)

Figure D23 BASF-(FS7)-24-6-B-DL-44-4 (a) Load-Deformation Plot, (b) Crack Propagation, (c) Cross-section Deformation, (d) Crack Width.

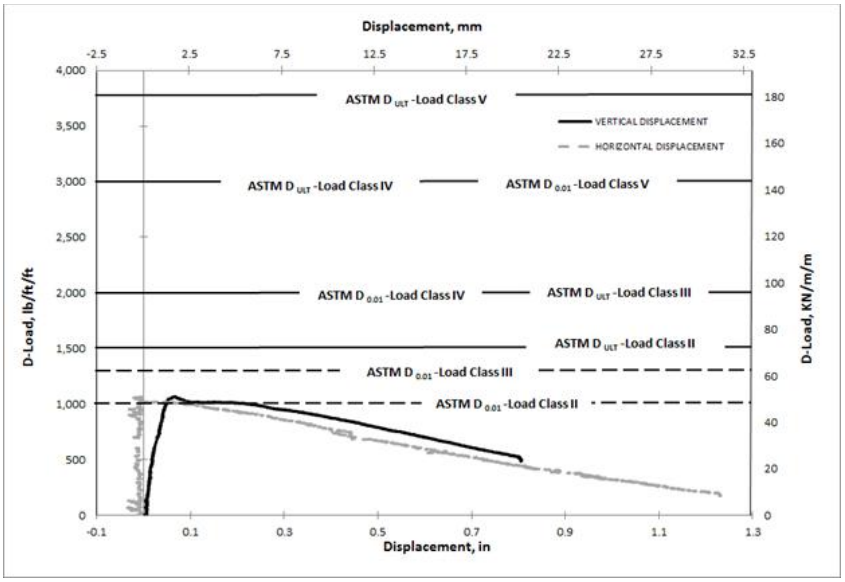

(a)

(b)

(c)

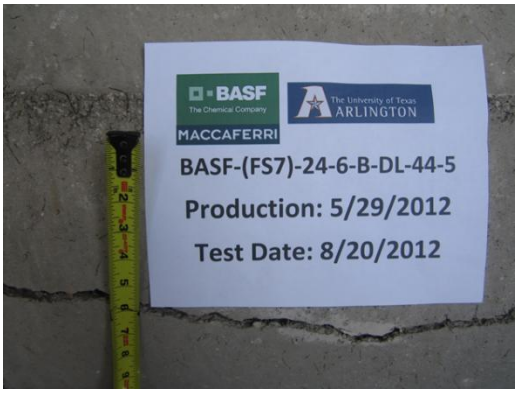

(d)

Figure D24 BASF-(FS7)-24-6-B-DL-44-5 (a) Load-Deformation Plot, (b) Crack Propagation, (c) Cross-section Deformation, (d) Crack Width.

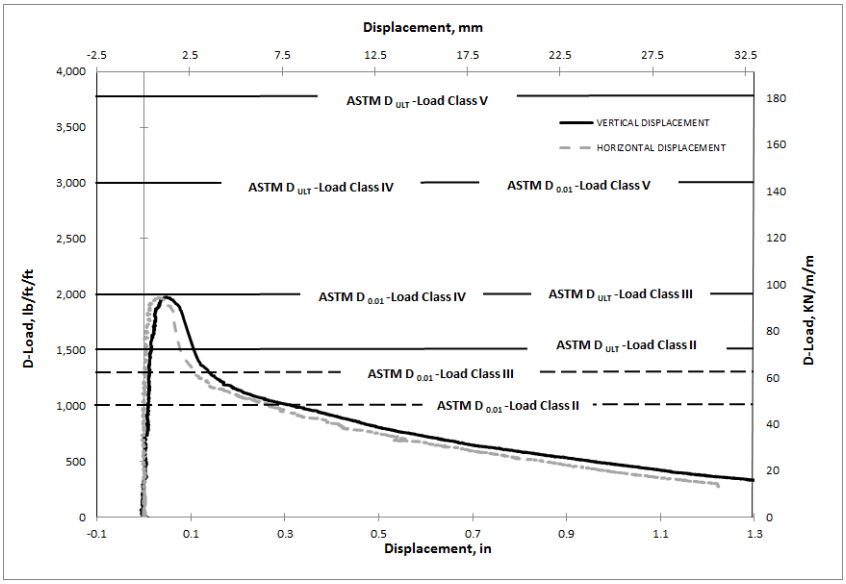

(a)

(b)

(c)

Figure D25 BASF-(FS7)-24-8-B-DL-44-2-LV (a) Load-Deformation Plot, (b) Crack Propagation and (c) Crack Width.

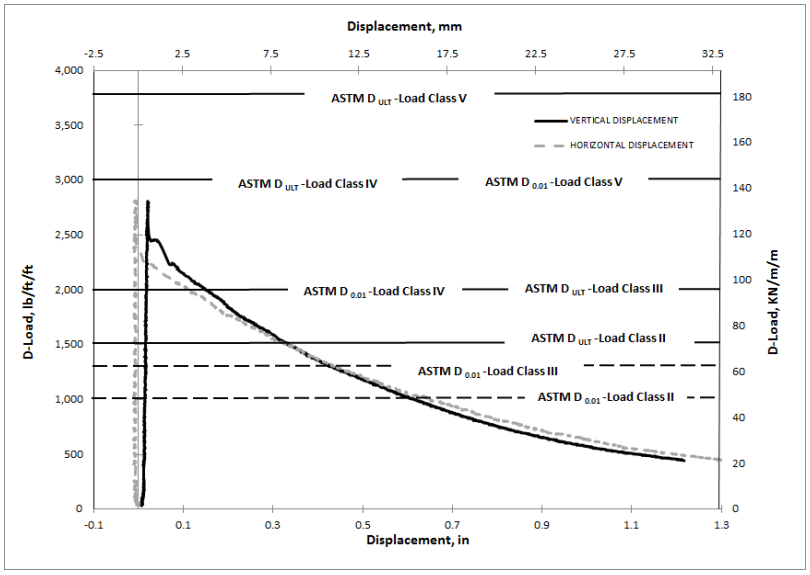

(a)

(b)

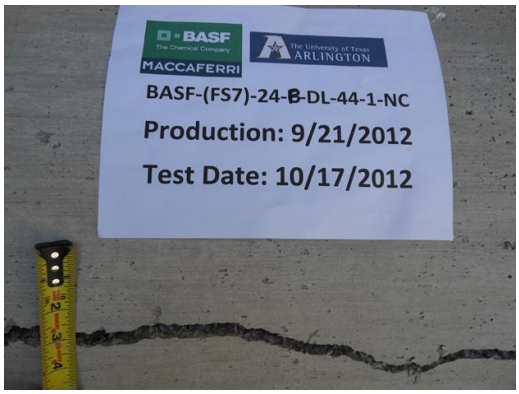

(c)

Figure D27 BASF-(FS7)-24-8-B-DL-44-1-NC (a) Load-Deformation Plot, (b) Crack Propagation and (c) Crack Width.

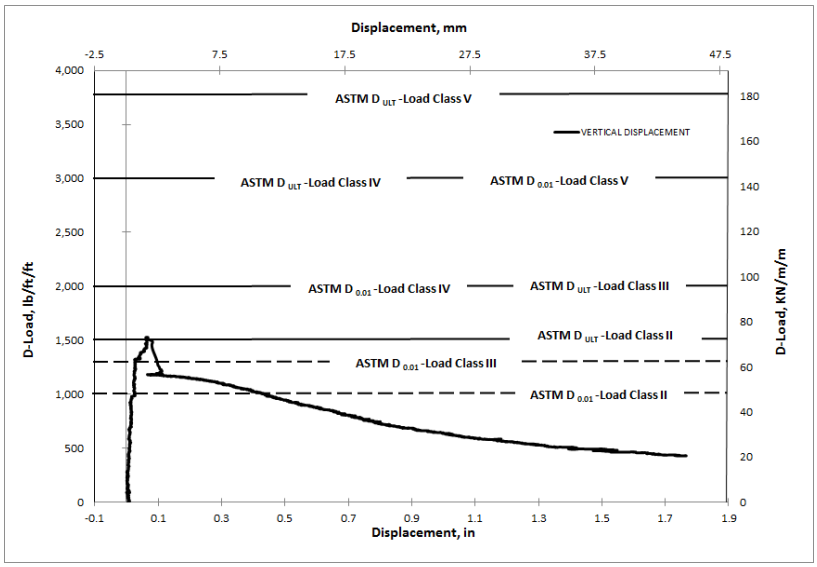

(a)

(b)

(c)

(d)

Figure D27 BASF-(FS7)-30-6-B-DL-33-1(a) Load-Deformation Plot, (b) Crack Propagation, (c) Cross-section Deformation, (d) Crack Width.

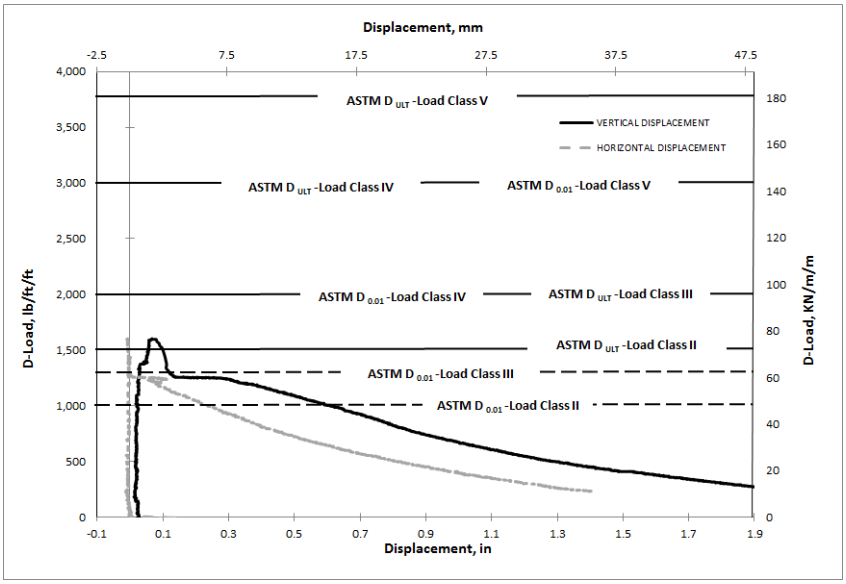

(a)

(b)

(c)

(d)

Figure D28 BASF-(FS7)-30-6-B-DL-33-2(a) Load-Deformation Plot, (b) Crack Propagation, (c) Cross-section Deformation, (d) Crack Width.

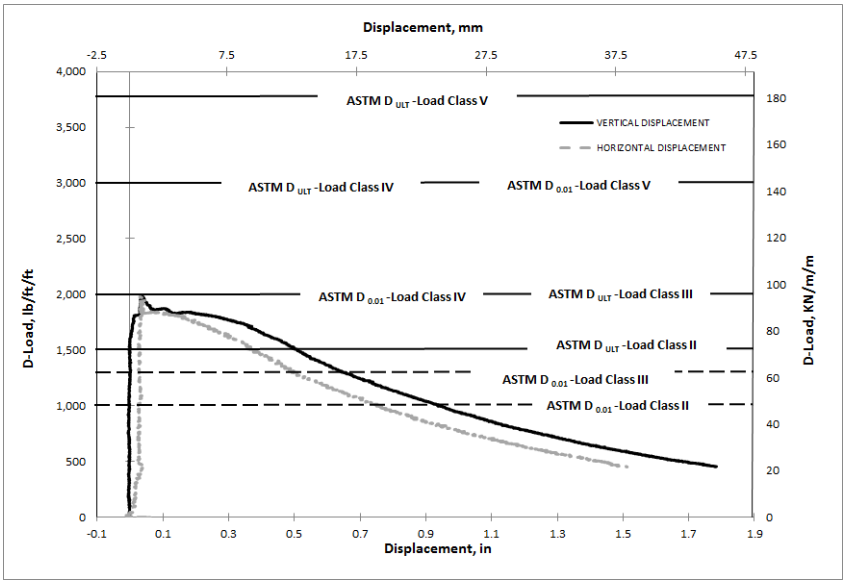

(a)

(b)

(c)

(d)

Figure D29 BASF-(FS7)-30-6-B-DL-44-2a) Load-Deformation Plot, (b) Crack Propagation, (c) Cross-section Deformation, (d) Crack Width.

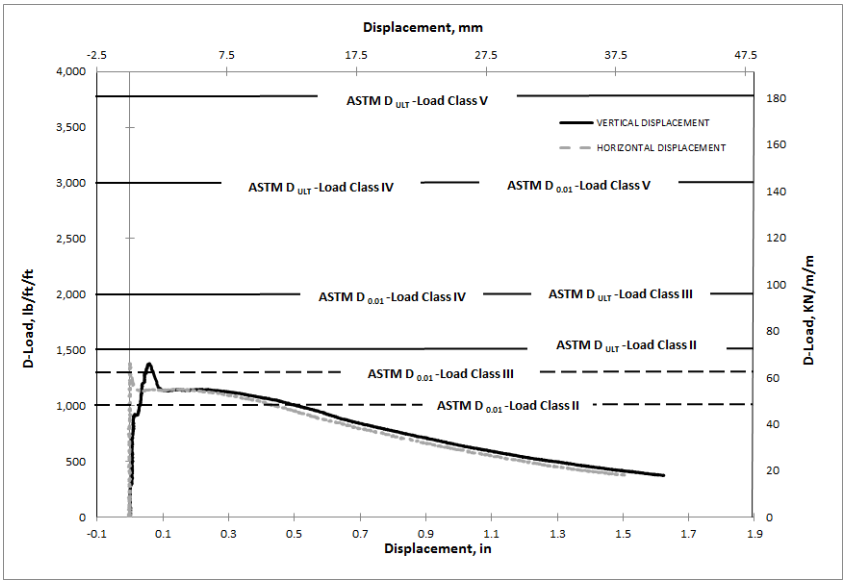

(a)

(b)

(c)

(d)

Figure D30 BASF-(FS7)-30-6-B-DL-66-1(a) Load-Deformation Plot, (b) Crack Propagation, (c) Cross-section Deformation, (d) Crack Width.

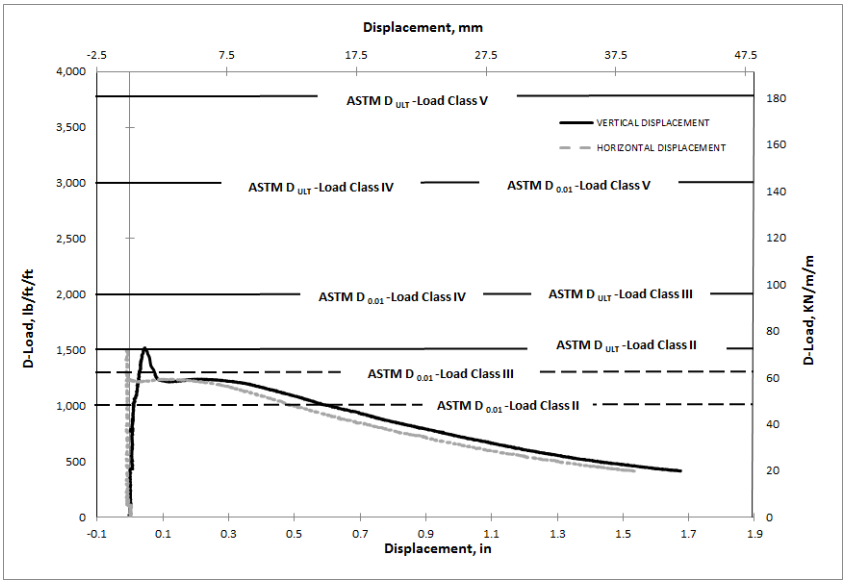

(a)

(b)

(c)

(d)

Figure D31 BASF-(FS7)-30-6-B-DL-66-2 (a) Load-Deformation Plot, (b) Crack Propagation, (c) Cross-section Deformation, (d) Crack Width.

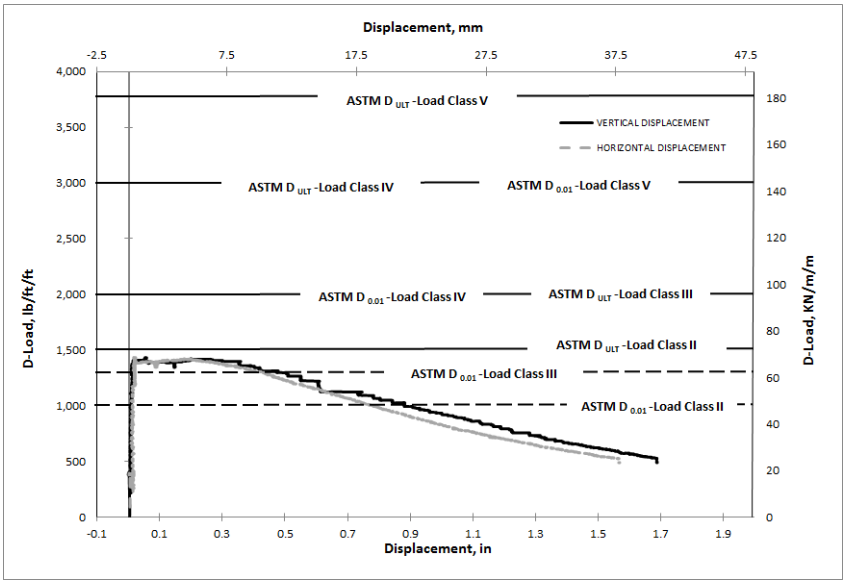

(a)

(b)

(c)

Figure D32 BASF-(FS7)-36-6-B-DL-44-1(a) Load-Deformation Plot, (b) Crack Propagation and (c) Crack Width.

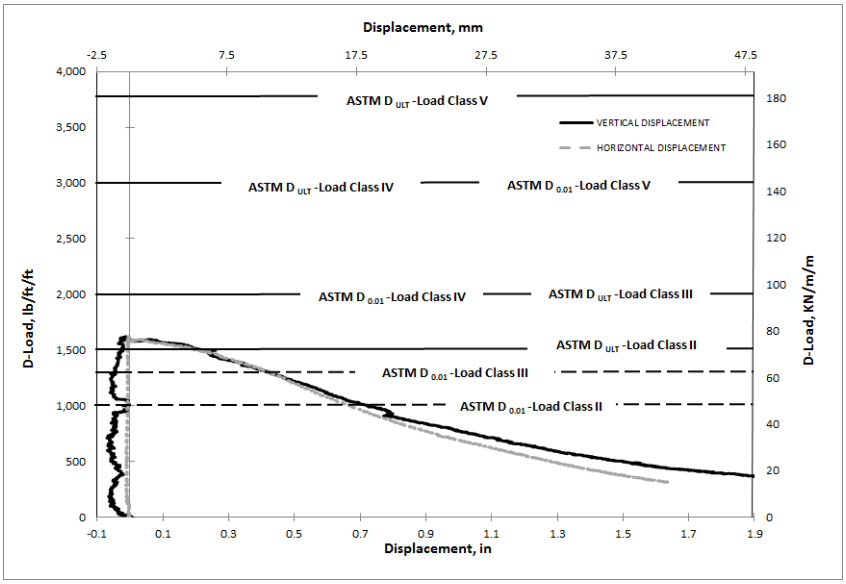

(a)

(b)

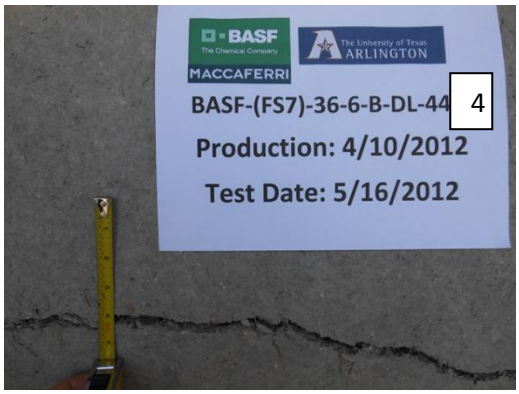

Figure D33 BASF-(FS7)-36-6-B-DL-44-4(a) Load-Deformation Plot, (b) Crack Propagation and (c) Crack Width.

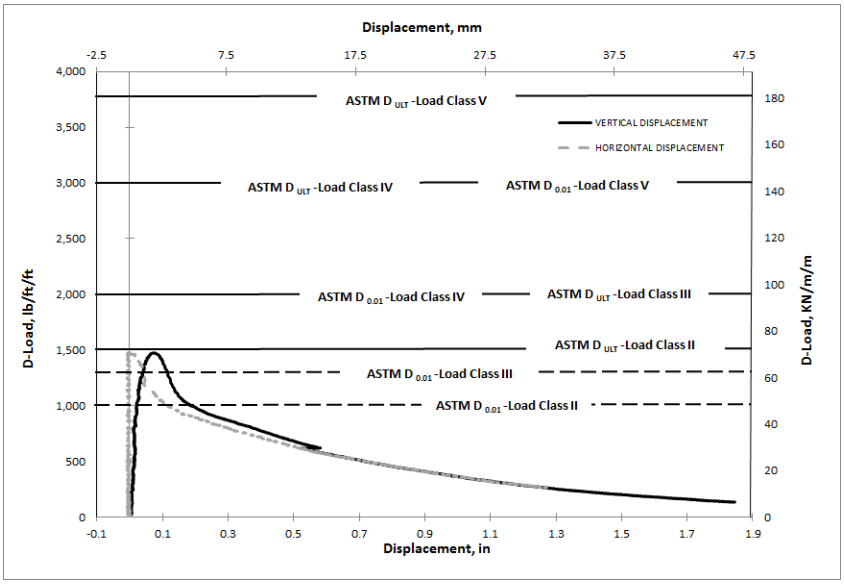

(a)

(b)

(c)

(d)

Figure D34 BASF-(FS7)-36-8-B-DL-44-2-LV (a) Load-Deformation Plot, (b) Crack Propagation, (c) Cross-section Deformation, (d) Crack Width.

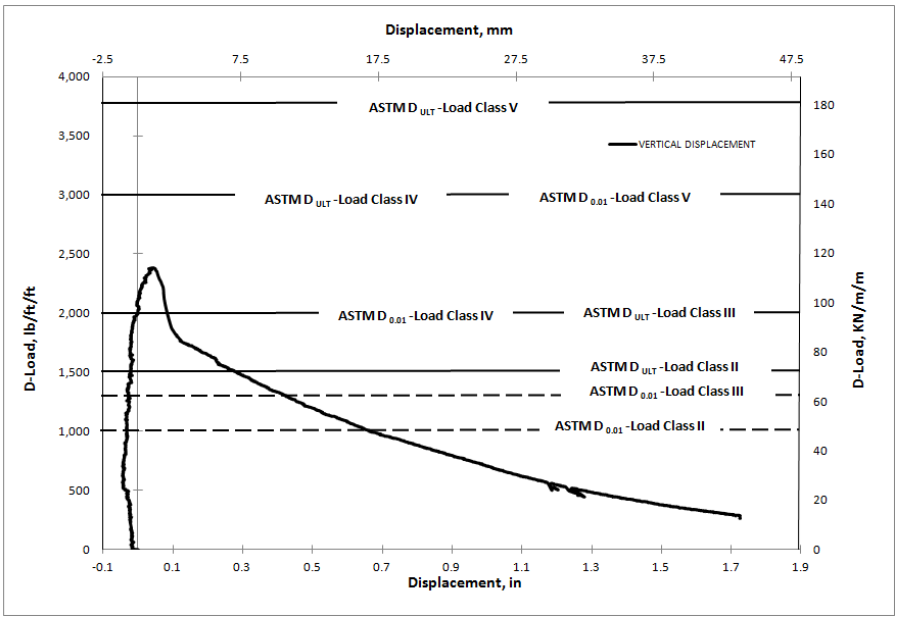

(a)

(b)

(c)

Figure D35 BASF-(FS7)-36-8-C-DL-44-1-NC(a) Load-Deformation Plot, (b) Crack Propagation and (c) Crack Width.

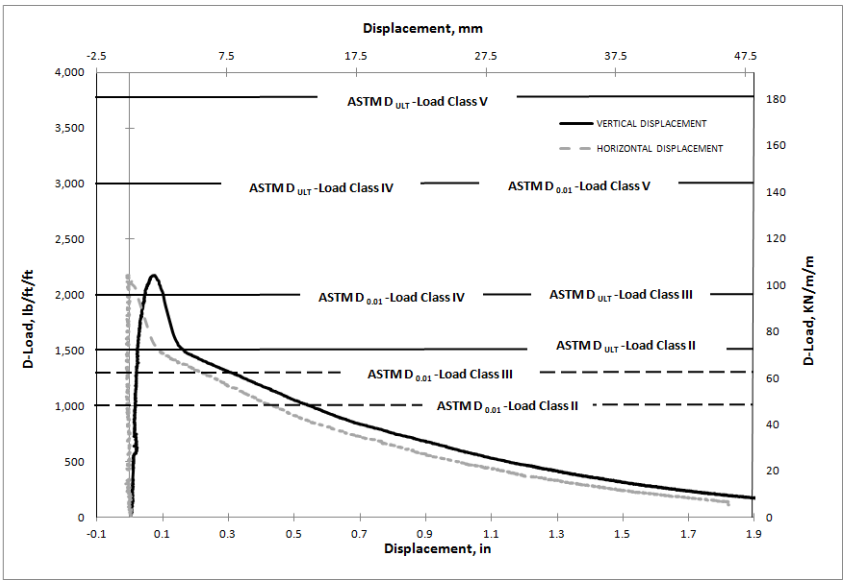

(a)

(b)

(c)

Figure D36 BASF-(FS7)-36-8-C-DL-44-2-NC(a) Load-Deformation Plot, (b) Crack Propagation and (c) Crack Width.

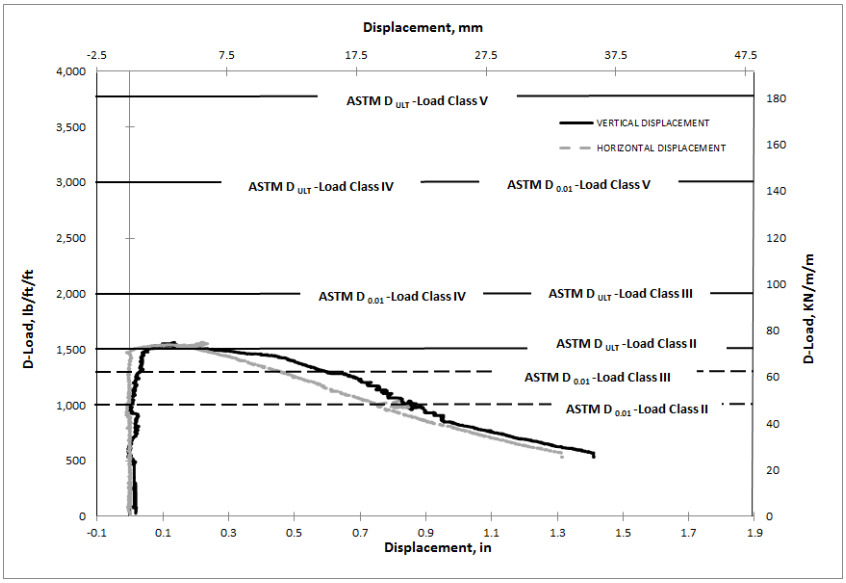

(a)

(b)

Figure D37 BASF-(FS7)-36-6-B-DL-66-1(a) Load-Deformation Plot and (b) Crack Propagation.

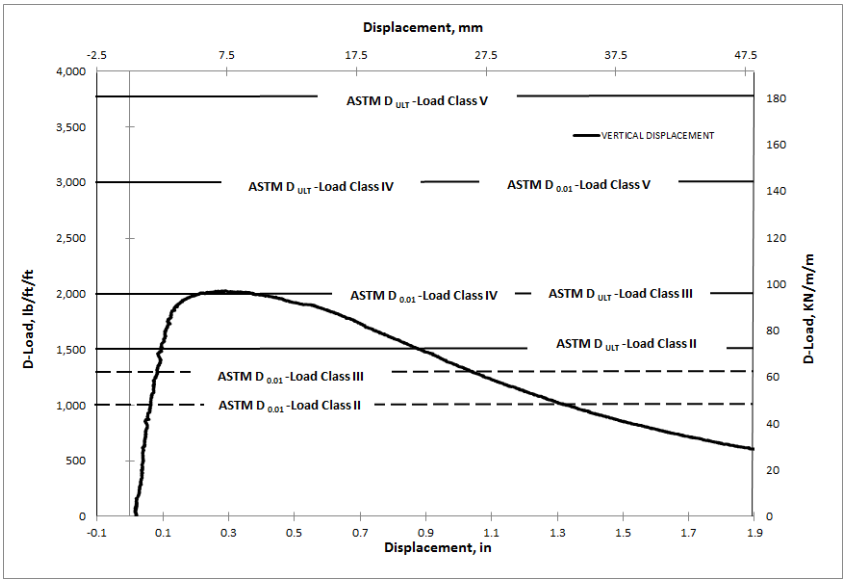

(a)

(b)

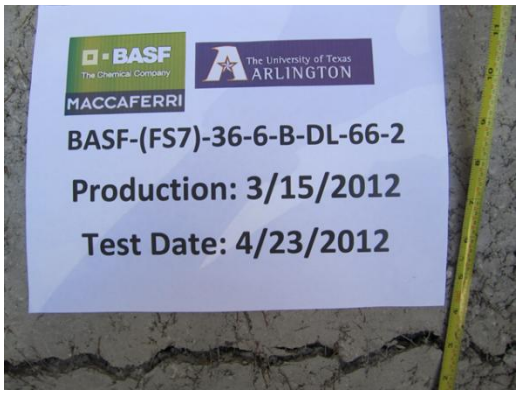

(c)

Figure D38 BASF-(FS7)-36-6-B-DL-66-2(a) Load-Deformation Plot, (b) Crack Propagation and (c) Crack Width.

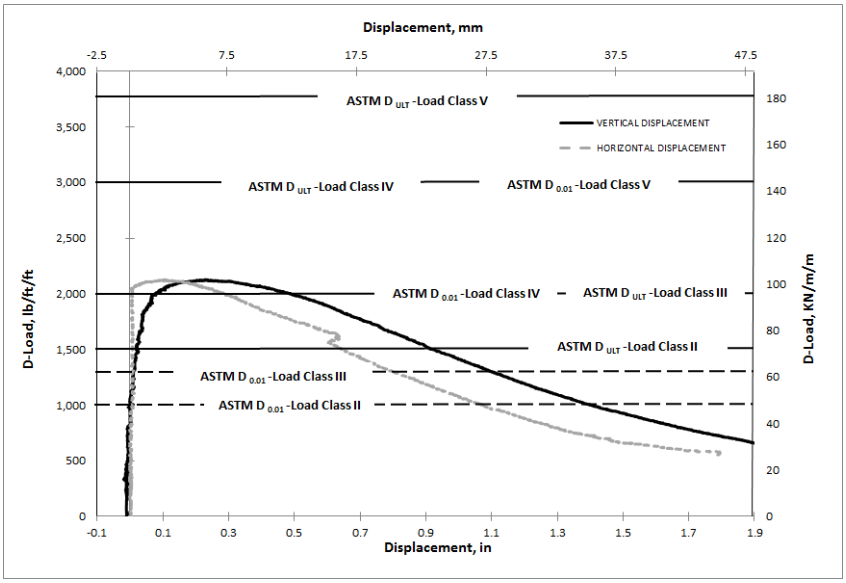

(a)

(b)

(c)

Figure D39 BASF-(FS7)-36-6-B-DL-66-3(a) Load-Deformation Plot, (b) Crack Propagation and (c) Crack Width.

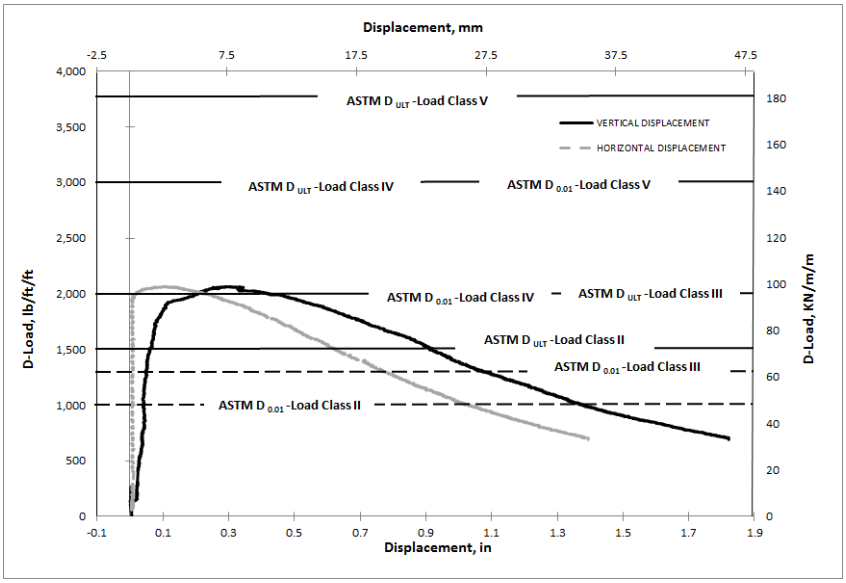

(a)

(b)

(c)

Figure D40 BASF-(FS7)-36-6-B-DL-66-4(a) Load-Deformation Plot, (b) Crack Propagation and (c) Crack Width.

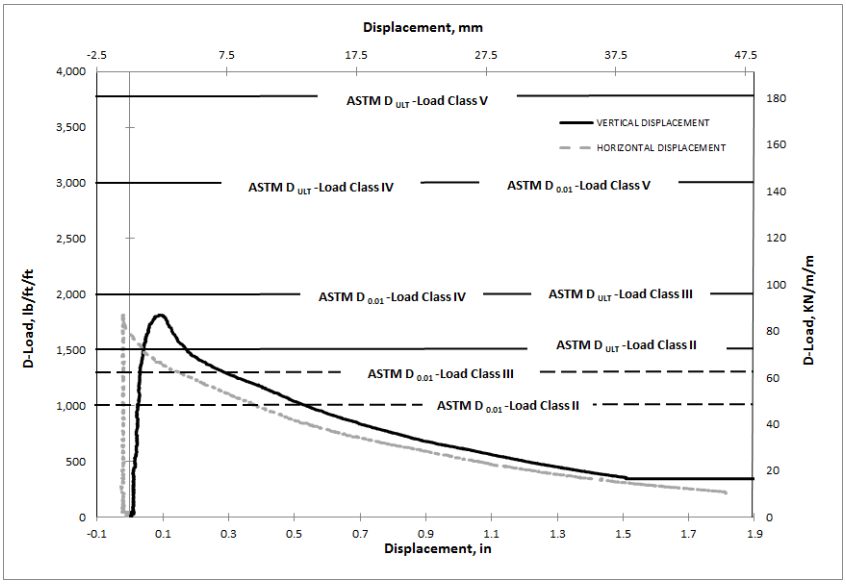

(a)

(b)

(c)

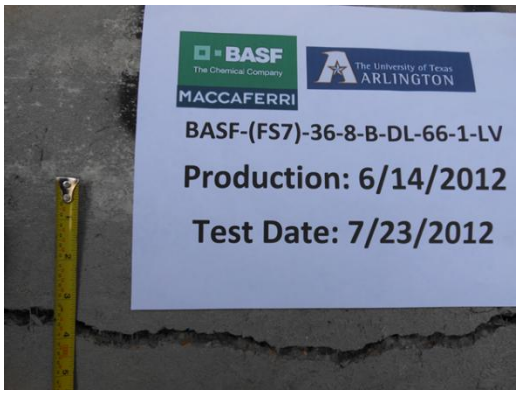

(d)

Figure D41 BASF-(FS7)-36-8-B-DL-66-1-LV (a) Load-Deformation Plot, (b) Crack Propagation, (c) Cross-section Deformation, (d) Crack Width.

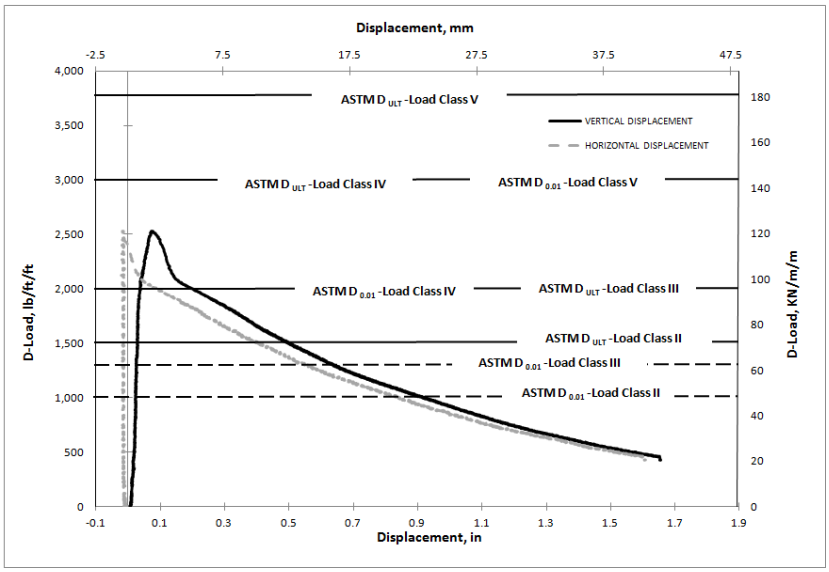

(a)

(b)

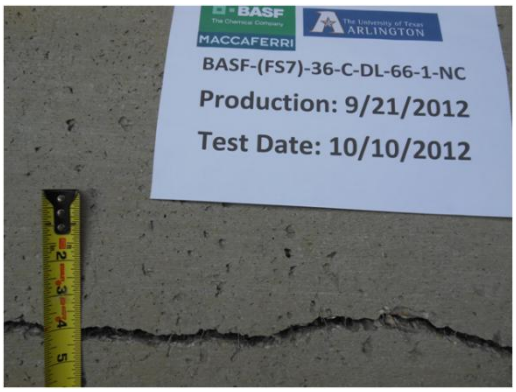

(c)

Figure D42 BASF-(FS7)-36-8-C-DL-66-1-NC(a) Load-Deformation Plot, (b) Crack Propagation and (c) Crack Width.

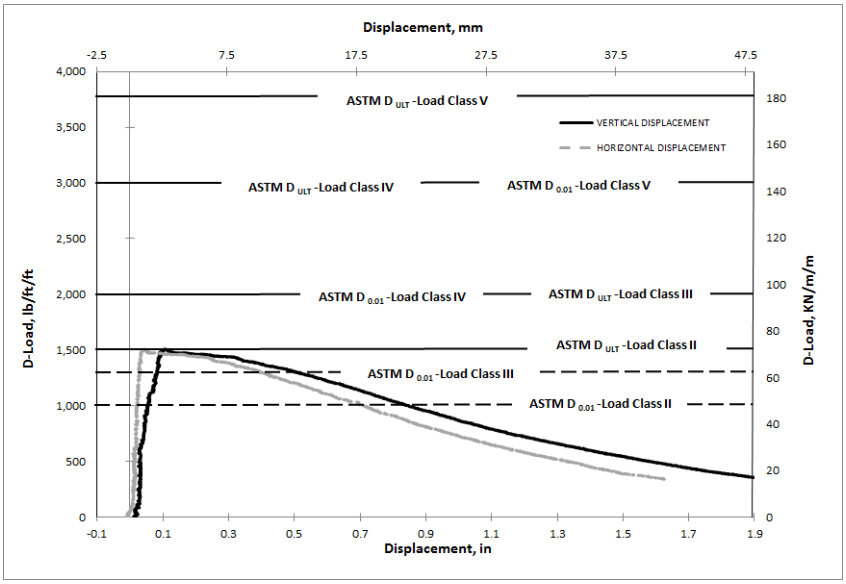

(a)

(b)

(c)

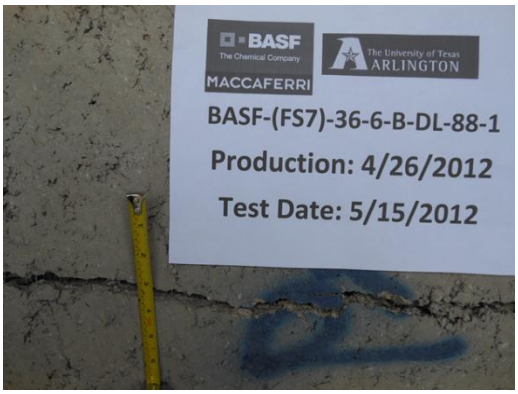

(d)

Figure D43 BASF-(FS7)-36-6-B-DL-88-1(a) Load-Deformation Plot, (b) Crack Propagation, (c) Cross-section Deformation, (d) Crack Width.

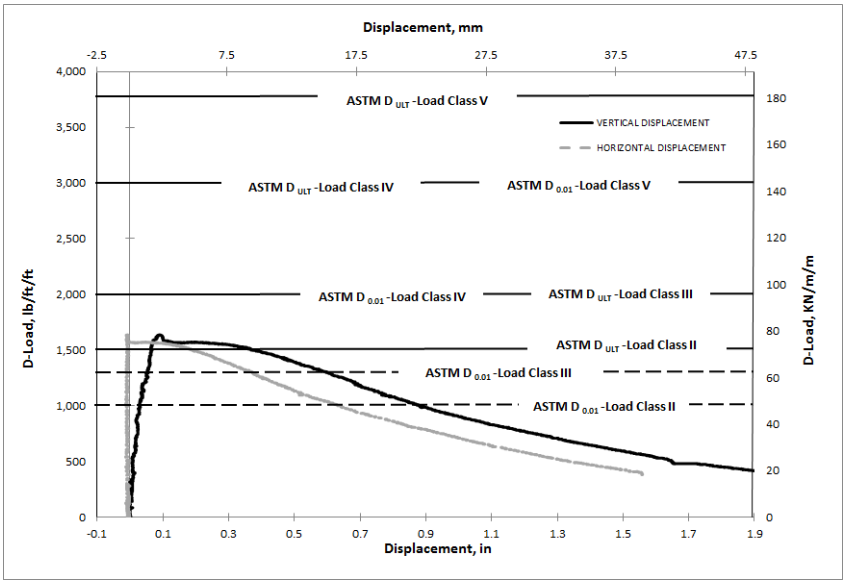

(a)

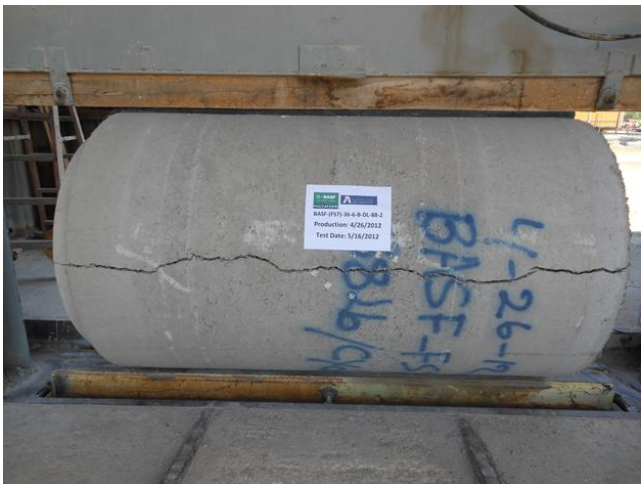

(b)

(c)

(d)

Figure D44 BASF-(FS7)-36-6-B-DL-88-2(a) Load-Deformation Plot, (b) Crack Propagation, (c) Cross-section Deformation, (d) Crack Width.

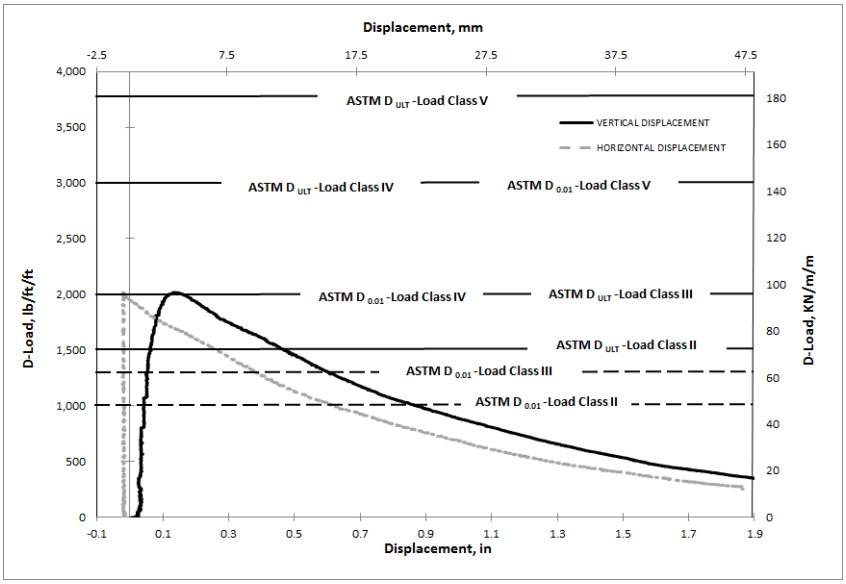

(a)

(b)

(c)

(d)

Figure D45 BASF-(FS7)-36-6-B-DL-88-1-LV (a) Load-Deformation Plot, (b) Crack Propagation, (c) Cross-section Deformation, (d) Crack Width.

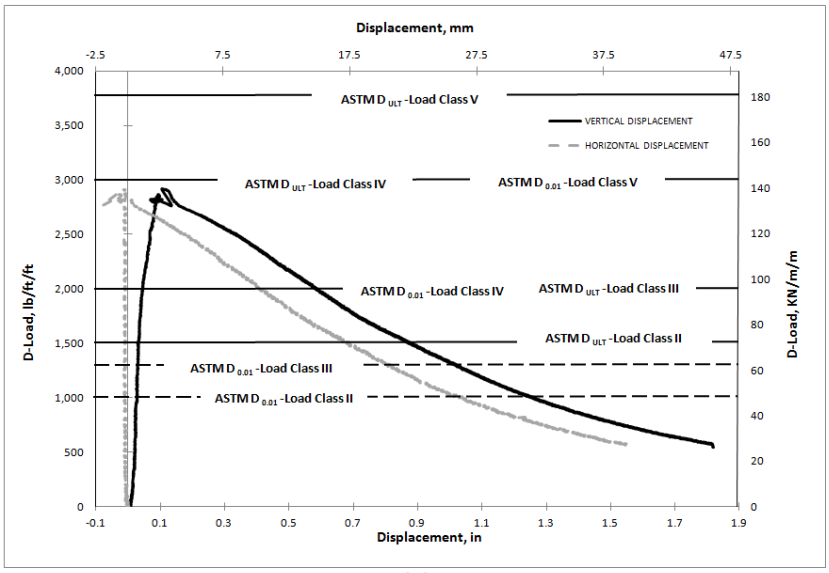

(a)

(b)

(c)

Figure D46 BASF-(FS7)-36-8-C-DL-88-1-NC(a) Load-Deformation Plot, (b) Crack Propagation and (c) Crack Width.

APPENDIX E

SYNTHETIC PIPE GRAPHS

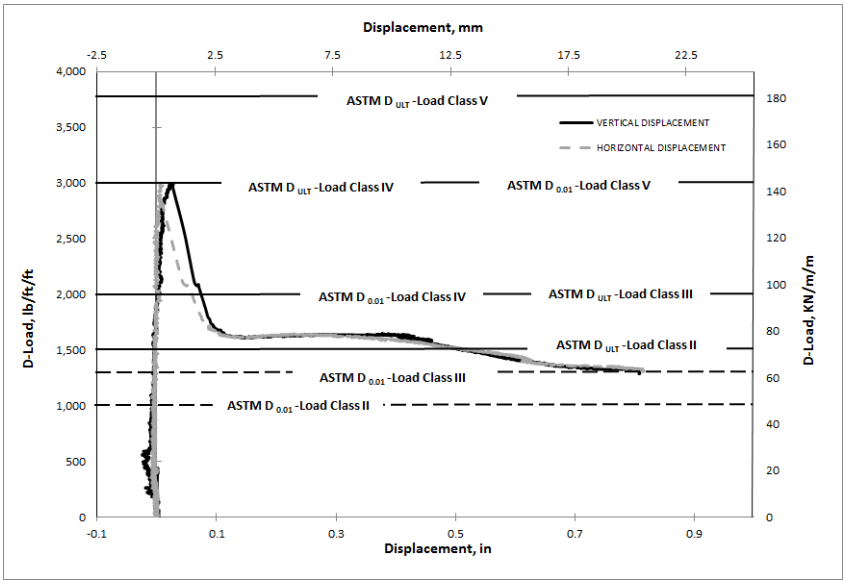

(a)

(b)

(c)

(d)

Figure E1 BASF-(SYN)-15-6-B-DL-8-1-LV (a) Load-Deformation Plot, (b) Crack Propagation, (c) Cross-section Deformation, (d) Crack Width.

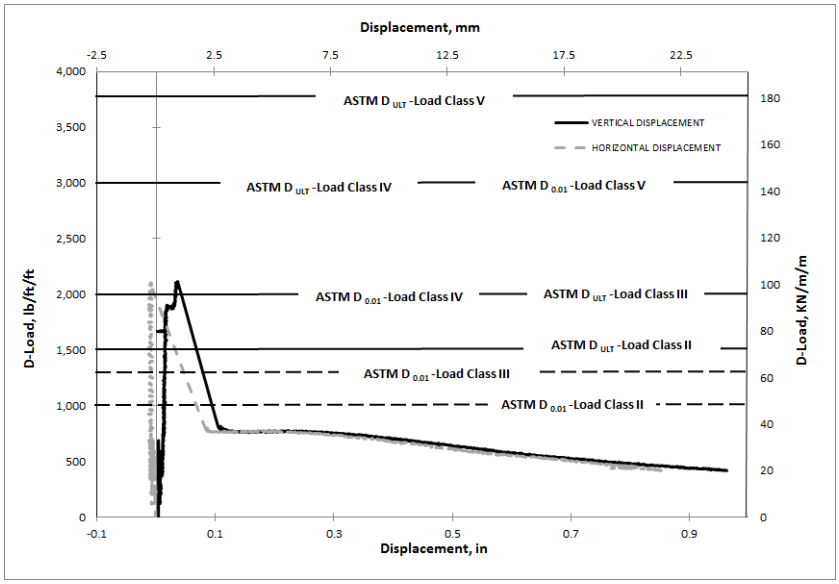

(a)

(b)

(c)

(d)

Figure E2 BASF-(SYN)-18-6-B-DL-4-1(a) Load-Deformation Plot, (b) Crack Propagation, (c) Cross-section Deformation, (d) Crack Width.

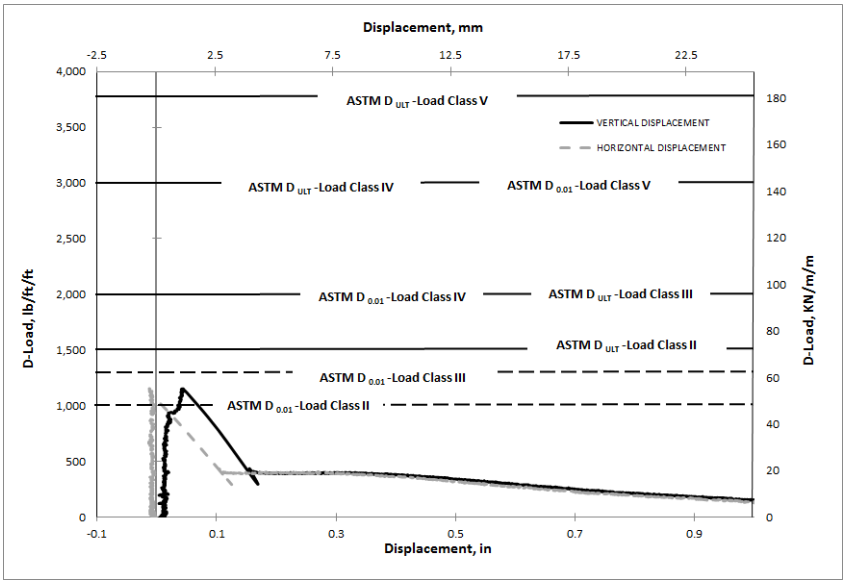

(a)

(b)

(c)

(d)

Figure E3 BASF-(SYN)-18-6-B-DL-4-3 (a) Load-Deformation Plot, (b) Crack Propagation, (c) Cross-section Deformation, (d) Crack Width.

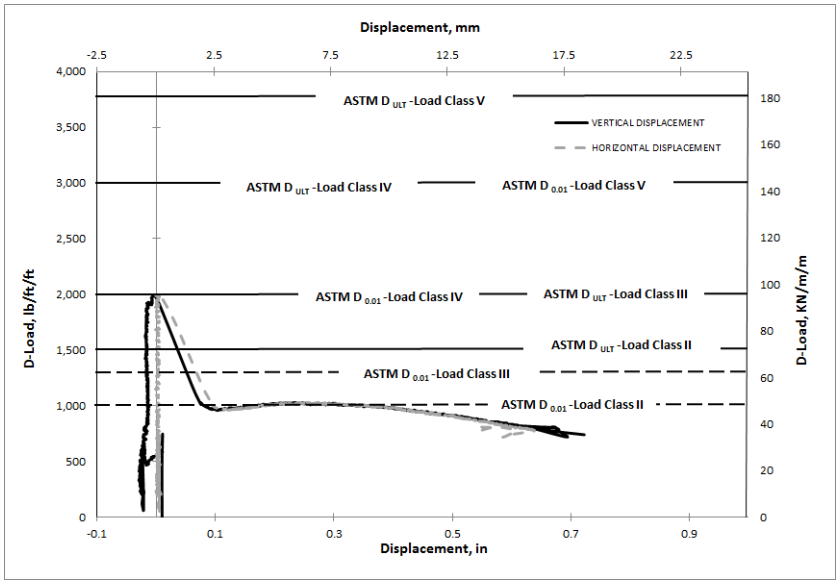

(a)

(b)

(c)

(d)

Figure E4 BASF-(SYN)-18-6-B-DL-6-1(a) Load-Deformation Plot, (b) Crack Propagation, (c) Cross-section Deformation, (d) Crack Width.

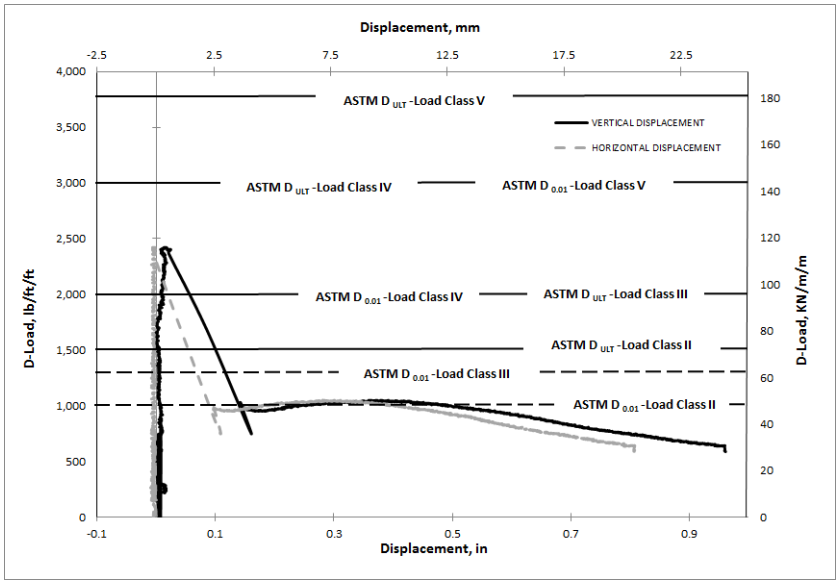

(a)

(b)

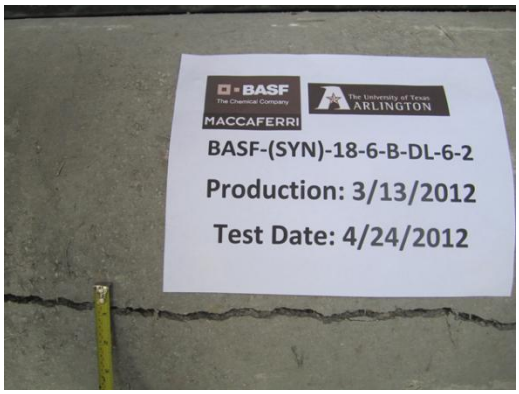

(c)

Figure E5 BASF-(SYN)-18-6-B-DL-6-2(a) Load-Deformation Plot, (b) Crack Propagation and (c) Crack Width.

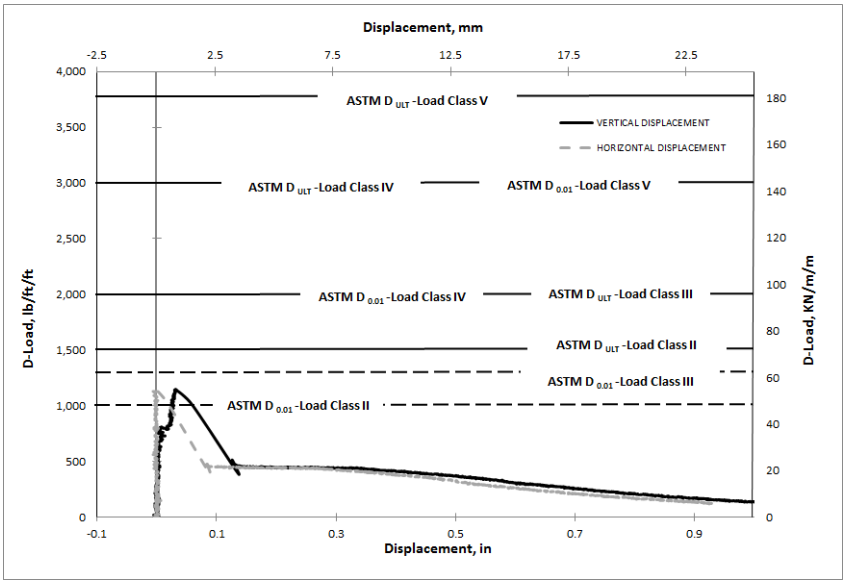

(a)

(b)

(c)

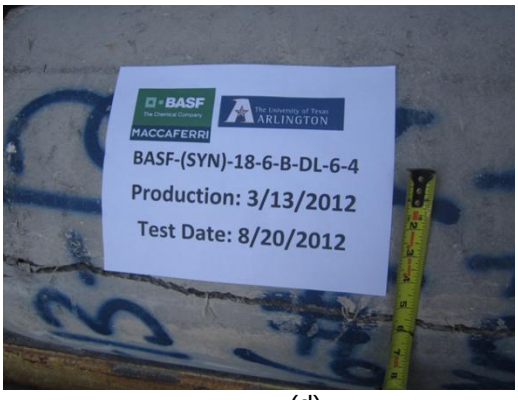

(d)

Figure E6 BASF-(SYN)-18-6-B-DL-6-3 (a) Load-Deformation Plot, (b) Crack Propagation, (c) Cross-section Deformation, (d) Crack Width.

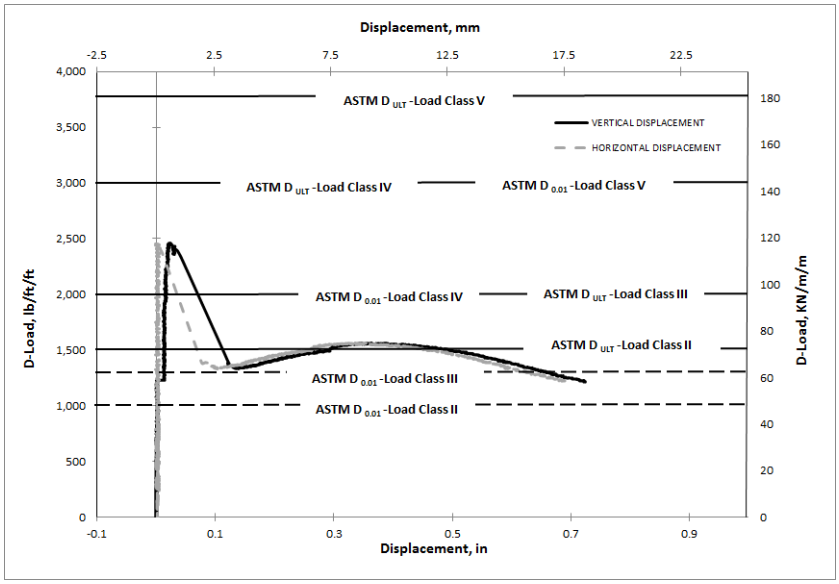

(a)

(b)

(c)

(d)

Figure E7 BASF-(SYN)-18-6-B-DL-8-1(a) Load-Deformation Plot, (b) Crack Propagation, (c) Cross-section Deformation, (d) Crack Width.

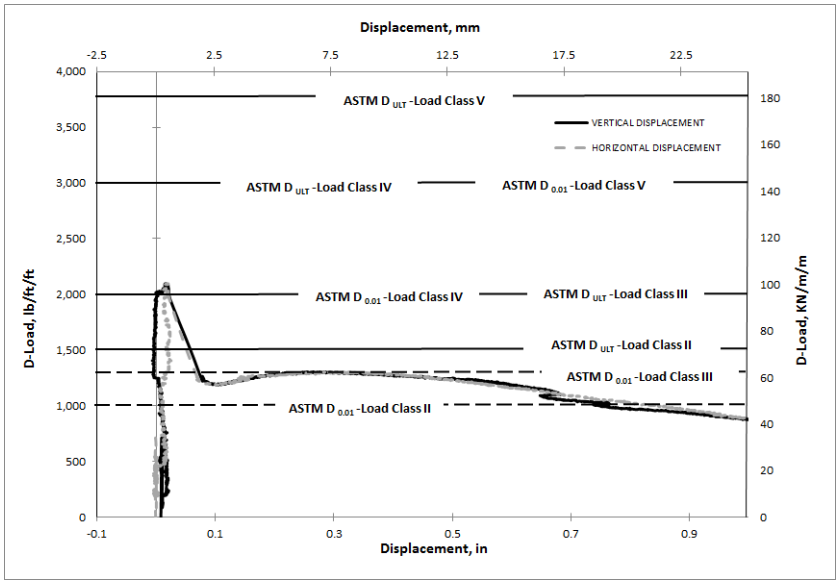

(a)

(b)

(c)

(d)

Figure E8 BASF-(SYN)-18-6-B-DL-8-2 (a) Load-Deformation Plot, (b) Crack Propagation, (c) Cross-section Deformation, (d) Crack Width.

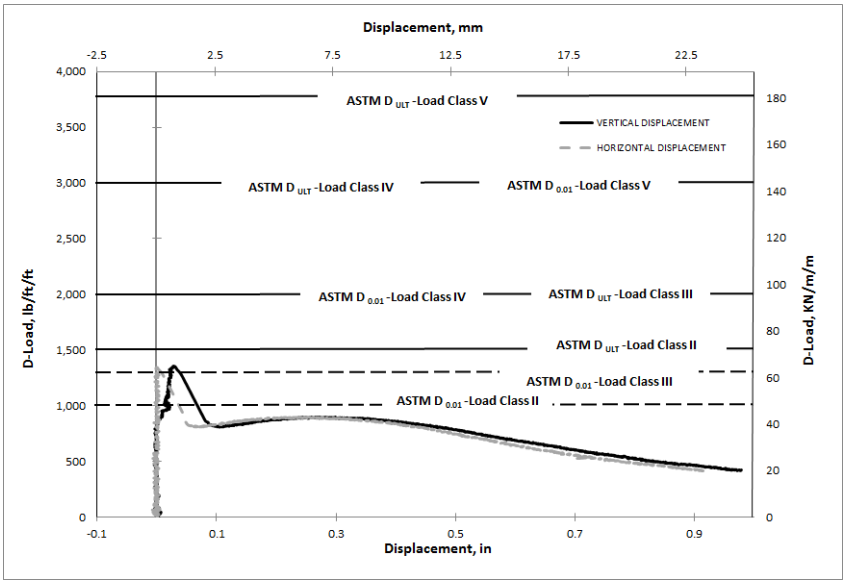

(a)

(b)

(c)

(d)

Figure E9 BASF-(SYN)-18-6-B-DL-8-3 (a) Load-Deformation Plot, (b) Crack Propagation, (c) Cross-section Deformation, (d) Crack Width.

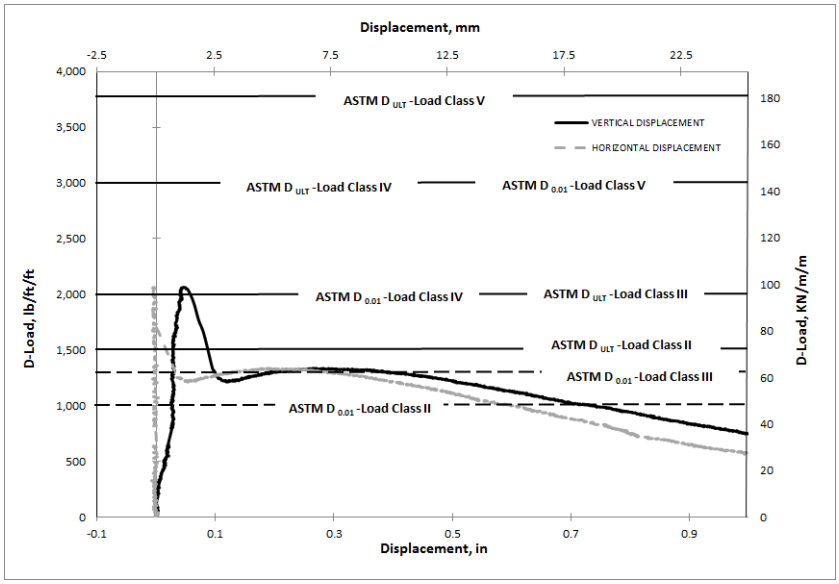

(a)

(b)

(c)

Figure E10 BASF-(SYN)-18-6-B-DL-10-1(a) Load-Deformation Plot, (b) Crack Propagation and (c) Crack Width.

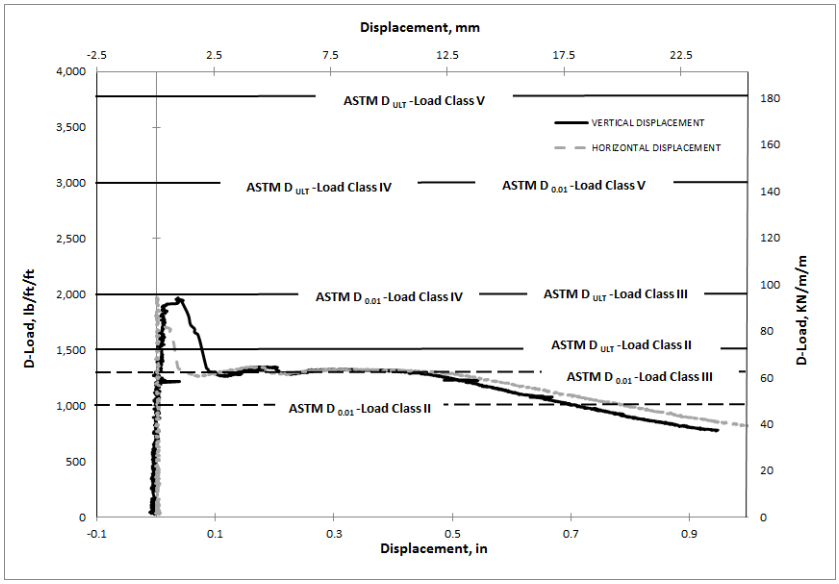

(a)

(b)

(c)

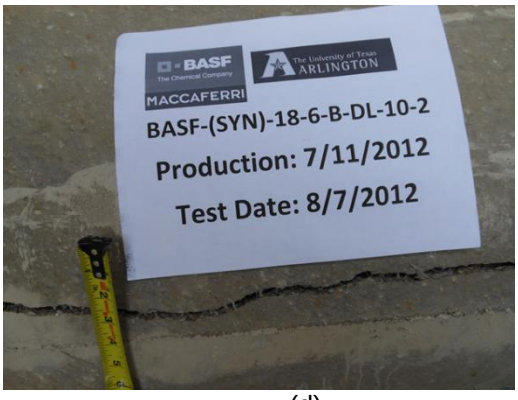

(d)

Figure E11 BASF-(SYN)-18-6-B-DL-10-2 (a) Load-Deformation Plot, (b) Crack Propagation, (c) Cross-section Deformation, (d) Crack Width.

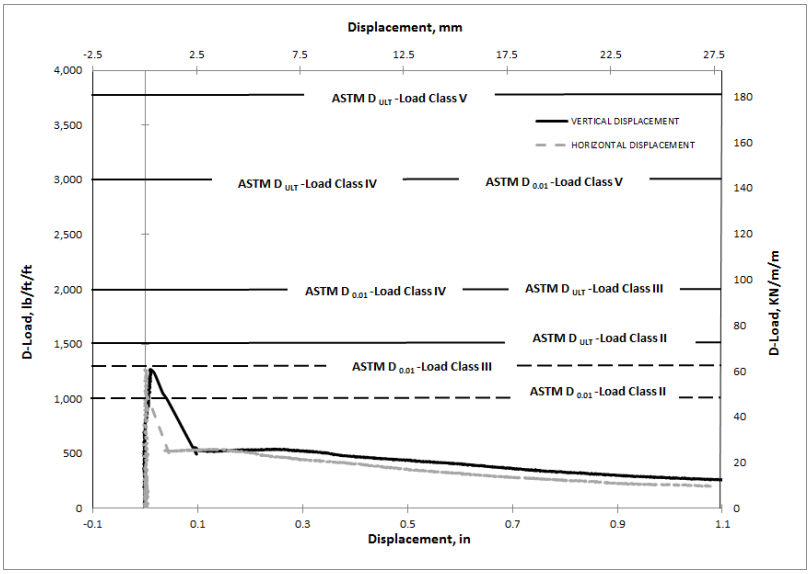

(a)

(b)

(c)

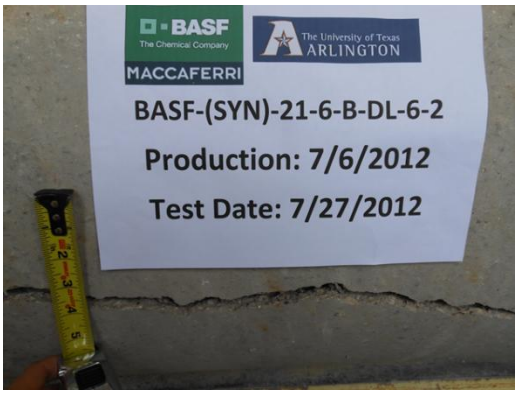

(d)

Figure E12 BASF-(SYN)-21-6-B-DL-6-2 (a) Load-Deformation Plot, (b) Crack Propagation, (c) Cross-section Deformation, (d) Crack Width.

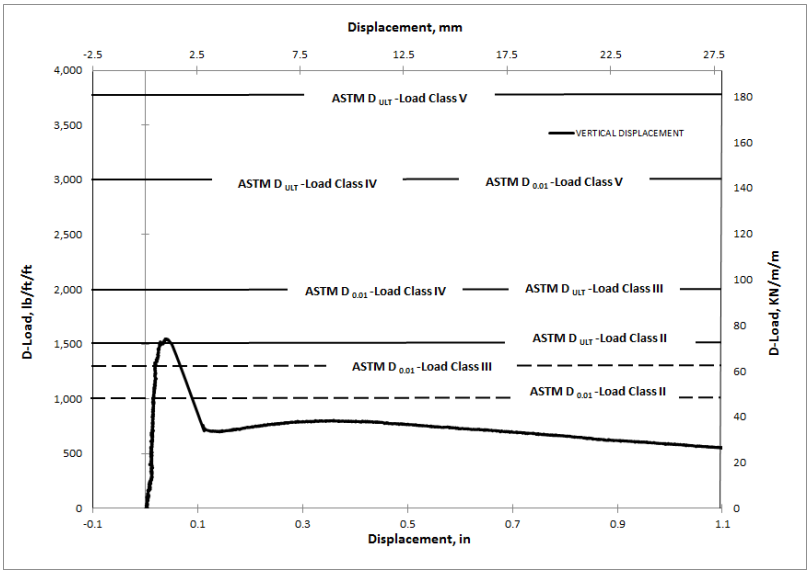

(a)

(b)

(c)

(d)

Figure E13 BASF-(SYN)-21-6-B-DL-8-2 (a) Load-Deformation Plot, (b) Crack Propagation, (c) Cross-section Deformation, (d) Crack Width.

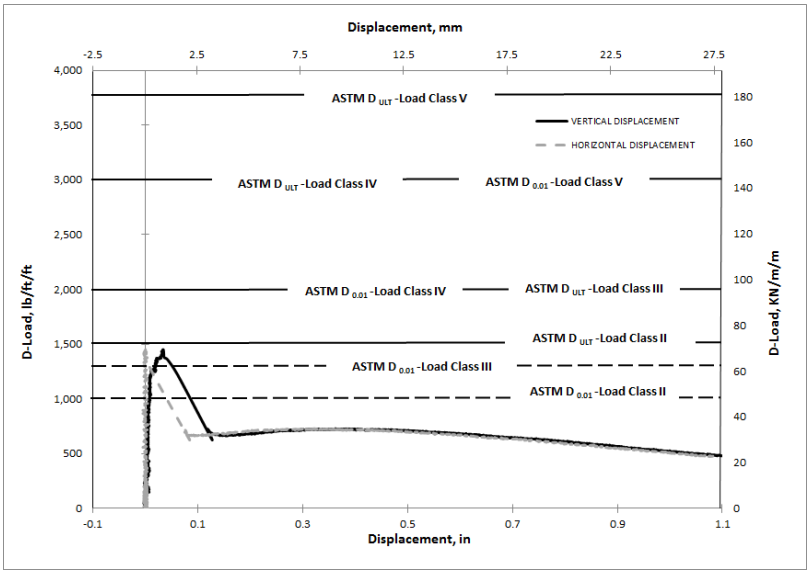

(a)

(b)

(c)

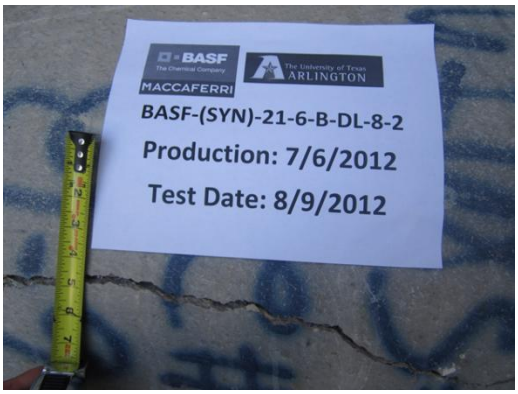

(d)

Figure E14 BASF-(SYN)-21-6-B-DL-8-3(a) Load-Deformation Plot, (b) Crack Propagation, (c) Cross-section Deformation, (d) Crack Width.

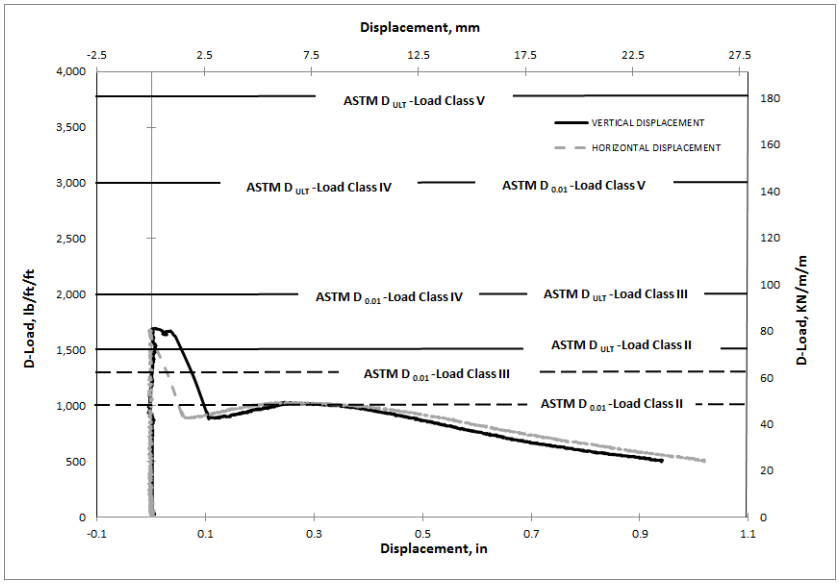

(a)

(b)

(c)

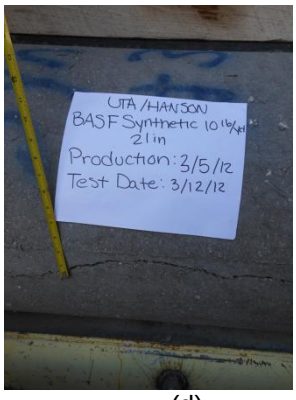

(d)

Figure E15 BASF-(SYN)-21-6-B-DL-10-1(a) Load-Deformation Plot, (b) Crack Propagation, (c) Cross-section Deformation, (d) Crack Width.

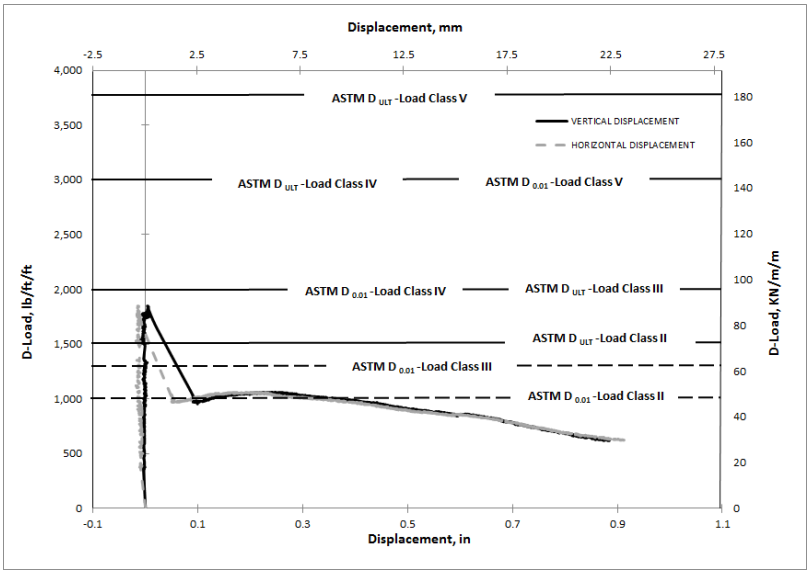

(a)

(b)

(c)

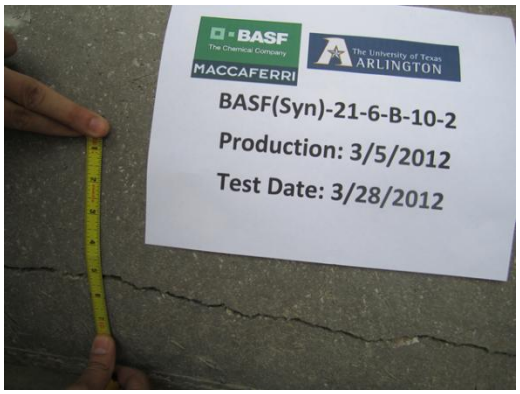

(d)

Figure E16 BASF-(SYN)-21-6-B-DL-10-2 (a) Load-Deformation Plot, (b) Crack Propagation, (c) Cross-section Deformation, (d) Crack Width.

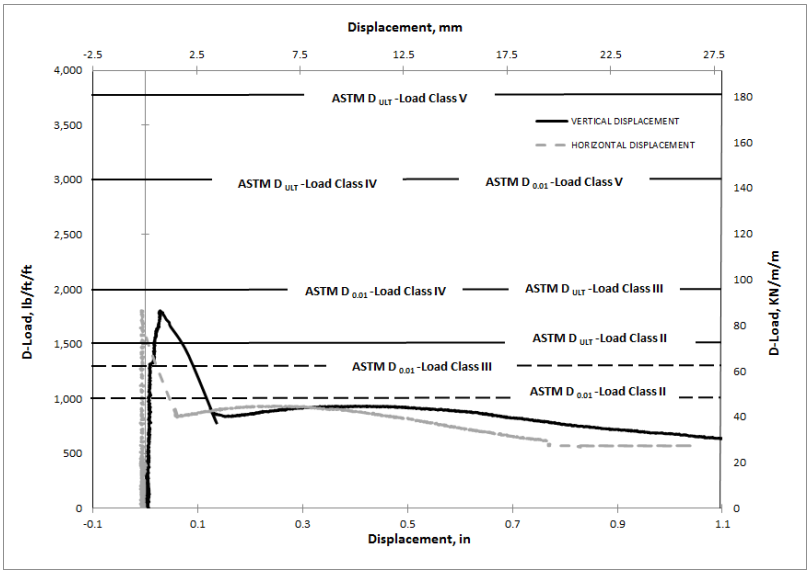

(a)

(b)

(c)

(d)

Figure E17 BASF-(SYN)-21-6-B-DL-10-3(a) Load-Deformation Plot, (b) Crack Propagation, (c) Cross-section Deformation, (d) Crack Width.

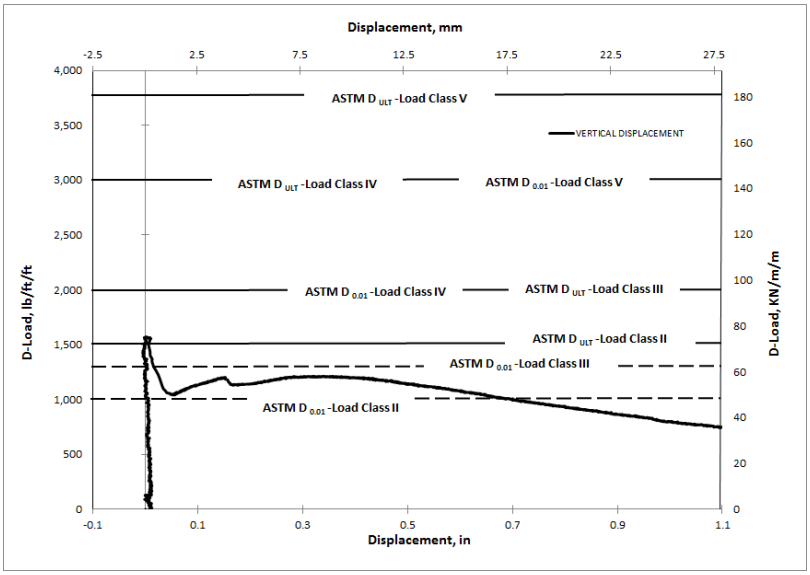

(a)

(b)

(c)

(d)

Figure E18 BASF-(SYN)-21-6-B-DL-12-1(a) Load-Deformation Plot, (b) Crack Propagation, (c) Cross-section Deformation, (d) Crack Width.

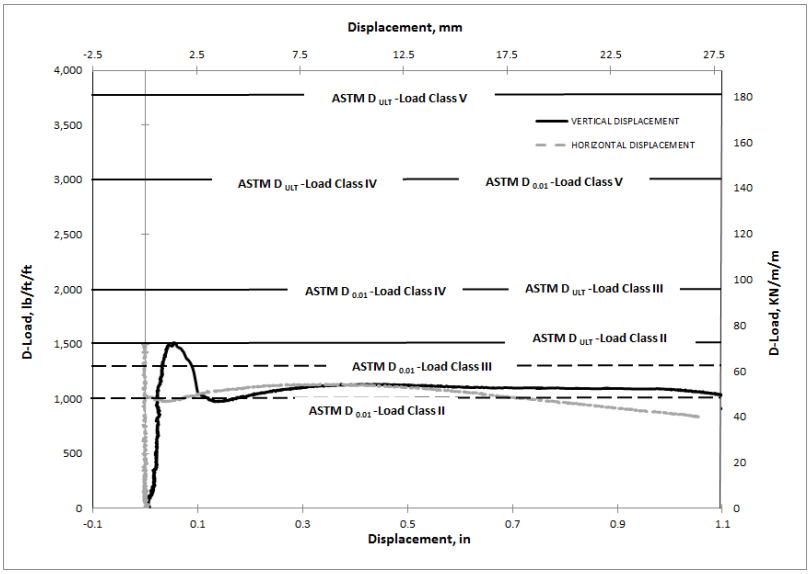

(a)

(b)

(c)

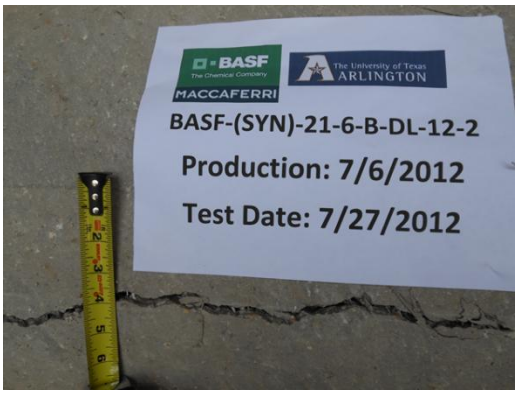

(d)

Figure E19 BASF-(SYN)-21-6-B-DL-12-2 (a) Load-Deformation Plot, (b) Crack Propagation, (c) Cross-section Deformation, (d) Crack Width.

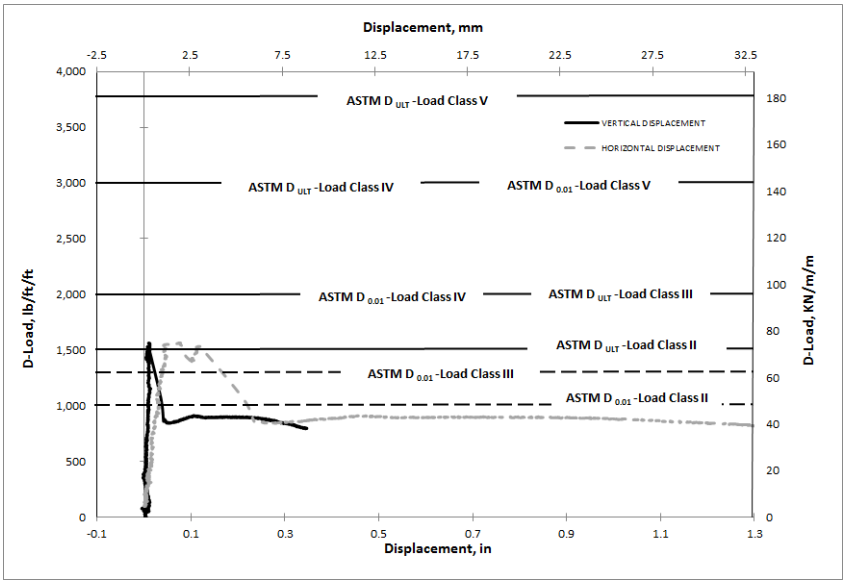

(a)

(b)

(c)

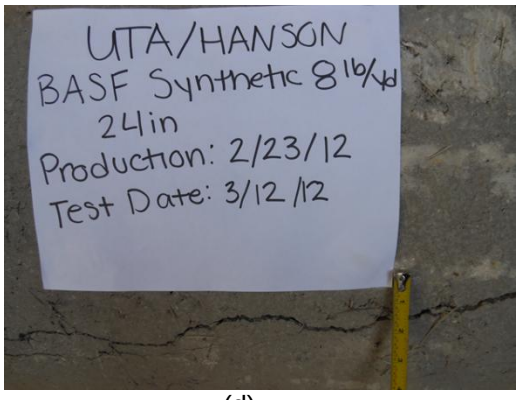

(d)

Figure E20 BASF-(SYN)-24-6-B-DL-8-1(a) Load-Deformation Plot, (b) Crack Propagation, (c) Cross-section Deformation, (d) Crack Width.

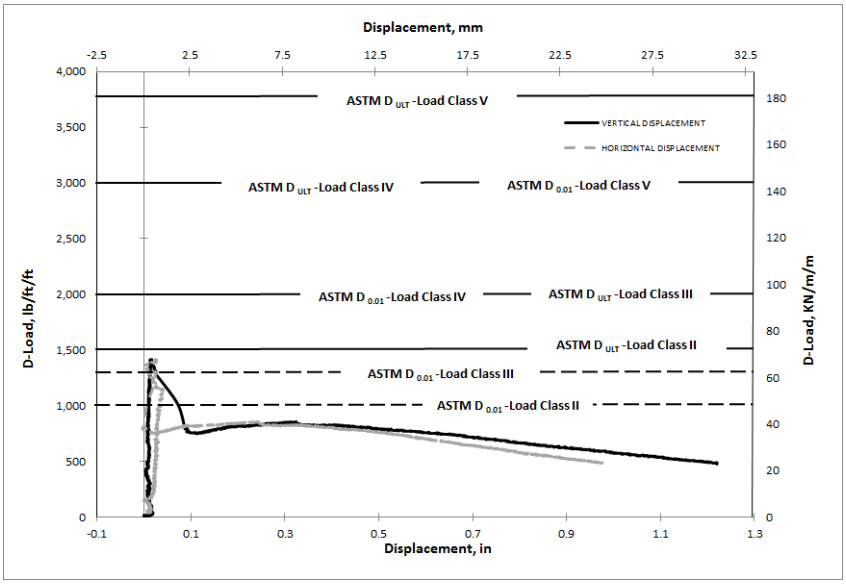

(a)

(b)

(c)

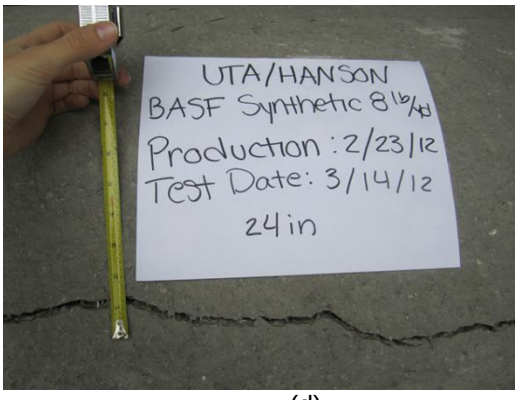

(d)

Figure E21 BASF-(SYN)-24-6-B-DL-8-2 (a) Load-Deformation Plot, (b) Crack Propagation, (c) Cross-section Deformation, (d) Crack Width.

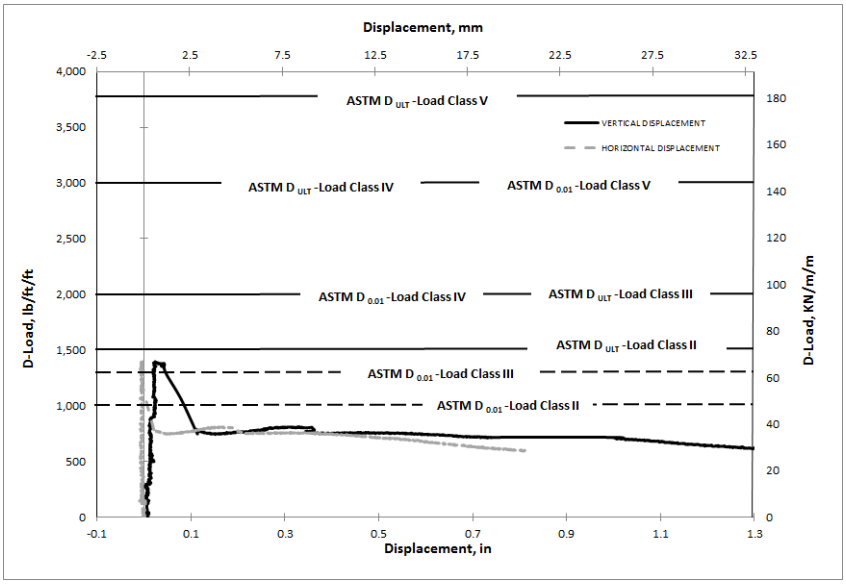

(a)

(b)

(c)

(d)

Figure E22 BASF-(SYN)-24-6-B-DL-8-3(a) Load-Deformation Plot, (b) Crack Propagation, (c) Cross-section Deformation, (d) Crack Width.

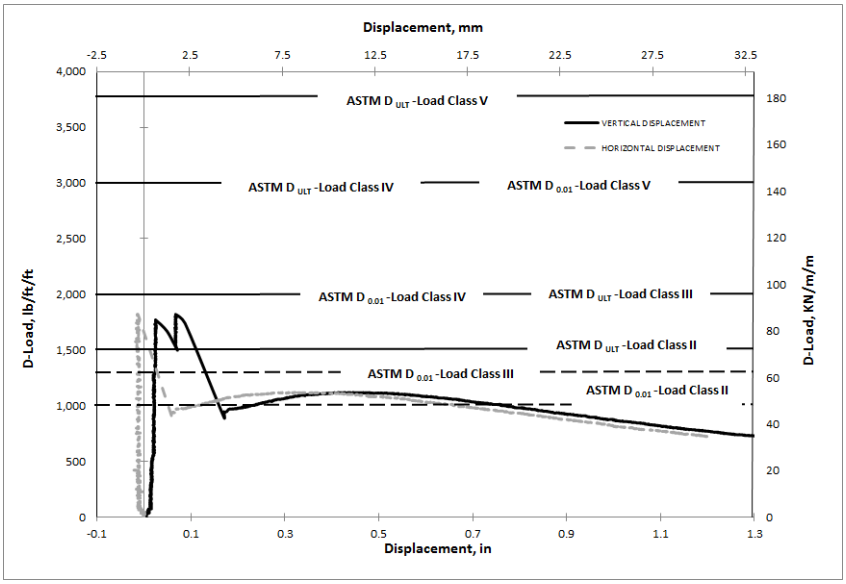

(a)

(b)

(c)

(d)

Figure E23 BASF-(SYN)-24-8-B-DL-8-4-LV(a) Load-Deformation Plot, (b) Crack Propagation, (c) Cross-section Deformation, (d) Crack Width.

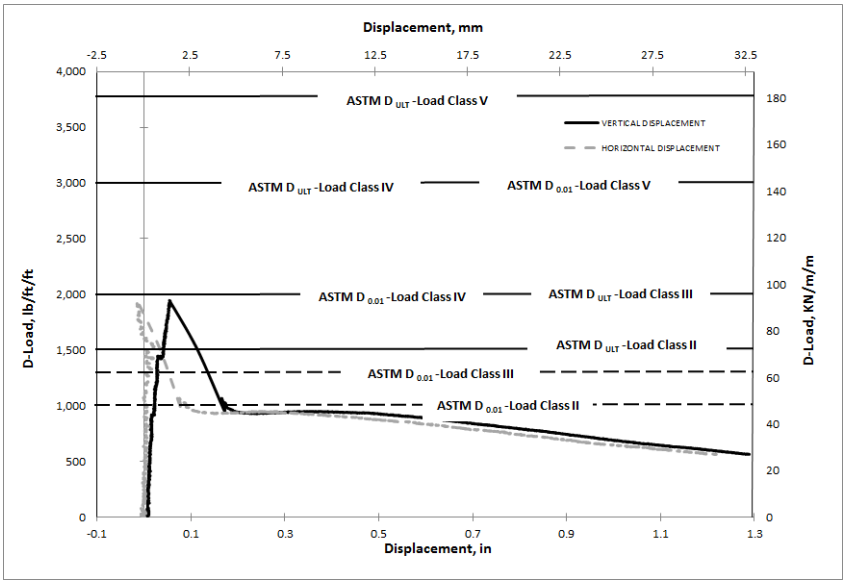

(a)

(b)

(c)

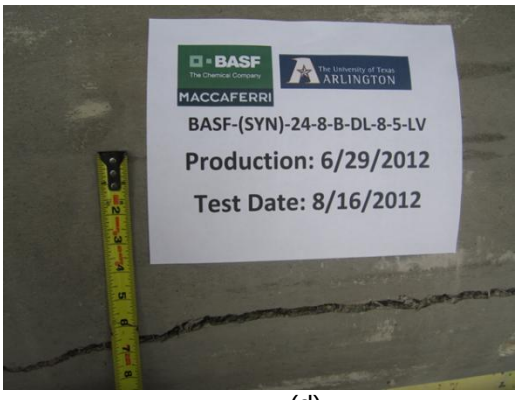

(d)

Figure E24 BASF-(SYN)-24-8-B-DL-8-5-LV(a) Load-Deformation Plot, (b) Crack Propagation, (c) Cross-section Deformation, (d) Crack Width.

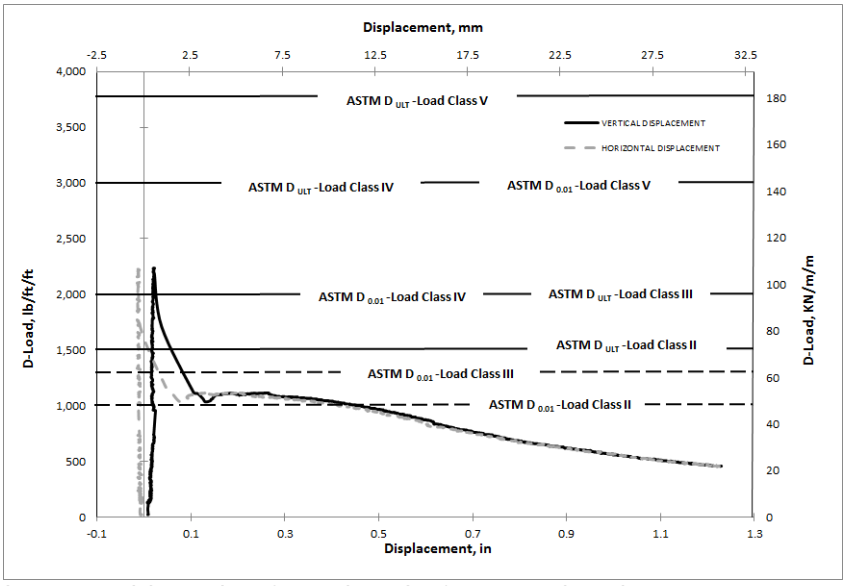

Figure E25 (a) Load-Deformation Plot for BASF-(SYN)-24-8-B-DL-8-1-NC

Figure E25 (b) Crack Propagation for BASF-(SYN)-24-8-B-DL-8-1-NC

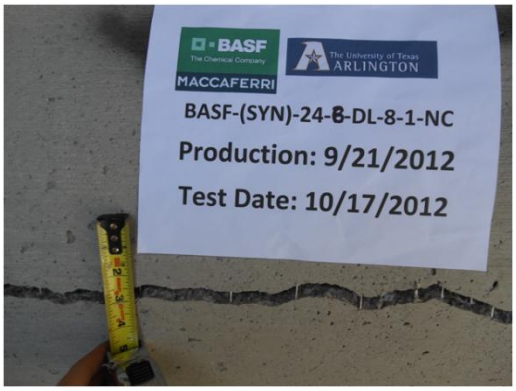

(c)

Figure E25 BASF-(SYN)-24-8-B-DL-8-1-NC (a) Load-Deformation Plot, (b) Crack Propagation and (c) Crack Width.

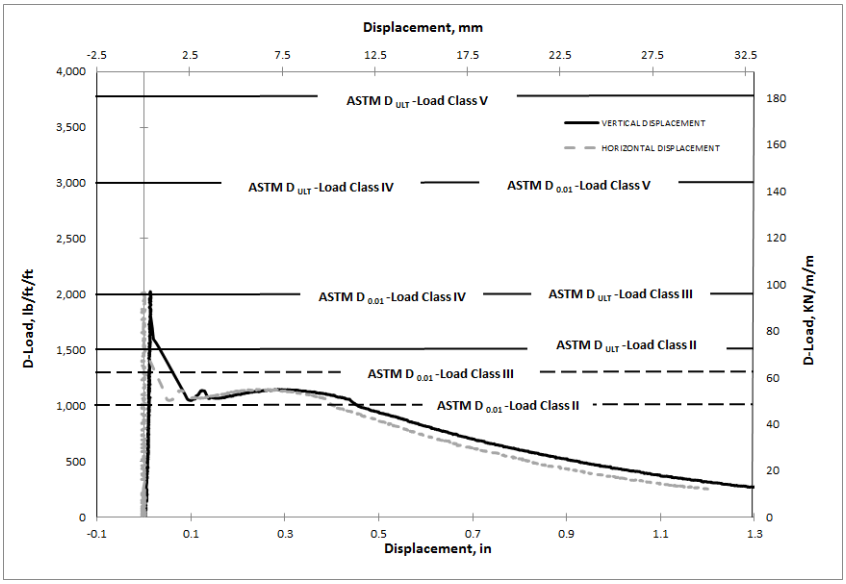

(a)

(b)

(c)

Figure E26 BASF-(SYN)-24-8-B-DL-8-2-NC (a) Load-Deformation Plot, (b) Crack Propagation and (c) Crack Width.

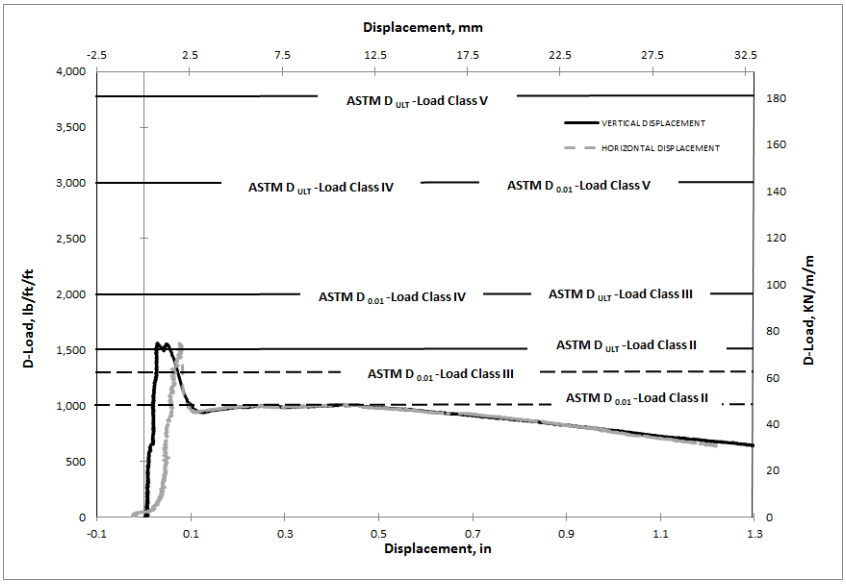

Figure E27 (a) Load-Deformation Plot for BASF-(SYN)-24-6-B-DL-10-1

Figure E27 (b) Crack Propagation for BASF-(SYN)-24-6-B-DL-10-1

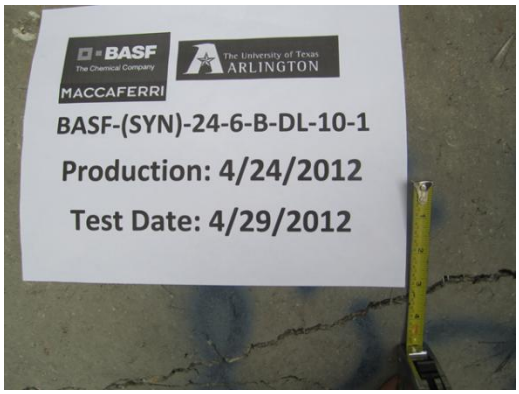

(c)

Figure E27 BASF-(SYN)-24-6-B-DL-10-1(a) Load-Deformation Plot, (b) Crack Propagation and (c) Crack Width.

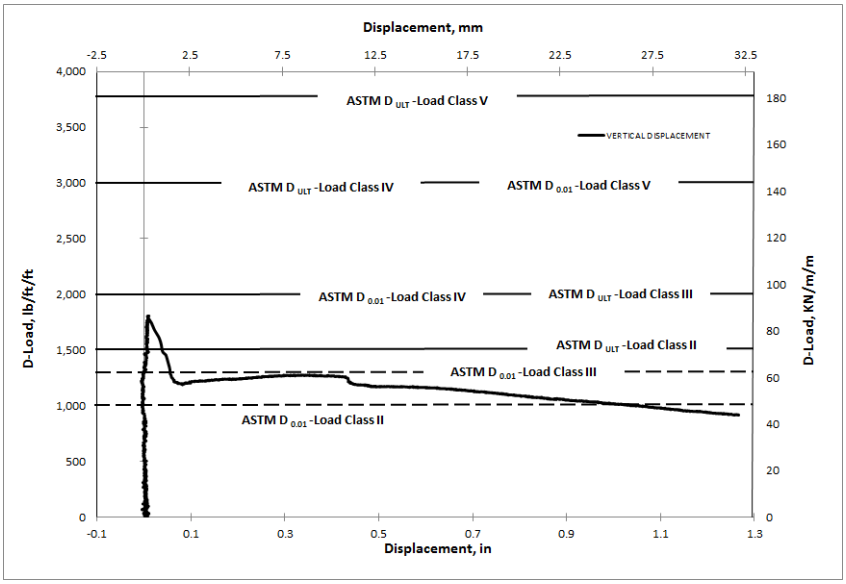

(a)

(b)

(c)

(d)

Figure E28 BASF-(SYN)-24-8-B-DL-10-1-LV (a) Load-Deformation Plot, (b) Crack Propagation, (c) Cross-section Deformation, (d) Crack Width.

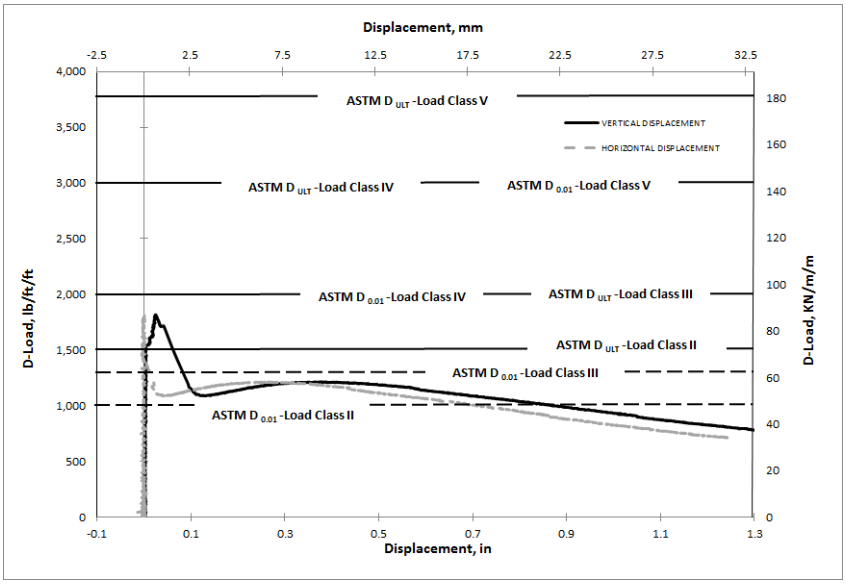

(a)

(b)

(c)

(d)

Figure E29 BASF-(SYN)-24-8-B-DL-10-2-LV (a) Load-Deformation Plot, (b) Crack Propagation, (c) Cross-section Deformation, (d) Crack Width.

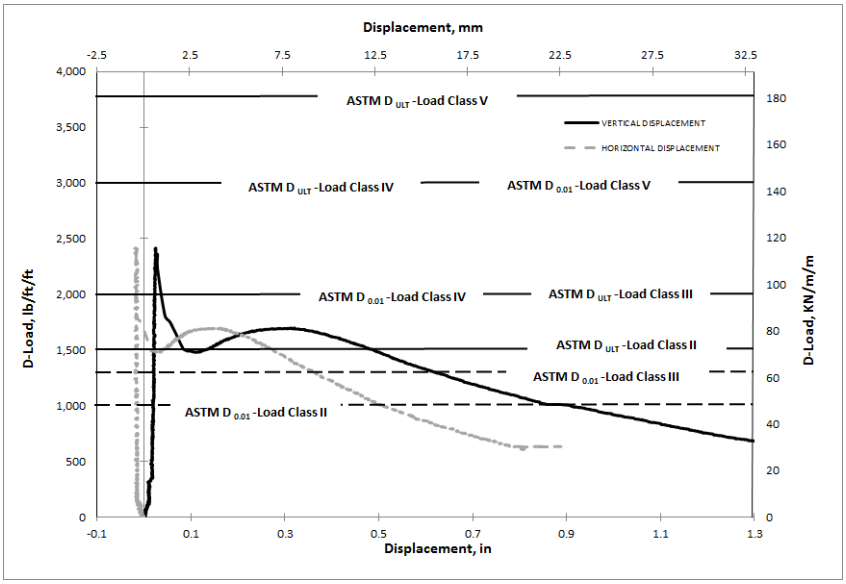

(a)

(b)

(c)

Figure E30 BASF-(SYN)-24-8-B-DL-10-2-NC (a) Load-Deformation Plot, (b) Crack Propagation and (c) Crack Width.

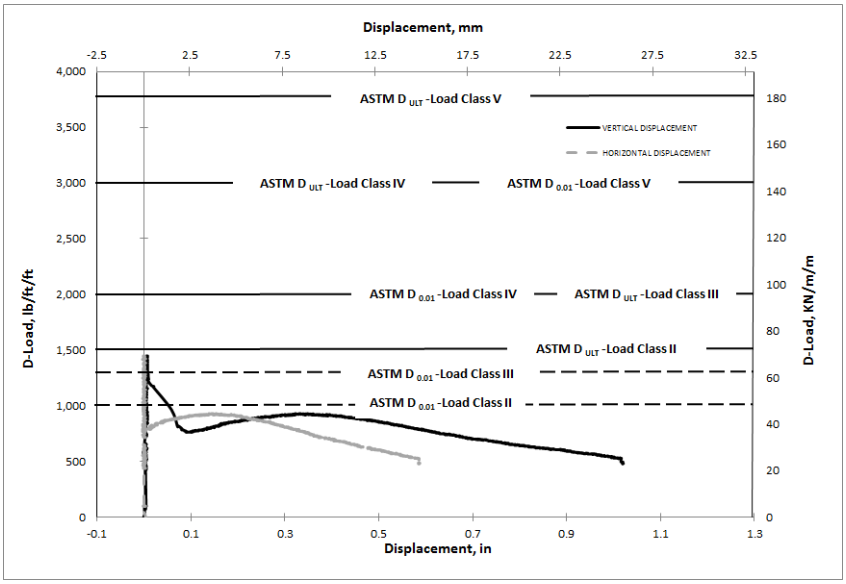

(a)

(b)

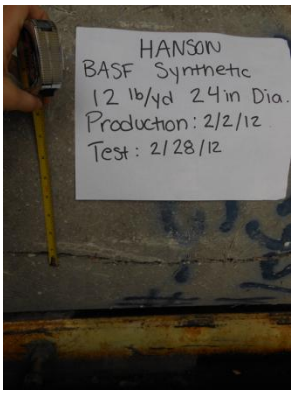

(c)

Figure E31 BASF-(SYN)-24-6-B-DL-12-4(a) Load-Deformation Plot, (b) Crack Propagation and (c) Crack Width.

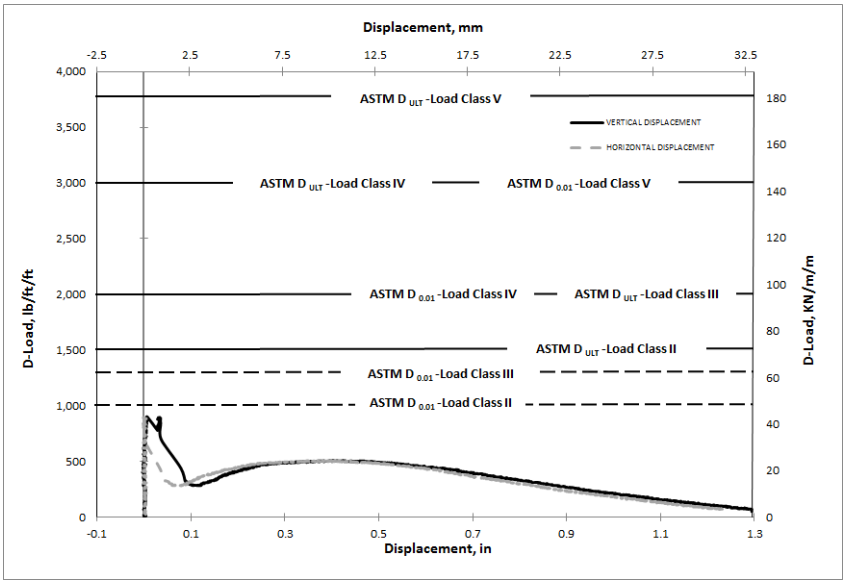

(a)

(b)

(c)

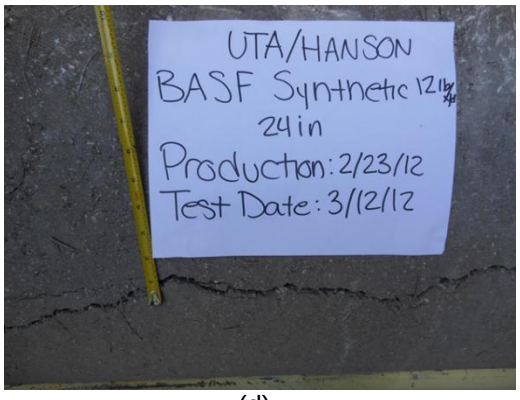

(d)

Figure E32 BASF-(SYN)-24-6-B-DL-12-5(a) Load-Deformation Plot, (b) Crack Propagation, (c) Cross-section Deformation, (d) Crack Width.

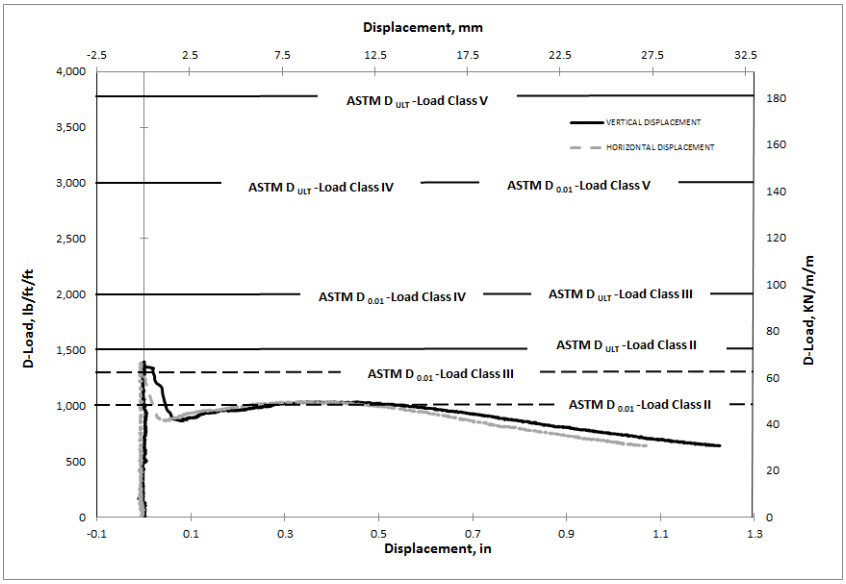

(a)

(b)

(c)

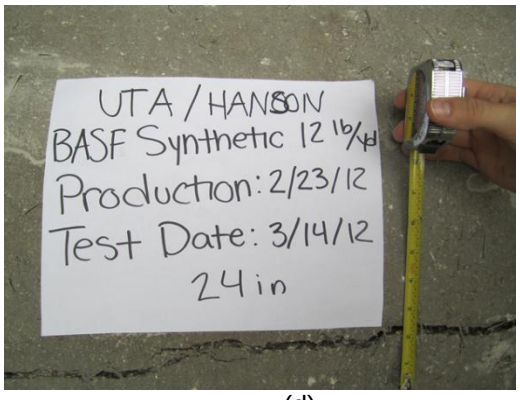

(d)

Figure E33 BASF-(SYN)-24-6-B-DL-12-6 (a) Load-Deformation Plot, (b) Crack Propagation, (c) Cross-section Deformation, (d) Crack Width.

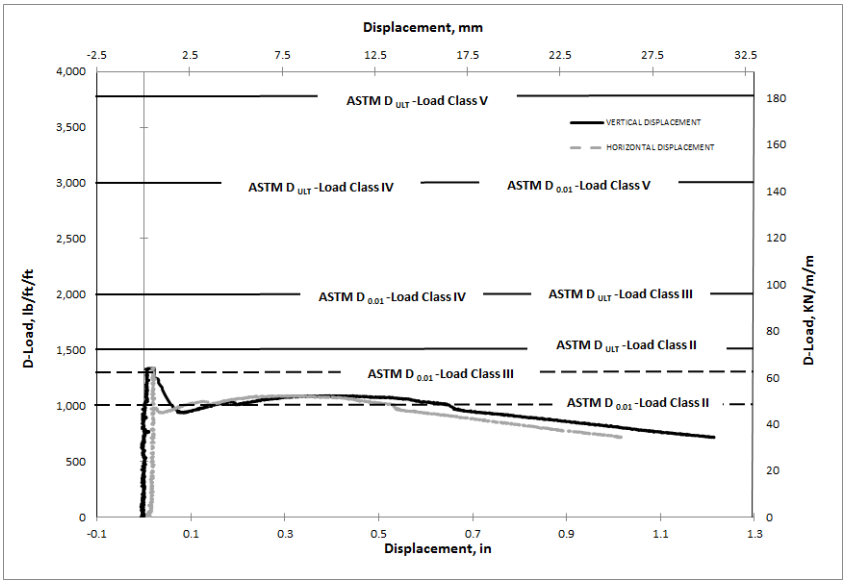

(a)

(b)

(c)

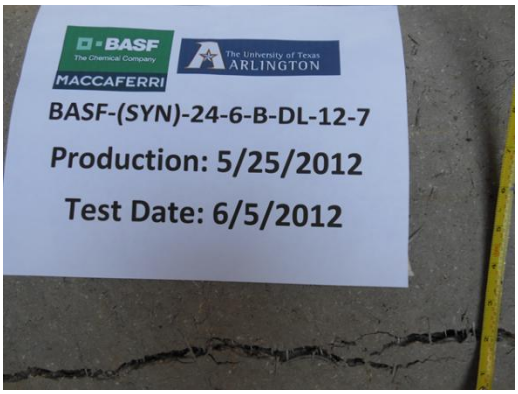

(d)

Figure E34 BASF-(SYN)-24-6-B-DL-12-7 (a) Load-Deformation Plot, (b) Crack Propagation, (c) Cross-section Deformation, (d) Crack Width.

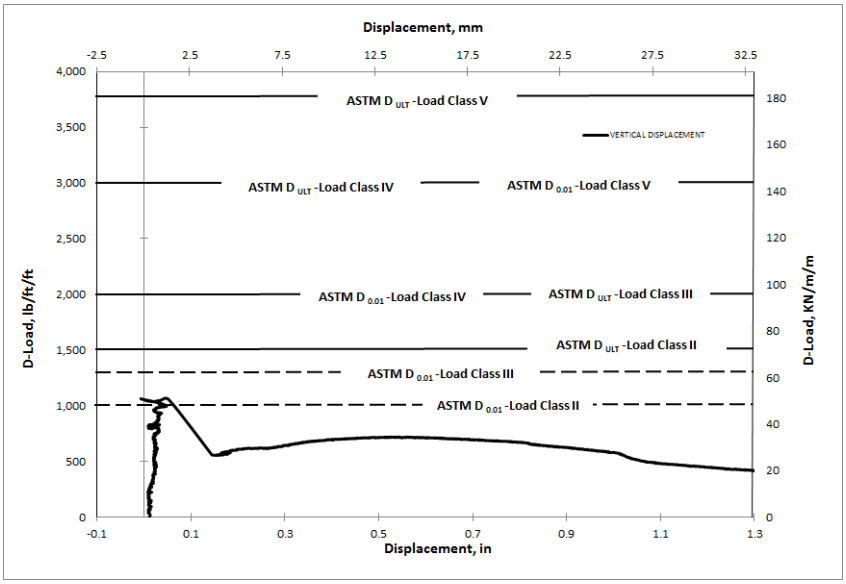

(a)

(b)

(c)

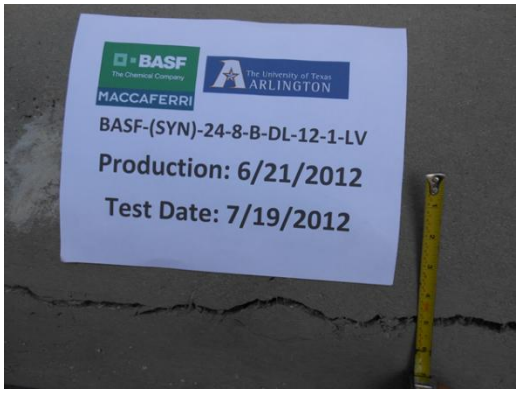

(d)

Figure E35 BASF-(SYN)-24-8-B-DL-12-1-LV (a) Load-Deformation Plot, (b) Crack Propagation, (c) Cross-section Deformation, (d) Crack Width.

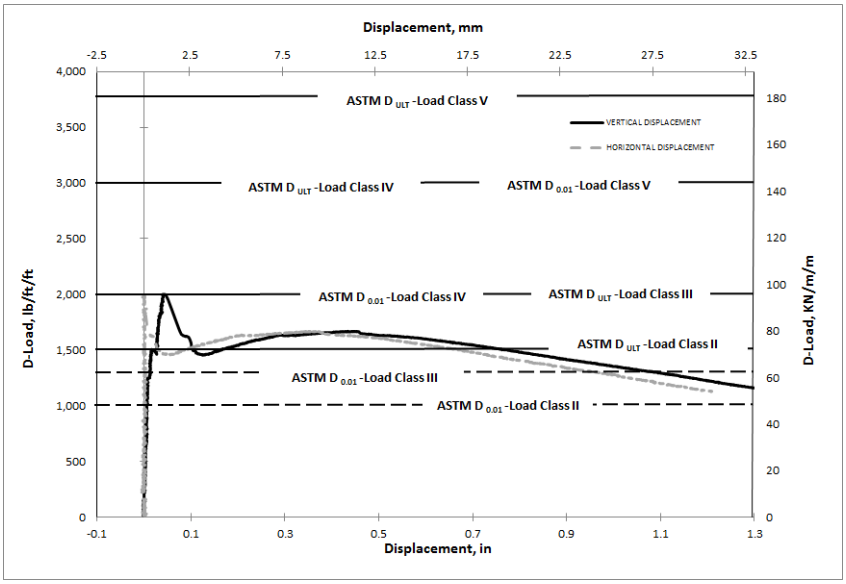

(a)

(b)

(c)

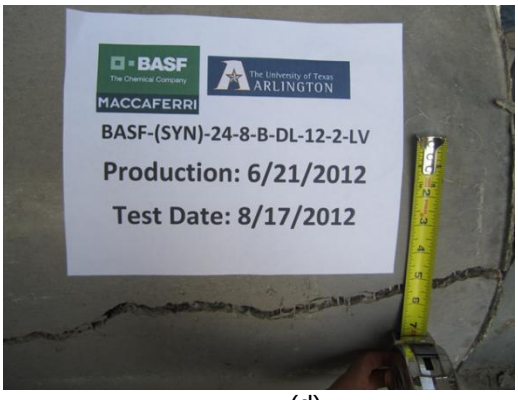

(d)

Figure E36 BASF-(SYN)-24-8-B-DL-12-2-LV (a) Load-Deformation Plot, (b) Crack Propagation, (c) Cross-section Deformation, (d) Crack Width.

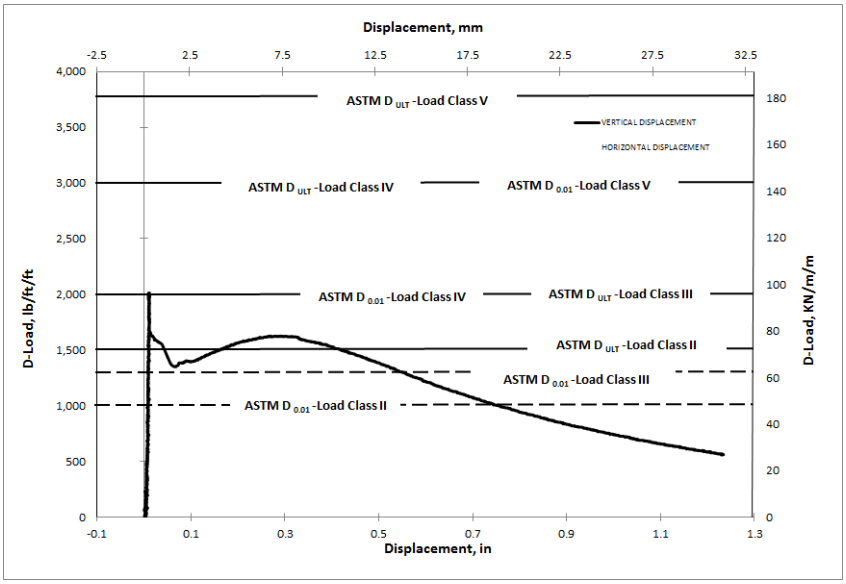

(a)

(b)

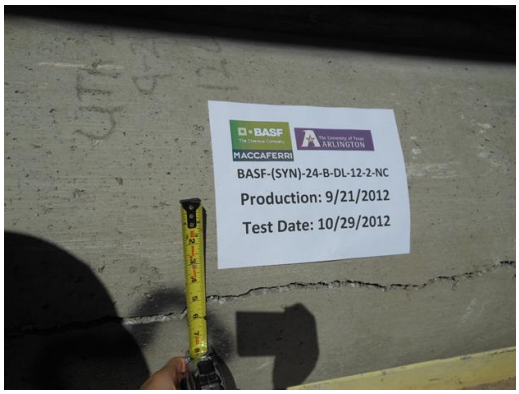

(c)

Figure E37 BASF-(SYN)-24-8-B-DL-12-1-NC (a) Load-Deformation Plot, (b) Crack Propagation and (c) Crack Width.

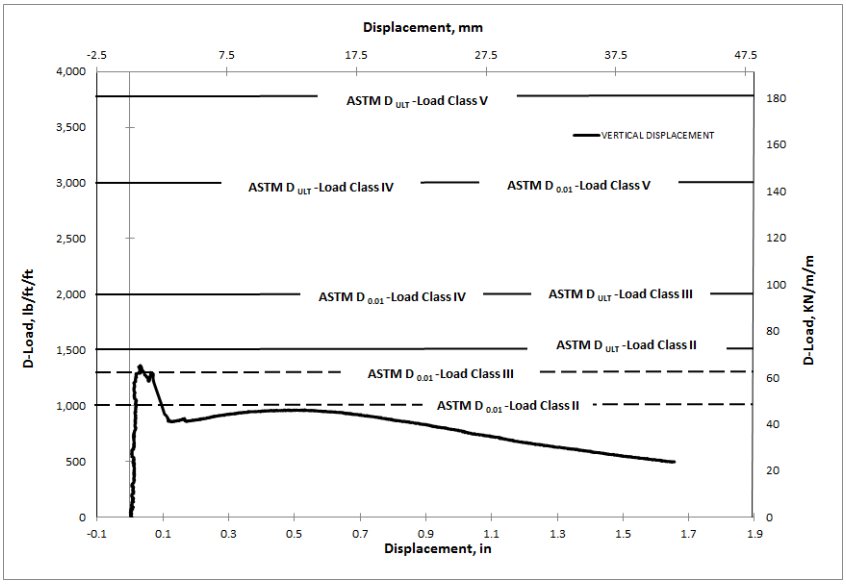

(a)

(b)

(c)

(d)

Figure E38 BASF-(SYN)-30-6-B-DL-10-2 (a) Load-Deformation Plot, (b) Crack Propagation, (c) Cross-section Deformation, (d) Crack Width.

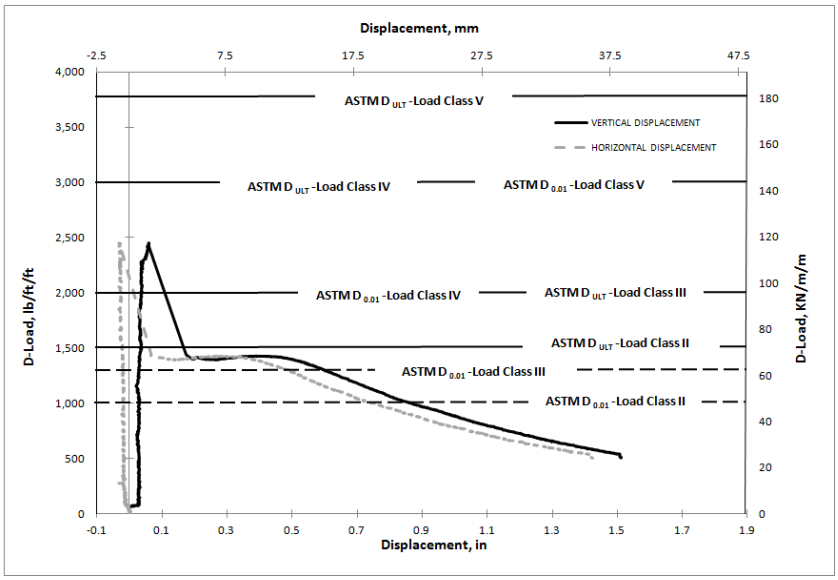

(a)

(b)

(c)

Figure E39 BASF-(SYN)-24-8-B-DL-10-1-NC(a) Load-Deformation Plot, (b) Crack Propagation and (c) Crack Width.

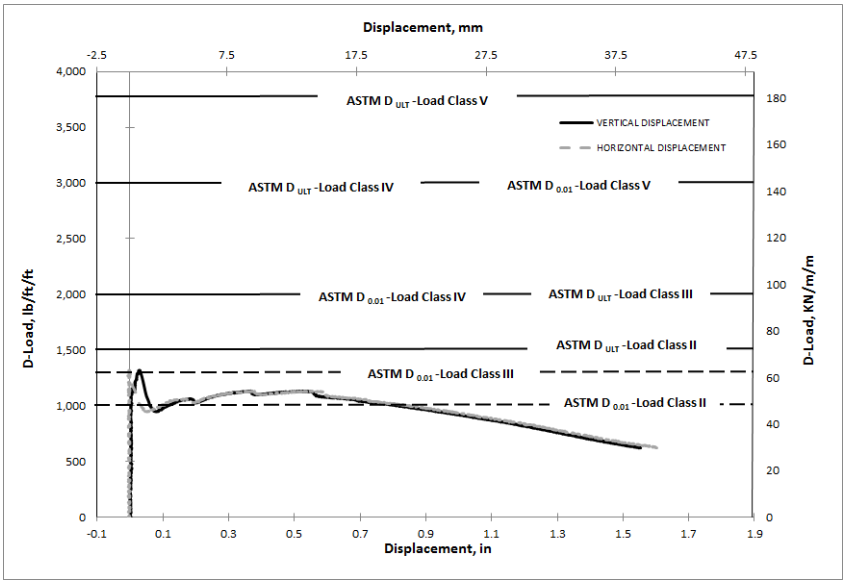

(a)

(b)

(c)

(d)

Figure E40 BASF-(SYN)-30-6-B-DL-12-1(a) Load-Deformation Plot, (b) Crack Propagation, (c) Cross-section Deformation, (d) Crack Width.

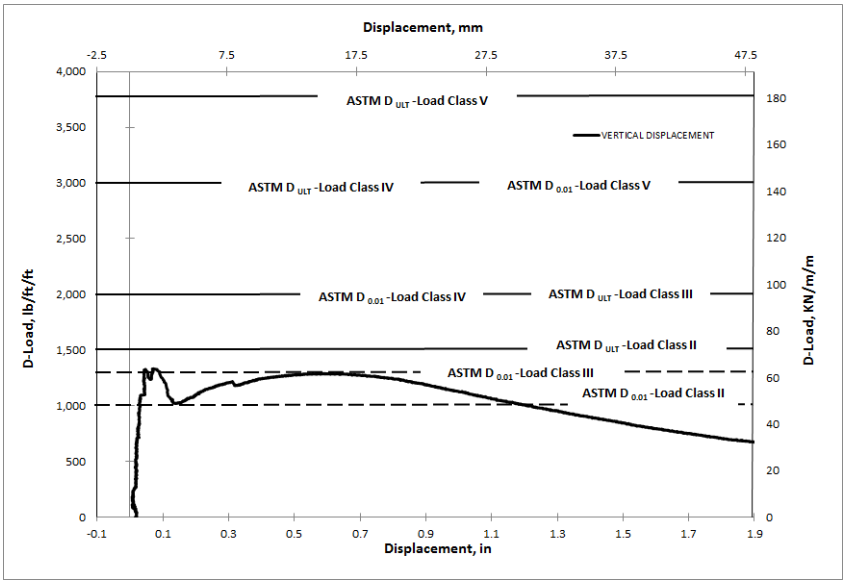

(a)

(b)

(c)

(d)

Figure E41 BASF-(SYN)-30-6-B-DL-12-2 (a) Load-Deformation Plot, (b) Crack Propagation, (c) Cross-section Deformation, (d) Crack Width.

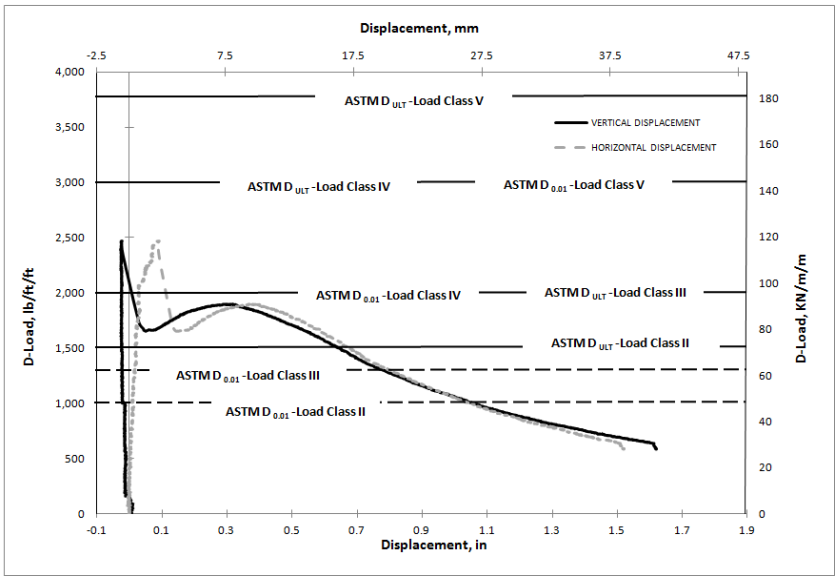

(a)

(b)

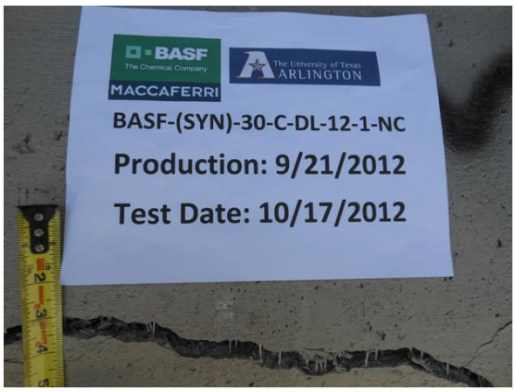

(c)

Figure E42 BASF-(SYN)-30-8-B-DL-12-1-NC (a) Load-Deformation Plot, (b) Crack Propagation and (c) Crack Width.

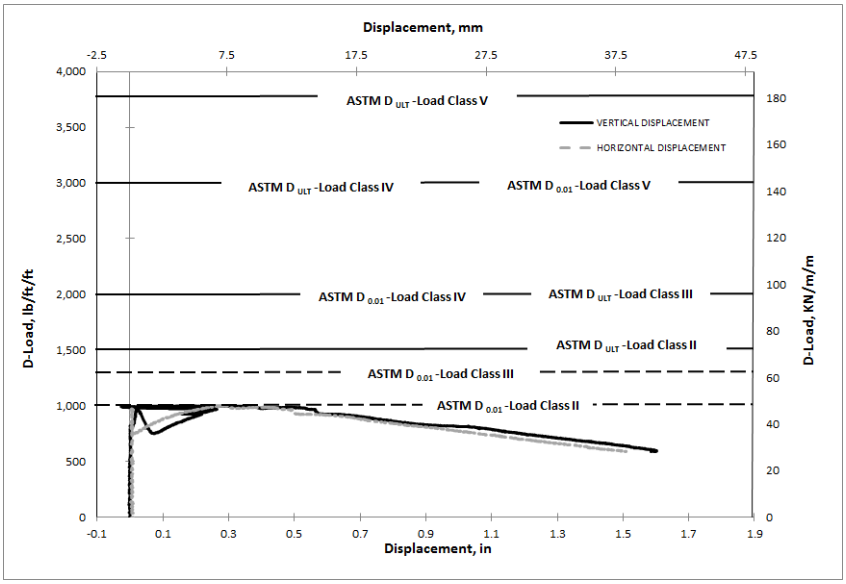

(a)

(b)

(c)

(d)

Figure E43 BASF-(SYN)-30-6-B-DL-16-1(a) Load-Deformation Plot, (b) Crack Propagation, (c) Cross-section Deformation, (d) Crack Width.

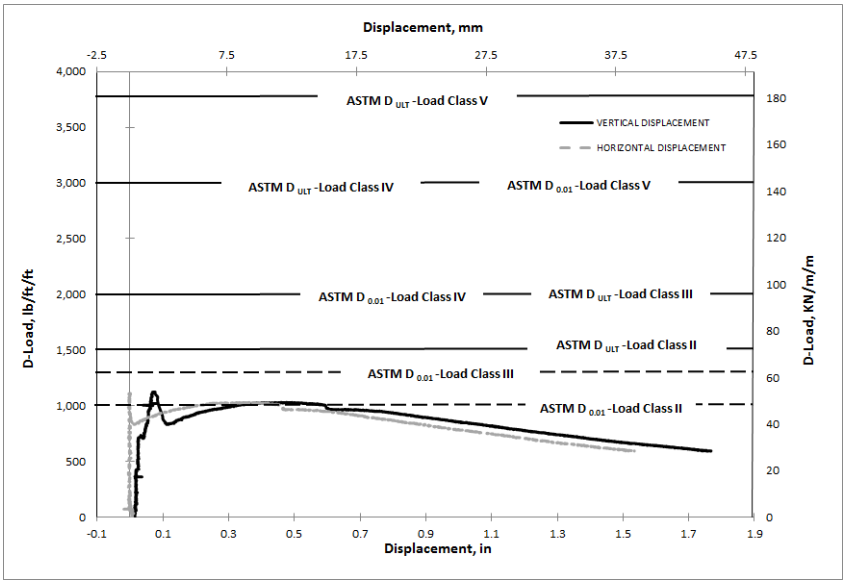

(a)

(b)

(c)

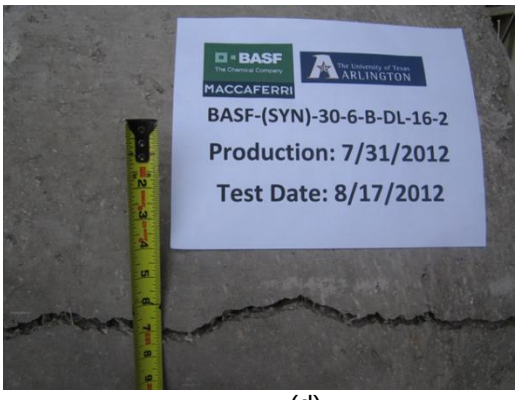

(d)

Figure E44 BASF-(SYN)-30-6-B-DL-16-2 (a) Load-Deformation Plot, (b) Crack Propagation, (c) Cross-section Deformation, (d) Crack Width.

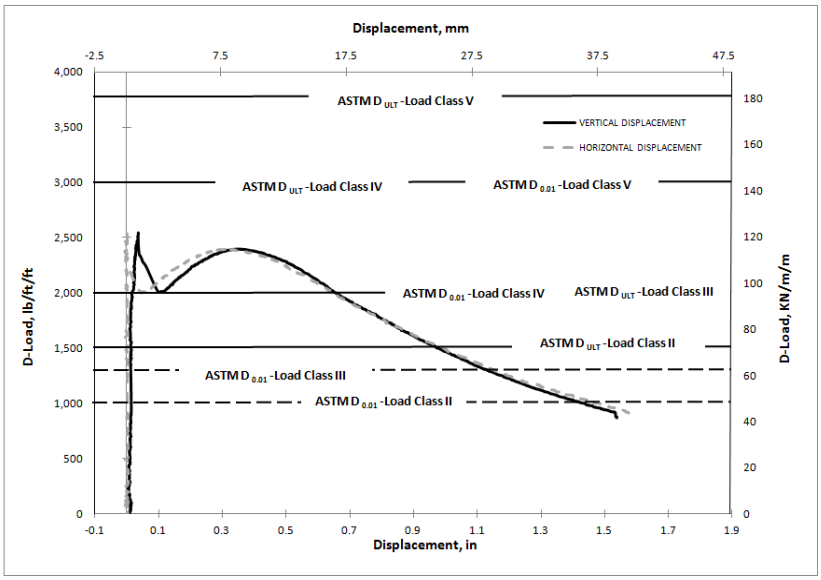

(a)

(b)

(c)

Figure E45 BASF-(SYN)-30-8-B-DL-16-1-NC (a) Load-Deformation Plot, (b) Crack Propagation and (c) Crack Width.

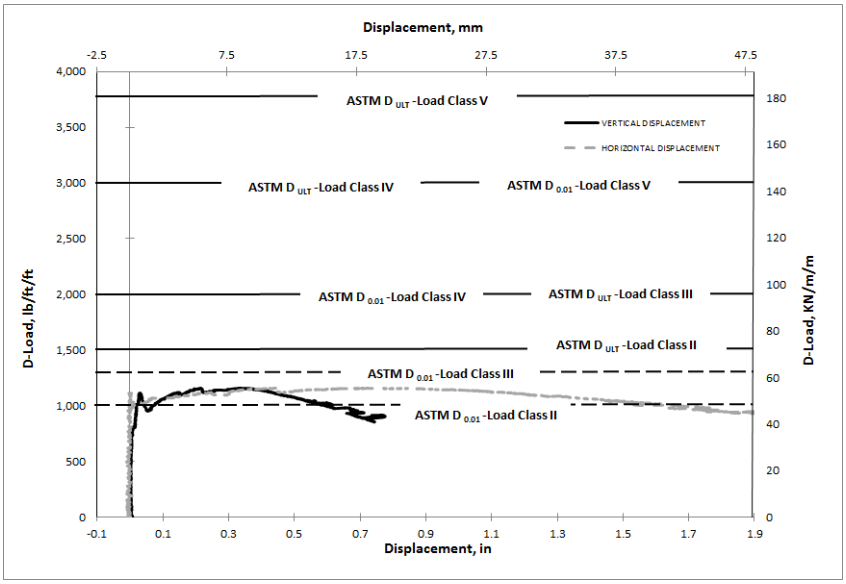

(a)

(b)

(c)

(d)

Figure E46 BASF-(SYN)-36-6-B-DL-12-1(a) Load-Deformation Plot, (b) Crack Propagation, (c) Cross-section Deformation, (d) Crack Width.

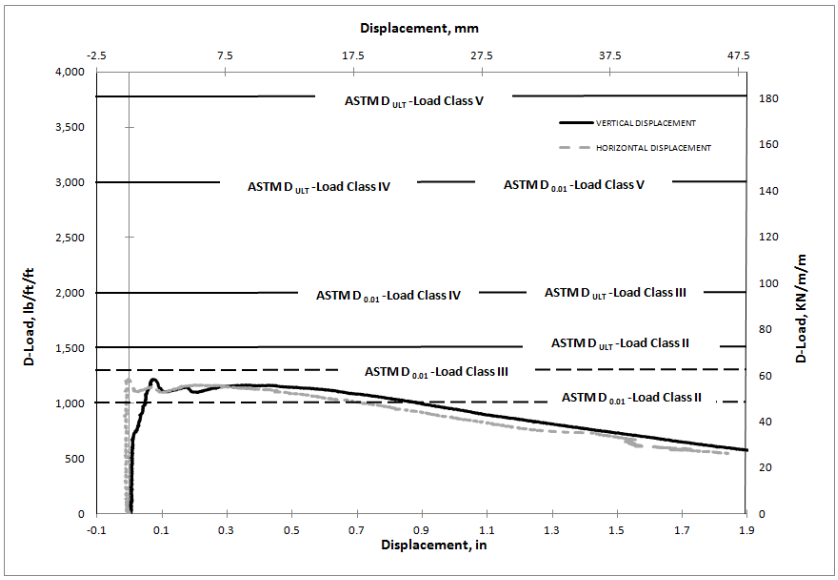

(a)

(b)

(c)

(d)

Figure E47 BASF-(SYN)-36-6-B-DL-12-2 (a) Load-Deformation Plot, (b) Crack Propagation, (c) Cross-section Deformation, (d) Crack Width.

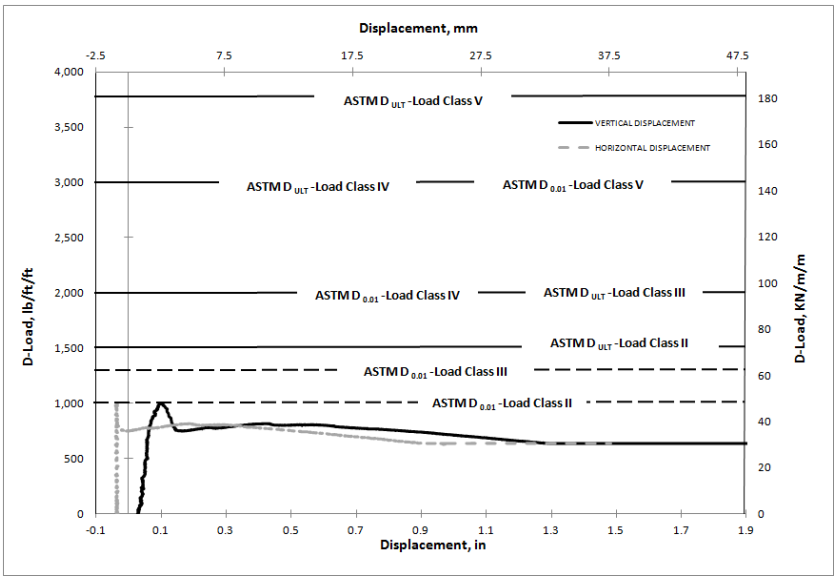

(a)

(b)

(c)

Figure E48 BASF-(SYN)-36-8-B-DL-12-1-LV(a) Load-Deformation Plot, (b) Crack Propagation and (c) Crack Width.

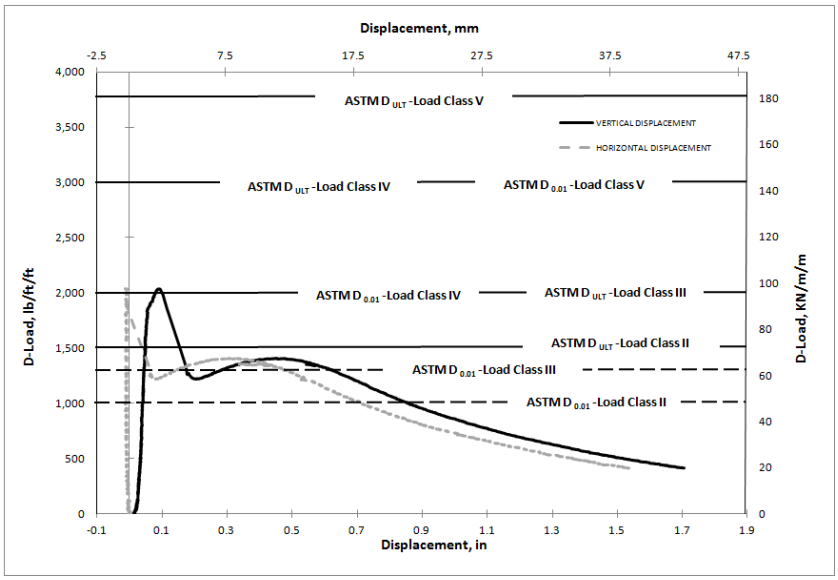

(a)

(b)

(c)

Figure E49 BASF-(SYN)-36-8-B-DL-12-1-NC (a) Load-Deformation Plot, (b) Crack Propagation and (c) Crack Width.

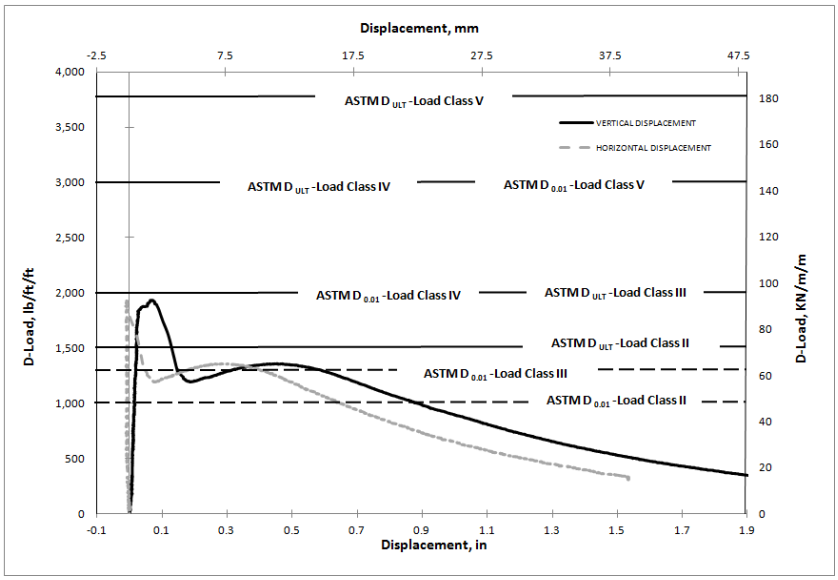

(a)

(b)

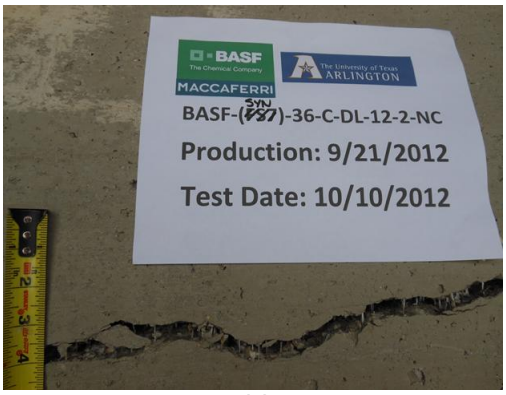

(c)

Figure E50 BASF-(SYN)-36-8-B-DL-12-2-NC (a) Load-Deformation Plot, (b) Crack Propagation, (c) Cross-section Deformation, (d) Crack Width.

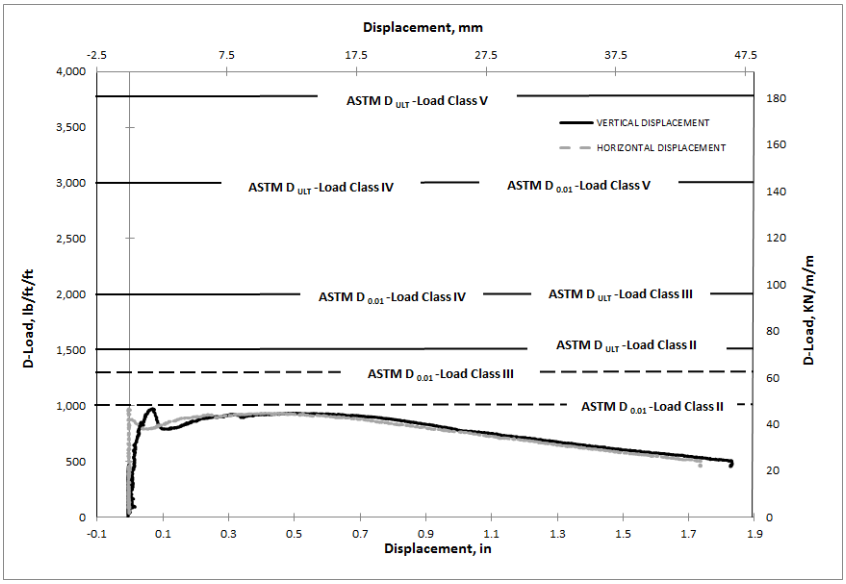

(a)

Figure E51 BASF-(SYN)-36-6-B-DL-16-1 (a) Load-Deformation Plot.

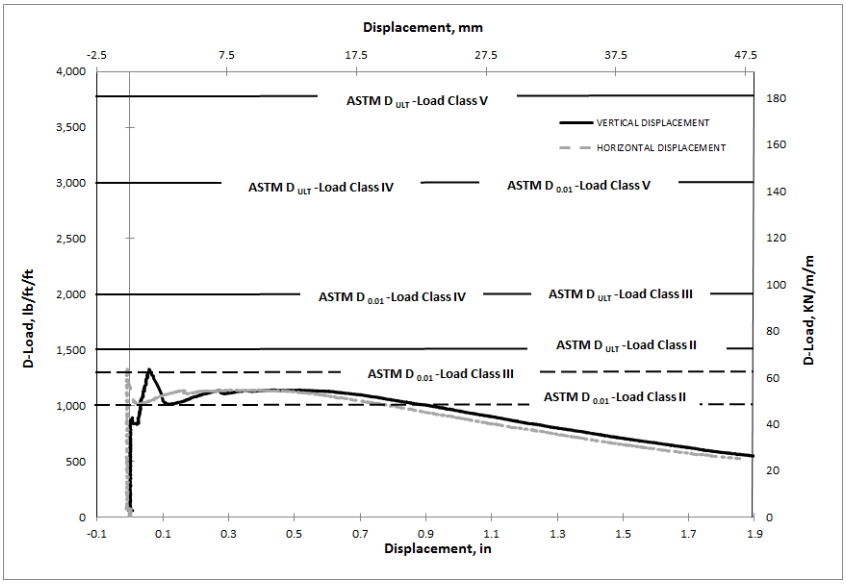

(a)

(b)

(c)

(d)

Figure E52 BASF-(SYN)-36-6-B-DL-16-2 (a) Load-Deformation Plot, (b) Crack Propagation, (c) Cross-section Deformation, (d) Crack Width.

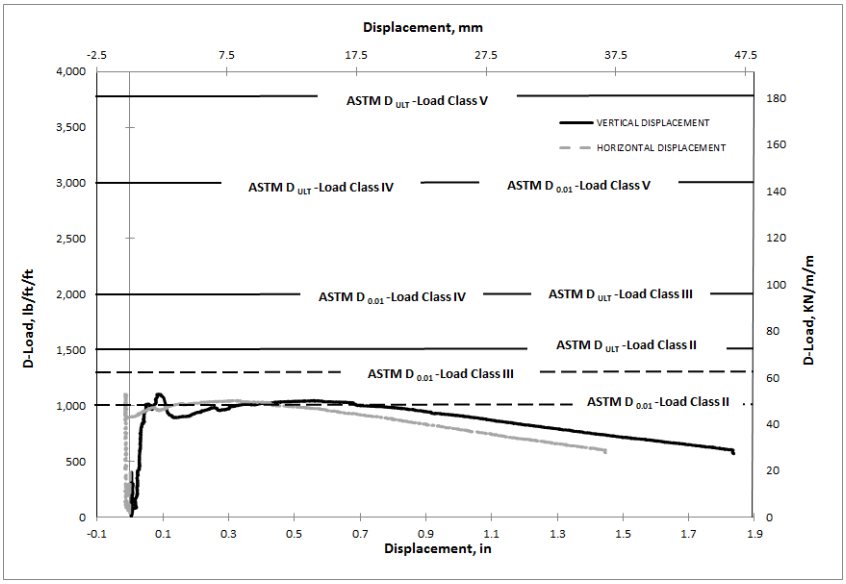

(a)

(b)

(c)

Figure E53 BASF-(SYN)-36-6-B-DL-16-3(a) Load-Deformation Plot, (b) Crack Propagation and (c) Crack Width.

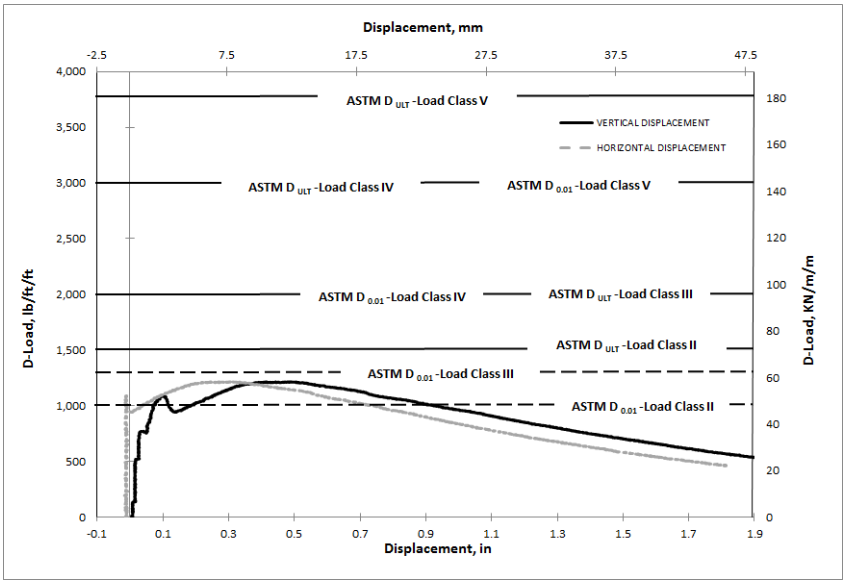

(a)

(b)

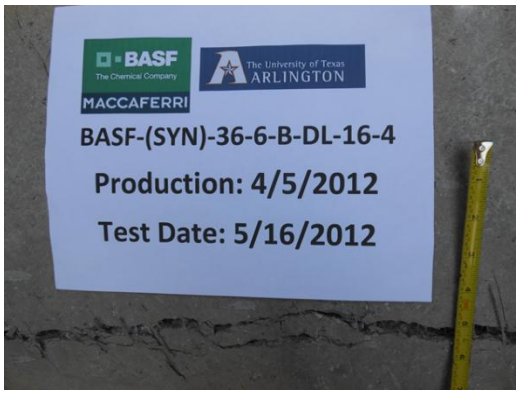

(c)

Figure E54 BASF-(SYN)-36-6-B-DL-16-4(a) Load-Deformation Plot, (b) Crack Propagation, and (c) Crack Width.

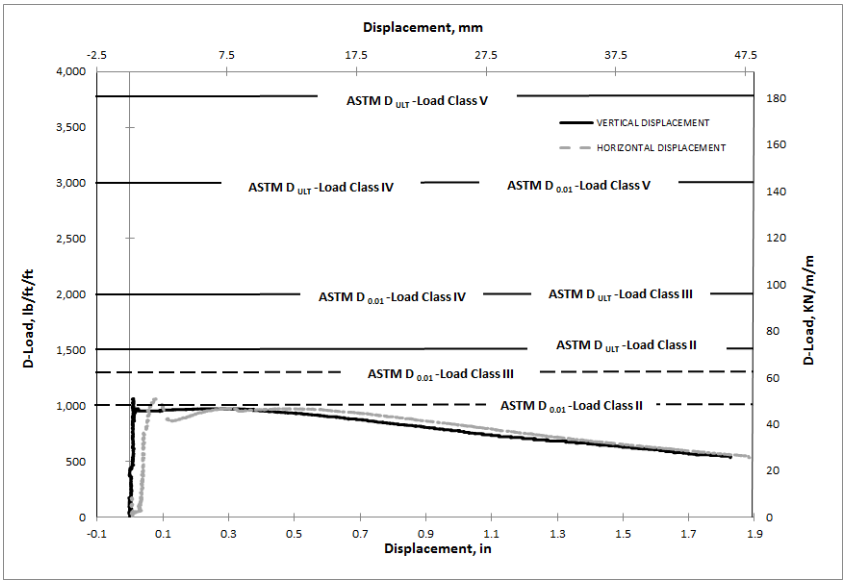

(a)

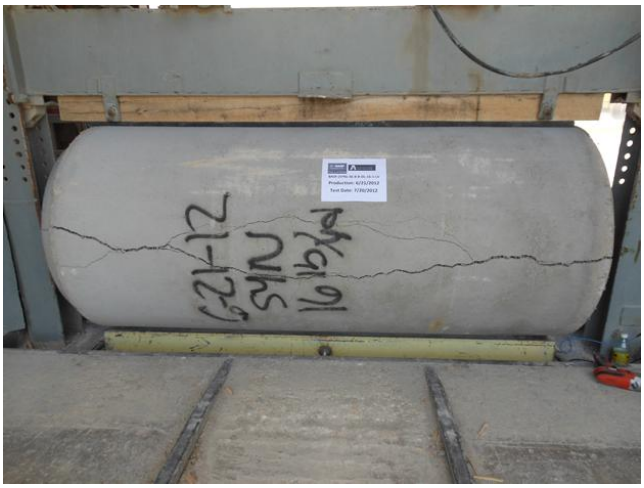

(b)

(c)

Figure E55 BASF-(SYN)-36-8-B-DL-16-1-LV (a) Load-Deformation Plot, (b) Crack Propagation and (c) Crack Width.

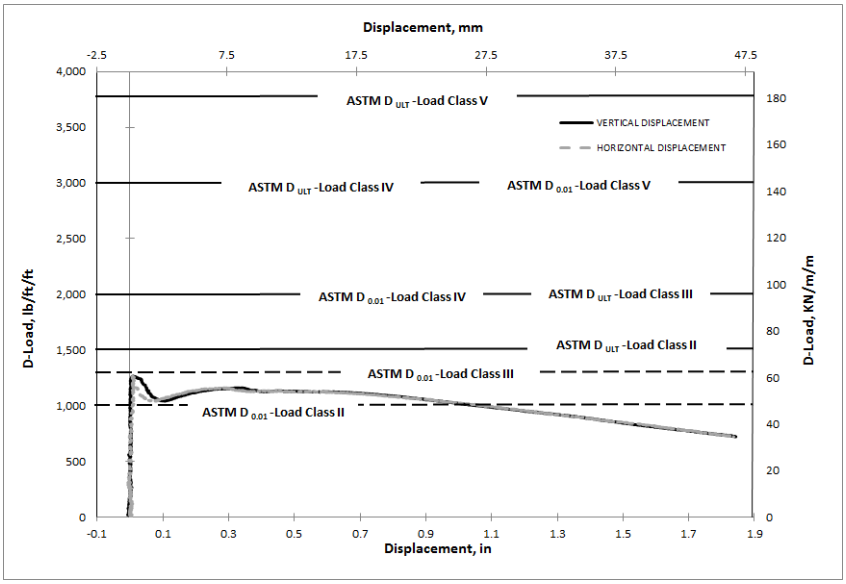

(a)

(b)

(c)

(d)

Figure E56 BASF-(SYN)-36-8-B-DL-16-2-LV (a) Load-Deformation Plot, (b) Crack Propagation, (c) Cross-section Deformation, (d) Crack Width.

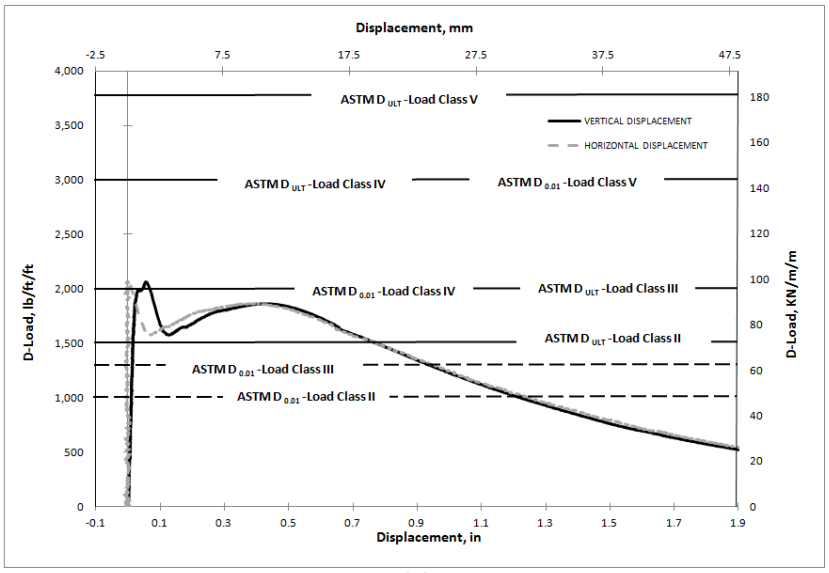

(a)

(b)

(c)

Figure E57 BASF-(SYN)-36-8-C-DL-16-1-NC (a) Load-Deformation Plot, (b) Crack Propagation and (c) Crack Width.

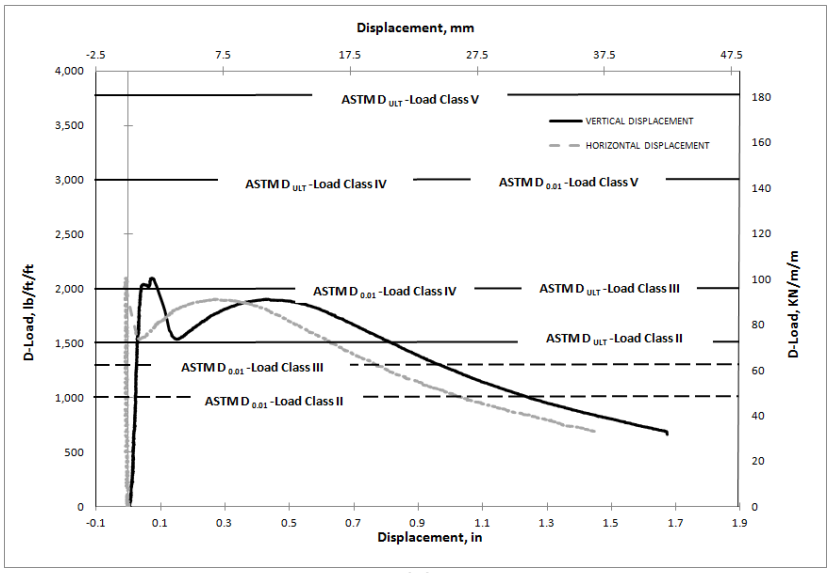

(a)

(b)

(c)

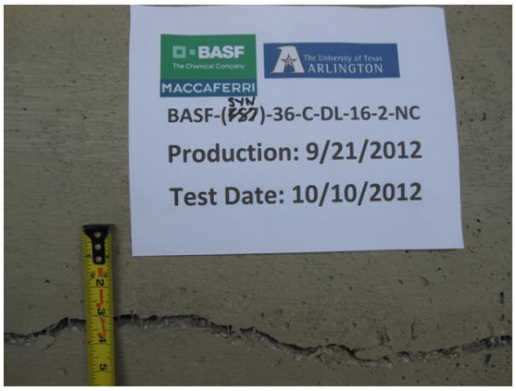

(d)

Figure E58 BASF-(SYN)-36-8-C-DL-16-2-NC (a) Load-Deformation Plot, (b) Crack Propagation, (c) Cross-section Deformation, (d) Crack Width.

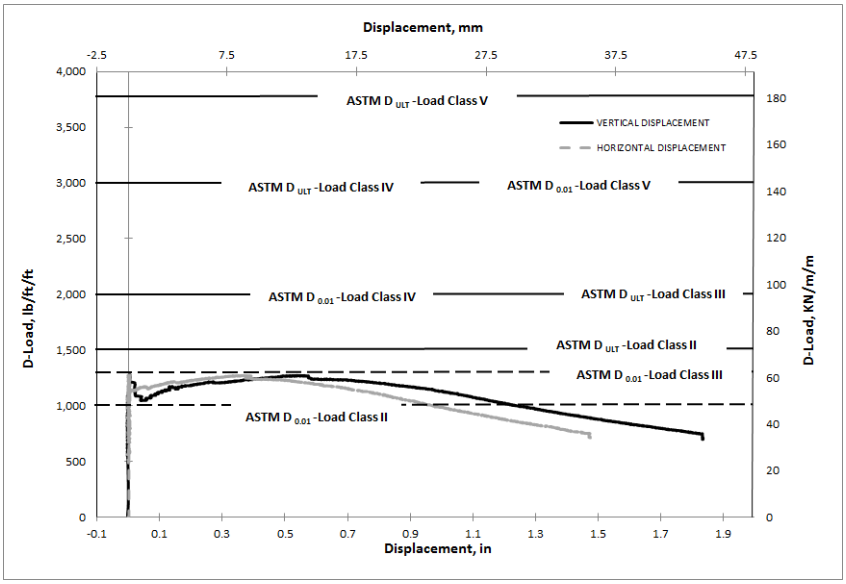

(a)

(b)

(c)

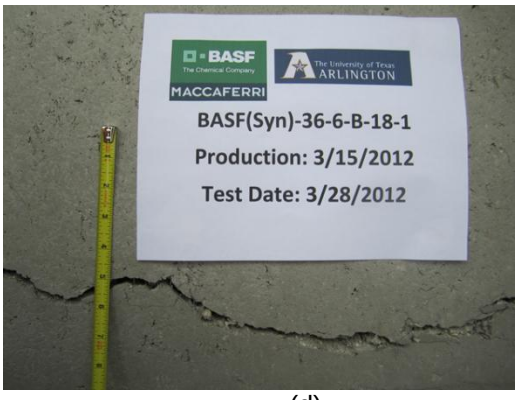

(d)

Figure E59 BASF-(SYN)-36-6-B-DL-18-1(a) Load-Deformation Plot, (b) Crack Propagation, (c) Cross-section Deformation, (d) Crack Width.

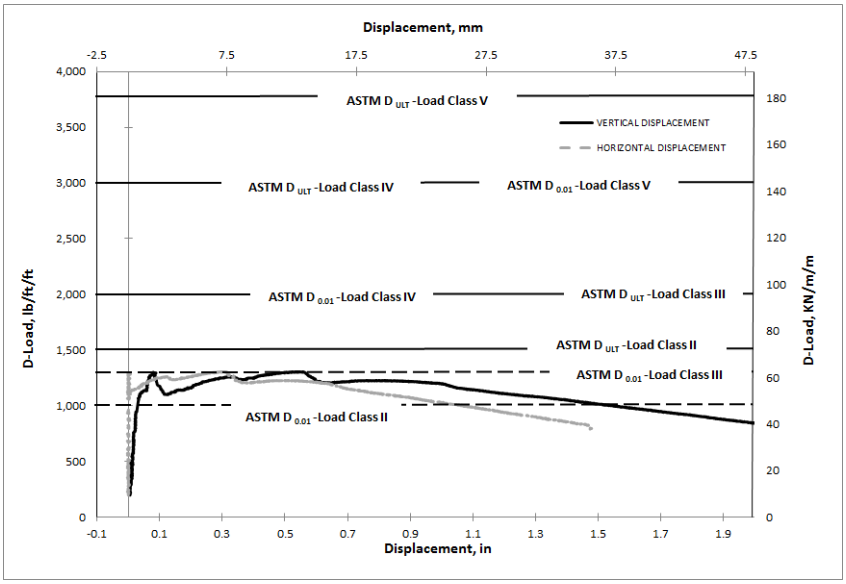

(a)

(b)

(c)

(d)

Figure E60 BASF-(SYN)-36-6-B-DL-18-2 (a) Load-Deformation Plot, (b) Crack Propagation, (c) Cross-section Deformation, (d) Crack Width.

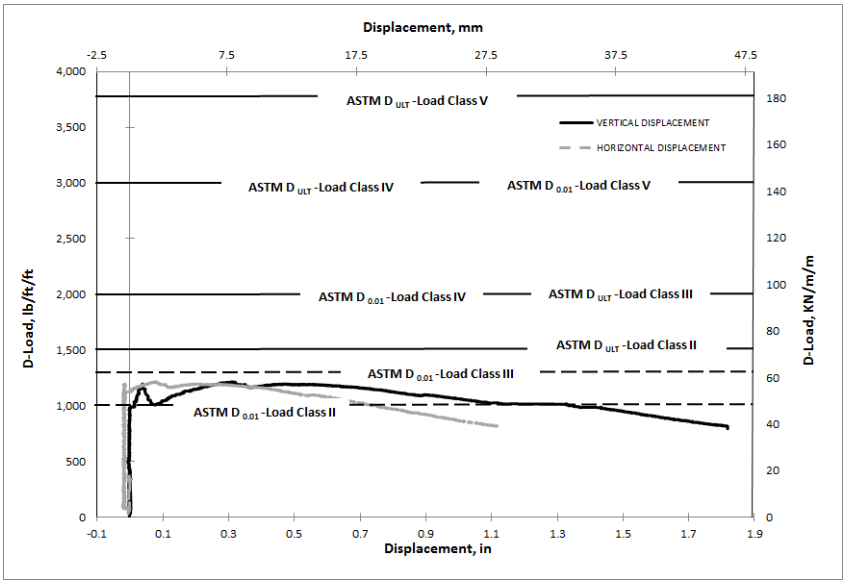

(a)

(b)

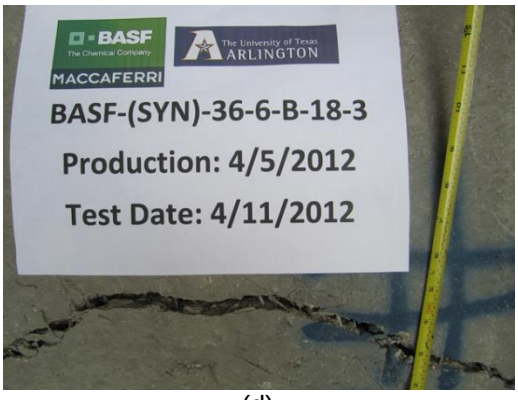

(c) (d)

Figure E61 BASF-(SYN)-36-6-B-DL-18-3 (a) Load-Deformation Plot, (b) Crack Propagation, (c) Cross-section Deformation, (d) Crack Width.

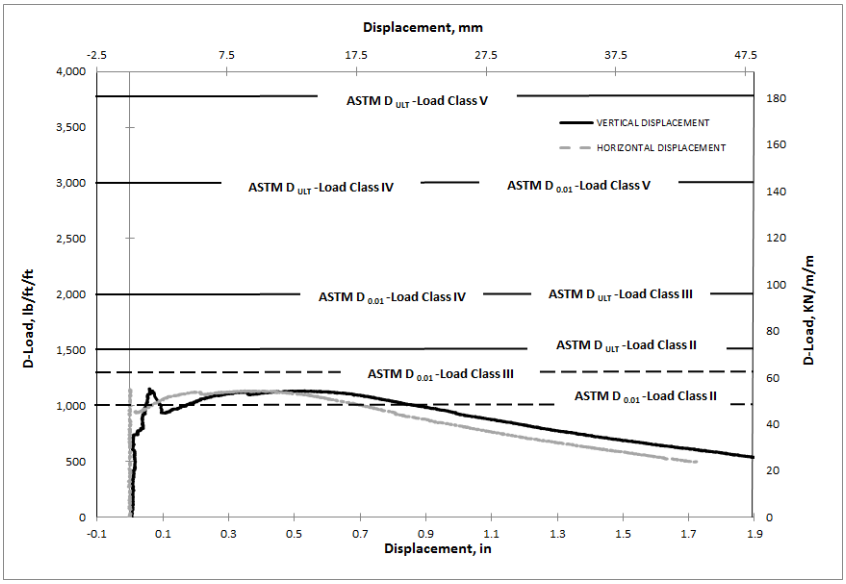

(a)

(b)

(c)

(d)

Figure E62 BASF-(SYN)-36-6-B-DL-18-4 (a) Load-Deformation Plot, (b) Crack Propagation, (c) Cross-section Deformation, (d) Crack Width.

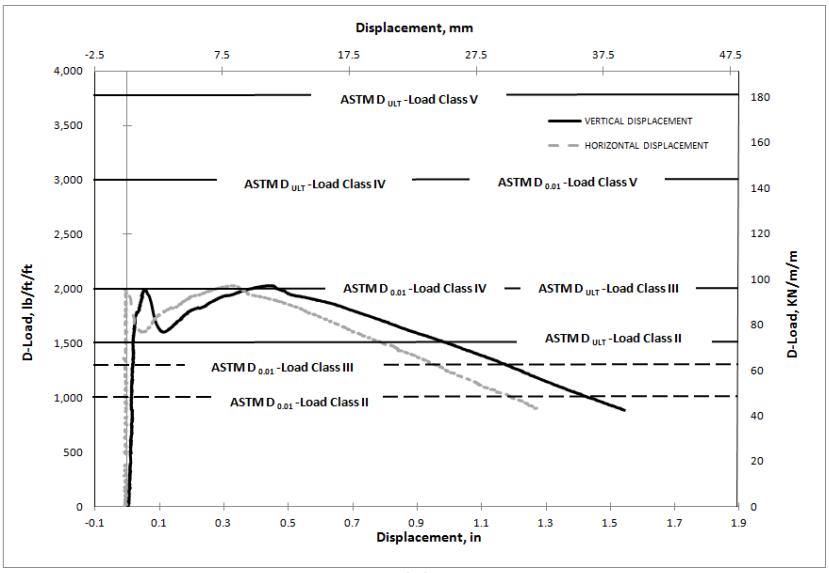

(a)

(b)

(c)

Figure E63 BASF-(SYN)-36-6-C-DL-18-1-NC(a) Load-Deformation Plot, (b) Crack Propagation and (c) Crack Width.

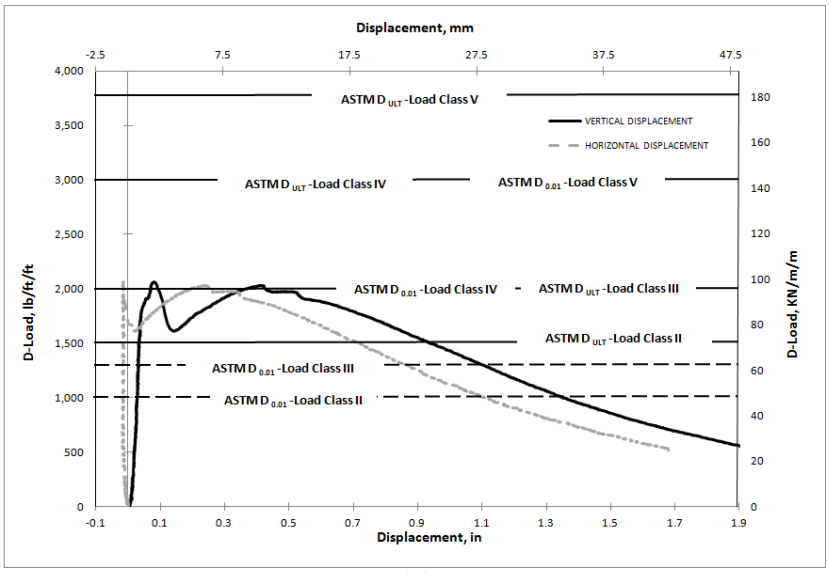

(a)

(b)

(c)

Figure E64 BASF-(SYN)-36-6-C-DL-18-2-NC(a) Load-Deformation Plot, (b) Crack Propagation, and (c) Crack Width.

APPENDIX F

TEST RESULTS TABLES

Table F1: Hanson Grand Prairie Steel (FS7) Pipe Test Results

Production Date	Test Date	Pipe Designation	D-Ultimate lb/ft/ft	Ultimate lb	Crack at 5%	Corresponding Class Based on ASTM C76 D-Ultimate
3/15/2012	3/28/2012	BASF-(FS7)-36-6-B-DL-44-1	1,434	25,812	3/8	<Class III
3/15/2012	5/1/2012	BASF-(FS7)-36-6-B-DL-44-2	1,586	28,550	1/4	<Class III
3/15/2012	3/21/2012	BASF-(FS7)-36-6-B-DL-66-1	1,564	28,148	-	<Class III
3/15/2012	4/24/2012	BASF-(FS7)-36-6-B-DL-66-2	2,028	36,514	1/4	Class III
3/22/2012	3/30/2012	BASF-(FS7)-24-6-B-DL-22-1	1,629	19,545	1/4	<Class III
3/22/2012	4/5/2012	BASF-(FS7)-24-6-B-DL-22-2	1,682	20,183	1/4	<Class III
3/22/2012	-	BASF-(FS7)-24-6-B-DL-22-3	Machine Stop	-	-	-
3/22/2012	4/5/2012	BASF-(FS7)-24-6-B-DL-44-1	2,291	27,486	1/4	Class III
3/22/2012	4/11/2012	BASF-(FS7)-24-6-B-DL-44-2	2,241	26,892	1/4	Class III
3/22/2012	4/30/2012	BASF-(FS7)-24-6-B-DL-44-3	2,472	29,661	3/8	Class III
4/10/2012	4/24/2012	BASF-(FS7)-36-6-B-DL-44-3	Machine Stop	-	-	-
4/10/2012	5/16/2012	BASF-(FS7)-36-6-B-DL-44-4	1,620	29,164	3/8	<Class III
4/10/2012	4/24/2012	BASF-(FS7)-36-6-B-DL-66-3	2,129	38,328	1/2	Class III
4/10/2012	5/1/2012	BASF-(FS7)-36-6-B-DL-66-4	2,065	37,176	1/4	Class III
4/24/2012	4/30/2012	BASF-(FS7)-24-6-B-DL-33-1	Machine Stop	-	-	
4/24/2012	5/16/2012	BASF-(FS7)-24-6-B-DL-33-2	1,871	22,452	3/8	<Class III
4/26/2012	5/15/2012	BASF-(FS7)-36-6-B-DL-88-1	1,509	27,155	1/2	<Class III
4/26/2012	5/16/2012	BASF-(FS7)-36-6-B-DL-88-2	1,637	29,471	1/2	<Class III
5/3/2012	5/16/2012	BASF-(FS7)-21-6-B-DL-44-1	1,459	15,315	3/8	<Class III
5/3/2012	-	BASF-(FS7)-21-6-B-DL-44-2	-	-	-	-
5/29/2012	6/6/2012	BASF-(FS7)-24-6-B-DL-22-4	1,625	19,498	1/8	<Class III
5/29/2012	7/16/2012	BASF-(FS7)-24-6-B-DL-22-5	Pipe Cracked	-	1/2	-
5/29/2012	6/6/2012	BASF-(FS7)-24-6-B-DL-44-4	2,074	24,886	1/4	Class III
5/29/2012	8/20/2012	BASF-(FS7)-24-6-B-DL-44-5	1,069	12,833	3/8	<Class III
6/12/2012	7/26/2012	BASF-(FS7)-30-6-B-DL-33-1	1,528	22,925	1/4	<Class III
6/12/2012	7/26/2012	BASF-(FS7)-30-6-B-DL-33-2	1,602	24,030	3/8	<Class III
6/12/2012	7/25/2012	BASF-(FS7)-30-6-B-DL-44-1	2,010	30,150	3/8	Class III
6/12/2012	7/26/2012	BASF-(FS7)-30-6-B-DL-44-2	1,981	29,715	3/8	<Class III
7/9/2012	8/3/2012	BASF-(FS7)-18-6-B-DL-22-1	2,636	23,724	1/4	Class III
7/9/2012	8/7/2012	BASF-(FS7)-18-6-B-DL-22-2	2,636	23,724	3/8	Class III
7/9/2012	8/3/202	BASF-(FS7)-18-6-B-DL-33-1	2,833	25,501	1/4	Class III
7/9/2012	8/7/2012	BASF-(FS7)-18-6-B-DL-33-2	2,487	22,381	1/4	Class III
7/11/2012	8/3/2012	BASF-(FS7)-18-6-B-DL-44-1	1,773	15,957	1/4	<Class III
7/11/2012	8/7/2012	BASF-(FS7)-18-6-B-DL-44-2	2,319	20,871	1/4	Class III
7/20/2012	8/9/2012	BASF-(FS7)-21-6-B-DL-22-1	1,463	15,362	1/4	<Class III
7/20/2012	8/9/2012	BASF-(FS7)-21-6-B-DL-22-2	1,393	14,627	3/8	<Class III
7/20/2012	8/9/2012	BASF-(FS7)-21-6-B-DL-33-1	1,609	16,895	1/4	<Class III
7/20/2012	8/9/2012	BASF-(FS7)-21-6-B-DL-33-2	1,533	19,097	1/4	<Class III
7/31/2012	8/17/2012	BASF-(FS7)-30-6-B-DL-66-1	1,379	20,680	3/8	<Class III
7/31/2012	8/17/2012	BASF-(FS7)-30-6-B-DL-66-2	1,520	22,807	3/8	<Class III

Table F2: Hanson Longview Steel (FS7) Pipe Test Results

Production Date	Test Date	Pipe Designation	D-Ultimate lb/ft/ft	Ultimate lb	Crack at 5%	Corresponding Class Based on ASTM C76 D-Ultimate
6/14/2012	6/22/2012	BASF-(FS7)-15-6-B-DL-33-1-LV	3581	26855	-	Class IV
6/14/2012	8/7/2012	BASF-(FS7)-15-6-B-DL-33-2-LV	3231	24234	-	Class IV
6/14/2012	8/2/2012	BASF-(FS7)-15-6-B-DL-33-3-LV	3408	25557	-	Class IV
6/14/2012	6/22/2012	BASF-(FS7)-24-8-B-DL-33-1-LV	2054	32857	-	Class III
6/14/2012	7/19/2012	BASF-(FS7)-24-8-B-DL-33-2-LV	1555	24886	1/4	<Class III
6/14/2012	8/16/2012	BASF-(FS7)-24-8-B-DL-33-3-LV	1610	25761	1/2	<Class III
6/14/2012	8/16/2012	BASF-(FS7)-24-8-B-DL-33-4-LV	1727	27628	3/8	<Class III
6/14/2012	6/22/2012	BASF-(FS7)-24-8-B-DL-44-1-LV	2142	34268		Class III
6/14/2012	7/19/2012	BASF-(FS7)-24-8-B-DL-44-2-LV	1975	311599	3/8	<Class III
6/14/2012	6/22/2012	BASF-(FS7)-36-8-B-DL-44-1-LV	1502	36058		<Class III
6/14/2012	7/23/2012	BASF-(FS7)-36-8-B-DL-44-2-LV	1475	35400	3/8	<Class III
6/14/2012	7/23/2012	BASF-(FS7)-36-8-B-DL-66-1-LV	1815	43560	3/8	<Class III
6/14/2012	7/20/202	BASF-(FS7)-36-8-B-DL-88-1-LV	2018	48426	3/8	Class III

Table F3: Northern Concrete Steel (FS7) Pipe Test Results

Production Date	Test Date	Pipe Designation	D-Ultimate lb/ft/ft	Ultimate lb	Crack at 5%	Corresponding Class Based on ASTM C76 D-Ultimate
9/21/2012	10/29/2012	BASF-(FS7)-24-8-B-DL-33-1-NC	2249	35984	1/2	Class III
9/21/2012	10/29/2012	BASF-(FS7)-24-8-B-DL-33-2-NC	2395	38320	1/4	Class III
9/21/2012	10/17/2012	BASF-(FS7)-24-8-B-DL-44-1-NC	2808	44928	1/2	Class III
9/21/2012	10/8/2012	BASF-(FS7)-36-8-C-DL-44-1-NC	2380	57123	1/4	Class III
9/21/2012	10/8/2012	BASF-(FS7)-36-8-C-DL-44-2-NC	2175	52207	1/2	Class III
9/21/2012	10/10/2012	BASF-(FS7)-36-8-C-DL-66-1-NC	2530	60716	3/8	Class III
9/21/2012	10/10/2012	BASF-(FS7)-36-8-C-DL-88-1-NC	2916	69980	3/8	Class III

Table F4: Hanson Grand Prairie Synthetic Pipe Test Results

Production Date	Test Date	Pipe Designation	D-Ultimate lb/ft/ft	Ultimate lb	Crack at 5% (in.)	Corresponding Class Based on ASTM C76 D-Ultimate
2/2/2012	2/9/2012	BASF-(SYN)-24-6-B-DL-12-1	1,844	22,133	-	<Class III
2/2/2012	2/17/2012	BASF-(SYN)-24-6-B-DL-12-2	1,934	23,212	-	<Class III
2/2/2012	2/23/2012	BASF-(SYN)-24-6-B-DL-12-3	1,833	22,000	-	<Class III
2/2/2012	2/28/2012	BASF-(SYN)-24-6-B-DL-12-4	1,448	17,370	1/4	<Class III
2/23/2012	3/12/2012	BASF-(SYN)-24-6-B-DL-12-5	902	10,824	3/8	<Class III
2/23/2012	3/14/2012	BASF-(SYN)-24-6-B-DL-12-6	1,394	16,728	1/2	<Class III
2/23/2012	3/12/2012	BASF-(SYN)-24-6-B-DL-8-1	1,564	18,768	1/8	<Class III
2/23/2012	3/14/2012	BASF-(SYN)-24-6-B-DL-8-2	1,416	16,992	1/4	<Class III
3/5/2012	3/12/2012	BASF-(SYN)-21-6-B-DL-10-1	1,695	17,796	1/8	<Class III
3/5/2012	3/28/2012	BASF-(SYN)-21-6-B-DL-10-2	1,848	19,403	1/4	<Class III
3/5/2012	4/10/2012	BASF-(SYN)-21-6-B-DL-10-3	1,805	18,954	1/8	<Class III
3/13/2012	4/10/2012	BASF-(SYN)-18-6-B-DL-4-1	2,114	19,025	1/4	Class III
3/13/2012	4/25/2012	BASF-(SYN)-18-6-B-DL-4-2	2,592	23,327	1/4	Class III
3/13/2012	8/20/2012	BASF-(SYN)-18-6-B-DL-4-3	1,153	10,375	1/4	<Class III
3/13/2012	4/5/2012	BASF-(SYN)-18-6-B-DL-6-1	1,993	17,938	1/4	<Class III
3/13/2012	4/25/2012	BASF-(SYN)-18-6-B-DL-6-2	2,421	21,790	1/4	Class III
3/13/2012	8/20/2012	BASF-(SYN)-18-6-B-DL-6-3	1,148	10,328	1/5	<Class III
3/13/2012	3/30/2012	BASF-(SYN)-18-6-B-DL-8-1	2,461	22,144	3/8	Class III
3/13/2012	4/10/2012	BASF-(SYN)-18-6-B-DL-8-2	2,096	18,859	3/8	Class III
3/13/2012	8/20/2012	BASF-(SYN)-18-6-B-DL-8-3	1,358	12,219	3/8	<Class III
3/15/2012	3/21/2012	BASF-(SYN)-36-6-B-DL-16-1	974	17,536		<Class III
3/15/2012	8/17/2012	BASF-(SYN)-36-6-B-DL-16-2	1,329	23,917	1/2	<Class III
3/15/2012	3/30/2012	BASF-(SYN)-36-6-B-DL-18-1	1,278	23,004	1/4	<Class III
3/15/2012	5/1/2012	BASF-(SYN)-36-6-B-DL-18-2	1,306	23,515	3/8	<Class III
4/5/2012	4/11/2012	BASF-(SYN)-36-6-B-DL-16-3	1,217	21,908	1/4	<Class III
4/5/2012	5/16/2012	BASF-(SYN)-36-6-B-DL-16-4	1,087	19,566	1/2	<Class III
4/5/2012	4/11/2012	BASF-(SYN)-36-6-B-DL-18-3	1,106	19,899	1/4	<Class III
4/5/2012	5/16/2012	BASF-(SYN)-36-6-B-DL-18-4	1,153	20,751	3/8	<Class III
4/24/2012	4/30/2012	BASF-(SYN)-24-6-B-DL-10-1	1,564	18,765	1/8	<Class III
4/24/2012	5/16/2012	BASF-(SYN)-24-6-B-DL-10-2	1,453	17,442	3/8	<Class III
4/26/2012	5/15/2012	BASF-(SYN)-36-6-B-DL-12-1	1,159	20,869	1/8	<Class III
4/26/2012	5/15/2012	BASF-(SYN)-36-6-B-DL-12-2	1,218	21,932	1/4	<Class III
5/25/2012	6/6/2012	BASF-(SYN)-24-6-B-DL-8-3	1,396	16,752	1/4	<Class III
5/25/2012	7/16/2012	BASF-(SYN)-24-6-B-DL-8-4	-	-	3/8	-
5/25/2012	6/5/2012	BASF-(SYN)-24-6-B-DL-12-7	1,341	16,092	3/8	<Class III
5/25/2012	8/20/2012	BASF-(SYN)-24-6-B-DL-12-8	473	5,652	1/4	<Class III
6/13/2012	7/26/2012	BASF-(SYN)-30-6-B-DL-10-1	1,456	21,840	1/8	<Class III
6/13/2012	7/26/2012	BASF-(SYN)-30-6-B-DL-10-2	1,361	20,415	1/2	<Class III
6/13/2012	7/23/2012	BASF-(SYN)-30-6-B-DL-12-1	1,319	19,758	3/8	<Class III
6/13/2012	7/26/2012	BASF-(SYN)-30-6-B-DL-12-2	1,333	19,994	3/8	<Class III
7/6/2012	7/27/2012	BASF-(SYN)-21-6-B-DL-6-1	1,519	15,950	3/8	<Class III
7/6/2012	7/27/2012	BASF-(SYN)-21-6-B-DL-6-2	1,269	13,325	3/8	<Class III
7/6/2012	7/27/2012	BASF-(SYN)-21-6-B-DL-8-1	1,436	15,078	1/5	<Class III
7/6/2012	7/27/2012	BASF-(SYN)-21-6-B-DL-8-2	1,549	16,265	1/4	<Class III
7/6/2012	8/9/2012	BASF-(SYN)-21-6-B-DL-8-3	1,450	15,225	1/4	<Class III
7/6/2012	7/27/2012	BASF-(SYN)-21-6-B-DL-12-1	1,571	16,496	1/4	<Class III
7/6/2012	7/27/2012	BASF-(SYN)-21-6-B-DL-12-2	1,513	15,887		<Class III
7/11/2012	8/3/2012	BASF-(SYN)-18-6-B-DL-10-1	2,064	18,576	3/8	Class III
7/11/2012	8/7/2012	BASF-(SYN)-18-6-B-DL-10-2	1,969	17,721	1/4	<Class III
7/31/2012	8/17/2012	BASF-(SYN)-30-6-B-DL-16-1	1,000	15,000	3/8	<Class III
7/31/2012	8/17/2012	BASF-(SYN)-30-6-B-DL-16-2	1,125	16,875	3/8	<Class III

Table F5: Hanson Longview Synthetic Pipe Test Results

Production Date	Test Date	Pipe Designation	D-Ultimate lb/ft/ft	Ultimate lb	Crack at 5%	Corresponding Class Based on ASTM C76 D-Ultimate
5/31/2012	6/7/2012	BASF-(SYN)-24-8-B-DL-8-1-LV	1,592	25,471	-	<Class III
5/31/2012	6/7/2012	BASF-(SYN)-24-8-B-DL-8-2-LV	1,671	26,735	-	<Class III
5/31/2012	6/7/2012	BASF-(SYN)-36-8-B-DL-8-1-LV	1,021	24,496	-	<Class III
6/21/2012	8/2/2012	BASF-(SYN)-15-6-B-DL-6-1-LV	2,670	20,023	-	Class III
6/21/2012	8/2/2012	BASF-(SYN)-15-6-B-DL-6-2-LV	2,802	21,013	-	Class III
6/21/2012	8/7/2012	BASF-(SYN)-15-6-B-DL-6-3-LV	2,920	21,902	-	Class III
6/21/2012	8/7/2012	BASF-(SYN)-15-6-B-DL-6-4-LV	2,709	20,315	-	Class III
6/21/2012	8/2/2012	BASF-(SYN)-15-6-B-DL-8-1-LV	2,984	22,381	1/8	Class III
6/21/2012	8/2/2012	BASF-(SYN)-15-6-B-DL-8-2-LV	3,585	26,890	1/4	Class IV
6/21/2012	6/29/2012	BASF-(SYN)-24-8-B-DL-8-3-LV	1,855	29,683	-	<Class III
6/21/2012	7/19/2012	BASF-(SYN)-24-8-B-DL-10-1-LV	1,807	28,912	1/4	<Class III
6/21/2012	8/17/2012	BASF-(SYN)-24-8-B-DL-10-2-LV	1,817	29,072	3/8	<Class III
6/21/2012	7/19/2012	BASF-(SYN)-24-8-B-DL-12-1-LV	1,064	17,024	1/4	<Class III
6/21/2012	8/17/2012	BASF-(SYN)-24-8-B-DL-12-2-LV	2,001	32,016	1/2	Class III
6/29/2012	8/16/2012	BASF-(SYN)-24-8-B-DL-8-4-LV	1,821	29,136	3/8	<Class III
6/29/2012	8/16/2012	BASF-(SYN)-24-8-B-DL-8-5-LV	1,945	31,120	1/4	<Class III
6/21/2012	7/20/2012	BASF-(SYN)-36-8-B-DL-12-1-LV	998	23,952	1/2	<Class III
6/21/2012	7/20/2012	BASF-(SYN)-36-8-B-DL-16-1-LV	1,065	25,536	1/2	<Class III
6/29/2012	7/20/2012	BASF-(SYN)-36-8-B-DL-12-2-LV	1,098	26,352	1/2	<Class III
6/29/2012	7/23/2012	BASF-(SYN)-36-8-B-DL-16-2-LV	1,267	30,417	1/2	<Class III

Table F6: Northern Concrete Synthetic Pipe Test Results

Production Date	Test Date	Pipe Designation	D-Ultimate lb/ft/ft	Ultimate lb	Crack at 5%	Corresponding Class Based on ASTM C76 D-Ultimate
9/21/2012	10/17/2012	BASF-(SYN)-24-8-B-DL-8-1-NC	2,236	35,782	1/2	Class III
9/21/2012	10/26/2012	BASF-(SYN)-24-8-B-DL-8-2-NC	2,025	32,400	1/2	Class III
9/21/2012	10/26/2012	BASF-(SYN)-24-8-B-DL-10-1-NC	2,246	35,936	1/2	Class III
9/21/2012	10/26/2012	BASF-(SYN)-24-8-B-DL-10-2-NC	2,415	38,640	1/4	Class III
9/21/2012	10/29/2012	BASF-(SYN)-24-8-B-DL-12-1-NC	2,013	32,208	1/4	Class III
9/21/2012	10/29/2012	BASF-(SYN)-24-8-B-DL-12-2-NC	1,929	30,864	1/8	<Class III
9/21/2012	10/17/2012	BASF-(SYN)-30-8-B-DL-10-1-NC	2,451	49,017	3/8	Class III
9/21/2012	10/17/2012	BASF-(SYN)-30-8-B-DL-12-1-NC	2,465	49,300	1/2	Class III
9/21/2012	10/17/2012	BASF-(SYN)-30-8-B-DL-16-1-NC	2,542	50,837	1/2	Class III
9/21/2012	10/10/2012	BASF-(SYN)-36-8-C-DL-12-1-NC	2,037	48,899	3/8	Class III
9/21/2012	10/10/2012	BASF-(SYN)-36-8-C-DL-12-2-NC	1,938	46,512	1/2	<Class III
9/21/2012	10/8/2012	BASF-(SYN)-36-8-C-DL-16-1-NC	2,067	49,608	1/2	Class III
9/21/2012	10/10/2012	BASF-(SYN)-36-8-C-DL-16-2-NC	2,100	50,411	3/8	Class III
9/21/2012	10/8/2012	BASF-(SYN)-36-8-C-DL-18-1-NC	2,027	48,639	1/2	Class III
9/21/2012	10/10/2012	BASF-(SYN)-36-8-C-DL-18-2-NC	2,061	49,466	1/2	Class III

Table F7: Hanson Grand Prairie Steel (FS7) Beam Test Results

Production Date	Test Date	Beam Designation	Peak Load (lbs)	Stress $f_{t,}$ (psi)	Stress $f_{c,}$ (psi)	η	Toughness (ft-lb)	E	Initial Stiffness Equation
3/15/2012	3/26/2012	BASF-(FS7)-36-6-B-BM-44-1	7,575	631	4,286	9.64	74.21	3,341,289	y = 3.34E+06x + 5.60E+02
3/15/2012	3/26/2012	BASF-(FS7)-36-6-B-BM-66-1	8,527	711	3,951	11.30	61.45	3,439,864	y = 3.44E+06x + 4.26E+02
3/22/2012	3/30/2012	BASF-(FS7)-24-6-B-BM-22-1	8,875	740	6,043	9.51	32.89	5,899,097	y = 5.90E+06x + 5.27E+02
3/22/2012	4/10/2012	BASF-(FS7)-24-6-B-BM-22-2	6,296	525	6,043	6.75	25.19	3,346,730	y = 3.35E+06x + 1.74E+01
3/22/2012	3/30/2012	BASF-(FS7)-24-6-B-BM-44-1	6,855	571	4,941	8.13	51.65	3,885,163	y = 3.89E+06x + 4.58E+02
3/22/2012	4/10/2012	BASF-(FS7)-24-6-B-BM-44-2	7,508	626	4,941	8.90	63.21	4,370,700	y = 4.37E+06x + 2.17E+02
4/10/2012	4/27/2012	BASF-(FS7)-36-6-B-BM-44-2	7,929	661	7,093	7.85	67.89	4,336,007	y = 4.34E+06x + 6.08E+02
4/10/2012	4/27/2012	BASF-(FS7)-36-6-B-BM-66-2	6,602	550	7,188	6.49	63.42	3,084,950	y = 3.08E+06x + 2.03E+03
4/10/2012	5/14/2012	BASF-(FS7)-36-6-B-BM-66-3	7,966	664	7,188	7.83	95.11	3,740,286	y = 3.74E+06x + 8.71E+02
4/24/2012	5/11/2012	BASF-(FS7)-24-6-B-BM-33-1	6,037	503	8,212	5.55	38.05	5,500,975	y = 5.50E+06x - 1.58E+04
4/24/2012	5/11/2012	BASF-(FS7)-24-6-B-BM-33-2	7,545	629	8,212	6.94	49.16	12,725,361	y = 1.27E+07x + 2.00E+03
4/26/2012	5/15/2012	BASF-(FS7)-36-6-B-BM-88-1	7,017	585	6,395	7.31	63.16	3,375,873	y = 3.38E+06x + 2.48E+02
4/26/2012	5/15/2012	BASF-(FS7)-36-6-B-BM-88-2	6,968	581	6,395	7.26	68.82	3,982,308	y = 3.98E+06x + 7.13E+02
5/3/2012	5/14/2012	BASF-(FS7)-21-6-B-BM-44-1	8,812	734	4,818	10.58	76.08	5,215,051	y = 5.22E+06x + 8.65E+02
5/29/2012	7/6/2012	BASF-(FS7)-24-6-B-BM-22-4	7,215	601	6,014	7.75	33.56	5,310,042	y = 5.31E+06x + 7.60E+02
5/29/2012	7/2/2012	BASF-(FS7)-24-6-B-BM-44-4	8,760	730	6,366	9.15	74.78	4,347,287	y = 4.35E+06x + 9.60E+02
6/12/2012	7/12/2012	BASF-(FS7)-30-6-B-BM-33-1	7,762	647	4,064	10.15	38.62	3,252,422	y = 3.25E+06x + 3.88E+02
6/12/2012	7/12/2012	BASF-(FS7)-30-6-B-BM-44-1	9,703	809	3,974	12.83	91.30	4,101,451	y = 4.10E+06x + 6.57E+02
7/9/2012	7/27/2012	BASF-(FS7)-18-6-B-BM-22-1	7,859	655	6,567	8.08	22.50	4,216,346	y = 4.22E+06x + 3.39E+02
7/9/2012	7/27/2012	BASF-(FS7)-18-6-B-BM-33-1	7,096	591	6,923	7.11	32.40	4,265,121	y = 4.27E+06x + 6.41E+02
7/11/2012	7/27/2012	BASF-(FS7)-18-6-B-BM-44-1	7,304	609	3,967	9.66	43.17	3,682,974	y = 3.68E+06x + 1.44E+02
7/20/2012	8/2/2012	BASF-(FS7)-21-6-B-BM-22-1	5,158	430	3,195	7.60	15.59	2,725,613	y = 2.73E+06x + 6.24E+02
7/20/2012	8/2/2012	BASF-(FS7)-21-6-B-BM-33-1	3,016	251	2,541	4.98	12.11	658,805	y = 6.59E+05x + 2.35E+02

Table F8: Hanson Longview Steel (FS7) Beam Test Results

Production Date	Test Date	Beam Designation	Peak Load (lbs)	Stress $f_{t,}$ (psi)	Stress $f_{c,}$ (psi)	η	Toughness (lb-ft)	E	Initial Stiffness Equation
5/31/2012	7/2/2012	BASF-(FS7)-B-BM-33-1-LV	7002	583	3,714	9.57	54	4,436,823	y = 4.44E+06x + 1.00E+03
5/31/2012	7/12/2012	BASF-(FS7)-B-BM-33-2-LV	7652	638	3,714	10.46	60	6,305,468	y = 6.31E+06x + 6.95E+02
6/14/2012	7/12/2012	BASF-(FS7)-B-BM-33-3-LV	7554	630	5,232	8.70	41	4,502,688	y = 4.50E+06x + 7.36E+02
6/14/2012	7/2/2012	BASF-(FS7)-B-BM-44-1-LV	7923	660	4,546	9.79	52	4,477,543	y = 4.48E+06x + 6.40E+02
6/14/2012	7/6/2012	BASF-(FS7)-B-BM-66-1-LV	8934	744	4,297	11.36	64	5,272,541	y = 5.27E+06x + 1.60E+03
6/14/2012	7/2/2012	BASF-(FS7)-B-BM-88-1-LV	7762	647	4,009	10.21	63	5,831,849	y = 5.83E+06x + 9.79E+02

Table F9: Northern Concrete Steel (FS7) Beam Test Results

Production Date	Test Date	Beam Designation	Peak Load (lbs)	Stress $f_{t,}$ (psi)	Stress $f_{c,}$ (psi)	η	Toughness (lb-ft)	E	Initial Stiffness Equation
9/21/2012	10/19/2012	BASF-(FS7)-B-BM-33-1-NC	11,442	954	3,646	15.79	68	4,255,396	y = 4.26E+06x + 1.13E+03
9/21/2012	10/19/202	BASF-(FS7)-C-BM-44-1-NC	12,498	1,042	5,109	14.57	-	-	-
9/21/2012	10/19/2012	BASF-(FS7)-C-BM-66-1-NC	11,009	917	3,456	15.60	73	4,673,904	y = 4.67E+06x + 1.31E+03
9/21/2012	10/19/2012	BASF-(FS7)-C-BM-88-1-NC	13,020	1,085	3,943	17.28	99	5,258,949	y = 5.26E+06x + 2.01E+03

Table G10: Hanson Grand Prairie Synthetic Beam Test Results

Production Date	Test Date	Beam Designation	Peak Load (lbs)	Stress f_t (psi)	Stress f_c (psi)	η	Toughness (lb-in)	E	Initial Stiffness Equation
2/23/2012	3/19/2012	BASF-(SYN)-24-6-B-BM-12-1	7,743	645	3,883	10.35	498	3,829,336	y = 3.83E+06x + 8.70E+01
2/23/2012	3/19/2012	BASF-(SYN)-24-6-B-BM-8-1	6,522	544	-	-	389	2,392,487	y = 2.39E+06x + 1.95E+02
3/5/2012	3/20/2012	BASF-(SYN)-21-6-B-BM-10-1	5,646	471	6,128	6.01	377	3,505,307	y = 3.51E+06x + 2.27E+02
3/5/2012	3/20/2012	BASF-(SYN)-21-6-B-BM-10-2	6,699	558	6,128	7.13	352	3,979,632	y = 3.98E+06x + 6.11E+02
3/13/2012	3/20/2012	BASF-(SYN)-18-6-B-BM-4-1	6,699	558	4,721	8.12	358	4,036,430	y = 4.04E+06x + 4.45E+02
3/13/2012	3/26/2012	BASF-(SYN)-18-6-B-BM-4-2	7,474	623	4,721	9.06	321	4,523,392	y = 4.52E+06x + 2.63E+02
3/13/2012	3/20/2012	BASF-(SYN)-18-6-B-BM-6-1	7,175	598	4,880	8.56	425	3,737,396	y = 3.74E+06x + 4.26E+02
3/13/2012	3/20/2012	BASF-(SYN)-18-6-B-BM-6-2	6,809	567	4,880	8.12	309	3,346,321	y = 3.35E+06x + 1.36E+02
3/13/2012	3/20/2012	BASF-(SYN)-18-6-B-BM-8-1	7,434	620	4,554	9.18	449	4,261,186	y = 4.26E+06x + 3.26E+02
3/13/2012	3/26/2012	BASF-(SYN)-18-6-B-BM-8-2	7,383	615	4,554	9.12	501	4,095,876	y = 4.10E+06x + 3.81E+01
3/15/2012	3/28/2012	BASF-(SYN)-36-6-B-BM-16-1	5,189	432	3,823	6.99	345	1,874,994	y = 1.87E+06x - 1.56E+01
3/15/2012	3/28/2012	BASF-(SYN)-36-6-B-BM-16-2	5,399	450	3,823	7.28	497	2,799,774	y = 2.80E+06x + 2.05E+02
3/15/2012	3/28/2012	BASF-(SYN)-36-6-B-BM-18-1	4,624	385	3,738	6.30	468	2,041,000	y = 2.04E+06x + 7.72E+01
3/15/2012	3/30/201	BASF-(SYN)-36-6-B-BM-18-2	6,037	503	3,738	8.23	647	2,926,857	y = 2.93E+06x + 2.56E+02
4/5/2012	4/10/2012	BASF-(SYN)-36-6-B-BM-16-3	6,999	583	6,799	7.07	613	4,818,275	y = 4.82E+06x + 9.96E+02
4/5/2012	4/27/2012	BASF-(SYN)-36-6-B-BM-16-4	9,617	801	6,799	9.72	701	3,846,894	y = 3.85E+06x + 1.65E+02
4/5/2012	4/10/2012	BASF-(SYN)-36-6-B-BM-18-3	6,141	512	5,399	6.96	594	3,111,005	y = 3.11E+06x + 4.92E+01
4/5/2012	4/27/2012	BASF-(SYN)-36-6-B-BM-18-4	5,946	495	5,399	6.74	567	4,601,670	y = 4.60E+06x + 3.25E+02
4/24/2012	5/11/2012	BASF-(SYN)-24-6-B-BM-10-1	8,052	671	8,106	7.45	657	4,809,354	y = 4.81E+06x + 6.49E+02
4/24/2012	5/14/2012	BASF-(SYN)-24-6-B-BM-10-2	7,545	629	8,106	6.98	553	3,726,078	y = 3.73E+06x - 1.08E+02
4/26/2012	5/14/2012	BASF-(SYN)-36-6-B-BM-12-1	6,574	548	6,218	6.95	555	4,035,690	y = 4.04E+06x + 1.42E+03
4/26/2012	5/14/202	BASF-(SYN)-36-6-B-BM-12-2	7,185	599	6,218	7.59	547	6,136,518	y = 6.14E+06x + 1.56E+03
5/25/2012	6/6/2012	BASF-(SYN)-24-6-B-BM-8-2	7,166	597	6,516	7.40	456	3,826,146	y = 3.83E+06x + 1.32E+02
5/25/2012	6/6/2012?	BASF-(SYN)-24-6-B-BM-12-2	7,033	586	6,159	7.47	562	4,741,819	y = 4.74E+06x + 2.88E+02
6/13/2012	7/12/2012	BASF-(SYN)-30-6-B-BM-10-1	7,511	626	7,789	7.09	574	4,790,355	y = 4.79E+06x + 6.11E+02
6/13/2012	7/12/2012	BASF-(SYN)-30-6-B-BM-12-1	6,678	557	7,234	6.54	609	3,487,778	y = 3.49E+06x + 4.07E+02
7/6/2012	7/27/2012	BASF-(SYN)-21-6-B-BM-6-1	7,017	585	2,346	12.07	308	3,487,579	y = 3.49E+06x + 1.08E+03
7/6/2012	7/27/2012	BASF-(SYN)-21-6-B-BM-8-1	6,293	524	1,738	12.58	286	3,266,677	y = 3.27E+06x + 2.06E+02
7/6/2012	7/27/2012	BASF-(SYN)-21-6-B-BM-12-1	4,572	381	1,760	9.08	274	1,783,173	y = 1.78E+06x + 5.07E+02
7/11/2012	8/2/2012	BASF-(SYN)-18-6-B-BM-10-1	6,178	515	2,698	9.91	289	2,806,560	y = 2.81E+06x + 8.68E+02
7/31/2012	8/9/2012	BASF-(SYN)-30-6-B-BM-16-1	6,519	543	2,778	10.31	509	2,939,606	y = 2.94E+06x + 1.63E+02

Table G11: Hanson Longview Synthetic Beam Test Results

Production Date	Test Date	Beam Designation	Peak Load (lbs)	Stress $f_{t,}$ (psi)	Stress $f_{c,}$ (psi)	η	Toughness (lb-ft)	E	Initial Stiffness Equation
5/31/2012	7/6/2012	BASF-(SYN)-B-BM-8-1-LV	7,218	602	5,486	8.12	35	4,591,140	y = 4.59E+06x + 4.21E+02
5/31/2012	7/6/2012	BASF-(SYN)-B-BM-8-2-LV	7,600	633	5,486	8.55	41	5,592,458	y = 5.59E+06x + 1.05E+03
6/21/2012	7/12/2012	BASF-(SYN)-B-BM-6-1-LV	6,445	537	4,084	8.40	26	5,643,893	y = 5.64E+06x + 6.56E+02
6/21/2012	7/6/2012	BASF-(SYN)-B-BM-8-3-LV	5,167	431	3,866	6.93	38	2,864,997	y = 2.86E+06x + 8.11E+02
6/21/2012	7/6/2012	BASF-(SYN)-B-BM-10-1-LV	5,094	425	3,442	7.24	31	3,973,023	y = 3.97E+06x + 7.38E+02
6/21/2012	7/12/2012	BASF-(SYN)-B-BM-12-1-LV	7,856	655	5,467	8.85	54	4,336,919	y = 4.34E+06x + 2.50E+02
6/21/2012	7/12/2012	BASF-(SYN)-B-BM-16-1-LV	6,818	568	4,251	8.71	42	7,003,746	y = 7.00E+06x + 9.33E+02

Table G12: Northern Concrete Synthetic Beam Test Results

Production Date	Test Date	Beam Designation	Peak Load (lbs)	Stress $f_{t,}$ (psi)	Stress $f_{c,}$ (psi)	η	Toughness (lb-ft)	E	Initial Stiffness Equation
9/21/2012	10/19/2012	BASF-(SYN)-B-BM-8-1-NC	9059	755	4,505	11.25	42	5,370,825	y = 5.37E+06x + 1.03E+03
9/21/2012	10/19/2012	BASF-(SYN)-B-BM-10-1-NC	11644	970	5,015	13.70	76	5,456,824	y = 5.46E+06x + 2.33E+03
9/21/2012	10/19/2012	BASF-(SYN)-C-BM-12-1-NC	11952	996	4,898	14.23	81	5,238,628	y = 5.24E+06x + 1.09E+03
9/21/2012	10/19/2012	BASF-(SYN)-C-BM-16-1-NC	11403	950	5,445	12.88	97	4,811,338	y = 4.81E+06x + 1.07E+03
9/21/2012	10/19/2012	BASF-(SYN)-C-BM-18-1-NC	9135	761	4,809	10.98	77	3,813,580	y = 3.81E+06x + 2.18E+02

Table G13: Hanson Grand Prairie Steel (FS7) Cylinder Test Results

Production Date	Test Date	Cylinder Designation	Peak Load (lbs)	Stress (psi)	Average Stress
3/15/2012	3/16/2012	BASF-(FS7)-36-6-B-CC-44-1	39,730	3,162	
3/15/2012	3/16/2012	BASF-(FS7)-36-6-B-CC-44-2	32,230	2,565	
3/15/2012	3/19/2012	BASF-(FS7)-36-6-B-CC-44-3	66,980	5,330	
3/15/2012	3/19/2012	BASF-(FS7)-36-6-B-CC-44-4	54,790	4,360	
3/15/2012	3/22/2012	BASF-(FS7)-36-6-B-CC-44-5	69,840	5,558	
3/15/2012	3/22/2012	BASF-(FS7)-36-6-B-CC-44-6	59,610	4,744	4,286
3/15/2012	3/16/2012	BASF-(FS7)-36-6-B-CC-66-1	36,390	2,896	
3/15/2012	3/16/2012	BASF-(FS7)-36-6-B-CC-66-2	27,500	2,188	
3/15/2012	3/19/2012	BASF-(FS7)-36-6-B-CC-66-3	50,650	4,031	
3/15/2012	3/19/2012	BASF-(FS7)-36-6-B-CC-66-4	53,870	4,287	
3/15/2012	3/22/2012	BASF-(FS7)-36-6-B-CC-66-5	68,070	5,417	
3/15/2012	3/22/2012	BASF-(FS7)-36-6-B-CC-66-6	61,440	4,889	3,951
3/22/2012	3/23/2012	BASF-(FS7)-24-6-B-CC-22-1	55,670	4,430	
3/22/2012	3/23/2012	BASF-(FS7)-24-6-B-CC-22-2	57,040	4,539	
3/22/2012	3/25/2012	BASF-(FS7)-24-6-B-CC-22-3	71,570	5,695	
3/22/2012	3/25/2012	BASF-(FS7)-24-6-B-CC-22-4	82,870	6,595	
3/22/2012	3/29/2012	BASF-(FS7)-24-6-B-CC-22-5	87,870	6,992	
3/22/2012	3/29/2012	BASF-(FS7)-24-6-B-CC-22-6	100,620	8,007	6,043
3/22/2012	3/23/2012	BASF-(FS7)-24-6-B-CC-44-1	59,830	4,761	
3/22/2012	3/23/2012	BASF-(FS7)-24-6-B-CC-44-2	45,140	3,592	
3/22/2012	3/25/2012	BASF-(FS7)-24-6-B-CC-44-3	53,320	4,243	
3/22/2012	3/25/2012	BASF-(FS7)-24-6-B-CC-44-4	56,590	4,503	
3/22/2012	3/29/2012	BASF-(FS7)-24-6-B-CC-44-5	75,000	5,968	
3/22/2012	3/29/2012	BASF-(FS7)-24-6-B-CC-44-6	82,680	6,579	4,941
4/10/2012	4/16/2012	BASF-(FS7)-36-6-B-CC-44-7	76,430	6,082	
4/10/2012	4/16/2012	BASF-(FS7)-36-6-B-CC-44-8	73,540	5,852	
4/10/2012	4/24/2012	BASF-(FS7)-36-6-B-CC-44-9	89,890	7,153	
4/10/2012	4/24/2012	BASF-(FS7)-36-6-B-CC-44-10	98,860	7,867	
4/10/2012	5/10/2012	BASF-(FS7)-36-6-B-CC-44-11	97,580	7,765	
4/10/2012	5/10/2012	BASF-(FS7)-36-6-B-CC-44-12	98,490	7,838	7,093
4/10/2012	4/16/2012	BASF-(FS7)-36-6-B-CC-66-7	76,940	6,123	
4/10/2012	4/16/2012	BASF-(FS7)-36-6-B-CC-66-8	71,360	5,679	
4/10/2012	4/24/2012	BASF-(FS7)-36-6-B-CC-66-9	109,980	8,752	
4/10/2012	4/24/2012	BASF-(FS7)-36-6-B-CC-66-10	91,260	7,262	
4/10/2012	5/10/2012	BASF-(FS7)-36-6-B-CC-66-11	102,280	8,139	
4/10/2012	5/10/2012	BASF-(FS7)-36-6-B-CC-66-12	90,160	7,175	7,188

Table G13: Hanson Grand Prairie Steel (FS7) Cylinder Test Results Cont.

Production Date	Test Date	Cylinder Designation	Peak Load (lbs)	Stress (psi)	Average Stress
4/24/2012	4/302012	BASF-(FS7)-24-6-B-CC-33-1	119,320	9,495	
4/24/2012	4/302012	BASF-(FS7)-24-6-B-CC-33-2	72,810	5,794	
4/24/2012	4/302012	BASF-(FS7)-24-6-B-CC-33-3	119,510	9,510	
4/24/2012	4/302012	BASF-(FS7)-24-6-B-CC-33-4	106,840	8,502	
4/24/2012	5/1/2012	BASF-(FS7)-24-6-B-CC-33-5	104,770	8,337	
4/24/2012	5/1/2012	BASF-(FS7)-24-6-B-CC-33-6	95,920	7,633	8,212
4/26/2012	5/3/2012	BASF-(FS7)-36-6-B-CC-88-1	62,880	5,004	
4/26/2012	5/3/2012	BASF-(FS7)-36-6-B-CC-88-2	77,930	6,201	
4/26/2012	5/12/2012	BASF-(FS7)-36-6-B-CC-88-3	87,700	6,979	
4/26/2012	5/12/2012	BASF-(FS7)-36-6-B-CC-88-4	91,990	7,320	
4/26/2012	5/17/2012	BASF-(FS7)-36-6-B-CC-88-5	103,090	8,204	
4/26/2012	5/17/2012	BASF-(FS7)-36-6-B-CC-88-6	58,600	4,663	6,395
5/3/2012	5/12/2012	BASF-(FS7)-21-6-B-CC-44-1	49,430	3,934	
5/3/2012	5/12/2012	BASF-(FS7)-21-6-B-CC-44-2	49,890	3,970	
5/3/2012	5/17/2012	BASF-(FS7)-21-6-B-CC-44-3	61,550	4,898	
5/3/2012	5/17/2012	BASF-(FS7)-21-6-B-CC-44-4	58,390	4,647	
5/3/2012	5/21/2012	BASF-(FS7)-21-6-B-CC-44-5	72,020	5,731	
5/3/2012	5/21/2012	BASF-(FS7)-21-6-B-CC-44-6	71,990	5,729	4,818
5/29/2012	6/1/2012	BASF-(FS7)-24-6-B-CC-22-7	52,470	4,175	
5/29/2012	6/1/2012	BASF-(FS7)-24-6-B-CC-22-8	55,390	4,408	
5/29/2012	6/5/2012	BASF-(FS7)-24-6-B-CC-22-9	90,130	7,172	
5/29/2012	6/5/2012	BASF-(FS7)-24-6-B-CC-22-10	72,360	5,758	
5/29/2012	6/26/2012	BASF-(FS7)-24-6-B-CC-22-11	87,110	6,932	
5/29/2012	6/26/2012	BASF-(FS7)-24-6-B-CC-22-12	96,000	7,639	6,014
5/29/2012	6/1/2012	BASF-(FS7)-24-6-B-CC-44-7	62,680	4,988	
5/29/2012	6/1/2012	BASF-(FS7)-24-6-B-CC-44-8	69,830	5,557	
5/29/2012	6/5/2012	BASF-(FS7)-24-6-B-CC-44-9	82,140	6,536	
5/29/2012	6/5/2012	BASF-(FS7)-24-6-B-CC-44-10	80,100	6,374	
5/29/2012	6/26/2012	BASF-(FS7)-24-6-B-CC-44-11	91,410	7,274	
5/29/2012	6/26/2012	BASF-(FS7)-24-6-B-CC-44-12	93,840	7,468	6,366
6/12/2012	6/13/2012	BASF-(FS7)-24-6-B-CC-33-7	41,420	3,296	
6/12/2012	6/15/2012	BASF-(FS7)-24-6-B-CC-33-8	47,830	3,806	
6/12/2012	6/19/2012	BASF-(FS7)-24-6-B-CC-33-9	63,950	5,089	4,064

Table G13: Hanson Grand Prairie Steel (FS7) Cylinder Test Results Cont.

Production Date	Test Date	Cylinder Designation	Peak Load (lbs)	Stress (psi)	Average Stress
6/12/2012	6/13/2012	BASF-(FS7)-24-6-B-CC-44-13	42,030	3,345	
6/12/2012	6/13/2012	BASF-(FS7)-24-6-B-CC-44-14	64,540	5,136	
6/12/2012	6/15/2012	BASF-(FS7)-24-6-B-CC-44-15	48,540	3,863	
6/12/2012	6/15/2012	BASF-(FS7)-24-6-B-CC-44-16	31,400	2,499	
6/12/2012	6/19/2012	BASF-(FS7)-24-6-B-CC-44-17	67,320	5,357	
6/12/2012	6/19/2012	BASF-(FS7)-24-6-B-CC-44-18	45,820	3,646	3,974
7/9/2012	7/20/2012	BASF-(FS7)-18-6-B-CC-22-1	47,590	3,787	
7/9/2012	7/20/2012	BASF-(FS7)-18-6-B-CC-22-2	77,640	6,178	
7/9/2012	7/26/2012	BASF-(FS7)-18-6-B-CC-22-3	93,200	7,417	
7/9/2012	7/26/2012	BASF-(FS7)-18-6-B-CC-22-4	74,710	5,945	
7/9/2012	8/7/2012	BASF-(FS7)-18-6-B-CC-22-5	85,320	6,790	
7/9/2012	8/7/2012	BASF-(FS7)-18-6-B-CC-22-6	116,710	9,287	6,567
7/9/2012	7/20/2012	BASF-(FS7)-18-6-B-CC-33-1	65,150	5,184	
7/9/2012	7/20/2012	BASF-(FS7)-18-6-B-CC-33-2	74,470	5,926	
7/9/2012	7/26/2012	BASF-(FS7)-18-6-B-CC-33-3	92,400	7,353	
7/9/2012	7/26/2012	BASF-(FS7)-18-6-B-CC-33-4	93,370	7,430	
7/9/2012	8/7/2012	BASF-(FS7)-18-6-B-CC-33-5	86,070	6,849	
7/9/2012	8/7/2012	BASF-(FS7)-18-6-B-CC-33-6	110,510	8,794	6,923
7/11/2012	7/20/2012	BASF-(FS7)-18-6-B-CC-44-1	37,980	3,022	
7/11/2012	7/20/2012	BASF-(FS7)-18-6-B-CC-44-2	51,600	4,106	
7/11/2012	7/26/2012	BASF-(FS7)-18-6-B-CC-44-3	42,460	3,379	
7/11/2012	7/26/2012	BASF-(FS7)-18-6-B-CC-44-4	55,310	4,401	
7/11/2012	8/9/2012	BASF-(FS7)-18-6-B-CC-44-5	55,350	4,405	
7/11/2012	8/9/2012	BASF-(FS7)-18-6-B-CC-44-6	56,400	4,488	3,967
7/20/2012	8/2/2012	BASF-(FS7)-21-6-B-CC-22-1	16,860	1,342	
7/20/2012	8/2/2012	BASF-(FS7)-21-6-B-CC-22-2	58,210	4,632	
7/20/2012	8/14/2012	BASF-(FS7)-21-6-B-CC-22-3	57,540	4,579	
7/20/2012	8/14/2012	BASF-(FS7)-21-6-B-CC-22-4	45,080	3,587	
7/20/2012	8/16/2012	BASF-(FS7)-21-6-B-CC-22-5	21,370	1,701	
7/20/2012	8/16/2012	BASF-(FS7)-21-6-B-CC-22-6	41,860	3,331	3,195
7/20/2012	8/2/2012	BASF-(FS7)-21-6-B-CC-33-1	24,530	1,952	
7/20/2012	8/2/2012	BASF-(FS7)-21-6-B-CC-33-2	20,750	1,651	
7/20/2012	8/14/2012	BASF-(FS7)-21-6-B-CC-33-3	49,680	3,953	
7/20/2012	8/14/2012	BASF-(FS7)-21-6-B-CC-33-4	34,700	2,761	
7/20/2012	8/16/2012	BASF-(FS7)-21-6-B-CC-33-5	23,420	1,864	
7/20/2012	8/16/2012	BASF-(FS7)-21-6-B-CC-33-6	38,540	3,067	2,541
7/31/2012	8/7/2012	BASF-(FS7)-30-6-B-CC-66-1	71,870	5,719	
7/31/2012	8/7/2012	BASF-(FS7)-30-6-B-CC-66-2	74,590	5,936	
7/31/2012	8/14/2012	BASF-(FS7)-30-6-B-CC-66-3	71,340	5,677	
7/31/2012	8/14/2012	BASF-(FS7)-30-6-B-CC-66-4	71,930	5,724	
7/31/2012	9/18/2012	BASF-(FS7)-30-6-B-CC-66-5	62,720	4,991	
7/31/2012	9/18/2012	BASF-(FS7)-30-6-B-CC-66-6	68,990	5,490	5,590

Table G14: Hanson Longview Steel (FS7) Cylinder Test Results

Production Date	Test Date	Cylinder Designation	Peak Load (lbs)	Stress (psi)	Average Stress (psi)
5/31/2012	6/18/2012	BASF-(FS7)-B-CC-33-1-LV	60,050	4,781	
5/31/2012	6/18/2012	BASF-(FS7)-B-CC-33-2-LV	64,270	5,117	
5/31/2012	6/28/2012	BASF-(FS7)-B-CC-33-5-LV	80,410	6,402	
5/31/2012	6/28/2012	BASF-(FS7)-B-CC-33-6-LV	75,170	5,985	3,714
6/14/2012	6/15/2012	BASF-(FS7)-B-CC-33-7-LV	60,400	4,809	
6/14/2012	6/15/2012	BASF-(FS7)-B-CC-33-8-LV	66,720	5,312	
6/14/2012	6/21/2012	BASF-(FS7)-B-CC-33-9-LV	66,560	5,299	
6/14/2012	6/21/2012	BASF-(FS7)-B-CC-33-10-LV	47,820	3,807	
6/14/2012	6/28/2012	BASF-(FS7)-B-CC-33-11-LV	82,290	6,552	
6/14/2012	6/28/2012	BASF-(FS7)-B-CC-33-12-LV	70,500	5,613	5,232
6/14/2012	6/15/2012	BASF-(FS7)-B-CC-44-1-LV	49,660	3,954	
6/14/2012	6/15/2012	BASF-(FS7)-B-CC-44-2-LV	39,480	3,143	
6/14/2012	6/18/2012	BASF-(FS7)-B-CC-44-3-LV	54,460	4,336	
6/14/2012	6/18/2012	BASF-(FS7)-B-CC-44-4-LV	59,590	4,744	
6/14/2012	6/21/2012	BASF-(FS7)-B-CC-44-5-LV	66,300	5,279	
6/14/2012	6/21/2012	BASF-(FS7)-B-CC-44-6-LV	73,090	5,819	4,546
6/14/2012	6/15/2012	BASF-(FS7)-B-CC-66-1-LV	51,380	4,091	
6/14/2012	6/15/2012	BASF-(FS7)-B-CC-66-2-LV	31,960	2,545	
6/14/2012	6/18/2012	BASF-(FS7)-B-CC-66-3-LV	61,370	4,886	
6/14/2012	6/18/2012	BASF-(FS7)-B-CC-66-4-LV	71,040	5,656	
6/14/2012	6/21/2012	BASF-(FS7)-B-CC-66-5-LV	55,850	4,447	
6/14/2012	6/21/2012	BASF-(FS7)-B-CC-66-6-LV	52,190	4,155	4,297
6/14/2012	6/15/2012	BASF-(FS7)-B-CC-88-1-LV	36,580	2,912	
6/14/2012	6/15/2012	BASF-(FS7)-B-CC-88-2-LV	44,040	3,506	
6/14/2012	6/18/2012	BASF-(FS7)-B-CC-88-3-LV	42,970	3,421	
6/14/2012	6/18/2012	BASF-(FS7)-B-CC-88-4-LV	55,240	4,398	
6/14/2012	6/21/2012	BASF-(FS7)-B-CC-88-5-LV	62,460	4,973	
6/14/2012	6/21/2012	BASF-(FS7)-B-CC-88-6-LV	60,860	4,846	4,009

Table G15: Northern Concrete Steel (FS7) Cylinder Test Results

Production Date	Test Date	Cylinder Designation	Peak Load (lbs)	Stress (psi)	Average Stress (psi)
9/21/2012	10/15/2012	BASF-(FS7)-B-CC-33-2-NC	150,040	5,307	
9/21/2012	10/18/2012	BASF-(FS7)-B-CC-33-3-NC	124,110	4,389	
9/21/2012	10/22/2012	BASF-(FS7)-B-CC-33-4-NC	187,820	6,643	
9/21/2012	10/26/2012	BASF-(FS7)-B-CC-33-5-NC	156,510	5,535	5,469
9/21/2012	10/15/2012	BASF-(FS7)-C-CC-44-2-NC	190,290	6,730	
9/21/2012	10/18/2012	BASF-(FS7)-C-CC-44-3-NC	215,150	7,609	
9/21/2012	10/22/2012	BASF-(FS7)-C-CC-44-4-NC	236,590	8,368	
9/21/2012	10/26/2012	BASF-(FS7)-C-CC-44-5-NC	224,680	7,946	6,131
9/21/2012	10/15/2012	BASF-(FS7)-C-CC-66-2-NC	223,010	7,887	
9/21/2012	10/18/2012	BASF-(FS7)-C-CC-66-3-NC	188,520	6,668	
9/21/2012	10/22/2012	BASF-(FS7)-C-CC-66-4-NC	174,850	6,184	6,913
9/21/2012	10/15/2012	BASF-(FS7)-C-CC-88-2-NC	223,410	7,902	
9/21/2012	10/18/2012	BASF-(FS7)-C-CC-88-3-NC	211,380	7,476	
9/21/2012	10/22/2012	BASF-(FS7)-C-CC-88-4-NC	234,100	8,280	7,886

Table G16: Hanson Grand Prairie Synthetic Cylinder Test Resul

Production Date	Test Date	Cylinder Designation	Peak Load (lbs)	Stress (psi)	Average Stress
2/2/2012	2/3/2012	BASF-(SYN)-24-6-B-BM-12-1	38,361	3,053	
2/2/2012	2/3/2012	BASF-(SYN)-24-6-B-BM-12-2	61,340	4,881	
2/2/2012	2/6/2012	BASF-(SYN)-24-6-B-BM-12-3	56,970	4,534	
2/2/2012	2/6/2012	BASF-(SYN)-24-6-B-BM-12-4	34,890	2,776	
2/2/2012	2/9/2012	BASF-(SYN)-24-6-B-BM-12-5	60,790	4,838	
2/2/2012	2/9/2012	BASF-(SYN)-24-6-B-BM-12-6	64,790	5,156	4,206
2/23/2012	2/24/2012	BASF-(SYN)-24-6-B-BM-12-7	36,160	2,878	
2/23/2012	2/24/2012	BASF-(SYN)-24-6-B-BM-12-8	37,180	2,959	
2/23/2012	2/27/2012	BASF-(SYN)-24-6-B-BM-12-9	43,540	3,465	
2/23/2012	2/27/2012	BASF-(SYN)-24-6-B-BM-12-10	53,690	4,273	
2/23/2012	3/1/2012	BASF-(SYN)-24-6-B-BM-12-11	38,010	3,025	
2/23/2012	3/1/2012	BASF-(SYN)-24-6-B-BM-12-12	61,870	4,923	
2/23/2012	3/22/2012	BASF-(SYN)-24-6-B-BM-12-13	45,620	3,630	
2/23/2012	3/22/2012	BASF-(SYN)-24-6-B-BM-12-14	74,290	5,912	3,883
3/5/2012	3/6/2012	BASF-(SYN)-21-6-B-CC-10-1	67,120	5,341	
3/5/2012	3/6/2012	BASF-(SYN)-21-6-B-CC-10-2	67,990	5,410	
3/5/2012	3/8/2012	BASF-(SYN)-21-6-B-CC-10-3	79,420	6,320	
3/5/2012	3/8/2012	BASF-(SYN)-21-6-B-CC-10-4	69,400	5,523	
3/5/2012	3/13/2012	BASF-(SYN)-21-6-B-CC-10-5	89,350	7,110	
3/5/2012	3/13/2012	BASF-(SYN)-21-6-B-CC-10-6	71,750	5,710	
3/5/2012	4/2/2012	BASF-(SYN)-21-6-B-CC-10-7	76,370	6,077	
3/5/2012	4/2/2012	BASF-(SYN)-21-6-B-CC-10-8	94,670	7,534	6,128
3/13/2012	3/14/2012	BASF-(SYN)-18-6-B-CC-4-1	33,840	2,693	
3/13/2012	3/14/2012	BASF-(SYN)-18-6-B-CC-4-2	47,690	3,795	
3/13/2012	3/16/2012	BASF-(SYN)-18-6-B-CC-4-3	60,450	4,810	
3/13/2012	3/16/2012	BASF-(SYN)-18-6-B-CC-4-4	57,030	4,538	
3/13/2012	3/20/2012	BASF-(SYN)-18-6-B-CC-4-5	90,630	7,212	
3/13/2012	3/20/2012	BASF-(SYN)-18-6-B-CC-4-6	66,340	5,279	4,721
3/13/2012	3/14/2012	BASF-(SYN)-18-6-B-CC-6-1	38,670	3,077	
3/13/2012	3/14/2012	BASF-(SYN)-18-6-B-CC-6-2	41,270	3,284	
3/13/2012	3/16/2012	BASF-(SYN)-18-6-B-CC-6-3	60,830	4,841	
3/13/2012	3/16/2012	BASF-(SYN)-18-6-B-CC-6-4	68,520	5,453	
3/13/2012	3/20/2012	BASF-(SYN)-18-6-B-CC-6-5	69,050	5,495	
3/13/2012	3/20/2012	BASF-(SYN)-18-6-B-CC-6-6	89,620	7,132	4,880
3/13/2012	3/14/2012	BASF-(SYN)-18-6-B-CC-8-1	41,370	3,292	
3/13/2012	3/14/2012	BASF-(SYN)-18-6-B-CC-8-2	34,600	2,753	
3/13/2012	3/16/2012	BASF-(SYN)-18-6-B-CC-8-3	71,430	5,684	
3/13/2012	3/16/2012	BASF-(SYN)-18-6-B-CC-8-4	63,060	5,018	
3/13/2012	3/20/2012	BASF-(SYN)-18-6-B-CC-8-5	55,240	4,396	
3/13/2012	3/20/2012	BASF-(SYN)-18-6-B-CC-8-6	77,660	6,180	4,554

Table G16: Hanson Grand Prairie Synthetic Cylinder Test Results Cont.

Production Date	Test Date	Cylinder Designation	Peak Load (lbs)	Stress (psi)	Average Stress
3/15/2012	3/16/2012	BASF-(SYN)-36-6-B-CC-16-1	31,380	2,497	
3/15/2012	3/16/2012	BASF-(SYN)-36-6-B-CC-16-2	41,980	3,341	
3/15/2012	3/19/2012	BASF-(SYN)-36-6-B-CC-16-3	69,630	5,541	
3/15/2012	3/19/2012	BASF-(SYN)-36-6-B-CC-16-4	53,350	4,245	
3/15/2012	3/22/2012	BASF-(SYN)-36-6-B-CC-16-5	51,150	4,070	
3/15/2012	3/22/2012	BASF-(SYN)-36-6-B-CC-16-6	40,730	3,241	3,823
3/15/2012	3/16/2012	BASF-(SYN)-36-6-B-CC-18-1	29,120	2,317	
3/15/2012	3/16/2012	BASF-(SYN)-36-6-B-CC-18-2	31,310	2,492	
3/15/2012	3/19/2012	BASF-(SYN)-36-6-B-CC-18-3	54,750	4,357	
3/15/2012	3/19/2012	BASF-(SYN)-36-6-B-CC-18-4	46,570	3,706	
3/15/2012	3/22/2012	BASF-(SYN)-36-6-B-CC-18-5	64,060	5,098	
3/15/2012	3/22/2012	BASF-(SYN)-36-6-B-CC-18-6	56,030	4,459	3,738
4/5/2012	4/9/2012	BASF-(SYN)-36-6-B-CC-16-7	73,190	5,824	
4/5/2012	4/9/2012	BASF-(SYN)-36-6-B-CC-16-8	61,020	4,856	
4/5/2012	4/16/2012	BASF-(SYN)-36-6-B-CC-16-9	95,390	7,591	
4/5/2012	4/16/2012	BASF-(SYN)-36-6-B-CC-16-10	84,100	6,692	
4/5/2012	5/3/2012	BASF-(SYN)-36-6-B-CC-16-11	106,340	8,462	
4/5/2012	5/3/2012	BASF-(SYN)-36-6-B-CC-16-12	92,590	7,368	6,799
4/5/2012	4/9/2012	BASF-(SYN)-36-6-B-CC-18-7	61,160	4,867	
4/5/2012	4/9/2012	BASF-(SYN)-36-6-B-CC-18-8	47,960	3,817	
4/5/2012	4/16/2012	BASF-(SYN)-36-6-B-CC-18-9	76,900	6,120	
4/5/2012	4/16/2012	BASF-(SYN)-36-6-B-CC-18-10	56,900	4,528	
4/5/2012	5/3/2012	BASF-(SYN)-36-6-B-CC-18-11	91,040	7,245	
4/5/2012	5/3/2012	BASF-(SYN)-36-6-B-CC-18-12	73,150	5,821	5,399
4/24/2012	4/30/2012	BASF-(SYN)-24-6-B-CC-10-1	103,710	8,253	
4/24/2012	4/30/2012	BASF-(SYN)-24-6-B-CC-10-2	102,450	8,153	
4/24/2012	4/30/2012	BASF-(SYN)-24-6-B-CC-10-3	111,930	8,907	
4/24/2012	5/1/2012	BASF-(SYN)-24-6-B-CC-10-4	94,860	7,549	
4/24/2012	5/1/2012	BASF-(SYN)-24-6-B-CC-10-5	96,350	7,667	8,106
4/26/2012	5/3/2012	BASF-(SYN)-36-6-B-CC-12-1	76,310	6,073	
4/26/2012	5/3/2012	BASF-(SYN)-36-6-B-CC-12-2	68,560	5,456	
4/26/2012	5/12/2012	BASF-(SYN)-36-6-B-CC-12-3	72,220	5,747	
4/26/2012	5/12/2012	BASF-(SYN)-36-6-B-CC-12-4	77,380	6,158	
4/26/2012	5/17/2012	BASF-(SYN)-36-6-B-CC-12-5	91,930	7,316	
4/26/2012	5/17/2012	BASF-(SYN)-36-6-B-CC-12-6	82,400	6,557	6,218

Table G16: Hanson Grand Prairie Synthetic Cylinder Test Results Cont.

Production Date	Test Date	Cylinder Designation	Peak Load (lbs)	Stress (psi)	Average Stress
5/25/2012	6/1/2012	BASF-(SYN)-24-6-B-CC-8-1	68,440	5,446	
5/25/2012	6/1/2012	BASF-(SYN)-24-6-B-CC-8-2	79,120	6,296	
5/25/2012	6/8/2012	BASF-(SYN)-24-6-B-CC-8-3	81,580	6,492	
5/25/2012	6/8/2012	BASF-(SYN)-24-6-B-CC-8-4	86,360	6,872	
5/25/2012	6/22/2012	BASF-(SYN)-24-6-B-CC-8-5	74,630	5,939	
5/25/2012	6/22/2012	BASF-(SYN)-24-6-B-CC-8-6	101,140	8,048	6,516
5/25/2012	6/1/2012	BASF-(SYN)-24-6-B-CC-12-15	62,260	4,954	
5/25/2012	6/1/2012	BASF-(SYN)-24-6-B-CC-12-16	81,750	6,505	
5/25/2012	6/8/2012	BASF-(SYN)-24-6-B-CC-12-17	81,580	6,492	
5/25/2012	6/8/2012	BASF-(SYN)-24-6-B-CC-12-18	86,360	6,872	
5/25/2012	6/22/2012	BASF-(SYN)-24-6-B-CC-12-19	82,570	6,571	
5/25/2012	6/22/2012	BASF-(SYN)-24-6-B-CC-12-20	69,830	5,557	6,159
6/13/2012	7/20/2012	BASF-(SYN)-30-6-B-CC-10-1	104,070	8,282	
6/13/2012	7/20/2012	BASF-(SYN)-30-6-B-CC-10-2	91,010	7,242	
6/13/2012	7/26/2012	BASF-(SYN)-30-6-B-CC-10-3	105,620	8,405	
6/13/2012	7/26/2012	BASF-(SYN)-30-6-B-CC-10-4	101,580	8,083	
6/13/2012	8/2/2012	BASF-(SYN)-30-6-B-CC-10-5	77,600	6,175	
6/13/2012	8/2/2012	BASF-(SYN)-30-6-B-CC-10-6	107,360	8,543	7,789
6/13/2012	7/20/2012	BASF-(SYN)-30-6-B-CC-12-1	92,610	7,370	
6/13/2012	7/20/2012	BASF-(SYN)-30-6-B-CC-12-2	102,330	8,143	
6/13/2012	7/26/2012	BASF-(SYN)-30-6-B-CC-12-3	76,580	6,094	
6/13/2012	7/26/2012	BASF-(SYN)-30-6-B-CC-12-4	88,550	7,047	
6/13/2012	8/2/2012	BASF-(SYN)-30-6-B-CC-12-5	84,750	6,744	
6/13/2012	8/2/2012	BASF-(SYN)-30-6-B-CC-12-6	100,630	8,008	7,234
7/6/2012	7/20/2012	BASF-(SYN)-21-6-B-CC-6-1	51,100	4,066	
7/6/2012	7/26/2012	BASF-(SYN)-21-6-B-CC-6-2	30,040	2,391	
7/6/2012	7/26/2012	BASF-(SYN)-21-6-B-CC-6-3	15,590	1,241	
7/6/2012	8/3/2012	BASF-(SYN)-21-6-B-CC-6-4	21,200	1,687	2,346
7/6/2012	7/20/2012	BASF-(SYN)-21-6-B-CC-8-1	16,970	1,350	
7/6/2012	7/20/2012	BASF-(SYN)-21-6-B-CC-8-2	23,010	1,831	
7/6/2012	7/26/2012	BASF-(SYN)-21-6-B-CC-8-3	32,600	2,594	
7/6/2012	7/26/2012	BASF-(SYN)-21-6-B-CC-8-4	14,030	1,116	
7/6/2012	8/3/2012	BASF-(SYN)-21-6-B-CC-8-5	22,230	1,769	
7/6/2012	8/3/2012	BASF-(SYN)-21-6-B-CC-8-6	22,220	1,768	1,738

Table G16: Hanson Grand Prairie Synthetic Cylinder Test Results Cont.

Production Date	Test Date	Cylinder Designation	Peak Load (lbs)	Stress (psi)	Average Stress
7/6/2012	7/20/2012	BASF-(SYN)-21-6-B-CC-12-1	12,130	965	
7/6/2012	7/26/2012	BASF-(SYN)-21-6-B-CC-12-2	24,540	1,953	
7/6/2012	7/26/2012	BASF-(SYN)-21-6-B-CC-12-3	36,190	2,880	
7/6/2012	8/3/2012	BASF-(SYN)-21-6-B-CC-12-4	15,620	1,243	1,760
7/11/2012	7/20/2012	BASF-(SYN)-18-6-B-CC-10-1	57,780	4,598	
7/11/2012	7/20/2012	BASF-(SYN)-18-6-B-CC-10-2	22,870	1,820	
7/11/2012	7/26/2012	BASF-(SYN)-18-6-B-CC-10-3	50,400	4,011	
7/11/2012	7/26/2012	BASF-(SYN)-18-6-B-CC-10-4	19,380	1,542	
7/11/2012	8/9/2012	BASF-(SYN)-18-6-B-CC-10-5	19,500	1,552	
7/11/2012	8/9/2012	BASF-(SYN)-18-6-B-CC-10-6	33,480	2,664	2,698
7/31/2012	8/7/2012	BASF-(SYN)-30-6-B-CC-16-1	47,940	3,815	
7/31/2012	8/7/2012	BASF-(SYN)-30-6-B-CC-16-2	17,270	1,374	
7/31/2012	8/14/2012	BASF-(SYN)-30-6-B-CC-16-3	18,910	1,505	
7/31/2012	8/14/2012	BASF-(SYN)-30-6-B-CC-16-4	55,510	4,417	2,778
8/31/2012	9/18/2012	BASF-(SYN)-30-6-B-CC-8-1	40,720	3,240	
8/31/2012	9/18/2012	BASF-(SYN)-30-6-B-CC-8-2	76,390	6,079	
8/31/2012	9/23/2012	BASF-(SYN)-30-6-B-CC-8-3	83,430	6,639	
8/31/2012	9/23/2012	BASF-(SYN)-30-6-B-CC-8-4	88,130	7,013	5,743
8/31/2012	9/18/2012	BASF-(SYN)-30-6-B-CC-10-7	72,100	5,738	
8/31/2012	9/18/2012	BASF-(SYN)-30-6-B-CC-10-8	53,960	4,294	
8/31/2012	9/23/2012	BASF-(SYN)-30-6-B-CC-10-9	73,070	5,815	
8/31/2012	9/23/2012	BASF-(SYN)-30-6-B-CC-10-10	46,720	3,718	4,891

Table G17: Hanson Longview Synthetic Cylinder Test Results

Production Date	Test Date	Cylinder Designation	Peak Load (lbs)	Stress (psi)	Average Stress
5/31/2012	6/15/2012	BASF-(SYN)-B-CC-8-1-LV	61,800	4,920	
5/31/2012	6/15/2012	BASF-(SYN)-B-CC-8-2-LV	64,590	5,143	
5/31/2012	6/18/2012	BASF-(SYN)-B-CC-8-3-LV	64,780	5,158	
5/31/2012	6/18/2012	BASF-(SYN)-B-CC-8-4-LV	64,120	5,105	
5/31/2012	6/28/2012	BASF-(SYN)-B-CC-8-5-LV	76,090	6,058	
5/31/2012	6/28/2012	BASF-(SYN)-B-CC-8-6-LV	82,050	6,533	5,486
6/21/2012	6/25/2012	BASF-(SYN)-B-CC-6-1-LV	53,080	4,226	
6/21/2012	6/25/2012	BASF-(SYN)-B-CC-6-2-LV	48,790	3,885	
6/21/2102	6/28/2012	BASF-(SYN)-B-CC-6-3-LV	33,300	2,651	
6/21/2012	6/28/2012	BASF-(SYN)-B-CC-6-4-LV	46,930	3,736	
6/21/2012	7/20/2012	BASF-(SYN)-B-CC-6-5-LV	58,760	4,678	
6/21/2012	7/20/2012	BASF-(SYN)-B-CC-6-6-LV	66,890	5,326	4,084
6/21/2012	6/25/2012	BASF-(SYN)-B-CC-8-7-LV	36,770	2,928	
6/21/2012	6/25/2012	BASF-(SYN)-B-CC-8-8-LV	57,720	4,596	
6/21/2012	6/28/2012	BASF-(SYN)-B-CC-8-9-LV	50,130	3,991	
6/21/2102	6/28/2012	BASF-(SYN)-B-CC-8-10-LV	34,030	2,709	
6/21/2012	7/20/2012	BASF-(SYN)-B-CC-8-11-LV	53,230	4,238	
6/21/2012	7/20/2012	BASF-(SYN)-B-CC-8-12-LV	59,460	4,734	3,866
6/21/2102	6/25/2012	BASF-(SYN)-B-CC-10-1-LV	30,250	2,408	
6/21/2012	6/25/2012	BASF-(SYN)-B-CC-10-2-LV	40,510	3,225	
6/21/2012	6/28/2012	BASF-(SYN)-B-CC-10-3-LV	47,120	3,752	
6/21/2012	6/28/2012	BASF-(SYN)-B-CC-10-4-LV	38,780	3,088	
6/21/2102	7/6/2012	BASF-(SYN)-B-CC-10-5-LV	41,900	3,336	
6/21/2012	7/6/2012	BASF-(SYN)-B-CC-10-6-LV	60,800	4,841	3,442
6/21/2012	6/25/2012	BASF-(SYN)-B-CC-12-1-LV	62,410	4,969	
6/21/2102	6/25/2012	BASF-(SYN)-B-CC-12-2-LV	56,550	4,502	
6/21/2012	6/28/2012	BASF-(SYN)-B-CC-12-3-LV	60,550	4,821	
6/21/2012	6/28/2012	BASF-(SYN)-B-CC-12-4-LV	68,270	5,436	
6/21/2012	7/20/2012	BASF-(SYN)-B-CC-12-5-LV	85,470	6,805	
6/21/2102	7/20/2012	BASF-(SYN)-B-CC-12-6-LV	78,780	6,272	5,467
6/21/2012	6/25/2012	BASF-(SYN)-B-CC-16-1-LV	54,080	4,306	
6/21/2012	6/25/2012	BASF-(SYN)-B-CC-16-2-LV	48,460	3,858	
6/21/2102	6/28/2012	BASF-(SYN)-B-CC-16-3-LV	52,230	4,158	
6/21/2012	6/28/2012	BASF-(SYN)-B-CC-16-4-LV	47,310	3,767	
6/21/2012	7/6/2012	BASF-(SYN)-B-CC-16-5-LV	51,890	4,131	
6/21/2012	7/6/2012	BASF-(SYN)-B-CC-16-6-LV	66,380	5,285	4,251

Table G18: Northern Concrete Synthetic Cylinder Test Results

Production Date	Test Date	Cylinder Designation	Peak Load (lbs)	Stress (psi)	Average Stress
9/21/2012	10/15/2012	BASF-(SYN)-B-CC-8-2-NC	132,130	4,676	
9/21/2012	10/18/2012	BASF-(SYN)-B-CC-8-3-NC	110,860	3,923	
9/21/2012	10/22/2012	BASF-(SYN)-B-CC-8-4-NC	115,710	4,094	
9/21/2012	10/26/2012	BASF-(SYN)-B-CC-8-5-NC	150,570	5,328	4,505
9/21/2012	10/15/2012	BASF-(SYN)-B-CC-10-2-NC	115,240	4,078	
9/21/2012	10/18/2012	BASF-(SYN)-B-CC-10-3-NC	114,240	4,042	
9/21/2012	10/22/2012	BASF-(SYN)-B-CC-10-4-NC	174,640	6,180	
9/21/2012	10/26/2012	BASF-(SYN)-B-CC-10-5-NC	162,800	5,761	5,015
9/21/2012	10/15/2012	BASF-(SYN)-C-CC-12-2-NC	156,880	5,551	
9/21/2012	10/18/2012	BASF-(SYN)-C-CC-12-3-NC	133,940	4,740	
9/21/2012	10/22/2012	BASF-(SYN)-C-CC-12-4-NC	144,770	5,123	
9/21/2012	10/26/2012	BASF-(SYN)-C-CC-12-5-NC	118,090	4,179	4,898
9/21/2012	10/15/2012	BASF-(SYN)-C-CC-16-2-NC	153,880	5,445	
9/21/2012	10/18/2012	BASF-(SYN)-C-CC-16-3-NC	140,970	4,988	
9/21/2012	10/22/2012	BASF-(SYN)-C-CC-16-4-NC	132,570	4,691	
9/21/2012	10/26/2012	BASF-(SYN)-C-CC-16-5-NC	188,040	6,654	5,445
9/21/2012	10/15/2012	BASF-(SYN)-C-CC-18-2-NC	153,270	5,424	
9/21/2012	10/18/2012	BASF-(SYN)-C-CC-18-3-NC	129,490	4,582	
9/21/2012	10/22/2012	BASF-(SYN)-C-CC-18-4-NC	136,990	4,847	
9/21/2012	10/26/2012	BASF-(SYN)-C-CC-18-5-NC	123,870	4,383	4,809

REFERENCES

1. Abolmaali, A., Mikhaylova A., Wilson, A., and Lundy, J. Performance of Steel Fiber Reinforced Concrete Pipes. *Transportation Research Board Journal*, In press.

2. Alhozaimy, A. M., Soroushian, P., and Mirza, F. Mechanical Properties of Polypropylene Fiber Reinforced Concrete and the Effects of Pozzalanic Materials. *Cement and Concrete Composites*, Vol. 18, 1996, pp.85-92.

3. Atis, C.D., Karahan, O., K. Ari, Sola, O.C., and Bilim, C. Relation between Strength Properties (Flexural and Compressive) and Abrasion Resistance of Fiber (Steel and Polypropylene)-Reinforced Fly Ash Concrete. *Journal of Materials in Civil Engineering*, Aug. 2009, Vol. 21, Issue 8, pp. 402-408. DOI:10.1061/(ASCE)0899-1561(2009)21:8(402).

4. ASCE 15-98 Standard Practice for Direct Design of Buried Precast Concrete Pipe Using Standard Installations (SIDD*). American Society of Civil Engineers*, 1998.

5. ASTM A820 Standard Specification for Steel Fibers for Fiber-Reinforced Concrete. *American Society for Testing and Materials*, 2011.

6. ASTM C39 Standard Test Method for Compressive Strength of Cylindrical Concrete Specimens. *American Society for Testing and Materials*, 2011.

7. ASTM C76 Standard Specification for Reinforced Concrete Culvert, Storm Drain and Sewer Pipe. *American Society for Testing and Materials*, 2011.

8. ASTM C76M Standard Specification for Reinforced Concrete Culvert, Storm Drain, and Sewer Pipe (Metric). *American Society for Testing and Materials*, 2011.

9. ASTM C497 Standard Test Method for Concrete Pipe, Manhole Sections, or Tile. *American Society for Testing and Materials*, 2005.

10. ASTM C1116 Standard Specification for Fiber-Reinforced Concrete. *American Society for Testing and Materials*, 2011.

11. ASTM C1609 Standard Test Method for Flexural Performance of Fiber-Reinforced Concrete (Using Beam With Third-Point Loading). *American Society for Testing and Materials*, 2011.

12. Banthia N., Bindiganavile, V., Jones, J., Novak, J. Fiber-reinforced concrete in precast concrete applications: Research leads to innovative products. *PCI Journal*, Summer 2012, pp.33-46.

13. Concrete Pipe Design Manual. *American Concrete Pipe Association,* 2007.

14. Concrete Pipe Handbook. *American Concrete Pipe Association*, 1998.

15. Concrete Pipe Technology Handbook. *American Concrete Pipe Association*, 1993.

16. Cunha, V.M., Barros, J.A., and Sena-Cruz, J. Pullout Behaivor of Steel Fibers in Self-Compacting Concrete. *Journal of Materials in Civil Engineering*, Jan. 2010, Vol. 22, Issue 1, pp. 1-9. DOI:10.1061/(ASCE)MT.1943-5533.0000001.

17. European Standard, BS EN 1916 Concrete Pipes and Fittings, unreinforced, steel fibre and reinforced. *European Committee for Standardization*, 2002.

18. Gencel, O., Bostow, W., Datashvili, T., and Thedfrod, M. Workability and Mechanical Performance of Steel Fiber-Reinforced Self-Compacting Concrete with Fly Ash. *Composite Interfaces*, April 2011, Vol. 18, Issue 2, pp. 169-184. DOI:10.1163/092764411X567567.

19. Henry H.L. An Investigation of Large Diameter Fiber Reinforced Concrete Pipe. *ACI Special Publications*, Vol. 44, Np. SP44-25, 1974, pp. 435-454.

20. Kurtz, S., and Balaguru, P. Postcrack Creep of Polymetic Fiber-reinforced Concrete in Flexure. *Cement and Concrete Research*, Vol. 30, 2000, pp. 183-190.

21. Kwak, Y-K., Eberhard, M., Kim, W-S., Kim, J. Shear Strength of Steel Fiber Reinforced Concrete Beams without Stirrups. *ACI Structural Journal*, July/August, No. 99-S55, 2002, pp. 530-538.

22. MacDonald, C.N., and Trangsrud, J. Steel Fiber Product Introduction through Pre-Cast Reinforced Concrete Pipe. *ACI Special Publications*, Vol. 222, No. SP222-13, 2004, pp. 185-198.

23. Roesler, J.R., Lange, D.A., Altoubat, S.A., Rieder, K., Ulreich, G.R. Fracture of Plain and Fiber-Reinforced Concrete Slabs under Monotonic Loading. *Journal of Matericals in Civil Engineering,* Sept/Oct 2004, Vol. 16, Issue 5, pp. 452-460. DOI:10.1061/(ASCE)0899-1561(2004)16:5(452).

24. Shende, A.M., and Pande, A.M. Comparative study on Steel fibre reinforced Cum control concrete under flexural and deflection. *International Journal of Applied Engineering Research, Dindigul*, 2011, Vol. 1, No. 4, pp. 942-950. ISSN-0976-4259.

25. Song, P.S., Hwang, S., Sheu, B.C. Strength properties of nylon- and polypropylene-fiber-reinforced concretes. *Cement and Concrete Research*, Vol. 35, 2005, pp. 1546-1550.

26. Sustersic, J., Ukrainczyk, V., Zajc, A., Sajna, A. Evaluation Of Crack Opening Resistance of SFRC. *Third International Conference on Concrete Under Severe Conditions*, 2001.

27. Swamy, R.N., and Kent, B. Some Practical Applications of Steel Fiber Reinforced Concrete. *American Concrete Institute*, Vol. 44, No. SP44-18, 1974, pp. 319-336.

28. Thomas, J., and Ramaswamy, A. Mechanical Properties of Steel Fiber-Reinforced Concrete. *Journal of Materials in Civil Engineering*, May 2007, Vol. 19, Issue 5, pp. 385-392. DOI:10.1061/(ASCE)0899-1561(2007)19:5(385).

29. Wang. Toughness Characteristics of Synthetic Fiber-Reinforced Cementitious Composites. *Fatigue & Fracture of Engineering Materials & Structures,* April 1998, Vol. 2, Issue 4, pp.521-531.

BIOGRAPHICAL INFORMATION

Ashley graduated from Northern Arizona University in the fall of 2009, receiving a Bachelor of Science Degree in Civil Engineering with a minor in Construction Management. Soon after graduation she began working for a local structural engineering firm in Arizona. She received her Engineering-In-Training Certificate in May 2010. In fall 2010 she moved to Texas to pursue her Master degree in Civil Engineering with a structural emphasis from the University of Texas at Arlington under the supervision of Dr. Ali Abolmaali. Ashley plans to begin her career working for Hanson Pipe and Precast in the Dallas/Ft. Worth area.